FTD-MT- 64-14

COPY 2 of 3 COPIES

TT 64-71188

TRANSLATION

NONFERROUS METALLURGY

249 p #6.00 hc
#1.25 mf

FOREIGN TECHNOLOGY DIVISION

AIR FORCE SYSTEMS COMMAND

WRIGHT-PATTERSON AIR FORCE BASE

OHIO

DISCLAIMER NOTICE

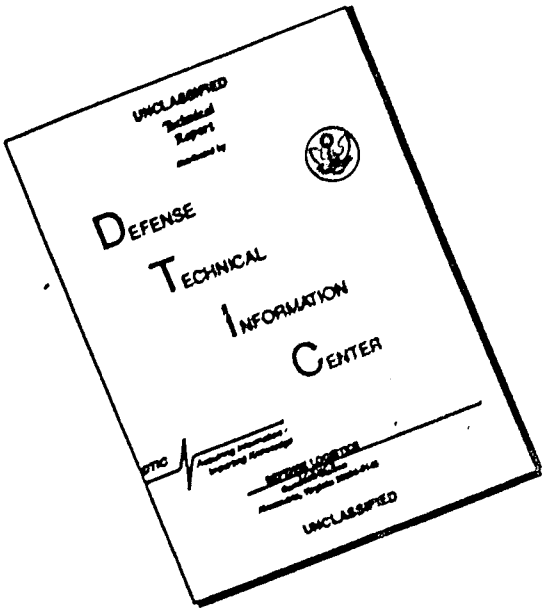

THIS DOCUMENT IS BEST QUALITY AVAILABLE. THE COPY FURNISHED TO DTIC CONTAINED A SIGNIFICANT NUMBER OF PAGES WHICH DO NOT REPRODUCE LEGIBLY.

FOREWORD

This document is a machine translation of Russian text which has been processed by the AN/GSQ-16(XW-2) Machine Translator, owned and operated by the United States Air Force. The machine output has been fully post-edited. Ambiguity of meaning, words missing from the machine's dictionary, and words out of the context of meaning have been corrected. The sentence word order has been rearranged for readability due to the fact that Russian sentence structure does not follow the English subject-verb-predicate sentence structure. The fact of translation does not guarantee editorial accuracy, nor does it indicate USAF approval or disapproval of the material translated.

CLEARINGHOUSE FOR FEDERAL SCIENTIFIC AND TECHNICAL INFORMATION, CFSTI
DOCUMENT MANAGEMENT BRANCH 410.11

LIMITATIONS IN REPRODUCTION QUALITY

Accession #

☑ 1. We regret that legibility of this document is in part unsatisfactory. Reproduction has been made from best available copy.

☐ 2. A portion of the original document contains fine detail which may make reading of photocopy difficult.

☐ 3. The original document contains color, but distribution copies are available in black-and-white reproduction only.

☐ 4. The original distribution copies contain color which will be shown in black-and-white when it is necessary to reprint.

☐ 5. The processing copy is available on loan at CFSTI.

☐ 6.

TJ-L-107-8/64

Processor: LA

EDITED MACHINE TRANSLATION

NONFERROUS METALLURGY

English Pages: 233

S/0149-063-000-003

PREPARED BY:

TRANSLATION DIVISION
FOREIGN TECHNOLOGY DIVISION
WP-AFB, OHIO.

Ministerstvo
Vysshego i Srednego Spetsial'nogo
Obrazovaniya SSSR

Izvestiya
Vysshikh Uchebnykh Zavedeniy

TSVETNAYA METALLURGIYA

3

1963
6-y god izdaniya

Izdaniye Severokavkazskogo
Gornometallurgicheskogo Instituta
g. Ordzhonikidze

Pages 1-171

Izvestiya VUZov: NONFERROUS METALLURGY

-USSR -

No 3, 1963

Following is a translation of the Russian-language journal Izvestiya Vysshikh Uchebnykh Zavedeniy: Tsvetnaya Metallurgiya (News of Higher Educational Institutions: Nonferrous Metallurgy), No 3, 1963, Ordzhonokidze, pp 1-166

TABLE OF CONTENTS

CHARACTERISTICS OF THE GEOLOGICAL STRUCTURE OF THE KADAT-KHAMPALADAGSKOYE ORE FIELD IN SEVERNAYA OSETIYA

By V.B. Tsogoyev, V.Ye. Gorelov, P.A. Polkvoy, V.S. Starikov, Northern Caucasian Mining and Metallurgical Institute, Chair of Geology and Mineralogy

Pages 3-10

The Kadat-Khampaladagskoye ore field, together with other polymetallic deposits and ore manifestations, forms part of the polymetallic zone of the Northern Caucasus and has long been known in the geological literature as one of the deposits of the "shale belt." It is located on the left side of the valley of the Fiagdon River, in the Kadat region, extending from there in a sublatitudinal direction along the valley of the Shagdar-adag River to the west.

The story of the discovery of polymetallic deposits in Jurassic shales is of great antiquity; mention of the presence of lead-zinc and silver deposits in Severnaya Osetiya is found in the account of the first Russian expeditions of 1768-1771. Serious attempts to prospect for these deposits were first made at the end of the last century and the beginning of this one. The first attempts at exploitation of these deposits were also made at that time. However, the low percentage of important metals in the ores and the imperfection of possible techniques for their enrichment caused these deposits to be undeservedly forgotten, since they were considered to hold no prospects. Work conducted in this direction during the last ten years, primarily by the geologists' collective of the "Sevkavtsvetmetrazvedka" Trust, sharply altered this opinion and there is now no doubt of the commercial character of the polymetallic deposits concentrated in the series of Jurassic shales.

All the polymetallic deposits and ore manifestations can be lumped into the so-called northern polymetallic belt, which traverses the entire territory of Severnaya Osetiya, running along the mountainous region, and emerges in the territory of the Checheno-Ingushskaya and Kabardino-Balkarskaya Autonomous Soviet Socialist Republics. Within Osetiya the deposits

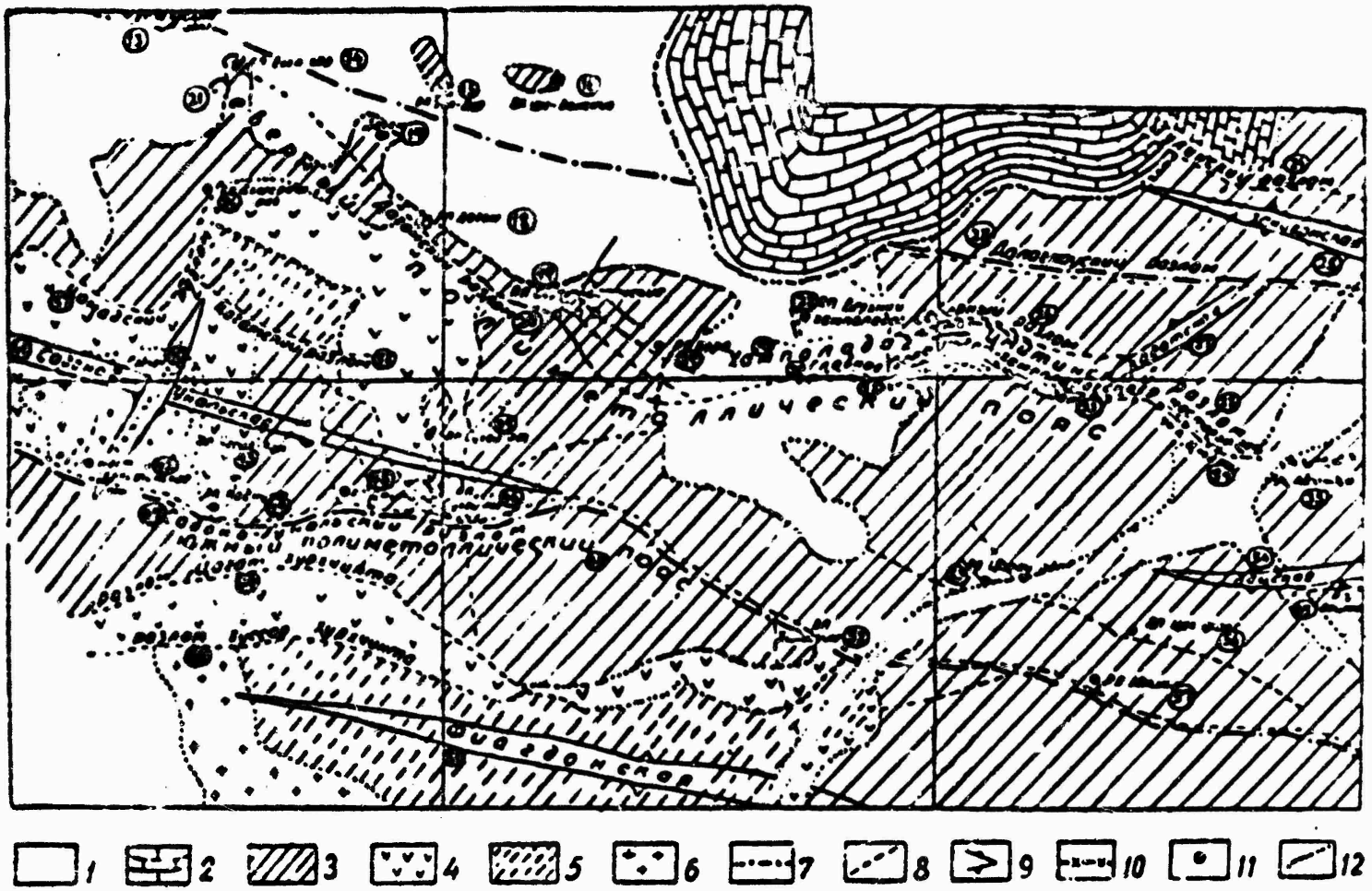

1 2 3 4 5 6 7 8 9 10 11 12

Fig. 1. Schematic structural-geological map of the Fiagdon-Ardon interfluve. 1) Quaternary deposits; 2) Upper Jurassic limestones; 3) Lower and Middle Jurassic sand-clay deposits; 4) Lower Jurassic keratophyre; 5) Paleozoic deposits; 6) granites; 7) boundaries of structural zones; 8) most important tectonic faults; 9) axes of anticlinal structures; 10) ore zones; 11) polymetallic ore manifestations; 12) geological boundaries; 13) Dolgokgoy; 14) Byl-Khor; 15) Uyel-Dur; 16) Urs-Don; 17) Dagom; 18) Dagom; 19) Verkhne-Dagomskoye; 20) Dagomskiy Fault; 21) northern polymetallic belt; 22) Verkhniy Khampaladag; 23) Dalagkauskiy Fault; 24) Gulinskiy Fault; 25) Khanikomskaya; 26) Northern Fault; 27) Kadatskaya; 28) Imitinskiy Fault; 29) Kora; 30) Khampaladag; 31) main zone of Kadat-Khampaladagskoye deposit; 32) Khandlodag; 33) Kadat section; 34) Tsmiti section; 35) Ansadur section; 36) Akh-

Continuation of key to Fig. 1: sharpirag; 37) Tsamadskiy Fault; 38) Tsagatskiy Fault; 39) Sukhoy-Log; 40) Loboyed; 41) Sadono-Unal'skaya; 42) Kholstinskor deposit; 43) Uarag-Kom; 44) Kadnunt; 45) Dzhimts; 46) Sukhoy-Log; 47) Sadono-Unal'skiy Fault; 48) southern polymetallic belt; 49) Tsagat-Khurkhchint Fault; 50) Khussar-Khurkhchint Fault; 51) Fiagdonskaya; 52) Kharshyatin; 53) Tsarachoda; 54) Latsskaya; 55) Latskoye; 56) Tsakh-Fars; 57) Yuzhnoye.

are controlled by regional longitudinal faults with sublatitudinal trends which complicate the wings of the Sadono-Unal'skiy and Fiagdonskiy anticlines, these having the same sublatitudinal trend (Fig. 1).

Paleozoic and Jurassic rocks occur in the geological structure of the region which we have described. Quaternary deposits are also widely distributed, especially in the Kadat-Khampaladagskoye ore field. The Paleozoic deposits, represented by series of crystalline shales and their faulting granites, are exposed only far to the south in the Fiagdon River valley. The cross-section of the Jurassic deposits is rather complicated, being characterized by great thickness and stratigraphic completeness, and has been described sufficiently well in the literature [1, 2]. Omitting a characterization of its lower levels, which are not exposed within the section that we have described, let us turn directly to a description of the deposits composing the Kadat-Khampaladagskoye ore field and adjacent regions.

The deposits of the Toarcian and Aalenian stages are ore-containing series and are an alternation of thin layers of clay and siltstone shales with thin layers of sandstones. It is sometimes possible to note a coarser alternation of blocks of clay shales enriched with layers of sand and blocks of material poor in sand. Within the series are lenses of light coarse-grained sandstones 15-20 m thick, whose trend is not maintained. Concretions of clay siderites of varying shape, the number of which increases toward the top, appear in the upper half of the series. It is interesting to note that in concretions near the ore-bearing zones it is frequently possible to observe cracks filled with comparatively large accumulations of pyrite, less frequently sphalerite, and very rarely galena. This phenomenon has also been noted in the Kakadur-Khanikomskoye deposit [3] and is the result of primary dispersion of the ore components caused by hydrothermal "steaming" of the surrounding rocks during the formation of the deposit.

Quaternary formations, represented by diluvial series (landslides, cave-ins, scree, and diluvial argillaceous soils), have developed very widely within the ore field; their thickness varies from 40 to 70 meters in individual sections (Kadatskoye deposit).

Tectonically, the regions is located wholly within the northern structural-facies zone, which was first distinguished by G.D. Azhgirey [4]. In vertical section three structural stages differing from each other in de-

gree of deformation and of rock metamorphism and character of metallogenesis are distinguishable quite distinctly.

The Lower Paleozoic stage is formed by metamorphized sedimentary and magmatic rocks. The middle stage is represented by plastic deposits of a Lower and Middle Jurassic shale complex and, to an insignificant degree, by volcanogenic formations. The upper stage is formed wholly by series of Upper Jurassic carbonate rocks and chalk. Inasmuch as polymetallic mineralization is adapted to rocks of the middle stage, a detailed structural characterization of it is given below.

As was already noted above, the territory described here is located wholly within the northern wing of the Caucasian anticline, the core of which exhibits Lower Paleozoic crystalline shales and their faulting granites. All series of Lower and Middle Jurassic shales form a series of folds complicated by rather numerous faults and zones of crumpling and brecciation. The folds in the brachyform region have a sublatitudinal trend and the most important faults and the zone of crumpling are usually oriented parallel to the latter.

The structural position of the Kadat-Khampaladagskoye deposit is relatively simple. Within the ore field a number of both plicative and disjunctive dislocations are distinguishable. The deposit is located on the north wing of the Fiagdonskiy anticline, which is a second-order structure. The north wing of the anticline is a monocline, called the Kora-Khareschinskiy monocline by A.P. Lebedev [5]. This monocline is formed by rocks of the Toarcian and Aalenian stages. The boundary monoclines at the south and the north are large tectonic dislocations (the Sadono-Unal'skiy and Main Ore Faults; see Fig. 1). The rocks in this section have a sublatitudinal trend and a northerly dip from 20 to 50°. Within the monoclines are sections characterized by the presence of intensive disharmonic folding and a series of intersecting faults with a northwesterly trend.

To the north of Kadat is the Kadatskiy anticline, which is formed by Lower and Upper Aalenian rocks. The fold has an asymmetric structure, its axis running in a northeasterly direction. Both wings of the Kadatskiy anticline are complicated by lower-order synclinal folds.

Of the large dislocations involving discontinuities, which play the main role in the localization of polymetallic mineralization, we should note the Khampaladag-Tsmitinskiy and Northern Faults (Fig. 2). The Khampaladag-Tsmitinskiy Fault extends through the whole Kadat-Khampaladagskoye ore field in a sublatitudinal direction, stretching far beyond its limits both eastward and westward. It is expressed superficially by a rather wide zone of rock crumpling and brecciation (up to 50 m). The latter is, in our opinion, the main ore-controlling structure, within which are localized a number of large polymetallic deposits and ore manifestations. Thus, on the eastern continuation of this fault is the Kakadur-Khanikomskoye deposit, with the Avsandur, Khanikom, Kakadur, and other sections. West of the Kadat-

Khampaladagskoye ore field the Zapadnyy Khampaladag, Kora, Dagomskoye, etc. ore manifestations gravitate to the same fault.

Within the area described here the fault has been traced in the Tsmiti, Kadat, and Khampaladag sections, both from the surface and underground, by means of worked-out mines and wells. The trend of the fault varies from latitudinal (270°) to northwesterly (295°) in individual sections. The dip of the fault (basically steep) is both northerly and southerly. Thus, in the Tsmiti section there is a quite steep (70-80°) southerly dip. On the northwest side of the Kadat section the fault is rather obliquely (40-50°) inclined to the north and, further on in the same direction (Khampaladag section), the angle of inclination increases to 80°, with the northerly dip direction preserved. The fault is a typical one with its north wing missing, as may be seen on the accompanying map (see Fig. 2). The amplitude of the displacement has not been accurately established, but, judging from the differences in the ages of the rocks in the northern and southern wings of the fault, it should be considerable.

The Khapaladag-Tsimitinskiy Fault is accompanied by a series of concomitant dislocations involving discontinuities, which sometimes also contain sulfide mineralization. The biggest and most interesting of them is the Northern Fault, which extends to the north of the main fault. It has been traced in the Kadat and Khampaladag Sections and was located by individual outcrops at the surface of the ore-bearing zone associated with its accompanying zone of rock crumpling and crushing. The dislocation has a latitudinal trend and a northerly dip at an angle of 60°. To the west the angle of incidence becomes greater and reaches 80°. In addition to the above-described faults, a number of small tectonic dislocations and zones of crumpling were detected within the ore field by means of worked-out mines; among these our attention is struck by dislocations having a submeridional trend and, for the most part, a westerly dip at angles of 40-50°. The thickness of the zones of crumpling observed reaches 20-30 m and individual cracks filled with attrition clay attain 3-10 cm. The displacement amplitudes for these dislocations have not been determined, but it may be assumed that they do not attain significant values. Individual sections of these zones are poorly mineralized.

Thus, the Kadat-Khampaladagskoye ore field is divided into two ore-bearing zones: the main zone is coordinated with the rock crushing area of the belt formed by the Khampaladag-Tsmitinskiy Fault and the northern zone lies in the vicinity of the Northern Fault (see Fig. 2). The localization of the industrial deposits within the Kadat-Khampaladagskoye ore field is related to the zones.

The main ore-bearing zone is a system of veinlets, veins, brecciated blocks, and lenticular bodies composed of quartz, carbonate, and quartz-carbonate with sulfide enrichment. The lenticular ore bodies observed in the zone are surrounded by a complicated network of quartz-carbonate-sulfide veins. The contacts between the ore bodies and the enclosing rocks

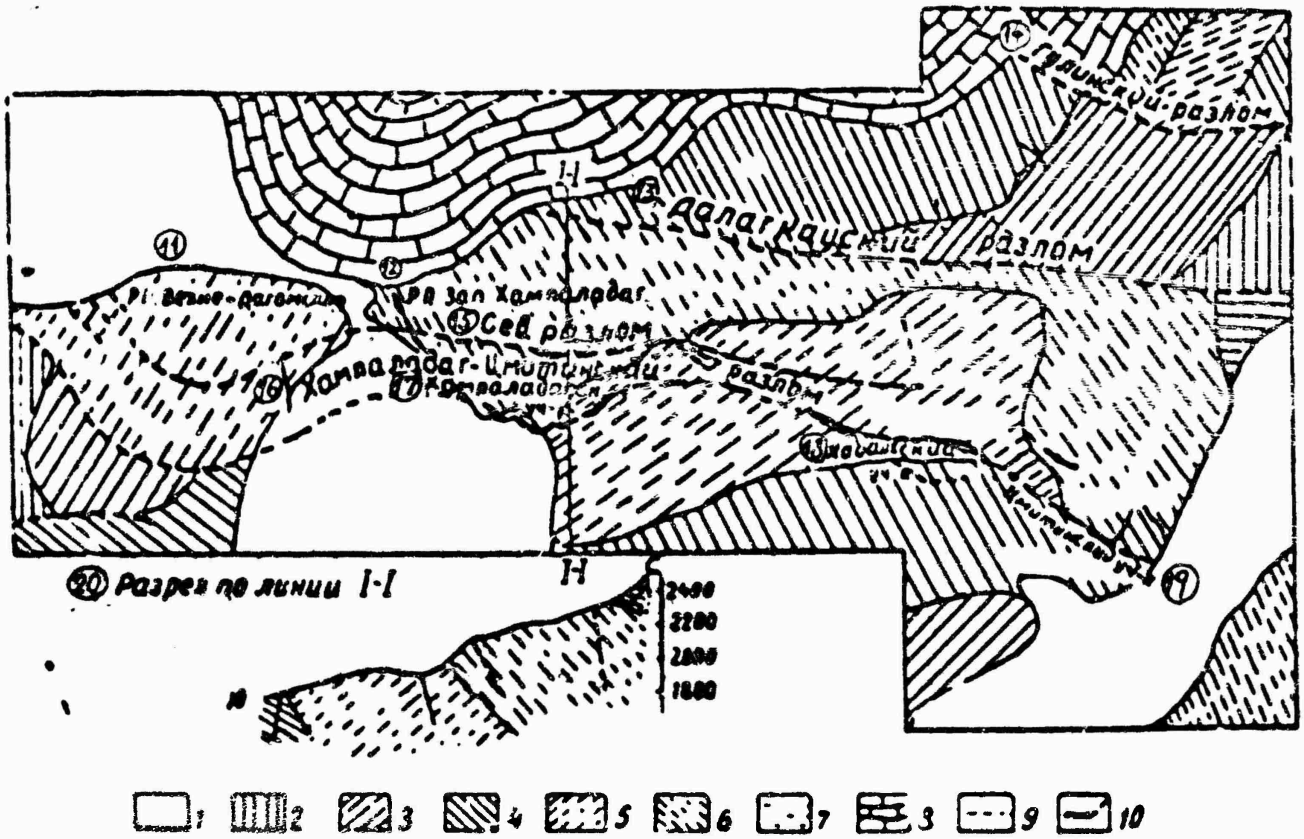

Fig. 2. Schematic geological map of the Kadatskoye ore field. 1) quaternary deposits (alluvium and diluvium); 2) Lower Toarcian clay deposits; 3) siltstones and sandstones with smaller quantity of Middle Toarcian clay rocks; 4) argillites and clay shales with layers of Upper Toarcian siltstones and sandstones; 5) argillites with blocks of Lower Aalenian siltstones and sandstones; 6) Upper Aalenian argillites, siltstones, and sandstones; 7) shistic siltstone clays and argillites of the Bajocian stage; 8) Upper Jurassic carbonate deposits; 9) tectonic dislocations; 10) ore-bearing zones; 11) Verkhne-Dagomskoye; 12) Zap. Khampaladag; 13) Dalagkauskiy Fault; 14) Gulinskiy Fault; 15) Northern Fault; 16) Khampaladag-Tsmitinskiy Fault; 17) Khampaladag section; 18) Kadat section; 19) Tsmiti section; 20) cross-section through I-I.

are usually gradual and have been established by assay.

A characteristic peculiarity of the ore-bearing zone is an echelon arrangement of the individual ore bodies within it. The presence of several parallel ore bodies is less frequent. The lenticular bodies are oriented along the trend of the ore-bearing zone. Their size (on the western and eastern sides) varies from 30 to 80 m along the trend, 3 to 5 m in thickness, and up to 100 m along the dip. In the center of the ore-bearing zone (Kadat section) lenses with [illegible] thickness have somewhat larger trend and dip dimensions.

The northern ore-bearing zone has been studied in less detail than the main zone. According to data obtained by trenching and drilling, the ore bodies discovered in the Kadat and Khampaladag sections attain thicknesses of 2.5 and 10 m respectively and have trends of several tens of meters. In addition to the increase in thickness established by tracing the ore bodies from east to west, there is a marked increase in the number of bodies.

The ore bodies in the main and northern ore-bearing zones do not have consistent thicknesses along either their trends or their dips; they are characterized by the presence of pinches, are frequently accompanied by apophyses, and taper out, forming a network of leaders which occasionally covers several tens of meters.

Sulfide mineralization is distributed very nonuniformly in the ore bodies, in the form of impregnation, veins, and pocket-like accumulations, and has developed both in lenticular bodies and vein networks.

Several characteristic textural types -- massif, breccial, and vein-network -- have been distinguished in studying the composition of the ores of the Kadat-Khampaladag group of deposits and ore manifestations. On examining the main ore-bearing zone from east to west it may clearly be seen that the vein-network type of deposit, which predominates in the Tsmiti section, gives way to the first two types of ore west of the junction (Khampaladag section).

The mineral composition of the ores is not complex. The principal primary ore minerals are pyrite, galena, sphalerite (marmatite and, more rarely, cleiophane), and chalcopyrite. Arsenopyrite, marcasite, covellite, and bornite are occasionally encountered in small quantities. The nonmetalliferous minerals include quartz, carbonates, and chlorite.

However, it should be noted that the character of the mineralization of the main and northern ore-bearing zones differs. While the main zone is characterized by a commercial concentration of lead and zinc (galena and sphalerite) with an insignificant content of copper, the northern zone displays poor contents of lead and zinc and, at the same time, an increased content of copper (chalcopyrite). This phenomenon, in our opinion, results from the appearance of a horizontal zonality in the deposits. The zone of

oxidation within the belt under consideration is poorly developed and of no practical importance. Among the minerals observed in it are limonites of various colors, pyromorphite, and lead ochre.

A hydrothermal change in the enclosing rocks is noted only in individual sections and takes the form of "bleaching" of the clay shales in direct proximity to the ore bodies, usually extending for only negligible distances (up to 0.5 m). Work conducted by the geologists of the Kadat GRP established the presence of a primary polymetallic dispersion aureole from the existence of very thin veins of varying mineralogical composition in the enclosing rocks. It was also proved that the zonal distribution of veins of a definite composition is a function of distance from the ore zone.

Thus, the geological structure of the Kadat-Khampaladagskoye ore field, which we have been considering, has its own specific peculiarities and is distinguished both from the deposits and ore manifestations in the southern polymetallic belt and from the deposits located to the east within the same shale belt. The Kadatskoye deposit is distinguished from the former, whose mineralization is localized in structures abutting the main ore-controlling faults (Sadono-Unal'skiy et al.) and forming the southern polymetallic belt, by the fact that it is located in rocks of a different composition and also by the fact that it is adapted to the zones of crushing and brecciation accompanying the main fault, which has a sublatitudinal trend.

The peculiar features of this deposit, as compared with other deposits in the same shale belt (Kakadur-Khanikom), consist primarily in differences in the structures favorable for the concentration of rich mineralization. In the Kakadur-Khanikomskoye deposit these structures are the intersections of the axes of the folds with the faults, while in the Kadat-Khampaladagskoye deposit they are flexure sites in the fault itself. Sections containing flexures in the fault zone are the most favorable for the formation of polymetallic sulfide bodies; the tectonic stresses, continuing after formation of the actual fault, open primarily the flexure zone, where cavities favorable for ore deposition are formed. It is not difficult to note that all of the ore blocks are located in precisely such sites (see Fig. 2).

CONCLUSIONS

1. The polymetallic deposits and ore manifestations of the Kadat-Khampaladagskoye ore field are located within the northern polymetallic belt and are adapted to a latitudinal fault accompanied by a zone of intensive crumpling and crushing of rock and related spatially to a belt in which Lower and Middle Jurassic sand-clay deposits have developed.

2. As a result of compressive stresses exerted from the flanks of the ore field, the flexure sites in the Khampaladag-Tsmitinskiy Fault were slightly opened in individual sections and the cavities most favorable for ore deposition were formed there.

3. The ore bodies are localized in zones of intensive crushing and cro-

sion accompanying the faults and are ore zones within which are observed individual lenses and veins, sections in which ore breccia have developed, or dense networks of thin quartz-carbonate veins with dispersed polymetallic mineralization.

4. The most favorable areas for prospecting for new polymetallic ore zones are the fault-flexure sections west of the Kadat-Khampaladagskoye ore field.

BIBLIOGRAPHY

1. L.A. Vardanyants, TsNIGRI /Central Scientific Research Institute for Prospecting for Nonferrous, Rare, and Precious Metals/, No. 25, 1935.

2. S.S. Kuznetsov, Geologiya Severnoy yurskoy depressii Digoro-Osetinskoy chasti Bol'shogo Kavkaza /Geology of the Northern Jurassic Depression in the Digoro-Osetiya Section of Bol'shoy Kavkaz/, Leningrad, 1947.

3. V.S. Starikov, G.P. Ol'khovskiy, Tr. SKGMI /Transactions of the Northern Caucasian Mining and Metallurgical Institute/, No. 16, 1961.

4. G.D. Azhgirey, Izv. VUZ /News of Higher Educational Institutions/, Geologiya i razvedka /Geology and Prospecting/, No. 4, 1953.

5. A.P. Lebedev, DAN SSSR /Proceedings of the Academy of Sciences USSR/, Vol. 58, No. 8, 1947-1948.

Manuscript submitted 19 December 1962

EXPERIENCE IN WORKING WITH THE NSM-2 LEVEL UNDER SUBTERRANEAN CONDITIONS

By L.A. Denisenko, Kommunar Mining and Metallurgical Institute, Chair of Surveying and Geodesy

Pages 11-15

Levels with self-adjusting sighting axes have lately found ever greater application in mine-surveying practice. Thus, the Khar'kov Mine Surveying Instrument Plant has put the self-adjusting NSM-2 level, intended for class I and II leveling in underground mine surveying and for surface leveling, into series production.

Automatic adjustment of the sighting axis to a horizontal position in the level is ensured by a lens compensator located in front of the objective tube. Because of the trapezoidal manner in which one of the lenses of the compensator is suspended on steel threads, when the tube is inclined the horizontal line of sight is refracted and the point image remains on a horizontal hair of the grid. The guaranteed limits of compensator functioning with satisfactory image quality are $\pm 2'$. The guaranteed precision of automatic adjustment of the line of sight to the horizontal position is $\pm 1''$. A detailed description of the compensator mechanism is given in the article by A.V. Meshcheryakov [1].

In order to obtain data for evaluating the accuracy ensured by the NSM-2 level and the maintenance of compensator adjustment and to determine the convenience of working with the level under subterranean conditions, traverses with a total length of more than 9 km were laid out in the production areas of the "Ukraina" Mine of the Kommunarskugol' Trust. In order to analyze the results obtained in this test preliminary calculations were made of the possible mean square error per kilometer of traverse.

It is known that leveling with the NSM-2 level involves errors which depend on a number of factors. Prime among these is nonparallelism of the sighting axis and the the compensator axis (angle i). The magnitude of angle

Table 1

Determination of Error in Adjustment of Compensator Line of Sight

Series I

a	Δ_1	d_1	b	Δ_2	d_2
93,379	— 0,0046		75,646	— 0,0155	
		+ 0,006			+ 0,002
93,373	+ 0,0014		75,644	— 0,0135	
93,369	+ 0,0054		75,647	— 0,0165	
		— 0,003			+ 0,003
93,372	+ 0,0024		75,644	— 0,0135	
93,379	— 0,0046		75,647	— 0,0165	
		+ 0,002			+ 0,002
93,377	— 0,0026		75,645	— 0,0145	
93,375	— 0,0006		75,632	— 0,0015	
		0,000			+ 0,007
93,375	— 0,0006		75,625	+ 0,0155	
93,375	— 0,0006		75,689	+ 0,0455	
		+ 0,005			— 0,005
93,370	+ 0,0044		75,590	+ 0,0405	
Среднее 93,3744 (1)			75,6305		
		$m_{x_1} = 0',33$			

1) Mean.

Series II

a	Δ_1	d_1	b	Δ_2	d_2
95,104	+ 0,0132		77,915	— 0,0101	
		— 0,004			— 0,003
95,108	— 0,0092		77,918	— 0,0176	
95,142	— 0,0248		77,911	— 0,0096	
		— 0,004			— 0,004
95,138	— 0,0208		77,915	— 0,0136	
96,138	— 0,0208		77,908	— 0,0066	
		— 0,007			— 0,002
95,131	— 0,0179		77,910	— 0,0086	
95,135	— 0,0178		77,869	— 0,0324	
		— 0,003			— 0,002
95,138	— 0,0208		77,871	— 0,0304	
95,068	— 0,0492		77,902	— 0,0006	
		— 0,002			— 0,007
95,070	— 0,0470		77,895	— 0,0064	
95,1172			77,9014		
		$m_{x_{II}} = 0',56$			

1) The results obtained are similar to those of A.V. Meshchyakov's investigation.

Table 1
Continued

Series III

a	Δ_1	d_1	b	Δ_2	d_2
95,106	— 0,0002		77,997	+ 0,0057	
		— 0,004			— 0,005
95,110	— 0,0042		77,992	+ 0,0107	
95,102	+ 0,0038		77,993	+ 0,0097	
		+ 0,000			+ 0,006
95,102	— 0,0038		77,987	+ 0,0157	
95,108	— 0,0022		77,995	+ 0,0077	
		+ 0,005			— 0,002
95,103	+ 0,0028		77,997	+ 0,0057	
95,106	— 0,0002		77,955	— 0,0423	
		+ 0,002			+ 0,005
95,104	+ 0,0018		77,950	— 0,0373	
95,107	— 0,0012		77,991	+ 0,0117	
		— 0,003			+ 0,001
95,110	— 0,0042		77,990	+ 0,0127	
95,1058			77,9127		
		$m_{z_{III}} = 0''.26$			

i in NSM-2 level No. 211 was determined by two-run leveling [2]. It was established from the results of six runs that i = 10,6".

Since the leveling was conducted from a central point under our conditions (the permissible deviation was no more than 1 m), the error in determining the overage at the stations resulting from angle i was insignificant.

The reading of the rod has a great influence on the magnitude of the error in determining the overage.

The main sources of error in rod reading are errors in sighting m_s and inaccuracies in adjusting the line of sight to the horizontal position m_c.

It is known that

6·S

$$m_s = \frac{100''}{\rho'' v} l,$$

where v is the magnification of the objective and l is the length of the sighting beam.

In the case in question the sighting beam is 40 m long and m_s thus equals 0.6 mm.

The accuracy of the adjustment of the sighting line to the horizontal position was investigated by the method proposed by A.V. Meshcheryakov (Table 1).

It is clear from the data of the three series of observations that the error in adjusting the compensator line of sight, in angular terms, is m_c =

= 0,36". With the length of the sighting beam l = 40 m, this error can be found in linear terms from the formula

К·с

$$m_u = \frac{0'',38}{\rho''} l = 0{,}07 \text{ мм}.$$

Consequently, the mean square error in reading the rod is

в·s

$$m_в = \pm \sqrt{m_в^2 + m_u^2} = \pm 0{,}61 \text{ мм}.$$

Taking into account the mean error in rod division, which was found to be $m_д$ = 0,20 mm by comparing two 1.5 m two-sided rods, the error in rod reading for one sighting, while reading from one hair, is

взг·гг
р·д

$$m_{вг} = \pm \sqrt{m_в^2 + m_р^2} = \pm 0{,}64 \text{ мм};$$

the error at the stations is

ст·st

$$m_{ст} = \pm m_{вг} \sqrt{2} = \pm 0{,}90 \text{ мм};$$

the error per km of traverse is

$$m_{км} = \pm m_{ст} \sqrt{\frac{1000}{80}} = \pm 3{,}2 \text{ мм}.$$

All sources of accidental error were not considered in calculating the mean error for a 1 km traverse. Since their influence can be regarded as negligible under our conditions, the errors caused by these deficiencies were disregarded.

Turning to an analysis of the results of subterranean testing of the level, it must be noted that the work was complicated by flooding of the production areas, continual haulage, and considerable ventilation. The level traverses laid out in the production areas consisted of three links (patterns). There was a total of 123 stations. The leveling was carried out in accordance with the class I program [3], from a central point, with a maximum sighting-beam length of 50 m and a minimum of 10 m. For a control, traverses were laid out in the forward and back directions (Table 2).

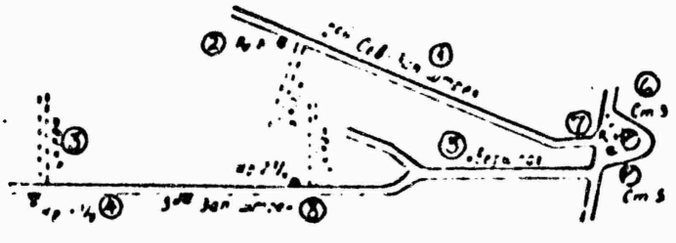

Diagram of class I level traverses
1) 2nd northwestern drift; 2) RpB; 3) inclination; 4) Rp2 z/u; 5) crosscut; 6) station; 7) Rp4; 8) 3rd western drift.

The mean square error per km of traverse, calculated from the differences among the overages /4/ obtained in the forward and back traverses, turned out to be equal to

$$m_{км} = \pm \sqrt{\left[\frac{d^2}{2L}\right] : n} \quad \pm 5{,}0 \text{ мм},$$

where d is the difference between the overages of the forward and back traverses, L is the length

Table 2

Results of Industrial Tests in the Ukraina Mine

1 Наименование ходов	2 Длина хода, км	3 Колич. станций	4 Невязка в ходе, м факт./доп.	5 Фактическая ошибка, мм: 6 на 1 км хода	7 на 1 станцию	8 Превышения	9 Время, затраченное на прокладывание ходов, час
10 Квершлаг гор. 290 от Rp1 до Rp2 з/у	2,96	43	−0,002 / ±0,135	±1,2	±0,3	+11,765 −11,767	5
11 3-й зап. откаточ. штрек от Rp3 з/у до Rp1 з/у	3,32	37	−0,019 / ±0,148	±10,3	+3,1	+6,093 −6,112	5,5
12 2-ой сев.-зап. откаточ. штрек от Rp4 до Rp Б	2,90	43	−0,015 / ±0,135	±8,8	±2,1	+7,536 −7,521	5

1) Designation of traverse; 2) length of traverse, km; 3) number of stations; 4) discrepancy in traverse, m, actual/permissible; 5) actual error, mm; 6) per km of traverse; 7) per station; 8) overages; 9) time expended in laying out traverses, hr; 10) crosscut through mountain 290 from Rp4 to Rp2 z/u; 11) 3rd western haulage drift, from Rp3 z/u to Rp4 z/u; 12) 2nd northwestern haulage drift, from Rp4 to RpB.

of the links between bench marks, and n is the number of links.

The actual mean error was somewhat larger than preliminarily calculated, but considerably less than the permissible value. The permissible relative error per km of traverses in class I leveling must not exceed ±15 mm [3].

Proceeding from the results of the work performed, it may be assumed that the NSM-2 level ensures accuracy of leveling class I, despite a number of unfavorable factors influencing the results of work under subterranean conditions.

The work performed under the conditions of the Ukraina Mine confirms that the wires on which the compensator lens is suspended and their mount have a sufficient margin of strength. The author also used this level to lay out class III level traverses more than 21 km long on the surface. This work was conjoined with transportation of the level over a distance of more than 1500 km by railroad and motor vehicle.

The time expended in the subterranean leveling indicates a rather high labor productivity, which to a considerable extent is ensured by the automatic adjustment of the line of sight and by the device which permits accu-

rate sighting of the objective of the level on the rod without application of the clamping screw. The level is simple in construction, light, and convenient to work with. As for shortcomings, it is possible to note only the narrow working range of the compensator.

Bibliography

1. A.V. Meshcheryakov, Geodeziya i kartografiya /Geodesy and Cartography/, No. 6, 1958.

2. Instruktsiya po nivelirovaniyu I, II, III, IV klassov /Instructions for Class I, II, III, and IV Leveling/, 1959.

3. Tekhnicheskaya instruktsiya po proizvodstvu marksheyderskikh rabot /Technical Instructions for the Conduct of Mine Survey Work/, 1959.

4. A.S. Chebotarev, Geodeziya /Geodesy/, Ch. II, Geodezizdat, 1949.

Manuscript submitted 3 January 1963

DRILLING WITH CAST CORE BITS

By M.A. Chopikashvili, Northern Caucasian Mining and Metallurgical Institute, Chair of Professional Training in Mining

Pages 16-21

In order to achieve high technical-economic indices in the shot drilling of hard rocks it is expedient to employ forced regimes, i.e., to work at high specific pressures and high drill speeds. It is not possible to work under these regimes with the usual bits, because of the rapid longitudinal wearing of the bits at high specific pressures, which decreases the pass time. At peripheral bit-rotation velocities of more than 1.2 m/sec the shot disrupts the feeding of the face in the case of direct washing.

It was long ago noted that when the wall thickness of core bits is increased the resistance of the shot to the face increases and the longitudinal wear decreases [1-4]. This makes it possible to have long passes and to employ forced operating regimes. However, because of the insufficient number of investigations confirming the economic feasibility of thin-walled bits, they have still not found practical application.

In order to determine the dependence of drilling speed on wall thickness and quality of bit material, laboratory and industrial test were conducted. The laboratory investigations were carried out on a drill stand at the Northern Caucasian Mining and Metallurgical Institute, while the industrial tests were performed at the Zverevo GRP of the Volga-Don Geological Administration and the Sadon GRP of the "Sevkavtsvetmetrazvedka" Trust. The laboratory stand was equipped with two drilling machines, a ZIF-300 and a PBS-2T, and the necessary measuring equipment.

The drilling was conducted on a dibasic metamorphic rock of class X drilling-resistance, with bits with wall thicknesses m = 6-20 mm. Steel chaff shot [drob'-sechka] 3.5 mm in diameter with a hardness of 50 HR_c and a crushing strength of 1200 kg was used. The tests were conducted at a constant drilling speed of 378 rpm. The water consumption amounted to 1-1.5

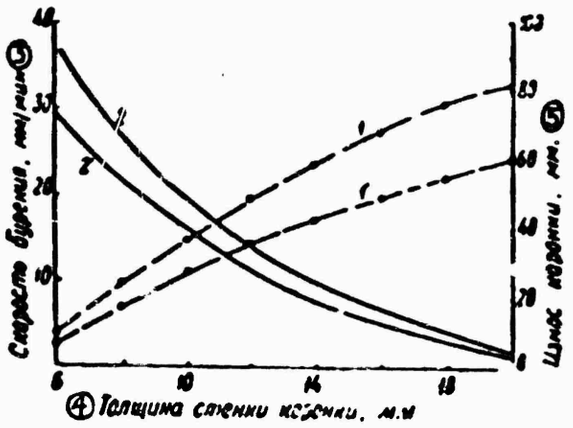

Fig. 1. Dependence of drilling speed 1, 1' and bit wear 2, 2' on wall thickness. 1, 2) at specific pressure of 40 kg/cm^2; 1', 2') at specific pressure of 30 kg/cm^2; 3) drilling speed, m/min; 4) thickness of bit wall, mm; 5) bit wear, mm.

l/min per centimeter of bit diameter. The core bits fabricated from steel 45 had various wall thicknesses. All of the bits had an outside diameter of 91 mm.

As the wall thickness increased within this range, i.e., m = 6-20 mm, an increase in technical drilling speed and a decrease in bit wear at an almost constant shot consumption were observed (Fig. 1). When the wall thickness of the bit was increased from 10 to 14 mm the drilling speed increased by 55% at a specific pressure of 30 kg/cm^2 and by 60% at a specific pressure of 30 kg/cm^2. In addition, the longitudinal wear on the bits decreased by 50 and 53%, respectively.

However, it should be noted that the practical application of thick-walled bits will be limited by the small yield of core sample in drilling. The yield of core sample might have been increased by using small shot, but this results in a larger shot consumption, while increasing the specific pressure in drilling with bits fabricated from comparatively soft steels entails intensive longitudinal bit wear, which in turn leads to a decrease in the drill pass speed (Table 1). This phenomenon is especially aggravated during the drilling of hard and very hard rocks.

It is possible to improve the boring properties of a core bit through the quality of the material used to fabricate it. N.I. Blinov [4] suggests the manufacture of core bits from U125, 30KhGS, 40Kh, and 45 steels heat-treated to a metal hardness of 25-30 HR_c. However, during the drilling of rocks of classes VII and VIII bits of this hardness do not ensure good contact with the shot and a high drilling speed. Therefore, in drilling rocks of average hardness with steel shot it is necessary to use bits having a lower hardness.

Consequently, the rate at which rock is broken up in shot drilling depends unconditionally primarily on the hardness of the bit metal, which in turn must ensure good contact with the shot with minimum wear.

In the drilling of rocks of average hardness with bits of high hardness there is a drop in drilling speed as compared with bits of lower hard-

Table 1

Results of Laboratory Tests on Bits 91 mm in Diameter Fabricated from Various Types of Steel. Drill Speed -- 378 rpm. Water Consumption -- 15 l/min. Magazine Width -- 1/5πD

1) Толщина коронки, мм	2) Площадь торца коронки, см²	3) Материал коронки	4) Удельное давление, кг/см²	5) Скорость бурения, мм/мин	6) Расход коронки, г/пог·м	7) Износ коронки по высоте, мм/пог·м	8) Стоимость коронки на 1 пог. м проходки, коп
10	19,84	9) прокат Ст.45	40	15	730	47	8,03
10	10) То же	То же	60	20	825	53	9,07
10	"	"	80	24	917	59	10,01
14	26,9	"	40	25	527	25	5,8
14	То же	"	60	31	655	31	7,2
14	"	"	80	35	718	34	7,9
10	19,84	11) литье Ст. 45	40	16	715	46	5,0
10	То же	То же	60	19	840	54	5,88
10	"	"	80	24	917	59	6,41
14	26,9	"	40	26	549	26	3,84
14	То же	"	60	30	654	31	4,57
14	"	"	80	34	698	33	4,88
10	19,84	12) прокат из легиров. стали	40	20	450	29	10,7
10	То же	То же	60	30	497	32	11,8
10	"	"	80	37	545	35	12,9
14	26,9	"	40	33	338	16	8,05
14	То же	"	60	43	443	21	10,5
14	"	"	80	50	528	25	12,5
10	19,84	13) литье из легиров. стали	40	21	435	28	4,35
10	То же	То же	60	29	514	33	5,14
10	"	"	80	38	590	36	5,90
14	26,9	"	40	33	359	17	3,59
14	То же	"	60	44	423	20	4,23
14	"	"	80	50	507	24	5,07

1) Bit thickness, mm; 2) area of bit face, cm^2; 3) bit material; 4) specific pressure, kg/cm^2; 5) drilling speed, mm/min; 6) bit consumption, g/running m; 7) longitudinal bit wear, mm/running m; 8) cost of bit per running m of pass, kop; 9) rolled steel 45; 10) the same; 11) cast steel 45; 12) rolled from alloy steel; 13) cast from alloy steel.

ness. In the drilling of hard rocks of class X with a soft bit (of hardness IIR_c = 9) shot-diverting channels will be formed on its face, as a result of which the drilling speed decreases. When the specific pressure is increased this phenomenon is enhanced and leads to rapid bit wear (Fig. 2).

Thus, in most cases rocks are not solid monoliths of the same class and it is impossible to propose a universal core bit having a high wear resistance and ensuring high drilling speed. Successful drilling can be ensured only by correct selection of the regime and the ratio of the hard-

Fig. 2. Shot-diverting channels formed on bit face.

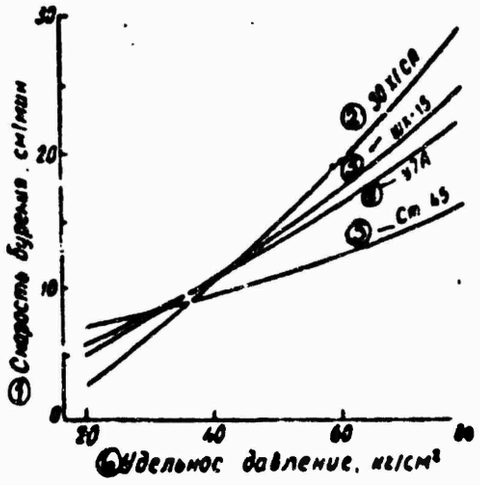

Fig. 3. Dependence of drilling speed on specific pressure in drilling with bits of various types of steel. 1) drilling speed, cm/min; 2) 30KhGSA; 3) ShKh-15; 4) U7A; 5) St-45; 6) specific pressure, kg/cm^2.

nesses of the bit, the shot, and the rock.

In order to find the optimum core-bit material for drilling hard rocks, castings and rolled-tubing bit blanks of the following types were fabricated and tested: St-45, ShKh-15, 30KhGSA, and U7A. Comparison of the results of the tests revealed that the best boring indices were those for the bits fabricated from 30KhGSA alloy steel. Therefore, we also took the results of the laboratory tests and the cost of bits of this steel for technical-economic comparison (see Table 1).

In drilling with bits fabricated from alloy steel the drilling speed rises when the specific pressure is increased. When the specific pressure was reduced to 20 kg/cm^2 the maximum drilling speed was observed for the bits fabricated from softer steel 45.

This, in our opinion, is explained by the fact that during bit drilling

Table 2

Dependence of Cost of Bit Blanks 500 mm Long on Method of Manufacture and Material, with 1 kg of Cast Stock Costing 0.07 rub for Carbon Steel and 0.1 rub for Alloy Steel and 1 kg of Rolled Stock Costing 0.11 rub for Carbon Steel and 0.238 rub for Alloy Steel

(2) Диаметр коронки, мм	(3) Толщина стенки коронки, мм	(4) Вес короночной заготовки, кг	(1) Стоимость, руб. (5) заготовки из прокатной углеродистой стали	(6) заготовки из прокатной легированной стали 30ХГСА	(7) литой короночной заготовки из углеродистой стали	(8) литой короночной заготовки из легирован. стали 30ХГСА
89	10	9,74	1,07	2,32	0,68	0,97
89	14	12,9	1,42	3,03	0,9	1,29
89	15	13,69	1,50	3,25	0,96	1,37
89	16	14,4	1,58	3,43	1,01	1,44
108	10	12,85	1,43	3,10	0,9	1,29
108	14	16,23	1,78	3,86	1,14	1,62
108	15	17,20	1,89	4,10	1,20	1,72
108	16	18,15	2,00	4,34	1,27	1,82

1) Cost, rubles; 2) bit diameter, mm; 3) thickness of bit wall, mm; 4) weight of bit blank, kg; 5) blank of rolled carbon steel; 6) blank of rolled 30KhGSA alloy steel; 7) cast bit blank of carbon steel; 8) cast bit blank of 30KhGSA alloy steel.

involving a high material hardness and a comparatively small specific load slippage of the bit occurs, i.e., there is insufficient contact with the shot.

As can be seen from Table 1, when the specific pressure is increased the drilling speed increases. In addition, bits with a wall thickness of 10 mm fabricated from alloy steel yield an increase in drilling speed as compared with the same bits of steel 45. The increase in drilling speed at a specific pressure of 40 kg/cm^2 amounts to 33%, while at 60 kg/cm^2 it is 50% and at 80 kg/cm^2 it is 54%. As compared with the same bits of carbon steel 45, bits of alloy steel with a wall thickness of 14 mm yield an increase in drilling speed of 32% at a specific pressure of 40 kg/cm^2, 39% at 60 kg/cm^2, and 43% at 80 kg/cm^2.

It must be noted that the drilling speed for cast bits is approximately the same as that for bits of rolled steel of the same types (see Table 1). The maximum drilling speed and minimum longitudinal bit wear were observed for bits fabricated from alloy steel. The cost of bit blanks of rolled 30KhGSA alloy steel is greater than that of rolled blanks of 45 carbon steel by a factor of 2.16. The cost of bits of rolled alloy steel per running m of pass is greater than that of bits of rolled carbon steel (see

Table 3

Results of Industrial Tests on Bits 91 mm in Diameter at Drill Speed of 128 rpm and Specific Pressure of 25-35 kg/cm^2; Bits with a Wall Thickness of 10 mm Were Standard and All Others Were Cast from Steel 45

(1) Толщина стенки коронки, мм	(2) Время чистого бурения, час	(3) Проходка за рейс, м	(4) Механическая скорость бурения, м/час	(5) Износ коронок по высоте, мм/пог·м	(6) Расход коронок, г/пог·м	(7) Площадь торца коронок, см^2	(8) Возможная длина рейса коронки до полного износа, м
(9) Породы VIII категории							
10	4,5	4,3	0,95	32	498	19,84	4,7
12	3,75	4,2	1,12	26	473	23,2	5,17
14	3,23	4,5	1,39	21	444	26,9	6,5
16	2,93	4,25	1,45	18	421	29,9	8,34
18	2,93	4,4	1,50	16	410	32,8	9,38
20	2,69	4,3	1,56	14	390	35,6	10
(10) Породы IX категории							
10	3,0	1,25	0,42	46	716	19,84	2,88
12	5,8	2,9	0,5	37	673	23,2	3,4
14	5,4	3,5	0,65	29	613	26,9	5,16
16	5,06	4,3	0,76	23	540	29,9	6,5
18	2,84	2,5	0,84	19	490	32,8	7,9
25	2,91	2,7	0,93	17	475	35,6	8,8
(11) Породы X категории							
6	5,4	0,216	0,040	170	1490	12,67	0,216
8	5,2	0,380	0,075	110	1425	16,5	1,96
10	5,4	0,700	0,130	90	1400	19,84	1,67
12	5,1	0,766	0,150	76	1380	23,2	1,98
14	4,4	0,928	0,210	65	1370	26,9	2,34
16	4,5	1,08	0,240	56	1312	29,9	2,68
18	4,2	1,172	0,280	49	1290	32,8	3,06
20	3,9	1,247	0,320	40	1120	35,6	3,75

1) Thickness of bit wall, mm; 2) pure drilling time, hr; 3) travel during pass, m; 4) mechanical drilling speed; 5) longitudinal bit wear, mm/running m; 6) bit consumption, g/running m; 7) area of bit face, cm^2; 8) possible length of bit travel to full wear, m; 9) class VIII rocks; 10) class IX rocks; 11) class X rocks.

Table 1). However, the cost of bits of cast alloy steel per running m of travel is less than that of rolled carbon steel, viz: at a bit-wall thickness of 10 mm and a specific pressure of 40 kg/cm^2 it is 84%, while at a wall thickness of 14 mm it is 61%.

The cost of bit blanks fabricated by casting and rolling is given in Table 2. It is clear from the data cited in Table 2 that the cost of 1 kg of stock cast from alloy steel is approximately equal to that of 1 kg of stock rolled from carbon steel. The cost of 1 kg of stock rolled from alloy steel is 2,16 times that of stock rolled from carbon steel. The cost

of 1 kg of cast stock of alloy steel was derived from calculations of the cost of simple cast spare parts fabricated from type 30KhGSA steel [5, 6].

Thus, cast core bits fabricated from alloy steel possess better boring properties and are cheaper than bits of rolled carbon steel.

Industrial tests completely confirmed the regularity of the change in drilling speed and longitudinal bit consumption obtained in the laboratory tests (Table 3).

Conclusions

1. When the wall thickness of a core bit is increased the drilling speed increases and the bit consumption per running meter of travel decreases.

2. Cast core bits prepared from 30KhGSA alloy steel have better boring properties in the drilling of hard rocks than bits fabricated from rolled steel 45 and are cheaper.

Bibliography

1. I.A. Ostroushko, Zaboynyye protsessy i instrumenty pri burenii gornykh porod [Mining Processes and Tools in Rock Drilling], Gosgorteknizdat, p. 226, 1962.

2. S.A. Volkov, Razvedka nedr [Mineral Prospecting], No. 3, 22 (1946).

3. A.N. Kirsanov, Razvedka nedr, No. 6, 19 (1957).

4. N.I. Blinov et al., Razvedka nedr, No. 12, 24 (1958).

5. Spravochnik tsen na materialy i oborudovaniye [Handbook of Material and Equipment Prices], Ch. V, Gosfinizdat, 1959.

6. Preyskurant No. 27-15 optovykh tsen na zapchasti k oborudovaniyu obshchego mashinostroyeniya [Price List No. 27-15 of Wholesale Prices for Spare Parts for General Machine Building Equipment], 1960.

Manuscript submitted 12 January 1963

DETERMINATION OF MINIMUM PERMISSIBLE WIDTH OF WORKING AREAS UNDER THE CONDITIONS OF THE "MEDVEZHIY RUCHEY" PIT

By B.P. Yumatov, V.G. Shitarev, Moscow Institute of Steel and Alloys, Chair of Exploitation of Deposits of Rare and Radioactive Metal Ores

Pages 22-28

Correct determination of the minimum permissible width of working areas, i.e., the least size which ensures normal functioning of loading, drilling, and transport equipment, is of great national-economic importance in the open-pit mining of deposits of useful minerals. Any decrease in the width of the working areas to less than the permissible minimum results in complication of the conduct of mining work on the terraces and disrupts the normal operation of the pit.

In order to improve the organization of mining work on the terraces and the development of transport communications it is neccesary to increase the width of the working areas. However, on the other hand, such an increase leads to a decrease in the angle of inclination of the working edge of the pit and this results in an increase in the volume of material removed and additional expenditures on mining operations.

The following factors are taken into account in the practical planning of the minimum of working areas in pits with railroad transport: width of fall of blasted material, width of transport strip, and, in addition to strip for main transport routes, marginal distance from latter to fall and safety bench to upper edge of underlying terrace. A strip for the parking and passage of auxiliary equipment is also occasionally a component of the minimum working area.

However, in connection with the state of mining operations and the specifications for the excavation of mined material, a rather peculiar determination of the minimum permissible working area has been arbitrarily adopted at the "Medvezhiy Ruchey" Pit. This is explained by the fact that ex-

ıvation of mined material, which is primarily hard, difficult-to-blast ɔck, results in the knocking-off of material from the edge of the terrace d the normal fall width in the pit is consequently rather significant, ɔounting to, calculating from the axis of the first row of holes, three mes or, in individual cases involving very hard rocks, four times the ight of the terrace. The height of the worked terraces in the pit is ta- n to be 15 m, with the exception of the three upper terraces, whose ight is 20 m.

The width of the working areas does not remain constant as mining op- ations progress in the pit, but varies within rather wide limits. The dy- mics of its change during the last few years of pit operations are shown the table, from which it follows that the current working areas have an erage size of 50-60 m. According to the determination cited, this working ea width is less than the permissible minimum, which should be 70-80 m, king into account the employment of two-row hole firing and the presence a strip for the parking and passage of auxiliary equipment, when the rraces are 15 and 20 m high. Widening the existing areas to this size in- lves excavation of an additional stripping volume (approximately 8 million

, which cannot be removed within a short period because of its consider- le size. The performance of mining operations on the working levels of the t is consequently carried out in accordance with arbitrary "instructions r terrace management" worked out at the pit; in these the minimum permis- ble working area width is determined from the disposition of the fall of asted material. The minimum permissible working area width in the mining terraces 15 and 20 m high is 60 and 75 m respectively.

Experience in the performance of mining operations has showed that, ler these conditions, it is expedient to carry out simultaneous blasting several adjacent terraces embracing part of the working zone of the pit. ch blasting methods have found wide application because they make it pos- ble to reduce the idle time of equipment by a factor of 1.5-2, despite drawbacks which exist in this case; on days when blasts are being pre- red and carried out the volume of recovery and excavation work in the pit sharply curtailed.

After a massive blast the loading operations are preceded by the cut- g of a route 12-14 m wide through the blasted material by an excavator; s is for the laying of railroad track and the installation of communica- ns and power lines, which are always removed from the section of the ter- e in the blast zone before the explosion. The loading of the broken-down erial is handled primarily in two excavator blocks 15 to 25 m wide on teen-meter terraces and in three such blocks on twenty-meter terraces. lling work usually starts on a given section of the terrace front during loading of the second block.

Thus, under current conditions the main factor determining the minimum king area width is the width of the fall, which depends on the number of

Dynamics of Change in Width of Working Areas during 1959-1962

① Рабочий горизонт	② Ширина рабочих площадок, м				
	на 1.1.1959	на 1.1.1960	на 1.1.1961	на 1.1.1962	на 1.VII.62
460	70	78	78	70	60
430	71	73	69	67	70
420	59	64	71	60	60
405	54	59	57	60	69
390	49	44	50	75	71
375	37	40	45	55	55
360	49	42	50	52	43
345	28	50	50	55	55
330	32	38	50	46	46
315	43	51	55	46	40
300	60	63	63	--	70

1) Working level; 2) width of working areas, m; 3) on.

rows fired.

The planning assignment and schedule for the progress of mining operations in the pit foresee both expansion of the working areas to 70-80 m and reduction of the fall of blasted material within the next 6-7 years. However, under the conditions of multirow blasting the width of the fall plays an important role in determining the size of the minimum permissible working area even in this case, since the width of the transport strip, with the scheme of routes along the cut described above, and the dimensions of the other components of the working area remain relatively constant.

However, considering the state of mining operations in the pit and the equipment used, the number of rows of holes fired cannot be taken arbitrarily; increasing it results in expanison of the working areas, which can be done only at the expense of the amount of excavation carried out. Furthermore, an increase in the number of rows of holes leads to an increase in fall height, which is limited by the conditions necessary for the safe performance of excavation operations. Under the conditions of the Medvezhiy Ruchey Pit the blasted material agglomerates and when the fall height exceeds the greatest depth to which the excavator can scoop "overhangs" and "lips" are formed; their removal is associated with considerable expenditures of material and labor.

The experience amassed in the use of multiple short-delay blasting in the pit shows that the fall width, measured from the axis of the first row of holes, does not depend on the number of rows fired and is the same as in single-row blasting. The full fall width is thus

p-f (in B_p) y-t
p-f (in m_p) б-v

$$B_p = m_p h_y + a(n-1).$$

where h_y is the height of the terrace in m, m_p is an index equal to the ratio of the width of the fall from the axis of the first row of holes to the height of the terrace, v is the distance separating the rows of holes, in m, and n is the number of rows fired. Figure 1 shows actual fall forms. The most frequently encountered form of fall, produced as a result of normal blasting, is depicted in diagram a. Its characteristic peculiarity is a decrease in the height of the fall relative to the height of the terrace in the section directly adjacent to the massif, as a result of which part of the latter is exposed. The planning and execution of massive blasting takes into account the production of such a reduced fall height, in order to guarantee safe conditions for excavation operations and the most favorable distribution of the blasted material over the width of the fall. The magnitude of the reduction in fall height in this section is characterized by the so-called "edge cave-in," which is the ratio of the height of the exposed part of the terrace to its full height h_t:

$$\eta = \frac{p}{h_y}.$$

On the other hand, this form of fall is characterized by the presence of a discontinuity in the direction of its slope (point C). Formation of the fall whose form is shown in diagram b is possible when the charge in the last row of holes is insufficient in magnitude. As may be seen from these diagrams, the height of the fall at the point of the discontinuity in its slope can be more or less than the height of the massif fall. The fall form depicted in diagram c is a particular case of the first two and is characterized by equality of the height of the fall at its point of inflection and the height of the massif.

The triangular fall form shown in diagram d is not characteristic under the conditions of the Medvezhiy Ruchey Pit and is formed primarily as a result of shortcomings in the planning and execution of multiple blasts. In this case the bottom of the terrace is frequently badly aligned.

Applying the principal of geometric comparison of the volumes of the blocks in the pillar and the fall referred to one running m of front, which was used by Prof. V.V. Rzhevskiy in calculating the parameters of trapezoidal and triangular falls, we may obtain the relationship between the height of the fall and its other parameters (for the fall forms shown in diagrams a and b):

p-f (in H_p)
p-d (in K_p)

$$H_p = \frac{h_y [2K_p A - L(1-\eta)]}{B_p},$$

where A is the width of the blasted block along the pillar, equal to w + v (n - 1) under the conditions of the pit, K_d is the coefficient of rock dis-

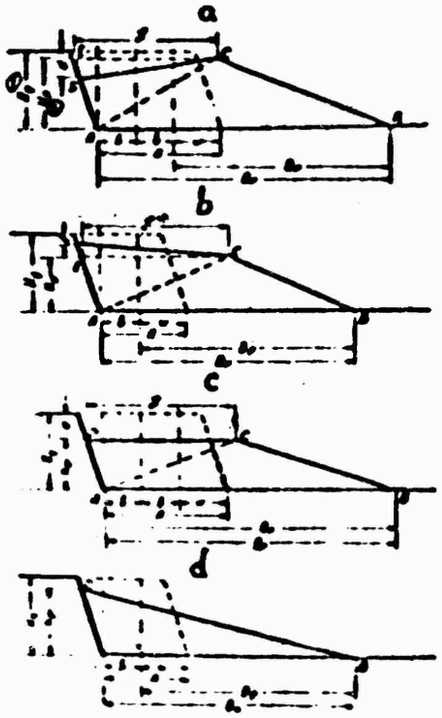

Fig. 1. Main forms of falls of blasted material in pit. 1) t; 2) f.

integration during blasting, and L is the horizontal distance from the point of inflection of the slope of the fall to the position of the slope of the terrace after blasting or its continuation if the height of point C is greater than that of the terrace. Under the conditions of the pit the magnitude of L varies from 20 to 30 m; H_f is the height of the fall at the point of discontinuity in its slope.

A more useful form of formula (1) for practical calculation of the value of H_f is obtained by substituting for B_f and A:

$$\begin{matrix} p=f\ (in\ Hp) \\ y=t \\ p=d\ (in\ K_p) \\ p=f\ (in\ m_p) \end{matrix} \quad \beta=\nu \qquad H_p = h_y \frac{2K_p\left[w+e(n-1)\right]-L(1-\gamma)}{m_p h_y + e(n-1)}. \qquad (2)$$

It must be noted that determination of the height of the fall from formula (2) when using hole charges BB, which are intended for loosening the material to be mined, cannot be carried out for any number of rows of holes, since the fall form shown in diagram a (see Fig. 1) will be maintained as the number of rows of holes increases to the value at which the height H reaches its maximum. When the number of rows of holes is further increased the value of H_f does not rise and the fall acquires the form shown in Fig. 2. It may be assumed that the greatest value of H_f for charges

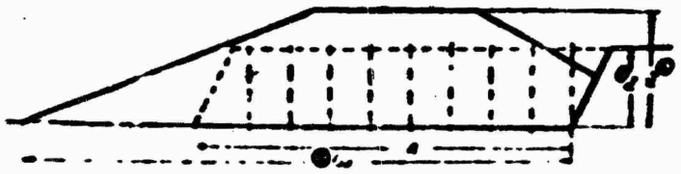

Fig. 2. Diagram of fall form produced on firing of a large number of rows of holes. 1) t; 2) f; 3) v.

BB, intended for loosening the material to be mined, will be $K_d h_t$. The number of rows of holes to which formula (2) will be valid is then determined by the expression

$$\begin{matrix} p = f\,(\text{in } m_p) \\ y = t \\ \theta = v \end{matrix} \qquad p = d\,(\text{in } K_p) \qquad n < \frac{m_p h_y - 2w}{a} + \frac{L(1-\gamma)}{K_p a} + 1.$$

With terrace heights of 15 and 20 m and arbitrary parameters for the multirow hole-arrangement grid (w = 10-12 m, v = 8-9 m) this number is 5-6.

From formula (2) one may determine the maximum permissible number of rows of holes to be fired for safe excavator operation

$$\begin{matrix} \text{доп} = per \\ p\text{-доп} = f.per \end{matrix} \qquad n_{доп} \leqslant h_y \frac{m_p H_{f.доп} + L(1-\gamma) - 2K_p w}{a(2h_y K_p - H_{f.доп})} + 1.$$

where $H_{f.per}$ is the permissible fall height, which is determined by the conditions for safe excavator operation, and should correspond to H_{sc} when the blasted material agglomerates and compacts (where H_{sc} is the greatest depth to which the excavator can scoop). In individual cases, when the mined material is well loosened, the fall height can be increased to 1.3-1.5.

The relationship $n_{per} = f(H_{f.per})$ is expressed by hyperbolae with asymptotes parallel to the coordinate axes and is shown in Fig. 3 for terraces 15 and 20 m high. In addition, the solid lines on the graph express this function for the existing fall width (m_f = 3), while the dash lines indicate a reduction in fall width to the value assumed in the planning assignment (m_f = 2.2). For current conditions and the existing fall width, the maximum number of rows of holes is determined from the operational conditions for EKG-8 excavators on the 20-meter terrace and EKG-4 excavators on the 15-meter terrace, since the latter and SE-3 excavators now predominate on these levels. At values of the permissible fall height corresponding to the greatest depth to which the excavator can scoop, the quantity n_{per}, determined from the graph in Fig. 3, is approximately 2 for both ledges. The full fall

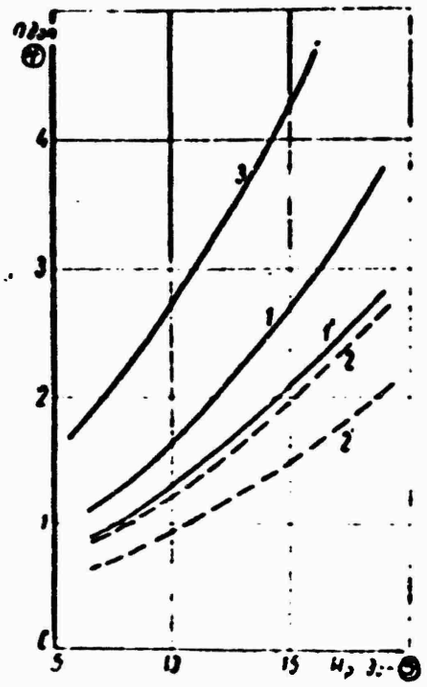

Fig. 3. Variation in permissible number of rows of holes fired n_{per} as a function of fall height $H_{f.per}$. 1 and 1') during multiple hole firing in rope-percussion drilling on terraces 15 and 20 m high, respectively, with m_f = = 3.0; 2 and 2') the same, with m_f = 2.2; 3) during multiple firing of oblique holes on terrace 15 m high, with m_f = 3.0; 4) per; 5) f.per.

width at an index m_f = 3 will be 53-54 m in the loosening of a terrace 15 m high and 69-70 m for a terrace 20 m high, this corresponding to the actual data.

At present, 2- and 3-row hole firing are used for loosening the material to be mined in the pit; the former is of predominant importance (accounting for up to 70-75% of the total volume of mined material), although 3-row blasting has been shown by experience to have certain advantages. The latter yields a higher drilling productivity (by 10-15%), improves the breaking-down of the mined material and thus increases excavator productivity by 8-10%, and increases the volume of mined material per running m of railroad track laid by 25-30%. This is explained by the fact that, in the 3-row blasting of terraces 15 m high, which are the principal component of the working face of the pit, the fall height frequently reaches a value close to that of the height of the terrace and sometimes exceeds it; this complicates operations and reduces the technical-economic indices of the EKG-4 and SE-3 excavators. Three-row blasting is employed primarily in the working of 20-meter terraces, although the fall height frequently exceeds

the greatest depth to which the excavators can scoop in this case.

In calculating the minimum permissible working area width for current conditions, taking into account the disposition of the fall, it is thus necessary to select a 2-row arrangement of vertical holes for rope-percussion drilling, this ensuring economical and safe loading conditions.

As experience has shown, in the drilling of terraces with oblique holes the basic pattern of fall location and form does not change, i.e., it may be assumed that when blocks of identical width are blasted from a pillar with oblique and vertical holes the fall parameters will be approximately identical. Curve 3 in Fig. 3 shows the expression $n_{per} = f(H_{f.per})$ for the use of oblique holes in drilling a 15-meter terrace; with $v = 6$ the permissible number of rows of holes may be assumes to be three. As calculated from these data, the minimum permissible working area width will correspond to that used in practice.

The conditions for loading operations on a terrace should not be further improved by expanding the working areas to more than the established sizes (60 and 75 m), which would result in an increase in the current stripping coefficient, but by reducing the fall width. The first industrial experiments performed on the use of controlled multiple blasting indicate the feasibility of this. When the index m_f is reduced to 2.2, as is provided for by the planning assignment, and EKG-8 excavators, with which it is proposed to carry out up to 75-80% of all loading of the mined material, are used, the permissible number of holes fired in working 15-meter terraces will also be equal to or approximately equal to two. In this case the full fall width will be 40-42 m. Such a reduction in fall width will make it possible to locate the transport strip on areas of this size in addition to the fall of blasted material; this may result in a significant improvement in the technical-economic indices of all aspects of the technological operations of the pit.

Conclusions

1. The calculation method presented herein makes it possible to determine the parameters of the fall of mined material and the rational number of rows of holes to be fired in multiple short-delay blasting.

2. The investigation carried out showed that, taking into account the current state of mining operations and the equipment used in the "Medvezhiy Ruchey" Pit, it is expedient to adopt 2-row hole firing as a basis; this ensures normal and economical conditions for the loading of the mined material and for pit operations without any substantial change in the current stripping coefficient.

3. It is recommended that the pit exploitation conditions be improved and the indices of the loading and transport equipment be increased both by

expanding the working areas to the minimum permissible size and by reducing the fall of blasted material by improving multiple short-delay blasting.

Manuscript submitted 23 February 1963.

USE OF ELECTRON MICROSCOPY IN STUDYING THE REACTION OF REAGENTS WITH INEVITABLE PULP IONS AND MINERAL SURFACES

By S.I. Pol'kin, A.M. Komelev, Ye.P. Petukhov, Moscow Institute of Steel and Alloys, Chair of Rare-Metal Ore Beneficiation

Pages 29-34

During the last few years electron diffraction methods have come to be employed ever more frequently in studying the structure of surface formations in metals and minerals. Electron microscopy is also widely used in studying the structure of metals and alloys. Great interest inh es in the application of these methods to the study of flotation processes in order to investigate the change which occurs in the structure and physicochemical properties of the surfaces of floatable minerals under the influence of reagents, water, atmospheric oxygen, and other agents.

Electron diffraction methods have been used in studying the change in the surface of galena under the action of flotation reagents [1], the fixation on sulfides of xanthogenate or xanthogenic acid, and the structure of copper xanthogenates on sphalerite surfaces [2, 3]. However, use of this method for studying the mechanism by which reagents react with mineral surfaces is limited by the fact that the latter must be smooth and minerals not having perfact cleavage must first be ground, polished, and etched. This undoubtedly changes the structure and surface properties of the minerals and can lead to incorrect conclusions about the character of the reaction of reagents with them. We know of no examples of the use of the electron microscope for studying flotation processes, but the electron photomicrographs of grains of martite and limonite (not treated with reagents) obtained at Mekhanobr' [4] made it possible to establish clearly the sharp difference in the microreliefs of the surfaces of these minerals. The rough surface of limonite has a specific surface 65 times as large as that of martite and this obviously determines the adsorptive capacity of the minerals.

We used electron microscopy for studying the interaction of sodium

oleate with inevitable pulp ions and the surfaces of certain minerals. In developing this method we attempted to make it possible to study the products of the reactions of various types of reagents with pulp ions and mineral surfaces and the reactions within the various classes of reagents themselves.

Flotation reagents can react with mineral surfaces and inevitable pulp ions either simultaneously or selectively, initially with the pulp cations and anions and then (the remaining portion of the reagent or the products of its reaction) with the mineral surfaces. In addition, after the reagents react with the pulp ions their initial properties change and their action on the flotation process may be intensified or greatly weakened. Thus, anion collectors of the fatty acid and fatty acid soap types undergo a sharp attenuation of their collecting properties when they react with cations of polyvalent metals, but during the formation of, for example, the oleates of iron, aluminum, and certain other metals the collecting properties of oleic acid are completely suppressed.

During the flotation of oxidized rare-metal ores the pulp contains up to 100-200 mg/l or more of soluble salts and hydroxides of calcium, magnesium, iron, aluminum, copper, lead, and others. This reaction with oleic acid, at various pH's, promotes the formation of neutral metal salts, basic oleates, or adsorption compounds of hydrated metal oxides and oleic acid $Me(OH)_n \cdot mOlH$ in the pulp. As was shown by earlier investigations [5], despite the fact that each of these compounds contains free unreacting oleic acid they have different collecting properties. The method used in the investigations made it possible to study certain physicochemical and flotation properties of oleates of calcium, iron, and tin.

This article describes the use of electron microscopy for studying the structure and certain of the physicochemical properties of oleates of calcium, magnesium, and iron in order to use the data obtained for determining the structure and physicochemical properties of the products of reactions of reagents with mineral surfaces.

In studying the products of the reaction of sodium oleate with "inevitable" pulp ions oleates of calcium, magnesium, and iron were obtained by a well-known method [5] at various pulp pH's. We first used the electron microscope to take standard photographs of the initial products ($CaCl_2$, $MgCl_2$, $FeCl_3$, $Ca(OH)_2$, $Mg(OH)_2$, and $Fe(OH)_3$), as well as sodium oleate and oleic acid, with which photographs of the products of the reaction between sodium oleate and the salts and hydrates indicated were later compared. The metal oleates obtained were thoroughly washed with water to free them from unreacting metal ions and residues of oleic acid.

The samples for electron-microscopic study were prepared in the following manner. A suspension of sodium oleate highly diluted in aviation gasoline (preliminarily purified of mechanical impurities; the sodium oleate

content was 100 mg/ℓ) was placed in a quantity of one or two drops on a collodion film formed on the object-stage grid; after evaporation of the gasoline the film was washed several times with pure gasoline. Several samples of gasoline without sodium oleate were prepared at the same time, in order to establish that gasoline does not react with a collodion film.

Samples of calcium, magnesium, and iron oleates were prepared in the same manner as for the sodium oleate, but distilled water was used instead of gasoline. The form of the crystals of $CaCl_2$, $MgCl_2$, $FeCl_3$, $Ca(OH)_2$, $Mg(OH)_2$, and $Fe(OH)_3$ was studied in samples prepared by the usual method [6]. Figure 1 shows photographs of sodium oleate taken at different magnifications in neutral and alkaline aqueous media. As may be seen, sodium oleate consists of fibrous particles 1.5-2 μ long and on the order of 0.1 thick.

In addition to the large particles there are smaller ones interconnected in various directions to form a dense network of fibers. The fibrous and ribbon-like structure of lithium and sodium fatty-acid soaps was earlier shown by a number of investigators [7-9]. It was established in this work that the shape and size of the fibers depends on the cooling temperature of the soap and on the various impurities in the fatty acids.

In our experiments the sodium oleate was prepared from oleic acid and chemically pure sodium hydroxide. For comparison, Fig. 2 shows photographs of the salt calcium chloride (magnesium chloride crystals have an analagous form) and hydrated magnesium oxide (hydrated calcium oxide has an analagous form). Crystals of the chlorine salts and hydroxides of calcium, magnesium, and iron have been rather well studied [10]. They are easily distinguishable in shape and size from crystals of the oleates of sodium, calcium, magnesium, et al.

Calcium oleate obtained from sodiun oleate and calcium chloride is a white, finely agglomerated precipitate. Its crystals take the form of square or elongated plates up to 1 μ long and 0.1 to 0.5 μ thick. They frequently form accumulations reminiscent of druse and, more rarely, individual long plates which reach 3-7 μ (Fig. 3a).

The size and shape of calcium oleate crystals undergo large changes with time from the instant of their formation. While only single crystals of calcium oleate are observed 2.5 hr after reaction (see Fig. 3b) and the entire remaining product is apparently a thin suspension of the acidic calcium soap, after 10-12 hr the entire mass has crystallized and after 30-50 hr the calcium oleate plate reaches 5-7 μ in length (see Fig. 3a).

In contrast to the other oleates which we studied, calcium oleate exhibits an alternation of light and dark strips across the crystal reminiscent in character of polysynthetic twins (plagioclase type). We did not determine the nature of these strips.

Magnesium oleate, like the calcium oleate, was obtained from sodium oleate and magnesium chloride. The mass obtained was a yellowish, easily dispersed powder. In contrast to calcium oleates, a characteristic peculiarity of magnesium oleate crystals is their tapering at an angle of approximately 60^0 (occasionally 90^0; Fig. 4). These crystals are plates 1.5-2 μ or more long and 0.2-0.4 μ thick. In contrast to the growth of calcium oleate crystals with time, magnesium oleate crystals are detected in the solution 0.5 hr after reaction (see Fig. 4b). After 10-12 hr the crystals attained a size of 2-3 μ and after 1.5-2 days they can be seen with the naked eye (see Fig. 4a).

Influence of pH of medium on formation of calcium and magnesium oleates. In order to obtain the calcium and magnesium oleates we used sodium oleate obtained from chemically pure oleic acid and calcium and magnesium chlorides in the form of distilled-water solutions (100 mg/ℓ) at a definite pH set up by HCl or NaOH; the solutions were combined and one day after the beginning of the reaction samples were selected under the electron microscope.

In an acid medium at a pH of 2 sodium oleate is almost completely converted to oleic acid, drops of which appear in the electron photomicrograph as large and small round black spots sharply differentiated from the fibrous structure of sodium oleate. Free particles of calcium chloride persist under these conditions. It may be judged from the results that no calcium oleate is formed at a pH of 2 and previously formed calcium oleate is decomposed.

In order to verify this conclusion we performed the following experiment. White, finely agglomerated calcium oleate powder was placed in water at a pH of 2 and drops of oleic acid were detected on the surface of the water after 18-20 hr; this proves that calcium oleate is decomposed to oleic acid and calcium chloride in water at a pH of 2.

The formation of calcium oleate starts at a pH of 4-4.5 and is especially intensive and a pH of 6. In the first case small square crystals ranging from 0.5 to 1 μ in size are formed in the first case while in the second case they reach a size of 2-3 μ. In a weakly alkaline medium (pH 8) calcium oleate is maintained in the form of small crystals; drops of oleic acid and significant quantities of calcium hydroxide and sodium oleate are also observed.

When the alkalinity of the solution is raised the content of sodium oleate and calcium hydroxide increases and the quantity of calcium oleate crystals decreases; the latter are completely absent at a pH of 12. In order to check this, the calcium oleate obtained in powder form was placed in water at pH 12. Sodium oleate and hydrated calcium oxide were detected after twenty-four hours (Fig. 5), i.e., the calcium oleate crystals were completely decomposed.

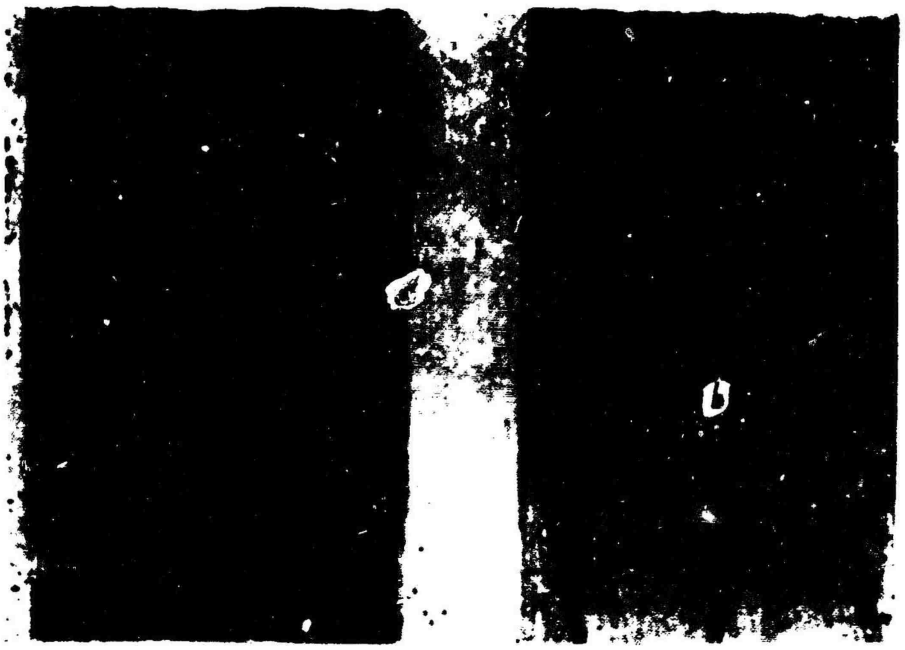

Fig. 1. Electron photomicrograph of sodium oleate. a) x3000; b) x9000.

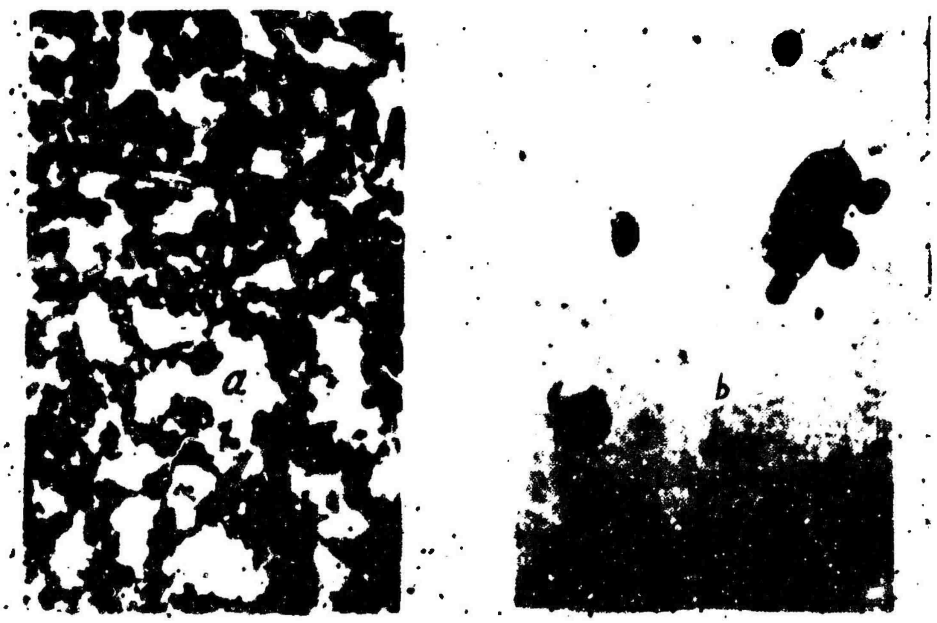

Fig. 2. Electron photomicrograph of calcium chloride (a) and magnesium hydroxide (b), x3000.

Fig. 3. Electron photomicrograph of calcium oleate taken at pH 6-7 (a) and 2.5 hr (b) and 12 hr (c) after beginning of reaction, x6000.

Fig. 4. Electron photomicrograph of magnesium oleate at pH 6.0, x6000 (a) and 0.5 hr after beginning of reaction, x9000 (b).

Fig. 5. Electron photomicrograph of calcium oleate after mixing in water at pH 12.

Fig. 6. Electron photomicrograph of calcium oleate taken during reaction of OlNa with calcite filtrate, x7500.

Fig. 7. Electron photomicrograph of calcite after treatment with sodium oleate for 0.5 hr, x6000 (a) and x18,000 (b).

Fig. 8. Calcite not treated with sodium oleate, x6000.

Fig. 9. Electron photomicrograph of calcite after treatment with sodium oleate for 50-70 hr, x6000 (a) and x 12,000 (b).

In contrast to calcium oleate, the formation of magnesium oleate crystals occurs at a pH of more than 5.0 (see Fig. 4). In an acid medium magnesium oleate is decomposed with the liberation of oleic acid and in an alkaline medium magnesium chloride is converted to hydrated magnesium oxide, while sodium oleate retains its fibrous structure.

Reaction of sodium oleate with a calcite surface. Finely ground calcite powder was agitated for 30 min in distilled water and a sample of the pulp was then removed and filtered. Sodium oleate was added to the filtrate and powdered calcite (1000 mg/l) and, after agitation, samples were removed for electron-microscopic study of the products of the reaction of sodium oleate with the mineral surfaces and the calcium ions which pass over in the filtrate.

After agitation for 30 min the pH of the water changed from 5.5-6 to 7.5-7.8, which indicates that part of the calcite passed into solution and that the calcium oleate crystals consequently must have been formed in the liquid phase.

Figure 6 shows an electron photomicrograph of the product of the reaction between the filtered portion of the solution and sodium oleate. It may be seen from this figure that the main product is calcium oleate, whose crystal form is identical to that of the calcium oleate obtained from $CaCl_2$ and sodium oleate.

Varying the time for which the calcite powder remaining on the filter is in contact with the sodium oleate has a considerable influence on the character of the bonding of the reagent to the minerals and the formation of calcium oleate and the manner in which it crystalizes on the mineral surfaces. Calcite particles treated with sodium oleate for 30 min (Fig. 7) do not have sharp projections, all points are rounded off, and formation of calcium oleate crystals starts only in individual sections; a large part of the mineral surface is apparently covered by uncrystalized calcium oleate and an oleic acid soap or oleic acid.

For comparison, Fig. 8 shows an electron photomicrograph of a calcite grain not treated with sodium oleate.

When the time for which the calcite is in contact with the reagent is increased to 1.5-3 days the entire surface of the particle is covered with calcium oleate crystals (Fig. 9), the quantity and growth of which increases continuously as a result of the increase in adsorption of sodium oleate from the solution, but may also be due to the calcium oleate formed in the pulp during the reaction of OlNa with the calcium ions.

Conclusions

1. The use of the electron microscope for studying flotation processes makes it possible to explain the structure and a number the physicochemical

properties of the products of the reaction of reagents with inevitable pulp ions and mineral surfaces.

2. As determined under the electron microscope, the external form and structure of sodium oleate and oleic acid, calcium and magnesium, the hydroxides of these metals, and particles of the minerals calcite and dolomite differ sharply from those of their reaction products.

3. The time for which the collector is in contact with calcite and dolomite surfaces and the soluble salts and hydroxides of calcium and magnesium has a considerable influence on the character of their bonding and on their crystal form.

A contact time close to that used under industrial conditions (10-30 min) ensures durable bonding of the collector to the calcite and, obviously, initial formation of monosubstituted calcium oleate bonded to the crystal lattice of the mineral, on which layers of the calcium oleic acid soap or oleic acid are retained. The rounded form of the projections on the mineral is characteristic of forms covered butyrous reagents.

When the contact time is increased to two or three days the monosubstituted layer of calcium oleate formed is converted to disubstitution products and begins to crystallize. When centers of crystallization are formed the rate at which the calcium oleate crystals grow increases at the expense of the oleate and calcium ions in the mineral and the liquid phase of the pulp. A single crystal is formed on further growth, small grains of calcite or calcium oleate (1-2 μ) growing in it. No free oleic acid is detected in the pulp in this case.

4. Study of the influence of pulp pH showed that calcium oleates are not formed in acid media at pH's of less than 3; when calcium oleate is placed in such a medium it is completely decomposed, with the formation of calcium chloride and small drops of oleic acid. Formation of calcium oleate starts at a pH of 4 or more. Marked decomposition sets in at pH 10, but at a pH of more than 12 calcium oleate is wholly decomposed, with the formation of sodium oleate and hydrated calcium oxide; this completely confirms the data obtained by other methods [5].

5. The crystal forms of calcium oleates obtained from calcium chloride (and hydrated calcium oxide) and sodium oleate in the pulp mass is identical to the crystal form and character of the bonding of the components of calcium oleates formed on calcite surfaces, while the time of contact with the collector has approximately the same influence on them.

6. Further improvement of electron microscopy as a method of investigating flotation processes in combination with other methods (radioactive isotopes, infrared spectroscopy, chemical processes) will, in the regular verification of theoretical investigations by direct flotation experiments, promote deeper study of the theoretical bases of flotation processes and an improvement of ore-processing technology.

Bibliography

1. S.V. Zatsepin, A.S. Ivoylov, Sb. nauchnykh trudov Irgiredmeta [Collection of Scientific Papers of the Irkutsk State Scientific Research and Design Institute for the Rare Metals Industry], No. 7, p. 82, Metallurgizdat, 1958.

2. H. Hagihohara, Uchikoshin, Nature, 174, 1 (1954).

3. R.I. Sato, Mining Inst. Japan, 70, 19 (1954).

4. N.Kh. Vladovskiy, S.I. Gorlovskiy, Obogashcheniye rud [Ore Beneficiation], No. 6, 15 (1961).

5. S.I. Pol'kin, Flotatsiya rud redkikh metallov i olova [Flotation of Rare-Metal and Tin Ores], Gosgortekhizdat, 1960.

6. Elektronnaya mikroskopiya [Electron Microscopy], Edited by Acad. A.A. Lebedev, 1954.

7. A.A. Trapeznikov, G.G. Shcheglov, I.I. Astakhov, Izv. AN SSSR [News of the Academy of Sciences USSR], ser. fiz. [Physics Series], 23, 6, 777 (1959).

8. A.A. Trapeznikov, G.G. Shcheglov, Kolloidnyy zhurnal [Colloid Journal], 1, 104 (1962).

9. V.V. Sinitsyn, Ye.V. Aleyeva, B.N. Kartinin, Kolloidnyy zhurnal, 1, 75 (1962).

10. Yu.V. Karyakin, Chistyye khimicheskiye reaktivy [Pure Chemical Reagents], Goskhimizdat, 1947.

Manuscript submitted 24 September 1962

INVESTIGATION OF THE MECHANISM OF THE REACTION OF THE CATION COLLECTOR ANP WITH APATITE AND CALCITE BY RADIOMETRY AND INFRARED SPECTROSCOPY

By S.F. Kuz'kin, V.I. Solnyshkin, Chen Yu-Lung, Moscow Institute of Steel and Alloys, Chair of Useful-Mineral Enrichment

Pages 35-39

Radiometric analysis methods and the study of the infrared spectra of powders of the natural minerals apatite and calcite treated with the appropriate flotation reagents are being used to obtain new information about the mechanism of cation-collector adsorption [1, 2]. We investigated laurylamine and ANP, a mixture of primary amines, as collectors. The mineral grains were selected by the sedimentation method, in which the fraction with a particle size of less than 5μ was isolated. The powder was treated at an ANP concentration of 666 mg/l. The contact time was 30 min from the instant at which the flotation reagents were introduced; the suspension was intensively agitated. After treatment the mineral grains were filtered. A suspension was prepared from the remaining powder and the mixture of primary amines was introduced into it. After filtration the mineral grains were precipitated from the aqueous medium onto fluorite substrate plates and the water was then carefully evaporated in a heater at 60-70°. In all of the experiments the thickness of the layer was 1.6 mg/cm^2.

The infrared spectra were photographed in a IKS-12 spectrometer with a halite prism, point by point (Fig. 1). The spectral curve of the mixture of primary amines was obtained with the liquid layer between the two fluorite plates 0.16 mm thick. The gap was regulated by contour spacers of copper and aluminum foils.

Figure 1 shows the absorption spectrum of the mixture of primary amines (ANP). Ten main absorption bands are observed in the region from 2 to 11 , these corresponding to the composition of the technical primary-amine mixture. According to the data in the literature, a limited number of bands is found for amines in the main region [3], those for absorption

by the primary amines themselves being the 1456, 1593, and 3310 cm^{-1} bands, which identify deformation oscillations of CH_3-N and NH_2 groups and valence oscillations of NH. The remaining bands are those of the amino groups and amino acids present in the technical product as amino acid hydrochlorides. It was impossible to interpret the 1018, 1161, and 1377 cm^{-1} bands. Judging from their intensity, they may be attributed to insignificant quantities of foreign impurities. The band at 1506 cm^{-1} is the second amide band, that at 1704 cm^{-1} is the band for the unionized acidic carbonyl groups of the amino acid hydrochlorides, and those at 1990 and 2655 cm^{-1} are the hydrochloride absorption bands; in addition, a complicated spectrum of bands located near one another appears in the region from 2500 to 3000 cm^{-1}. They merge into a wide high-intensity band, to which the absorption band for the amino group valence oscillations. Finally, the 3950 cm^{-1} band is the first harmonic of the absorption at 1990 cm^{-1} [3].

The infrared spectrum of ANP makes it possible to classify this flotation reagent as a mixture of primary amine and amino acid hydrochlorides. As a result of the acid form of the amines, the carboxyl groups of the amino acids are unionized and their reactive capacity is sharply reduced. This situation gives every reason for comparing the experimental results obtained with tagged laurylamine and the technical flotation reagent ANP.

The infrared spectra of apatite and calcite were obtained during comparison of the spectra of untreated I_0 and treated I samples in order to isolate the absorption bands of the minerals. After apatite is treated (see Fig. 1b) bands appear which indicate the presence in the diffusion layer of adsorbed NH groups (3485 cm^{-1}). It is possible to attribute the absorption at 1443 and 2923 cm^{-1} to valence oscillations of CH_2 groups. There is a band at 1541 cm^{-1} which relates to deformation oscillations of the ionized group NH_3^+, being located between 1485 and 1550 cm^{-1} for amino compounds [3]. The presence of CH_2, NH, and NH_3^+ absorption bands in the spectrum indicates that during the treatment of apatite with ANP not only the amino acids and primary amines in molecular form, but also their ions $RCOOHNH_3^+$ and RNH_3^+ are adsorbed on the surfaces; the ions enter into the equilibrium reaction

$$RNH_2Cl \rightleftarrows RNH_3^+ + Cl^-.$$

The 1704 and 1780 cm^{-1} absorption bands indicate that the carboxyl groups of the amino acids remain unionized during adsorption on apatite.

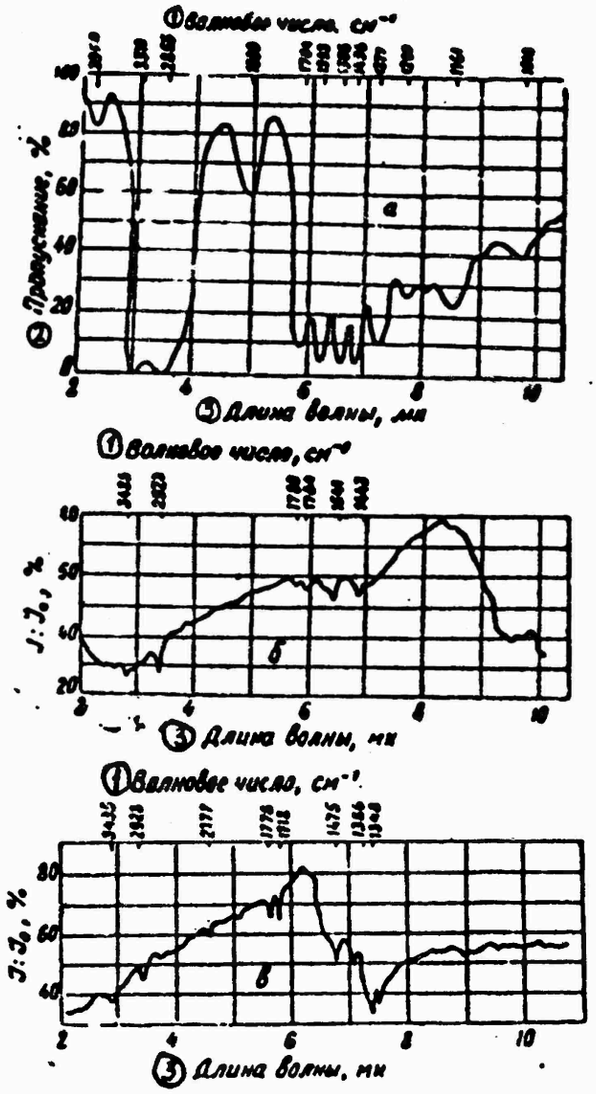

Fig. 1. Spectral curves for technical cation collector ANP (a), apatite (b), and calcite (c). b and c) after treatment with 5 kg/t of ANP; 1) wave number, cm^{-1}; 2) pass, %; 3) wavelength, μ.

Considering the mineralogical structure of apatite, it must be noted that only two hydroxyls, one acidic formed with a phosphorus atom and one basic formed with a calcium atom, can operate here. Their positioning close to one another leads to both hydroxyls being in an equilibrium ionic state, since the neutralization reaction does not go to completion, because of the fixed positions of the phosphorus and calcium atoms in the mineral lattice. In this case we should observe one of the forms of ion-exchange adsorption encountered for ion-exchange resins and related to physical adsorption [4]. The cations of amines and amino acids play a large role in the formation of the monomolecular layer on apatite, but only in the presence of the chlorine ion, which neutralizes the influence of the calcium atoms in the surface

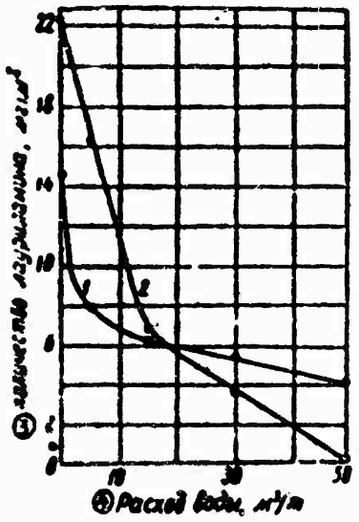

Fig. 2. Curves for desorption of tagged laurylamine from mineral grain surface. 1) calcite; 2) apatite; 3) quantity of laurylamine, mg/m^2; 4) water consumption, m^3/t.

layer. In other words, fixation of the flotation reagent in a monolayer requires the presence of an acid medium, which is created in the diffusion layer by the hydrochloric acid chemically bonded to the amino groups of the molecules. The presence of chlorine ions suppresses ionization of the carboxyl radicals of the amino acids.

Washing the mineral with water leads to full desorption of the flotation reagent from its surface and restoration of the original calcium and phosphorus atoms. This has been confirmed by experiments on the desorption of tagged laurylamine from the surfaces of calcite and apatite grains. Figure 2 shows curves for the desorption of the amine after washing with distilled water. With a water consumption of 50 mg/l, the laurylamine is completely removed from the apatite surface. One might call this type of adsorption hydrolytic adsorption, in contrast to ion exchange, in which the adsorption-desorption process may involve ions of molecules and of complexes of chemical compounds. In the mineral which we studied the exchange occurs between ions of the flotation reagents and water molecules.

The spectrum of calcite (see Fig. 1c) indicates hydrocarbon and amine absorption. The 2923 and 1475 cm^{-1} bands are those of the NH of the primary amines and of CH_2 [3]. The absorption at 1712, 1778, and 3435 cm^{-1} denotes unionized carboxyl groups, while the latter band is the first harmonic of the absorption at 1712 cm^{-1}. All three absorption bands are associated with the presence of the carbonyl group C-O in the chemical formula of the molecules. The 1348 cm^{-1} band also relates to the carbonyl group, being located between 1200 and 1350 cm^{-1}, but it is absent for the corresponding hydro-

carbons and is not caused by valence oscillations of the C-O radical in organic compounds [3].

Since ANP is a hydrochloride of amines and amino acids, the equilibrium reaction

$$RNH_3Cl \rightleftarrows RNH_2 + HCl.$$

is observed in aqueous media. Free acid can act on calcite to form chlorcarbonate:

$$CaCO_3 + 2HCl \rightleftarrows CaCl_2 + H_2CO_3;$$

$$H_2CO_3 \rightleftarrows 2H^+ + CO_3^{2-};$$

$$2HCl + CO_3^{2-} \rightleftarrows CO_2Cl_2 + H_2O.$$

An ion of a complex compound which yields an absorption band at 1348 cm^{-1} is formed when the chlorcarbonate acts on the amines and amino acids in the diffusion layer:

$$RNH_3^+ + CO_2Cl_2 \rightleftarrows (RNH_3Cl_2)CO_2^+.$$

Formation of a compound of the type $[Ca(RNH_3)]_nCl_2$, which is chemosorbically bonded to the calcium atoms in the crystal lattice of the mineral, is possible in the monomolecular layer. This is confirmed by the results of the experiments with the tagged laurylamine (see Fig. 2). Desorption from the surface of calcite goes rapidly at first, but falls sharply at water consumption of 5 ml/g and no more reagent is washed off. In washing at 50 ml/g 27.4 % of the chemosorbed laurylamine remains on the calcite, while it is completely desorbed from the surface of apatite, despite the fact that the quantity of flotation reagent fixed on apatite during adsorption is considerably greater.

The flotation experiments showed that apatite is floated on addition of ANP to the pulp, while calcite has almost no flotation activity at all [1]. Summarizing the data obtained, it must be noted that RNH_3^+ ions exhibit flotation activity during the flotation of apatite and calcite with the cation collector ANP. The amines and amino acids, being in the form of molecules and ions of complex compounds, do not promote adhesion of air sacs to the particles.

The amines and amino acids form strong hydrogen bonds between their amino groups and the solvent molecules. When the surface potential rises the flotation reagent passes from the molecular into the ionic form as we approach the boundary between the particle and sac phases, forming polymolecular layers (see structural formula below). These layers are the main factor regulating the strength and elasticity of the adhesion of the air sacs to the mineral grains [5]. In molecular form the flotation reagent does

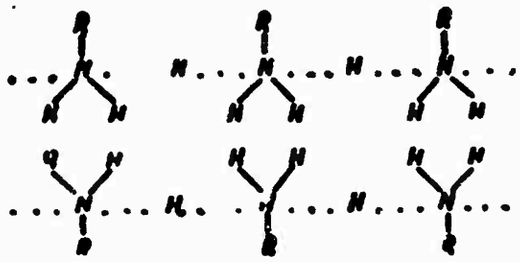

participate directly in the formation of the mineral-sac aggregate, but sets up the requisite concentration of the ionic form.

Conclusions

1. The spectrum of the cation collector ANP, which is a mixture of primary amines and amino acids in hydrochloride form, was photographed by infrared spectroscopy.

2. Physical adsorption of ANP in the form of molecules and ions of amines and amino acids occurs in the diffusion layer on the surface of apatite.

3. The diffusion layer formed by ANP on the surface of calcite consists of complex compounds of amines and amino acids with carbonic acid; ANP is also chemosorbed in the form of complex salts of the amino groups.

4. These infrared spectra and radiometry show that the cations of the primary amines and amino acids exhibit flotation activity during the flotation of apatite and calcite with ANP, forming polymolecular layers in the diffusion layer by hydrogen bonding; the molecular form of flotation reagents does not participate directly in the formation of this layer, but is necessary as the source of ions when the surface potential at the particle-sac boundary rises.

Bibliography

1. S.F. Kuz'kin, Chen Yu-Lung, Izv. VUZ. Tsvetnaya metallurgiya /News of Higher Educational Institutions, Nonferrous Metallurgy/, No. 1, 42 (1963).

2. I.N. Plaksin, V.I. Solnyshkin, DAN SSSR /Proceedings of the Academy of Sciences USSR/, Vol. 139, No. 4, 936 (1961); Vol. 144, No. 1, 186 (1962).

3. L. Bellami, Infrakrasnyye spektry molekul /Infrared Spectra of Molecules/, IL, 1957.

4. K.M. Saldadze, Ionoobmennyye vysokomolekulyarnyye soyedineniya /High-Molecular-Weight Ion-Exchange Compounds/, Goskhimizdat, 1958.

5. V.I. Saldadze, Nauchnyye soobshcheniya IGD AN SSSR /Scientific Reports of the Mining Institute of the Academy of Sciences USSR/, No. 6, 117 (1960).

Manuscript submitted 8 October 1962

STATE OF THE DOUBLE ELECTRIC LAYER OF TANTALITE AND CERTAIN CONCOMITANT MINERALS DURING FLOTATION

By T.B. Nayfonov, S.I. Pol'kin, E.Sh. Shafeyev, Moscow Institute of Steel and Alloys, Chair of Rare-Mineral Ore Beneficiation

Pages 40-46

The work of Soviet investigators [1,2] has established that the surface charge on minerals affects the adsorption of surface-active organic substances, this being one of the main factors governing the floatability of minerals. The electrical state of the surface of mineral particles is characterized by thermodynamic and, particularly, electrokinetic potentials.

Soviet and foreign investigators have recently paid considerable attention to electroosmosis methods and the potential which the course of this process involves in studying the peculiarities of the mechanism by which flotation reagents react with the surfaces of various minerals and in developing improved technological schemes for the flotation of various ores.

This article describes a study of the character of the change in this potential under various flotation conditions, which was conducted in order to explain certain questions about the interaction of flotation reagents with tantalite-columbite, garnet (almandine), and tourmaline, and measurement of the adsorption potential of oleic acid on tantalite surfaces.

The elctrokinetic potential was measured by electroosmosis with a Gortikov device [3-5], being calculated from the equation [6]

$$\zeta = \frac{4\pi\eta}{D} \cdot \frac{V\varkappa}{i}, \text{ mV,}$$

where η is the viscosity in poises, Γ is the dielectric constant of water, V is the minute volume of liquid transferred in ml/min, i is the current in ma, and $\varkappa$ is the specific electrical conductivity of the solution in $ohm^{-1} \cdot cm^{-1}$.

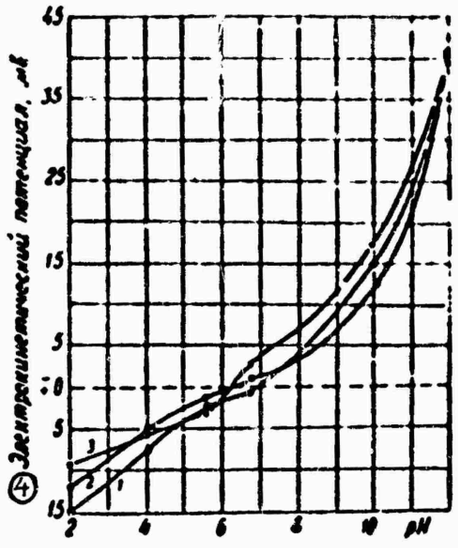

Fig. 1. Influence of pH of medium on variation in electrokinetic potential of minerals. 1) Tantalite; 2) tourmaline; 3) garnet; 4) electrokinetic potential, mv.

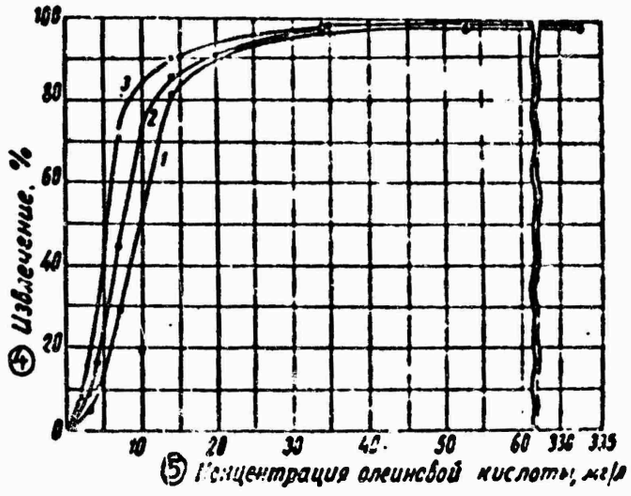

Fig. 2. Extraction of minerals as a function of oleic acid concentration (pH = 6.5). 1) Tantalite; 2) tourmaline; 3) garnet; 4) extraction, %; 5) oleic acid concentration, mg/l.

This research was carried out with monomineral powders 0.043 mm in size. Figure 1 shows the results of experiments on the variation in the electrokinetic potential of minerals as a function of the pH of the medium. The pH was varied by introducing hydrochloric acid and an alkali (KOH) into the distilled water. It must be noted that the pH of the medium has a considerable effect on the value of the electrokinetic potential.

Table 1

Variation in ζ-Potential and Electrokinetic Index as a Function of pH of Medium

pH среды	Электрокинетический потенциал, мв						Электрокинетический показатель, мв		
	Концентрация олеиновой кислоты, мг/л								
	0			33,3					
	танталит	турмалин	гранат	танталит	турмалин	гранат	танталит	турмалин	гранат
2	+15	+11,8	+9,3	+15,5	+12,2	+9,7	+0,5	+0,4	+0,4
4	+7,5	+4,8	+5,5	+7,8	+5,2	+5,8	+0,3	+0,4	+0,3
5,5	+2,4	+1,4	+1,8	+2,3	+1,9	+1,3	−0,1	−0,4	−0,5
6,7	+0,5	−1,5	−3,0	−2,4	−6,5	−7,8	−1,9	−5,0	−4,8
8,0	−5,0	−5,5	−7,0	−8,5	−11,5	−12,0	−3,5	−6,0	−5,0
10,0	−15,0	−12,5	−17,5	−16,0	−13,5	−18,5	−1,0	−1,0	−1,0
12,0	−39,0	−42,5	−40,0	−39,0	−42,5	−40,0	0,0	0,0	0,0

1) Electrokinetic potential, mv; 2) oleic acid concentration; 3) pH of medium; 4) tantalite; 5) tourmaline; 6) garnet; 7) electrokinetic index, mv.

When the pH is increased to 6-7 the isoelectric point of the surface is reached and a further increase in the pH of the medium causes a sharp rise in the negative value of the ζ-potential of all the minerals investigated. In this case the change in the electrokinetic potentials of tantalite, tourmaline, and garnet probably results from adsorption of the potential-governing ions H^+ and OH^-, which have a substantial effect on the surface properties of the minerals investigated. Table 1 gives data which show the variation of the electrokinetic potential and electrokinetic index of oleic acid adsorption for the minerals investigated as a function of the pH of the medium in the presence of an oleic acid emulsion. The oleic acid concentration is taken as optimum, corresponding to the maximum extraction of the minerals investigated (Fig. 2).

As has been shown in certain works [7, 8], the electrokinetic index* enables us to determine the influence of individual reagents simultaneously present in a pulp on the flotation properties of minerals.

It is clear from the data in Fig. 1 and Table 1 that the adsorbing ions H^+ and OH^- exert a powerful action on the state of the surface properties of minerals in acid and alkaline media, reducing the adsorption of oleic acid. The maximum electrokinetic index obviously corresponds to the greatest oleic acid adsorption and the best mineral floatability. This has been confirmed

*The electrokinetic index of reagent adsorption is the difference between the electrokinetic potentials of the mineral surface in the presence and in the absence of the reagent [7].

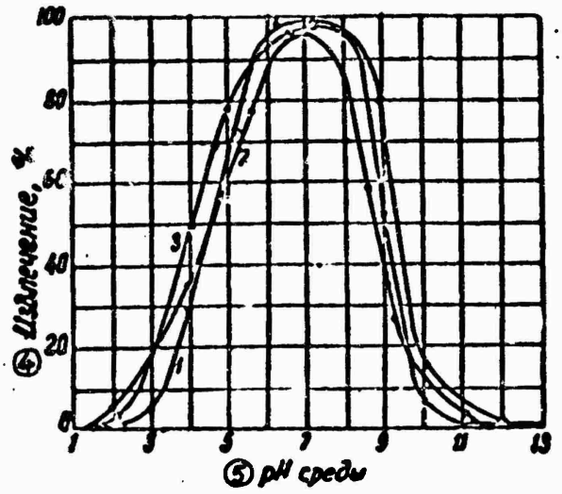

Fig. 3. Influence of pH of medium on extraction of minerals at an oleic acid concentration of 33.3 mg/ℓ. 1) Tantalite; 2) tourmaline; 3) garnet; 4) extraction, %; 5) pH of medium.

by the flotation experiments depicted in Fig. 3. It is clear from the results produced by varying the electrokinetic index that the ξ-potential of mineral surfaces remains virtually unchanged at high and low medium pH's in the presence of oleic acid. At these pH values the values of the electrokinetic index lie within the limits of the error in measurement.

However, it must be kept in mind that strongly acidic and strongly alkaline media promote the passage of polyvalent metal cations into solution from the surface of minerals; these bond part of the oleic acid into low-solubility oleates, reducing the concentration of oleic acid in the pulp [9]. Furthermore, a change in surface charge may take place as a result of partial dissolution of the minerals and exposure at their surface of positively charged metal cations or anions of their lattices. It is consequently possible to assume that there is virtually no adsorption of oleic acid on mineral surfaces in very acid or alkaline media.

The absence of flotation of the minerals investigated in acid media is obviously a result of the fact [10] that the oleic acid is in molecular form and its fixation on the mineral surfaces is hampered. The increase in the negative value of the ξ-potential in an alkaline medium may be associated with intensive surface hydration, which causes the absence of flotation. As was noted in References [7, 8], in this case the best conditions for oleic acid adsorption are created at or near the isoelectric point, i.e., when the surface charge is at its minimum. The maximum mineral extraction at various medium pH's corresponds to the minimum absolute value of the isoelectric potential or the maximum value of the electrokinetic index of oleic acid adsorption. The increase in the ξ-potential of the surface of the minerals investigated in the presence of oleic acid in slightly acid and alkaline media

Table 2

Variation in Electrokinetic Potential and Electrokinetic Index as a Function of Oleic Acid Consumption

1) Расход олеиновой кислоты		4) Электрокинетический потенциал, мв			8) Электрокинетический показатель, мв		
2) г/т	3) мг/л	танталит 5)	турмалин 6)	гранат 7)	танталит	турмалин	гранат
0	0	+0,5	—1,5	—3,0	0	0	0
100	6,66	—0,8	—2,0	—3,8	—1,3	—0,5	—0,8
200	13,32	—1,5	—4,5	—5,4	—2,0	—3,0	—2,4
500	33,3	—2,4	—6,5	—7,8	—2,9	—5,0	—4,8
1000	66,6	—3,5	—9,4	—9,9	—4,0	—7,9	—6,8
3000	199,8	—6,8	—12,7	—13,2	—7,3	—11,2	—10,2
5000	333,3	—11,5	—15,8	—15,6	—12,0	—14,3	—12,6

1) Oleic acid consumption; 2) g/t; 3) mg/l; 4) electrokinetic potential, mv; 5) tantalite; 6) tourmaline; 7) garnet; 8) electrokinetic index, mv.

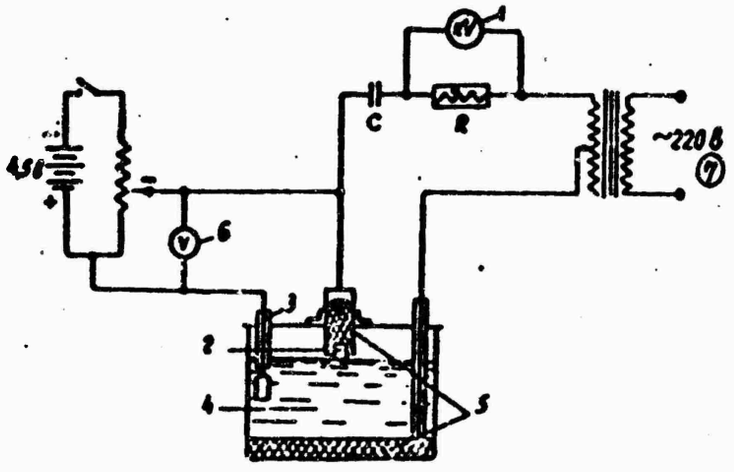

Fig. 4. Basic scheme of determination of relative capacitance of double layer. 1) Cathode voltmeter; 2) tantalite electrode; 3) platinum electrode; 4) medium in which capacitance is measured; 5) mercury; 6) 3v voltmeter; 7) v.

probably results from chemosorption of this reagent on the mineral particles. At high and low medium pH's the flotation capacities of the minerals in the presence of oleic acid will be determined by adsortpion of the potential-governing ions H^+ and OH^-.

We studied the problem of the reaction of this collector with the surface of tantalite, tourmaline, and garnet from the standpoint of the change

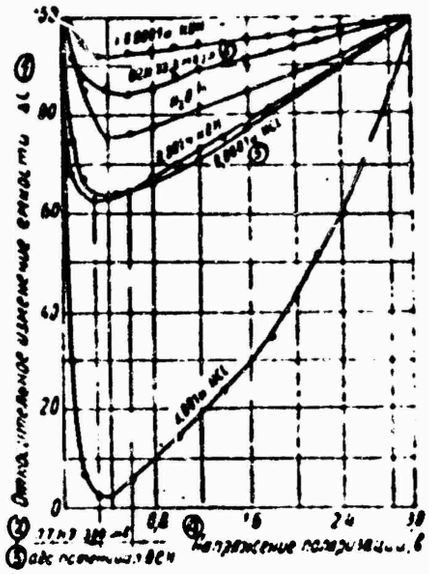

Fig. 5. Variation in capacitance of double layer as a function of polarization voltage. 1) Relative change in capacitance, ΔC; 2) potential of null-charge point, 300 mv; 3) ads. potential of oleic acid; 4) polarization voltage, v; 5) N; 6) mg/l.

in the eletrokinetic potential as a function of the oleic acid concentration. Table 2 shows the influence of the oleic acid concentration on the variation in the ζ-potential and the electrokinetic index. When the initial oleic acid concentration is increased the absolute value of the negative electrokinetic potential increases for all of the minerals investigated. The increase in negative electrokinetic potential in these minerals is obviously associated with the chemical adsorption of oleic acid. This assumption is in accord with the conclusions of a number of investigators. Thus, analysis of certain published works shows that the value of the electrokinetic potential of oxidized minerals increases with a rise in the concentration of an anion collector. These conclusions were reached by O'Connor for scheelite under the action of sodium oleate [11], by M.A. Eygeles and A.V. Mash'yanova for ilmenite under the action of tallol [12], by O'Connor and Buchanau for cassiterite [13], etc.

The potential of the null-charge point on a tantalite surface and the adsorption potential of oleic acid may be determined experimentally, by several methods [2, 14]: from the position of the maximum of the electrocapillary curve, from the position of the minimum of the curve for the capacitance of the double electric layer of the electrode as a function of the potential of the mineral surface, from the variation in the magnitude of the wetting angle as a function of the surface potential, etc.

In our experiments we determined the null-charge point from the position

of the minimum of the curve for the capacitance of the double electric layer of the electrode in dilute solutions. The measurements were made in accordance with a somewhat modified version of the scheme described in References [2, 15]. The basic circuit is shown in Fig. 4. Instead of a null-indicator we employed a cathode voltmeter of the A4-M2 type, which makes it possible to measure the capacitance of the double electric layer directly. The data obtained in the experiments are shown in Fig. 5.

As a result of measurement with an alternating voltage of the capacitance of the double electric layer as a function of the polarization voltage we determined the potential of the null-charge point on a tantalite surface, which equals 400 mv in distilled water. In measuring the capacitance of the double electric layer in dilute solutions of HCl and KOH we observed a displacement of the null-charge point toward more positive surface potentials. In the presence of an oleic acid emulsion the null-charge point is displaced in the negative direction. From the magnitude of this displacement we determined the adsorption potential V_{ex} of oleic acid on tantalite surfaces, which equals -300 mv at an oleic acid concentration of 33.3 mg/l. Further increasing the oleic acid concentration does not affect the value established for its adsorption potential. This adsorption-potential value probably corresponds to the optimum oleic acid concentration in tantalite flotation, which corresponds to the maximum occupation of the tantalite surface by oleic acid anions under the conditions used. This assumption is confirmed by the flotation experiments, in which it was shown that tantalite extraction depends on the oleic acid concentration (see Fig. 5).

The quantity of oleic acid fixed on the tantalite surfaces was tentatively calculated from the magnitude of the adsorption potential. The area occupied by one oleic acid molecule is assumed to be 20 A^2, the surface area of the electrode is equal to twice its geometric surface $0.25 \times 2 = 0.5$ cm^2, and the dipole moment of oleic acid is $1.6 \cdot 10^{-18}$ esu. According to the Helmholtz equation [6], the change in potential during the adsorption of oleic acid anions is

теор - theor

$$V_{теор} = 4\pi n\mu,$$

where n is the number of oleic acid molecules per cm^2 of mineral surface and μ is the dipole moment of oleic acid. Substituting numerical values into this formula we obtain $V_{theor} = 1500$ mv. Comparing the value of the potential difference calculated from the Helmholtz equation with the experimental value of the adsorption potential and assuming in first approximation that the number of oleic acid anions is proportional to the change in the surface potential [16], we can determine what portion of the tantalite surface is occupied by oleate ions:

экс - ex

$$\Delta s = \frac{V_{эксп}}{V_{теор}} 100 = \frac{300}{1500} 100 = 20\% .$$

This enables us to assume that oleic acid is not fixed on the entire surface of tantalite, but only on portions of it amounting to approximately 20% of the ideal monolayer. This was shown earlier for cassiterite by S.I. Pol'kin, who used the radiographic method [9].

Conclusions

1. Tantalite, tourmaline, and garnet are floated well by oleic acid at pH's of 6-8, where their surface has its maximum electrokinetic index during adsorption of the collector on the minerals.

2. The increase in the negative ξ-potential in the presence of oleic acid makes it possible to assume that the latter is fixed chemosorbically on the surfaces of the minerals investigated.

3. From the change in the capacitance of the double electric layer we determined the null-charge point in distilled water at various concentrations of HCL and KOH and calculated the adsorption potential of oleic acid on tantalite surfaces.

Bibliography

1. B.N. Kabanov, A.V. Gorodetskaya, Electrokapillyarnyye yavleniya i smachivayemost' metallov [Electrocapillary Phenomena and the Wettability of Metals], Zh. fiz. khimii [Journal of Physical Chemistry], 1933.

2. A.N. Frumkin, V.S. Bagotskiy, Z.A. Nofa, B.N. Kabanov, Kinetika elektrodnykh protsessov [Kinetics of Electrode Processes], Izd-vo MGU [Publi : House of Moscow State University], 1952.

3. V.M. Gortikov, Kolloidnyy zhurnal [Colloid Journal], Vol. 1, No. 3, 1935.

4. O.N. Grigorov, I.F. Karpova, Z.P. Koz'mina, D.A. Fridrikhsberg, Rukovodstvo k prakticheskim zanyatiyam po kolloidnoy khimii [Handbook of Practical Information on Colloid Chemistry], Izd-vo LGU [Publishing House of Leningrad State University], 1955.

5. P.M. Soloshenkin, S.A. Tikhonov, S.M. Yasyukevich, Metallurgiya tsvetnykh metallov, sb. nauchnykh trudov Mintsvetmetzolota [Metallurgy of the Nonferrous Metals, Collection of the Scientific Papers of the Ministry of the Nonferrous Metals and Gold Industry], No. 31, 1958.

6. I.I. Zhukov, Kolloidnaya khimiya [Colloid Chemistry], Izd-vo LGU, 1949.

7. B.M. Borisov, DAN SSSR [Proceedings of the Academy of Sciences USSR], Vol. XCIX, No. 3, 1959.

8. V.I. Klassen, V.A. Mokrousov, Vvedeniye v teoriyu flotatsii [Introduc-

tion to Flotation Theory/, Gosgortekhizdat, 1959.

9. S.I. Pol'kin, Flotatsiya rud redkikh metallov i olova /Flotation of Rare-Metal and Tin Ores/, Gosgortekhizdat, 1960.

10. V.G. Danilov, Nauchno-informatsionnyy byulleten' in-ta Mekhanobr /Scientific-Information Bulletin of the Mekhanobr Institute/, No. 3, 40 (1948).

11. D.I. O'Connor, Electrokinetic properties and surface reaction of sheelite, Chem. Dept. Univ. of Melbourne, Australia, 1956.

12. M.A. Eygeles, A.V. Mash'yanova, Flotatsiya silikatov i okislov /Flotation of Silicates and Oxides/, Gosgeoltekhizdat, 1961.

13. D.I. O'Connor, A.S. Buchanau, Electrokinetic properties of cassiterite, Austral. J. Chem., Vol. 66, No. 3, 278 (1954).

14. V.V. Skorchelleti, Teoreticheskaya elektrokhimiya /Theoretical Electrochemistry/, Goskhimizdat, 1959.

15. V.L. Kheyfets, D.K. Avdeyev, L.S. Reyshakhrit, Praktikum po teoreticheskoy elektrokhimii /Handbook of Theoretical Electrochemistry/, Izd-vo LGU, 1954.

16. E.K. Raydil, Khimiya poverkhnostnykh yavleniy /Chemistry of Surface Phenomena/, ONTI, Khimteoret, 1936.

Manuscript submitted 20 February 1963

NAPTHAZOLETHIONES AS POTENTIAL COLLECTORS FOR OXIDE AND SULFIDE MINERALS OF LEAD AND COPPER

By G.N. Tyurenkov, I.A. Kakovskiy, Ural Polytechnic Institute, Chair of Precious-Metal Metallurgy

Pages 47-50

Benzimidazole-2-thione or, as it is called, "Captax" is quite often used as the collector in the flotation of sulfide and oxide minerals of lead and copper /1-4/. Reference /5/ shows the possibility of floating galena, serussite, and malachite with substituted derivatives of benzimidazole-2-thione having the structure

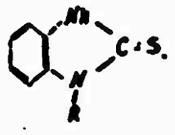

where R is an alkyl or aryl radical.

In this connection it is of interest to synthesize analagous derivatives of the naphthalene series and to study their physicochemical and flotation properties in comparison with those of benzene derivatives, since replacement of the C_6H_5 group by the $C_{10}H_7$ group in heteropolar organic reagents is accompanied by a significant increase in chemical activity, i.e., the ability to yield low-solubility salts with ions of heavy nonferrous metals (by a factor of approximately 2), and ensures a large wetting angle when covering mineral surfaces, i.e., sets up the prerequisites for an increase in their flotation acitvity.

Naphthazolethiones, having the general formula

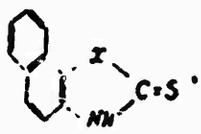

where X is O, NH, or S, were synthesized from the corresponding naphthylamines and carbon bisulfide in a pyridine medium by heating at 80° for 4-6 hr. The compounds obtained, high-melting colorless crystalline substances, were poorly soluble in water, but highly soluble in alkalies, ammonia, pyridine, and dioxane and somewhat less soluble in alcohol. The table shows certain data on the properties of these compounds with various X (their solubility in water was determined by extrapolation of data on their solubility in water-alcohol mixtures). For evaluation of their relative chemical activities the activity products of the silver salts of the corresponding benzene derivatives and the ratio of the activity products of the silver salts of benzene and naphthol derivatives are given [6].

Naphthazolethiones, like the derivatives of the benzene series, form low-solubility compounds with ions of heavy nonferrous metals (bismuth, copper, silver, lead, palladium, et al.); these exhibit high melting temperatures and are insoluble in the majority of organic solvents (acetone, benzene, alcohol, chloroform, and ether). The results of chemical analysis indicate the stoichiometric composition of these compounds. Thus, the composition found for the silver salt of naphth-/2,1/-imidazole-2-thione was (in %) 7.86 N and 31.35 Ag, while the calculated composition was 8.16 N and 31.43 Ag.

A number of works, [7-13] for example, cite data on the fact that benzazolethiones can be used in analytic chemistry as precipitation reagents for heavy metal ions, as well as in hydrometallurgy. Comparing the magnitudes of the activity products of the silver salts of benzazolethiones and naphthazolethiones (approximately the same ratio will be maintained for salts of other metals [6]) and taking into account the stoichiometric composition of the latter, we may conclude that the use of naphthazolethiones for gravimetric analysis in analytic chemistry is more expedient than the use of their benzene analogues.

It also follows from the material presented that naphthazolethiones are typical anionic sulfhydryl reagents with a high chemical activity and a rather hydrophobic radical; this furnished a basis for testing them as collection reagents in flotation. Since the flotation properties of mercaptobenzothiazole ("Captax") have been rather well studied, it was decided to conduct comparative tests on benzazolethiones and naphthazolethiones with different structures under identical conditions.

The experimental conditions were flotation of an artificial mixture of quartz and galena, malachite or serussite (the latter without preliminary sulfidization in a "Nigrizoloto" device with a chamber for a 100-g batch at a solid:liquid ratio of 1:3. The mixture contained 90% quartz (-0.208 mm) and 10% floatable mineral (-0.147 mm). The collector was added to the pulp in portions (0.2 - 0.3 - 0.5 - 0.5 - 0.5...g·mole/t) at intervals of 2, 2, 5, 5, 5... min, in the form of the corresponding sodium salt. The frothing agent in the flotation of galena was isoamyl alcohol (40 g/t), while that in the flotation of the oxide minerals was pine oil (100 g/t). The results of

BLANK PAGE

Properties of Naphthazolethiones

(1) X в формуле нафт-[2,1]-азол-2-тиона	(2) Температура плавления, °С	(3) Брутто формула	(4) Содержание азота, %		(7) Растворимость в воде, г · моль/л	(8) Произведение активности серебряной соли		
			(5) найдено	(6) вычислено		(9) нафтазол-2-тиона	(10) бензазол-2-тиона	(11) отношение этих величин
NH	>300	$C_{11}H_8N_2S$	14,34	13,99	$4 \cdot 10^{-5}$	$3,1 \cdot 10^{-22}$	$1,6 \cdot 10^{-20}$	52
O	241–243	$C_{11}H_7NOS$	7,03	6,96	$5 \cdot 10^{-5}$	$5,3 \cdot 10^{-22}$	$2,0 \cdot 10^{-19}$	377
S	219–221	$C_{11}H_7NS_2$	6,28	6,45	$1 \cdot 10^{-5}$	$2,0 \cdot 10^{-22}$	$2,4 \cdot 10^{-20}$	120

1) X in formula of naphth-/2,1/-azole-2-thione; 2) melting temperature, °C; 3) empirical formula; 4) nitrogen content, %; 5) observed; 6) calculated; 7) solubility in water, g·mole/l; 8) activity product of silver salt; 9) naphthazole-2-thione; 10) benzazole-2-thione; k) ratio of these quantities.

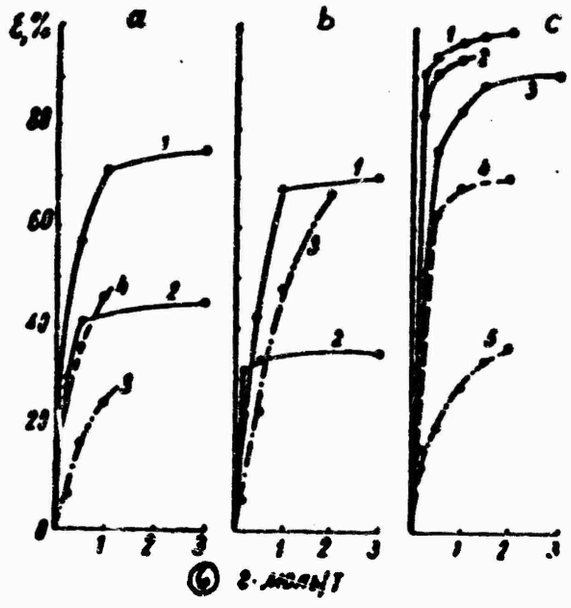

a) Flotation with imidazolethiones: 1 and 2) malachite and galena with naphthimidazolethione; 3 and 4) malachite and galena with benzimidazolethione; b) flotation with oxazolethiones: 1 and 2) malachite and galena with naphthoxazolethione; 3) galena with benzoxazolethione; c) flotation with thiazolethione: 1, 2, and 3) galena, cerussite, and malachite with thiazolethione; 4 and 5) galena and malachite with thiazolethione. The solid lines indicate flotation with derivatives of the naphthalene series and the dotted lines indicate flotation with benzene derivatives. 6) g-mole/t.

the experiments are shown in the figure.

As follows from the data cited, naphthazolethiones have a significantly higher flotation activity than the benzol derivatives. It must be noted that all the flotation experiments were conducted under identical but not optimum conditions (coarse and unsedimented minerals, flotation in the absence of soda, etc.) and even mercaptobenzothiazol, the strongest of the azolethiones of the benzene series, thus ensures extraction of only 70% of the galena in the foam product. However, this was done intentionally, for clearer demonstration of the advantages of derivatives of the naphthalene series over benzene derivatives. By the same token, flotation of the oxide minerals (malachite and serussite) was carried out without sulfidization.

Although the activity products of imidazolethiones, oxazolethiones, and thiazolethiones are of approximately the same order of magnitude, their flotation properties differ (apparently because of the crystallochemically different fixation on the mineral surfaces and the varying degree of hydrophobization).

The flotation activity of imidazolethiones and oxazolethiones is approximately identical and is less than that of thiazolethiones. It is interesting to note that the reagents studied float malachite better than serussite without sulfidization (with imidazolethiones and oxazolethiones the latter virtually fails to pass into the foam).

Thiazolethiones are the most active collectors of those studied, but the advantages of naphthalene derivatives over benzene derivatives appear clearly in this case (see figure). Naphthazolethiones ensure that all three of the minerals studied pass into the foam (serussite and malachite without preliminary sulfidization) in quantities of more than 90%, while benzothiazolethione, at a consumption of 2 g·mole/t, extracts only 70% of the galena and 37% of the malachite and virtually does not float serussite at all. These results accord well with the advantages of derivatives of the naphthalene series over benzene derivatives predicted on the basis of study of their physicochemical properties.

Introduction of a substitute in position 3 of the imidazole ring of naphthimidazole-2-thione did not yield the marked positive result which might have been expected by analogy with benzimidazole-2-thione and its 1-phenyl derivative; this apparently may be explained by the conditions of reagent fixation on the mineral surfaces.

Thus, on the basis of the investigation conducted, it may be concluded that naphthazolethiones are more effective collectors than benzazolethiones in the flotation of the sulfide and oxide ores of nonferrous metals. The best reagent and the one recommended for industrial application must be considered to be naphth-/2,1/-thiazole-2-thione (which may be called "Naphthax"), which has significantly better flotation properties than the currently used mercaptobenzothiazole ("Captax"), considering that its raw materials are readily available and that its synthesis is analagous to that of "Captax" ("Naphthax" may be obtained in an autoclave at 220° by reacting 3-naphthylamine with carbon bisulfide and sulfur). It is especially desirable to use "Naphthax" in the flotation of copper and lead oxide ores without preliminary sulfidization (when these ores contain significant quantities of precious metals) and, as might be assumed, in the flotation of precious-metal ores.

Bibliography

1. Spravochnik po obogashcheniyu poleznykh iskopayemykh pod red. A.F. Taggarta /Handbook on Useful-Ore Beneficiation Edited by A.F. Taggart/, Vol. 3, p. 425, Metallurgizdat, Moscow, 1952.

2. A.K. Livshits, in collection of scientific and technical information entitled Flotatsiya /Flotation/, p. 31, NITOtsvetmet i Metallurgizdat, Moscow, 1956.

3. A.Ye. Babin, Bynll. TsIIN tsvetmet /Bulletin of the Central Scientific Research Institute for Nonferrous Metallurgy/, No. 23, 9 (1957).

4. I.W. Mark, K.L. Sutherland, Trans. AIME, Vol. 134, 53 (1939).

5. G.N. Tyurenkova, Ye.I. Silina, I.Ya. Postovskiy, Zh. prikl. khimii [Journal of Applied Chemistry], Vol. 34, 2327 (1961).

6. I.A. Kakovskiy, Tr. IGD AN SSSR [Transactions of the Mining Institute of the Academy of Sciences USSR], Vol. III, p. 286, Izd. AN SSSR, Moscow, 1956.

7. V.I. Kuznetsov, Zavodskaya laboratoriya [Plant Laboratory], Vol. 11, No. 7-8, 656; No. 9, 768 (1945).

3. A.N. Kul'berg, Sintezy organicheskikh reaktivov [Syntheses of Organic Reagents], p. 86, Goskhimizdat, 1947.

9. A.K. Majumdar, M.K. Chakrabartty, Z. analyt. Chem., 162, No. 2, 96 and 101 (1958); Analyt chim acta, 20, No. 4, 379 (1959).

10. T.F. Burneo, Rev. farm. y biogim.; Univ. nacl. San Marcos (Lima, Peru), 15, 67 (1953); C.A. 49, 9449 (1955).

11. C. Duval, Analyt. chim. acta, 4, 159 (1950).

12. I. Ubaldini, Gazz. chim. ital., 78, 293 (1948).

13. I.A. Kakovskiy, K.A. Karasev, Tsvetnyye metally [Nonferrous Metals], No. 4, 16 (1959).

Manuscript submitted 10 January 1963

STUDY OF THE INFLUENCE OF CERTAIN REAGENTS ON THE FLOTATION PROPERTIES OF THE MINERALS OF CARBONATITE ROCKS

By D.I. Kogan, V.A. Rychagov, Irkutsk State Scientific Research Institute for Rare Metals

Pages 51-57

The flotation properties of pyrochlore and concomitant minerals have not as yet been sufficiently well studied. This article presents the main results of work conducted to study the influence of reagents on the flotation of pyrochlore and concomitant minerals from a carbonatite deposit.

For these investigations we selected the pure minerals pyrochlore, calcite, and magnetite from a carbonatite deposit and pyrochlore from a pegmatite deposit*, all with elemental contents close to the theoretical (table), and used the following reagents: sulfonated oxidized recycle (ORS), octadecylamine, ANP-14, sodium hydroxide, soda, salt, hydrofluoric and sulfuric acids, sodium silicate, sodium sulfide, and calcium and iron salts.

In order to study the influence of these reagents on the flotation of pyrochlore and concomitant minerals we employed:

1. Measurement of the electrokinetic potential of the mineral surfaces, which was determined by the electroosmosis method with an instrument designed by the VIMS [All-Union Scientific Research Institute for Mineral Resources] [1].
2. Incorporation of the isotopes C^{14}, S^{35}, Cl^{36}, Ca^{45}, and Fe^{59} into the reagents: soda, sulfuric and hydrochloric acids, calcium chloride, and ferrous sulfate.
3. Monobubble flotation.
4. Flotation of minerals and mixtures in a flotation apparatus with a volume of 75 cm^3.

Influence of pH of medium on floatability of minerals. One of the most widely used methods of controlling the flotation process is the creation of

*Henceforth, the pyrochlore of the carbonatite deposit is designated as pyrochlore II and that of the pegmatite deposit as pyrochlore I.

Results of Chemical and Spectral Analyses of Minerals (in %)

Элемент (1)	Пирохлор I	Пирохлор II	Магнетит (3)	Кальцит (4)
SiO_2	3,50	3,15	++	+
Nb_2O_5	65,25	63,90	+	+
CaO	15,07	16,60		49,93
MgO	0,50	0,91	+	+ +
Fe_2O_3	0,07			
FeO	0,16	1,7	24,15	
Fe (2)		+ +	69,60	+ +
TiO_2	4,70	3,50	+ +	ca.
Al_2O_3	+	+	+	+
ThO_2	0,07	0,09		
CeO_2	0,06	0,58		
Th	0,97	0,54		
U	0,01	0,009		
Na_2O	6,60	5,73		
Sr	++	+		+
La	++	+ +		
Pb	ca.			
Mn	ca.	+ + +	+	+
Zr	ca.	+ +		
Re	ca.	ca.		
Y	ca.	+		+
Ba		+	ca.	+
V		ca.	+	
Zn			+	
Cu			ca.	ca.
Sn				ca.
Yb				ca.

Note: +++ indicates percents, ++ tenths of a percent, and + hundredths of a percent; sl indicates traces. 1) Elements; 2) pyrochlore I; 3) magnetite; 4) calcite; 5) total.

a definite concentration of hydrogen and hydroxyl ions in the pulp. Study of the influence of the hydrogen and hydroxyl ion concentrations on the variation in the surface charge on the minerals (Fig. 1) showed that, for the group of minerals investigated, the OH^- are the potential-governing ions; when their concentration rises there is a sharp increase in the negative surface charge of the minerals, which probably results from sorption of hydroxyl ions on the inner face of the double electric layer (all of the minerals have a negative surface charge). When the hydrogen ion concentration rises the surface charge of the minerals decreases, approaching zero.

Experiments have shown that when the pH of the medium rises the floatability of pyrochlores and magnetite by sulfonated oxidized recycle is sharply reduced, while the floatability of calcite remains constant. Thus, at a medium pH of 12 the extraction of calcite (ORS -- 100 mg/l) is 90%, that of pyrochlore II is 40%, that of magnetite is 8%, and that of pyrochlore I is

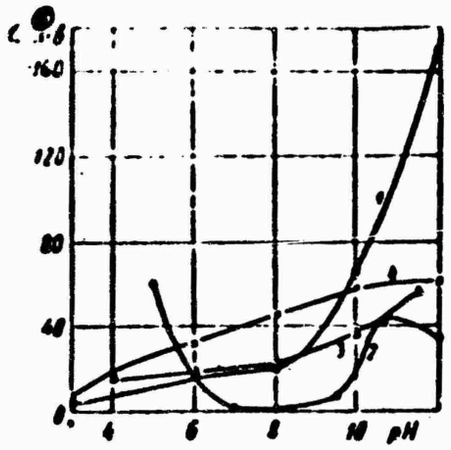

Fig. 1. Influence of pH of medium on electrokinetic potential of minerals. 1) Calcite; 2) magnetite; 3) pyrochlore I; 4) pyrochlore II; 5) ζ, mv.

6%. It is thus possible to separate calcite from pyrochlore and magnetite in strongly alkaline media with ORS.

Mineral flotation has a different character under the action of cation collectors. As was determined earlier [2], hydrophobization of mineral surfaces during the use of cation reagents results from amine ions or molecules, the selective sorption of which depends on the electrochemical properties of the mineral surfaces and the state of the disolved amine.

In the case in question the minerals have a small negative surface charge in acid media and the amine is in ionic form. The flotation of calcite and magnetite with ANP-14 or octadecylamine (Fig. 2) proceeds sluggishly in strongly acid media. When the pH of the medium rises, i.e., when the negative surface charge of the minerals increases, their flotation by cation collectors is significantly improved. On shifting to strongly alkaline media (see Fig. 2a) there is a marked impairment of the floatability of all the minerals. The negative surface charge probably exceeds the optimum value for improved flotation. The maintenance of the flotation activity of the minerals during flotation with octadecylamine at pH 12 (see Fig. 2b) depends to a considerable extent on the reactions of its hydrocarbon chains among themselves, these promoting fixation of the amine on the mineral surfaces (i.e., it is possible that there is another optimum value for the negative surface charge of the minerals during flotation with octadecylamine).

Acid treatment of minerals. Preliminary acid treatment [3-5], which results in an improvement of the selective separation of minerals, has recently found wide application in the flotation of nonsulfide mineral ores. It is known that acid treatment promotes removal of various salts, ions, hydroxides, and other foreign impurities from mineral surfaces and exposure of the natural surfaces. Just as removal of "inevitable" ions from pulp by

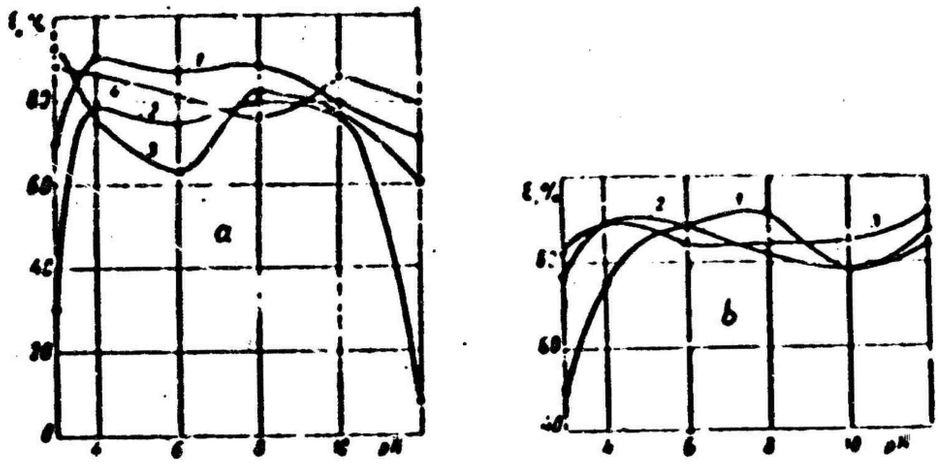

Fig. 2. Influence of pH of medium on floatability of minerals at an ANP-14 concentration of 50 mg/l (a) and an octadecylamine concentration of 25 mg/l (b). 1) Calcite; 2) magnetite; 3) pyrochlore I; 4) pyrochlore II.

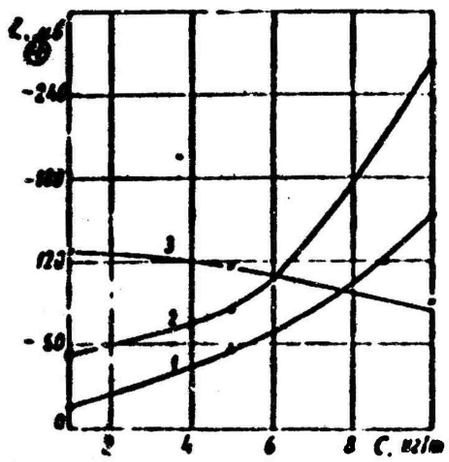

Fig. 3. Effect of acid treatment on electrokinetic potential of pyrochlore I. 1) HF; 2) HCl; 3) H_2SO_4; 4) mv.

acid treatment and subsequent washing, this improves the selectivity of the process. As a result of acid treatment cations in the crystal lattice of the mineral may be "washed" from the surface layers; impoverishment of their surfaces in cations can decrease the ability of minerals to react with an anion collector. The formation of new surface compounds with a greater or lesser chemical activity than the initial compounds is possible in the acid treatment of mineral surfaces [3].

In this work we studied the action of preliminary treatment with hydrofluoric, hydrochloric, and sulfuric acids on minerals. Preliminary treatment of pyrochlore I with hydrofluoric and hydrochloric acids causes a sharp in-

crease in the surface charge of the mineral (Fig. 3). Changing the HF and HCl consumtions from 1 to 10 kg/t leads to an increase in the electrokinetic potential, from 22 and 55 mv to 155 and 258 mv respectively. Despite the fact that hydrofluoric acid is more reactive than hydrochloric acid, it produces a smaller change in the surface potential of pyrochlore. This obviously is associated with the fact that the crystal lattice of the mineral contains F^+, which has a greater protective action against HF than against HCl. The increase in the negative surface charge of the mineral may occur as a result of the selective removal of iron, titanium, and calcium cations from the surface of pyrochlore during treatment with hydrofluoric and hydrochloric acids; furthermore, we cannot exclude the possibility that the surface layers of the mineral dissolve. Hydrofluoric and hydrochloric acids have an analogous but somewhat weaker action on magnetite. Hydrofluoric acid, being more reactive, has a stronger influence on magnetite than hydrochloric acid.

Treatment with sulfuric acid, which results in a decrease in the negative surface charge of pyrochlore I and magnetite, has a completely different character. The decrease in the electrokinetic potentials of the minerals enables us to assume that low-solubility compounds of the sulfate type are formed on their surfaces. This assumption of the formation of new surface compounds based on SO_4^{2-} on minerals has been confirmed by sorption experiments. We studied the fixation of hydrochloric and sulfuric acids on calcite, magnetite, and pyrochlore with the aid of "tagged" chlorine and sulfur atoms incorporated into the acids. The hydrochloric acid consuption in the experiments varied from 1 to 4 kg/t, but sorption of chlorine atoms was not observed on a single one of the minerals. The sorption of sulfuric acid was studied at a consumption of 2.4 and 10 kg/t. The sorption of SO_4^{2-} increases with the acid consumption. The maximum sorption was observed on magnetite (this also being manifested in a sharp decrease in surface charge).

The action of sulfuric acid on pyrochlore I is interesting. On reaching a H_2SO_4 consumtion of 4 kg/t its sorption remains virtually constant; at this sulfuric acid consumption the cations on the mineral surfaces probably all enter into compounds with SO_4^{2-} to form low-solubility sulfates.

Action of sodium silicate on mineral floatability. Despite the fact that sodium silicate has been the subject of a considerable number of investigations, the mechanism of the depressive action of this reagent is still not sufficiently clear. The action of sodium silicate was determined at a medium pH of less than 8, i.e., when the pulp contains primarily undissociated silicic acid.

As measurements of the electrokinetic potentials of the minerals showed, the action of sodium silicate on them varies (Fig. 4a). The action of sodium silicate on pyrochlore I is manifested in a sharp drop in the negative surface charge, which probably results from sorption of undissociated silicic acid (in the form of micelles) on the surface of the pyrochlore, thus causing a sharp depression of pyrochlore I. For the remaining minerals the action

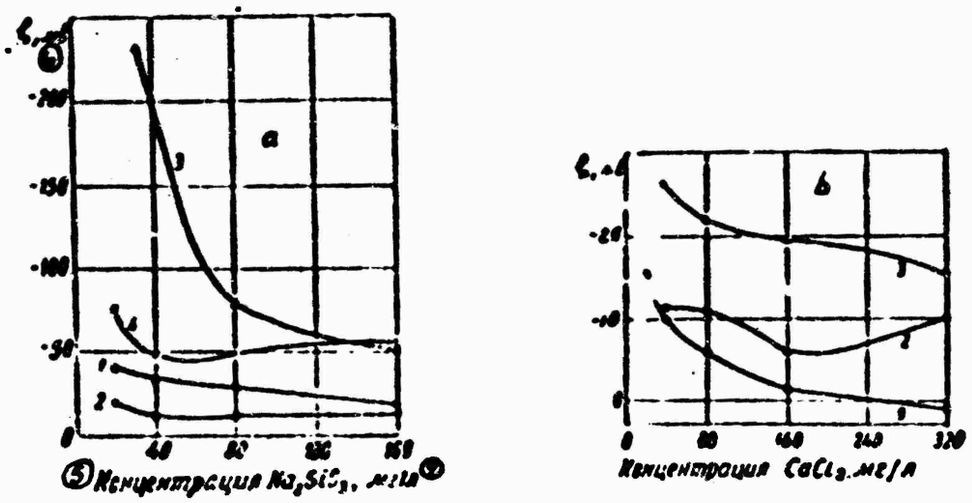

Fig. 4. Action of sodium silicate (a) and calcium chloride (b) on the electrokinetic potential of minerals. 1) Calcite; 2) magnetite; 3) pyrochlore I; 4) pyrochlore II; 5) concentration; 6) mv; 7) mg/l.

of sodium silicate is not so strongly manifested. The salicic acid micelles are probably concentrated primarily in the diffusion layer, creating an unusual "screen". The creation of such a "screen" of salicic acid micelles increases the hydrophilia of the surface, as a result of which one might expect a depression of the minerals weaker than that which occurs on sorption of salicic acid micelles on their surfaces. Thus, during flotation with ORS sodium silicate causes an insignificant depression of calcite, a greater depression of pyrochlore I, and a sharp suppression of the floatability of pyrochlore II and magnetite. At a sodium silicate concentration of 100 mg/l the extraction of pyrochlore II amounts to 59%, that of pyrochlore I to 6%, and that of magnetite to 8%.

Depressive action of sodium sulfide. The possibility of using sodium sulfide in the flotation of nonsulfide minerals has recently been noted. Reference [6] acknowledges the use of sodium sulfide in conjunction with soda to be the most expedient method in the flotation of pyrochlore ores, since in this case the activating action of both iron and calcium ions is eliminated. However, little research has as yet been done on the problem of the action of sodium sulfide on the flotation properties of minerals.

In this work experiments on the action of sodium sulfide were conducted in distilled water; on introduction of Na_2S the pH of the pulp increased as a function of the sodium sulfide concentration, to 8 at 160 mg/l Na_2S and to 10.7 at 500 mg/l Na_2S, i.e., sulfhydryl ions predominated in the pulp.

Experiments on the action of sodium sulfide on pyrochlore I and calcite

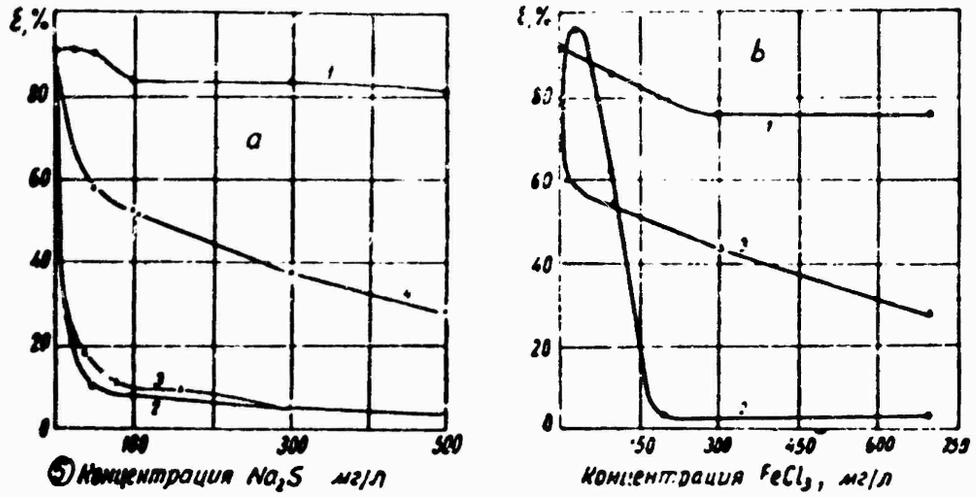

Fig. 5. Influence of sodium sulfide (a) and ferric chloride (b) on the floatability of mineral at an ORS concentration of 100 mg/ℓ. 1) Calcite; 2) magnetite; 3) pyrochlore I; 4) pyrochlore II; 5) concentration, mg/ℓ.

showed that increasing the Na_2S concentration in the pulp causes a significant increase in the negative surface charge of pyrochlore I. There is almost no change in the electrokinetic potential of calcite under these conditions. It may be assumed that the sorption of sulfhydryl ions and molecules of hydrogen sulfide on pyrochlore and calcite differs in character. Sorption on pyrochlore I probably occurs on the inner face of the double electric layer, while on calcite it occurs in the diffusion layer; this predetermines the differing influence of the reagent on the floatability of these minerals. Thus, in the flotation of minerals with ORS in the presence of Na_2S there is an insignificant drop in the floatability of calcite and a complete depression of pyrochlore and magnetite (Fig. 5a). At concentrations of 300 mg/ℓ Na_2S and 100 mg/ℓ ORS the extraction of calcite amounts to 84%, that of pyrochlore II to 37%, and that of pyrochlore I and magnetite to 6%. Flotation of the minerals with a medium pH of more than 12 showed that introduction of sodium sulfide has no effect in this case.

Influence of calcium and iron salts on mineral flotation. We studied the action of calcium and iron salts on the floatability of calcite, pyrochlore, and magnetite. The presence of small concentrations of calcium ions in the pulp leads to a significant decrease in the negative surface charge of the minerals (see Fig. 4b). Further increasing the concentration of Ca^{2+} slightly alters the electrokinetic potential of the minerals. Sorption of Ca^{2+} obviously occurs on the mineral surfaces; on saturation of the inner face of the double layer with calcium ions the ion concentration moves to the outer face and the diffusion layer. This assumption has been confirmed

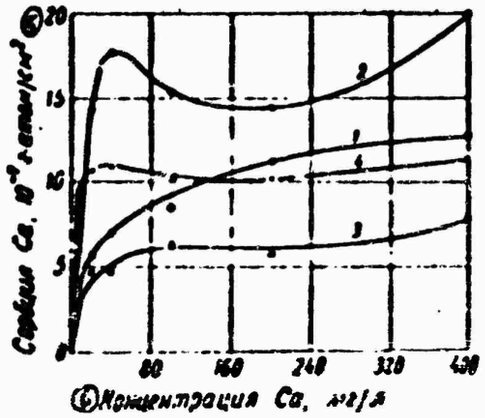

Fig. 6. Sorption of calcium on minerals as a function of concentration. 1) Calcite; 2) magnetite; 3) pyrochlore I; 4) pyrochlore II; 5) sorption of Ca, 10^{-7} g-atom/cm^2; 6) Ca concentration, mg/l.

by sorption experiments which showed the large sorption capacity of the minerals for calcium at low concentration and the insignificant change in sorption when the $CaCl_2$ concentration is increased (Fig. 6).

The flotation experiments show the decrease in mineral floatability at low calcium chloride concentrations. The improvement in the floatability of the minerals with ORS when the $CaCl_2$ concentration is increased is probably explained by concentration of the calcium cations in the diffusion layer on the one hand and by the formation of calcium alkylsulfate on the other; the latter is based on sulfonated oxidized recycle, the intensity of its collecting action being somewhat higher than that of true ORS.

Ferric salts have a somewhat different action. When the concentration of trivalent iron in the pulp is low the electric state of the surfaces changes sharply. The electrokinetic potential of calcite falls to zero, while the surfaces of pyrochlore and magnetite are charged. An increase in reagent concetration may lead to its sorption on the outer face, which results in a drop in the electrokinetic potential of the minerals.

All the minerals are characterized by a greater sorption capacity for iron cations than for calcium cations. Sorption of small quantities of iron probably leads to completion of the crystal lattices of the minerals. Increasing the concentration of trivalent iron in the pulp causes a decrease in the floatability of all the minerals during flotation with ORS (see Fig. 5b), since ferric alkylsulfate is formed; this compound is of low solubility and usually either does not have collecting properties (flotation occurs as a result of the ORS unreacted with the iron) or possesses only weak ones. The sharp depression of magnetite is enhanced by sorption of ferric hydroxide, which strongly hydrophilizes its surface.

Conclusions

1. The surfaces of the minerals studied carry a negative charge; pyrochlore II has a larger negative charge than pyrochlore I and this to some extent determines the difference in their flotation properties.

2. Hydrogen and hydroxyl ions are the potential-governors for this group of minerals.

3. Small concentrations of sodium silicate sharply reduce the electrokinetic potential of pyrochlore. This action of sodium silicate on the surface of the mineral may result chiefly from the sorption of silicic acid micelles.

4. The selective depressive action of sodium sulfide on pyrochlore and magnetite at pH 8-11 is apparently manifested in the sorption of sulfhydryl and hydroxyl ions and hydrogen sulfide molecules on their surfaces.

5. Preliminary treatment of mineral surfaces with hydrofluoric and hydrochloric acids probably promotes the washing off of foreign impurities. Furthermore, we cannot exclude the possibility that formation of new surface compounds of the sulfate type occurs under the action of sulfuric acid.

6. Calcium and ferric ions are actively sorbed on mineral surfaces; it is possible that the presence of low concentrations of these ions leads to completion of the crystal lattices of the minerals.

Bibliography

1. M.L. Volova, V.P. Kuznetsov, O primenenii elektrokineticheskikh metodov issledovaniya pri izuchenii deystviya flotatsionnykh reagentov /Use of Electrokinetic Research Methods in Studying the Action of Flotation Reagents/, Byull. VIMS /Bulletin of the All-Union Scientific Research Institute for Mineral Resources/, No. 34, 1960.

2. A.A. Abramov, Obogashcheniye rud /Ore Beneficiation/, No. 5, 1960.

3. S.I. Pol'kin, Ting-P'eng-Hai, K izucheniyu mekhanizma kislotnoy obrabotki mineralov pered flotatsiyey /Study of the Mechanism of the Acid Treatment of Minerals Before Flotation/, Byull. TsIINtsvetmet /Bulletin of the Central Scientific Research Institute for Nonferrous Metallurgy/, No. 21, 1959.

4. M.A. Eygel's, L.A. Grekulova, V.P. Kuznetsov, Byull. TsIINtsvetmet, No. 15, 1961.

5. F.N. Belash, Kislotnaya depressiya i aktivatsiya okislennykh mineralov pri flotatsii /Acid Depression and Activation of Oxidized Minerals before Flotation/, Obogashcheniye poleznykh iskopayemykh /Enrichment of Useful Minerals/, No. 1, 1958.

6. S.I. Pol'kin, Yu.A. Bykov, G.M. Shapovalov, Flotatsiya pirokhlora i tsirkona /Flotation of Pyrochlore and Zircon/, Moscow, 1959.

Manuscript submitted 30 July 1962

Recommended by the Chair of Beneficiation, Irkutsk Polytechnic Institute

INVESTIGATION OF THE KINETICS OF THE REACTION OF CARBON WITH OXYGEN DISSOLVED IN COPPER AND TIN

By P.M. Shurygin, V.I. Kryuk, Ural Polytechnic Institute, Chair of Metallurgical Process Theory

Pages 58-63

A knowledge of the kinetic mechanisms of the reaction of carbon with oxygen dissolved in molten copper is necessary for analysis of the technological characteristics of the poling and deoxidation of this metal, as well as for the theory of the oxidative smelting of copper [1, 2]. Despite the fact that the equilibrium of the process is very greatly shifted toward the formation of carbon monoxide [3], its rate is apparently small, the physicochemical constants of the reaction rates have not as yet been studied; we do not know the limiting stage, the influence of temperature, or the mechanism, specific rates, or order of the reaction. This work makes an attempt to investigate the kinetics of the reaction of solid carbon with oxygen in molten copper and tin at various temperatures and under various experimental conditions.

As was noted earlier [4, 5], the use of revolving disks with equal surfaces available in the diffusion sense makes it possible to obtain simple and reproducible results for the kinetics of heterogeneous reactions under controlled melt-movement conditions. For the mixed mode, when the rates of the chemical process and the delivery of reagents to the reaction front are commensurable, the rate of the entire process V is defined by the expression [4]

$$V = \frac{C - C_e}{1.61 D^{\frac{2}{3}} \nu^{-\frac{1}{6}} \omega^{0.5} + \frac{1}{K}}, \qquad (1)$$

where C and C_e are the equilibrium and given concentrations of oxygen in the copper in g/cm^3, D is the diffusion coefficient in cm^2/sec, ν is the kinematic fusion viscosity in cm^2/sec, ω is the angular rotation velocity in

sec^{-1}, and K is the chemical reaction-rate constant, cm/sec.

The first item in the denominator of Equation (1) characterizes the diffusion resistance R_d and the second characterizes the kinetic resistance R_k. When $R_d > R_k$ the reaction is in the diffusion mode and its rate increases with ω. When $R_d \ll R_k$, V does not depend on ω and is determined by the chemical process. It is easy to see that a four- or five-fold change in R_d or R_k makes it possible to emerge from the mixed mode and facilitates evaluation of the character of the limiting stage of the process. In the case of the diffusion mode one can determine the value of D in the process under study from the measured V.

The technique of experiments with revolving disks in melts is described in Reference [5]. Samples of very pure graphite (99.999% C) were inserted in ceramic casings and set in rotation in the molten metal. The latter was in an alumina crucible. An oxidizing atmosphere was maintained in the furnace and, furthermore, pure Cu_2O was supplied to the surface of the molten copper, this promoting maintenance of the equilibrium oxygen content in the melt at the experimental temperature.

Inasmuch as there are indications in the literature [6] of the possibility of supersaturating copper with oxygen, we made additional measurements of the solubility of Cu_2O in copper at temperatures of 1300, 1400, and 1520°. For this purpose samples of the metal were drawn off through a quartz tube, deoxidized with aluminum, and then analyzed for quantity of Al_2O_3 formed. Despite the fact that such a method cannot pretend to special accuracy, the results of the measurements corresponded almost exactly to those in the literature [7]. At the temperatures indicated the oxygen content turned out to be 1.71, 1.96, and 2.18% by weight, respectively.

From the decrease in the weight of the samples (40-100 mg out of a total weight of 350-400 mg), the surface area of the disk, and the period of rotation (1.5-5 min) we determined the rate of the process V (in $mg/cm^2 \cdot sec$). It must be emphasized that the decrease in the weight of the rotating sample does not result from mechanical abrasion by the melt. This is confirmed by data from control experiments. Samples were rotated in molten copper and tin in graphite crucibles and thus virtually deprived of oxygen for a period of 15-20 min; nevertheless, the change in their weight was negligible.

The results of the experiments are shown in Fig. 1, from which it is clear that the rate of the process V rises linearly as the square root of the angular velocity of disk rotation. With stationary samples the values of V are very small, although not zero because of molecular diffusion and convection currents within the melt. The rate of the reaction of carbon with oxygen dissolved in this metal is in the diffusion region and the kinetic resistance in Equation (1) is negligible as compared with the diffusion resis-

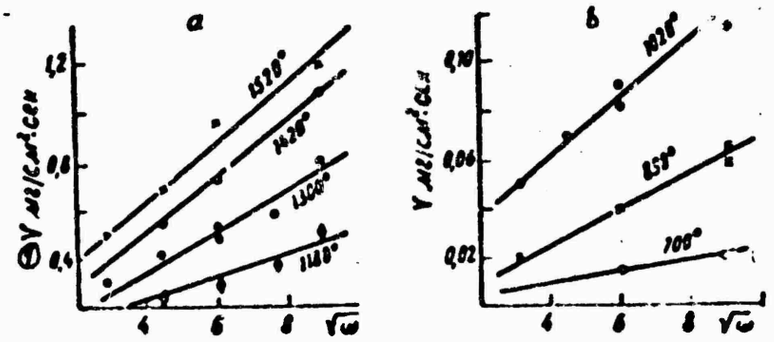

Fig. 1. Change in kinetics of reaction of carbon with oxygen dissolved in copper (a) and tin (b) as a function of angular rotation velocity. 1) V, mg/cm^2·sec.

tance. A decrease produced in the latter by ω causes a rise in V; we were unable to attain the kinetic mode by the methods available to us.

In connection with the aforementioned, Equation (1) is transformed into the expression

$$V = 0{,}62\,D^{\frac{2}{3}}\nu^{-\frac{1}{6}}(C - C_p)\sqrt{\omega}, \qquad (2)$$

from which one may determine the diffusion coefficient.

It is obvious that under the experimental conditions the destruction of the graphite crystal lattice, breaking of the oxygen-copper bonds, and formation of new oxygen-carbon bonds, as well as formation of the gas phase (SO), occur more rapidly than the transfer of particles within the melt. This apparently enhances the properties of the copper-graphite boundary, with its nonuniform force field and excess oxygen content, to a considerable extent [8], facilitating the course of the chemical reaction and the formation of SO bubbles in the graphite pores not wetted by the melt.

As is well known [7], the solubility of carbon in liquid copper is negligibly small, amounting to only $1{,}5\cdot10^{-4}$% by weight or approximately $2{,}0\cdot10^{-3}$ g/cm^3 at 1300°. By substituting this value into Equation (2) it is easy to obtain the possible values of the diffusion coefficient of carbon D = 0,03 cm^2/sec from the measured V and . There is no satisfactory justification for such a large valuc, since the D of the carbon is cast iron [9] amounts to only $4{,}3\cdot10^{-5}$ cm^2/sec at the same temperature (1350°), i.e., is less by three orders of magnitude. The solubility of carbon in tin is usually negligible and cannot account for the measured process rates at ordinary values of D. It is thus only the transport of oxygen to the reaction front which can control the rate.

The value of the oxygen concentration C_e in equilibrium with the carbon

can be determined from thermodynamic data [3] on the oxidation reactions of carbon and copper:

тв = solid
ж = liquid

$$2C_{тв} + O_2 = 2CO,\ \Delta Z_2 = -53400 - 41{,}9T;$$

$$4Cu_{ж} + O_2 = 2Cu_2O_{ж},\ \Delta Z_3 = -65260 + 21{,}44T;$$

$$C_{тв} + Cu_2O_{ж} = CO + 2Cu_{ж},\ \Delta Z_1 = \frac{1}{2}\Delta Z_2 - \frac{1}{2}\Delta Z_3 = 5930 - 31{,}17T.$$

On the other hand, $\Delta Z_1 = RT \ln \frac{P_{CO} a_{Cu}^2}{a_{Cu_2O} a_c}$. Taking P_{CO} = 1 atm and $a_{Cu} = a_c = 1$ and assuming in first approximation that the solution of cuprous oxide in the metal is ideal, i.e., $a_{Cu_2O} = C_{Cu_2O}$, it is easily found that, at 1300°, $\lg \frac{1}{C_{Cu_2O}} = 6$, whence $C_{Cu_2O} = 10^{-6}$.

In other words, the value of the item C_e can be disregarded in Equation (2) against the background of C. This is also valid for solutions of oxygen in tin.

The values of the diffusion coefficient of oxygen in copper and tin calculated from Equation (2), taking into account the solubility of oxygen [7] and the density [8, 10] and viscosity [11, 12] of the metal, are shown in Fig. 2 as a temperature function plotted on semilogarithmic coordinates.

Just as the process rate, the diffusion coefficient increases by the exponential law

$$D_{Cu} = 1{,}55 \cdot 10^{-4} \exp\left(-\frac{35000}{RT}\right) \quad \text{and} \quad D_{Sn} = 1{,}97 \cdot 10^{-3} \exp\left(-\frac{82000}{RT}\right),$$

where the activation energy of diffusion in copper (35,000) and in tin (82,000) is expressed in joules/mole.

For copper at 1180 and 1520° the values of D are $0{,}72 \cdot 10^{-5}$ and $1{,}18 \cdot 10^{-5}$ cm^2/sec respectively, while those for tin at 700 and 1020° are $1{,}0 \cdot 10^{-6}$ and $4{,}17 \cdot 10^{-6}$ cm^2/sec. As one might have been led to expect the high energy consumption in the elementary act of oxygen fusion in tin and the consequently large values of the activation energy explain the smaller values of D as compared with those for molten copper at corresponding temperatures.

However, it should be taken into account that the reliability of the calculation of D in tin is to a significant extent limited by the approximate character of the data on the solubility of oxygen in it [7]. More precise determination of these data will make it possible to recalculate D. Nevertheless, the basic conclusion about the diffusion mode of the reaction

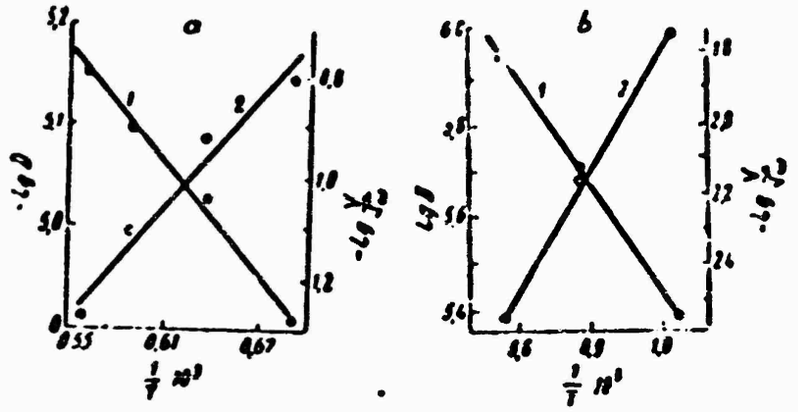

Fig. 2. Rate of process (1) and coefficient of oxygen diffusion (2) as a function of temperature in copper (a) and tin (b).

process remains independent of the degree of accuracy of the experimental data on the oxygen content of tin.

An approximate evaluation of the effective particle radius of oxygen in diffusion can be made from the Stokes-Einstein formula

$$D = \frac{kT}{4\pi\eta r},$$

where η is the dynamic viscosity.

For molten tin r = 1.45 A and this virtually coincides with the radius of a two-charge ion according to Pauling. This calculation yields r = 5.6 A for molten copper, i.e., an excessive value. The cause of this discrepancy apparently lies both in the limited applicability of the Stokes-Einstein formula to melts and in the rather low values of the experimental data.

It is appropriate to note here that the decrease in the surface tension of copper when its oxygen content rises [6] to some extent indicates possible separation of the Cu-O-Cu bonds in the melt and displacement of this group to the interphase boundary. However, despite the large value obtained for the radius from the Stokes-Einstein equation, there is apparently not yet sufficient basis for accepting it as the structural unit in the diffusion process. The forms of stationary and diffusing particles may differ, since their energy states may vary considerably during translation. This is indicated by the value of the activation energy.

On the other hand, certain diffusion theories have recently advanced the concept [13] of the possible simultaneous direct displacement of five, six or more atoms in liquids, as well as of the nonactivation displacement of any particle of the melt, while the very notion of effective atomic jumps is changing. From this standpoint, the size of the vacancies, which may be

evaluated approximately from the equation

$$\frac{4}{3}\pi r^3 = 0{,}68\left(\frac{kT}{e}\right)^{\frac{3}{2}}.$$

should not directly affect the displacement of single particles. Indeed, the radii of the "holes" for tin and copper have similar values, of the order of 10^{-8} cm, while the value of the activation energy of diffusion for tin is twice as large as for copper. Unfortunately it is impossible to make a direct comparison of our diffusion coefficients with analagous data. The only data on D for oxygen in molten iron at 1600° ($0{,}73 \cdot 10^{-2}$ cm^2/sec) must be assumed to be excessive as a result of convection transfer in the capillaries [14].

In conclusion it must be emphasized that high pyrorefining temperatures create favorable conditions for the chemical processes at the interphase boundaries and investigation of the kinetics of similar reactions should thus to a considerable extent reduce to a study of diffusion mechanisms within melts. There is every reason to assume that the deoxidation of copper by mazut and hydrocarbons also occurs in the diffusion mode. The deoxidation and poling process should therefore be accelerated by expanding the reaction surface in every way possible, e.g., by blowing in generator gas or charcoal dust [15] and intensifying agitation. The latter is important not only from the standpoint of mass transfer within the melt (and it is quite important here), but primarily with respect to improvement of conditions for the transport of matter to the immediate vicinity of the interphase boundary, where the conditions for convection diffusion improve as the linear velocity of the liquid increases.

Conclusions

1. The use of equal available surfaces on revolving disks was employed to investigate the kinetics of the reaction of carbon with oxygen dissolved in copper and tin. It was found that the process rate is limited by the diffusion of the oxygen in the metal.

2. The coefficients of oxygen diffusion in copper and tin and their temperature functions were experimentally determined. The order of D for copper was 10^{-5} cm^2/sec, while that for tin was 10^{-6} cm^2/sec; the activation energy of diffusion in tin and copper was 82,000 and 35,000 joules/mole respectively.

3. It was shown that poling and deoxidation should be accelerated by increasing the reaction surface and intensifying agitation.

Bibliography

1. D.M. Chizhikov, Metallurgiya tyazhelykh tsvetnykh metallov [Metallurgy of the Heavy Nonferrous Metals], Izd-vo AN SSSR, 1948.

2. V.I. Smirnov, Metallurgiya medi i nikelya [Metallurgy of Copper and Nickel], Metallurgizdat, 1950.

3. R. Raddl, Fizicheskaya khimiya pirometallurgii medi [Physical Chemistry of the Pyrometallurgy of Copper], Moscow, IL, 1955.

4. V.G. Levich, Fiziko-khimicheskaya gidrodinamika [Physicochemical Hydrodynamics], Moscow, Fizmatizdat, 1959.

5. P.M. Shurygin, V.N. Boronenkov, V.I. Kryuk, Izv. VUZ. Tsvetnaya metallurgiya [News of Higher Educational Institutions, Nonferrous Metallurgy], No. 3, 59 (1962).

6. V.N. Yeremenko, Yu.V. Naydich, A.A. Nosonovich, Zh. fiz. khimii [Journal of Physical Chemistry], 34, No. 5 (1960).

7. M. Khansen, K. Anderko, Struktury dvoynykh splavov [Structures of Double Alloys], Moscow, 1962.

8. Yu. V. Naydich, V.N. Yeremenko, L.F. Kirichenko, Zh. neorg. khimii [Journal of Inorganic Chemistry], 2, No. 7, 333 (1962).

9. D.W. Morgan, I.A. Kitchener, Trans. Faraday Soc., 1, 50, 51 (1951).

10. N.I. Koshkin, M.G. Shirkevich, Spravochnik po elementarnoy fizike [Handbook of Elementary Physics], Fizmatizdat, 1962.

11. A.A. Vertman, A.M. Samarin, Stroyeniye i svoystva zhidkikh metallov [Structure and Properties of Molten Metals], Moscow, page 138, 1960.

12. V.G. Shvidkovskiy, Nekotoryye voprosy vyazkosti rasplavlennykh metallov [Certain Problems of the Viscosity of Molten Metals], Gosizdat tekh.-teoret. literatury, 1955.

13. Ling Jang, Metallurg. Soc. Conference, 7, 503 (1961).

14. V.I. Kozlov, A.F. Vishkarev, A.G. Zil'berman, V.I. Yavoyskiy, Izv. VUZ. Chernaya metallurgiya [News of Higher Educational Institutions, Ferrous Metallurgy], No. 11, 1961.

15. M.M. Lakernik, N.N. Sevryukov, Metallurgiya tsvetnykh metallov [Metallurgy of the Nonferrous Metals], Metallurgizdat, Moscow, 1957.

Manuscript submitted 10 November 1962

THERMODYNAMIC PROPERTIES OF MOLTEN LEAD SILICATES

By V.I. Minenko, N.S. Ivanova, Khar'kov Engineering-Economic Institute, Chair of Chemistry

Pages 64-69

Melts of the system $PbO-SiO_2$ are of interest for the metallurgy of lead and the technology of glass, enamels, and glazes and have been studied rather thoroughly [1-9]. However, the data on them are not always in agreement. Thus, for example, according to published data [8, 9], component activity and other thermodynamic quantities vary monotonically as a function of composition. Meanwhile, on the basis of data obtained in investigations of other properties [2-7], including information on the electromotive forces of concentration chains composed of melts of $PbO-SiO_2$ [6, 7], one would expect a change in the character of the dependence of the thermodynamic properties at points corresponding to definite stoichiometric component ratios.

The work described herein was carried out in order to check certain thermodynamic data [10] and make a more precise determination of them. We used the electromotive-force method, which makes it possible to determine a number of differential and integral properties directly.

The subjects of the investigation were the chemical chains

$$Pb\,|x\,PbO + (1-x)\,SiO_2|O_2\,(P_{O_2} = 1\ atm),\ Pt$$

The electrolytic measuring cells consisted of one or two corundum crucibles (one inserted into the other in the latter case) containing silicate melts, electrodes, and current conductors and were formed in a manner analogous to that described in References [10, 11]. Melts of "granular pure" quality lead and platinum wire (or tubing) washed by a stream of oxygen were used as the electrodes. The lead electrode was connected to the leads to the measuring device with tungsten, iron, or nichrome wire insulated from the silicate melt by alundum tubing. Another formed alundum tube, containing the platinum

electrode, served to supply oxygen to the area in the vicinity of the electrode.

The silicate melts were prepared from chemically pure lead oxide and silica, by a previously described method [6], and varied by 1-2% by weight PbO from experiment to experiment.

The emf measurements were conducted under isothermal conditions with an accuracy of ±1 mv, with the aid of a Raps potentiometer and a mirror galvanometer. A platinum/platinum-rhodium thermocouple and a PP-1 potentiometer were used to measure the temperature.

The emf values became constant after 20-30 min and the discrepancy in the results of parallel experiments did not usually exceed 4 mv, reaching 6-7 mv in rare cases (for melts with compositions close to those of the compounds formed).

Fig. 1 shows the results of emf measurements made at temperatures of 800, 900, 940, 1000, and 1200° after elimination of the thermoelectric forces the tungsten-platinum, iron-platinum, and nichrome-platinum pairs. Comparison of these results with the data obtained by other authors /11, 12/, which are also given in Fig. 1, indicates their close similarity.

It is clear from Fig. 1 that the emf rises when the temperature decreases and the content of lead oxide and similar compounds expressed by the simplest formulas $4PbO \cdot SiO_2$, $2PbO \cdot SiO_2$, $3PbO \cdot 2SiO_2$, $PbO \cdot SiO_2$, and $2PbO \cdot 3SiO_2$, according to the data in References [6, 7], undergoes more or less marked changes in the character of its dependence. The existence of certain of these compounds has recently been confirmed by other authors [13].

The emf's of the chemical chains investigated are determined by the potential difference between the platinum-oxygen and lead electrodes and, according to References [14, 15], at P_{O_2} = const depend on the activity of the oxygen and lead ions in the melt:

$$E_1 = E_0 - \frac{RT}{2F} \ln a_{O^{2-}} \cdot a_{Pb^{2+}}.$$

On the basis of the common assuption that $a_m = a_+ \cdot a_-$ (or $Ka_m = a_+ \cdot a_-$ and K = const) we may substitute in $a_{Pb^{2+}} \cdot a_{O^{2-}} \sim a_{PbO}$ and assume that $E_1 = E_0 - RT/2F \ln a_{PbO}$.

Using this expression and the relationships:

M36 • exc $\Delta Z_0 = -nFE_0$; $\Delta Z_1 = -nFE_1$; $\Delta \bar{Z}_1 = \Delta Z_1 - \Delta Z_0$; $\frac{d(\Delta \bar{Z}_1)}{dT} = -\Delta \bar{S}$

$\Delta \bar{Z}_1 = \Delta \bar{H}_1 - T\Delta S_1$; $\Delta Z_{1\,ид} = \Delta Z_1 = 2.3RT \lg N_1$; $\Delta S_{1\,ид} = \Delta S_1 + 2.3R \lg N_1$

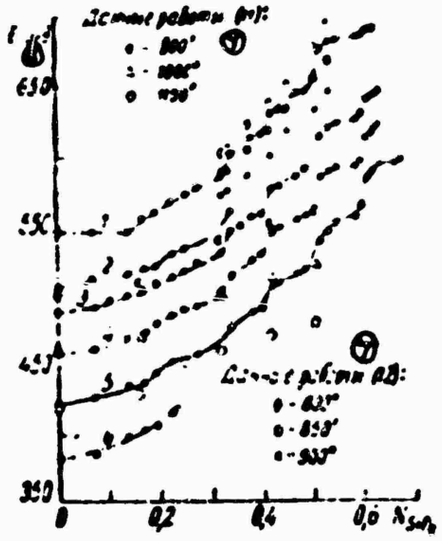

Fig. 1. Emf isotherms of chemical chains. Authors' data: 1) 800°; 2) 900°; 3) 940°; 4) 1000°; 5) 1100°; 6) 1200°. 7) Data from Reference [12]; 8) emf; 9) data from Reference [11].

and $\lg a_1 = \frac{\Delta \bar{Z}_1}{2.3RT}$, we calculated the isobaric-isothermal potentials of the formation of lead oxide in melts of pure oxide ΔZ_0 and melts with the concentrations indicated ΔZ_1, the change in the isobaric-isothermal potentials $\Delta \bar{Z}_1$, enthalpy $\Delta \bar{H}_1$, and entropy $\Delta \bar{S}_1$ during the transfer of one mole of lead oxide from the pure oxide melt to the melts with the concentrations indicated, the excess isobaric-isothermal potentials ΔZ_{1exc} and entropy ΔS_{1exc}, which characterize the deviation of these melts from the ideal state, and the activity of the lead oxide a_1.

The values obtained were in turn used for finding the values for silicon dioxide with the aid of the Gibbs-Duhem-Margolies-Lewis equations.

As an example, Table 1 shows the activity of lead oxide and silica calculated from the emf values for 800, 940, 1000, and 1100°.

The values obtained for the thermodynamic properties of the oxides in melts of the system $PbO-SiO_2$ agree satisfactorily with the data of O.Ye. Yesin, B.M. Lepinskiy, and V.I. Musikhin [17] and other authors [8, 9, 12]. However, in contrast to the data of these authors, they show a more or less marked change in the character of the dependence as a function of composition near points corresponding to the stoichiometric component ratios of $4PbO \cdot SiO_2$, $2PbO \cdot SiO_2$, $3PbO \cdot 2SiO_2$, $PbO \cdot SiO_2$, and $2PbO \cdot 3SiO_2$*.

*These peculiarities of the variation in the properties could not be detected by the authors mentioned, due to the small quantity of melt investigated /11, 12/ and the insufficient accuracy of the determination [8, 9].

Table 1

Activity of Lead Oxide and Silica in Melts of the System PbO-SiO_2 as a Function of Composition and Temperature

Molar fraction SiO_2	a_{PbO}				a_{SiO_2}			
	900	940	1000	1100	840	940	1000	1100
0.	1,000	1,000	1,000	1,000	0	0	0	0
0,070	1,000	0,914	0,964	0,989		0,00267	0,00361	0,00346
0,103	1,000	0,909				0,00124		
0,134	1,000	0,811	0,831	0,863	0	0,00085	0,00882	0,0138
0,164	0,805	0,765	0,789	0,777	0,00813	0,0118	0,0116	0,0106
0,192	0,723	0,682	0,695	0,690	0,0126	0,0202	0,0203	0,0209
0,219	0,655	0,632	0,622	0,612	0,0204	0,0274	0,0355	0,0432
0,244	0,570	0,585	0,579	0,612	0,0280	0,0351	0,0424	—
0,269	0,512	0,517	0,548	0,544	0,0387	0,0425	0,0495	0,0653
0,315	0,419	0,474	0,474	0,500	0,0523	0,0724	0,0703	0,0777
0,356	0,318	0,343	0,371	0,402	0,107	0,118	0,114	0,127
0,354		0,350			—	0,129		
0,373	0,240	0,283	0,306	0,333	0,170	0,158	0,163	0,173
0,396	0,239	0,278	0,284	0,322	0,183	0,172	0,175	0,185
0,414	0,166	0,200	0,212	0,212	0,283	0,291	0,269	0,280
0,432	0,159	0,186	0,205	0,218	0,303	0,355	0,295	0,289
0,466	0,125	0,166	0,183	0,211	0,395	0,366	0,338	0,334
0,482	0,123	0,153	0,174	0,201	0,454	0,391	0,363	0,354
0,512	0,0614	0,0950	0,108	0,146	0,684	0,643	0,596	0,488
0,526	0,0563	0,0863	0,0987	0,125	0,790	0,707	0,645	0,565
0,540	0,0539	0,0813	0,0952	0,117	0,897	0,74.	0,671	0,586
0,579	0,0527	0,0769	0,0918	0,109	0,916	0,773	0,691	0,517
0,591	0,0516	0,0700	0,0853	0,0940	0,939	0,828	0,731	0,696
0,603	0,0494	0,0578	0,0826	0,0668	0,946	0,923	0,909	0,874
0,610	0,0473	0,0566	0,0603	0,0636	0,975	0,953	0,923	0,908
0,614	0,0453	0,0535	0,0571	0,0614	1,000	0,965	0,940	0,922
0,625	—	0,0535	0,0542	0,0578	—	1,000	0,966	0,968
0,657	—	—	0,0512	0,0570	—	—	1,000	—
0,667	—	—	—	0,0546	—	—	—	1,000

1) Molar fraction.

We used the values of the thermodynamic properties of the oxides in the equation

$$G = N_1\bar{G}_1 + N_2\bar{G}_2,^*$$

to determine the integral values of the isobaric-isothermal potential, enthalpy, and entropy of melt formation and the isobaric-isothermal potentials, enthalpy, and entropy of the formation of compounds of lead oxide and silica from molten lead oxide and tridymite.

The isobaric-isothermal potentials of the formation of these compounds were determined as the sum of the changes in the isobaric-isothermal potentials during the transfer into the compound melt of a corresponding number of moles of oxides from pure lead oxide melts and melts saturated with si-

*Here G, G_1, and G_2 are the integral and differential values for the solution and the components, while N_1 and N_2 are the molar component fractions.

Table 2

Isobaric-Isothermal Potentials, Enthalpy, and Entropy of the Formation of Lead Oxides and Silicates

④ Формула соединения	① ΔZ ± 200 кал/г-моль, при температурах					Среднее значение ② 800 1100°	
		800°	900°	1000°	1100°	③ ΔH = 200 кал/г-моль	⑤ ΔS = 0,3 кал/г-моль·град
PbO	—	—	−22,600	−21,220	−19,510	−15,260	18,69
9 PbO·SiO$_2$	—	−13,120	−12,800	−13,000	13,650	−6,160	5,0
4 PbO·SiO$_2$*	−10,500	—	—	—	—	—	—
2 PbO·SiO$_2$	—	−9,570	−10,250	−10,900	10,150	−6,700	2,95
2 PbO·SiO$_2$*	−9,110	—	—	−11,090	−10,990		
3 PbO·2 SiO$_2$	—	−16,740	−17,540	17,830	−18,310	−11,120	5,26
PbO·SiO$_2$	—	−6,230	−6,640	−6,870	−7,170	−2,850	3,16
PbO·SiO$_2$*	−6,010	—	—	−7,010	−6,900	—	—
2 PbO·3 SiO$_2$	—	−13,120	−14,070	−14,850	15,150	−4,200	7,95

*According to the data of Richardson and Webb [87].
1) ΔZ ± 200 cal/g·mole, at temperatures of; 2) mean value; 3) cal/g·mole; 4) formula of compound.

lics, for which $\Delta\bar{Z}_{PbO}$ and $\Delta\bar{Z}_{SiO_2}$ are by definition equal to zero*

The data obtained by calculating the values of the thermodynamic properties of the melts are given in Fig. 2 and those for the compounds are given in Table 2.

Table 2 also shows the experimentally obtained values of the isobaric-isothermal potential of the formation of lead oxide by the reaction

ж·liquid $\qquad Pb_ж + 0.5O_2 = PbO_ж$

and the data obtained by other authors.

The isobaric-isothermal potentials shown in Table 2 for the formation of the compounds are satisfactorily expressed in the form of linear functions of temperature and agree among themselves.

*Melts saturated with silica and melts of pure lead oxide were selected as standard in calculating the activities of the oxides; for these $a_{PbO} = 1$ and $a_{SiO_2} = 1$.

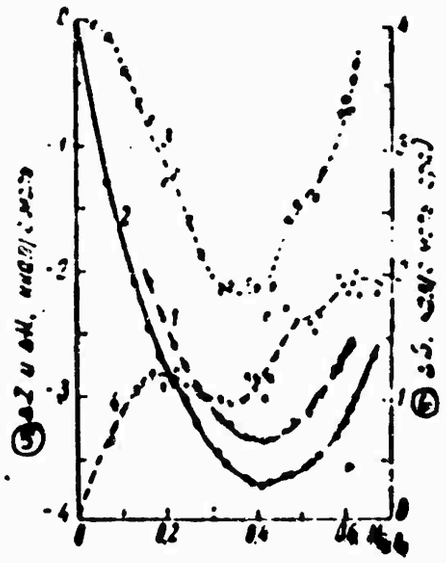

Fig. 2. Integral values of isobaric-isothermal potential at 800° (1) and 1100° (2), enthalpy ΔH (3), and entropy ΔS (4) of the formation of melts of PbO-SiO_2 mixtures from molten lead oxide and tridymite, 5) ΔZ and ΔH, kcal/g·mole; 6) ΔS, cal/g·mole·degrees.

The data obtained explain the cause of the changes in the character of the dependence of a number of physicochemical properties on composition at compositions close to those corresponding to certain other compounds formed by lead oxide and silica, a phenomenon manifested more clearly at elevated temperatures, and permit us to estimate the isobaric-isothermal potentials, enthalpy, and entropy of the reactions of lead silicates with one another.

Conclusions

1. We measured the emf of the chemical chains

$$Pb|x\,PbO + (1-x)\,SiO_2|O_2(P_{O_2} = 1\ atm),\ Pt$$

at temperatures of 800, 900, 940, 1000, 1100, and 1200° within the range of concentrations in which the system PbO·SiO_2 is homogeneous.

2. Using the results of these measurements as our basis we calculated the isobaric-isothermal potentials of the formation of lead oxide in melts of PbO and mixtures of PbO and SiO_2, the change in the isobaric-isothermal potential, enthalpy, and entropy during the transfer of one mole of lead oxide from a pure oxide melt and one mole of silicon dioxide from a melt saturated with silica into a melt of a given concentration, as well as the integral values of the isobaric-isothermal potential, enthalpy, and entropy of the formation of melts from molten lead oxide and tridymite.

3. It was shown that the electromotive forces of the chemical chains and the other properties of melts of the system $PbO-SiO_2$ undergo a change in the character of their dependence on composition at points corresponding to the stoichiometric component ratios of $4PbO \cdot SiO_2$, $2PbO \cdot SiO_2$, $3PbO \cdot 2SiO_2$, $PbO \cdot SiO_2$, and $2PbO \cdot 3SiO_2$.

4. We determined the isobaric-isothermal potentials, enthalpy, and entropy of the formation of compounds of lead oxide with silica.

Bibliography

1. E.F. Geller, A.S. Creamer, E.N. Bunting, J. Res. Nat. Bur. Standards, 13, 23, (1934).

2. M.M. Skornyakov, Fiziko-chimicheskiye svoystva troynoy sistemy okis' natriya -- okis' svintsa -- kremnezem /Physicochemical Properties of the Ternary System Sodium Oxide -- Lead Oxide -- Silica/, Collection edited by I.V. Grebenshchikov, Izd-vo AN SSSR, Moscow-Leningrad, p. 39, 1949.

3. K.S. Yevstrop'yev, Collection edited by I.V. Grebenshchikov, Izd-vo AN SSSR, Moscow-Leningrad, p. 83, 1949.

4. J.B.M. Bockris, C.W. Mellors, J. Phys. Chem., 60, 1321 (1956).

5. A.S. Kheynman, L.I. Rybakova, Izv. AN SSSR OTN /News of the Academy of Science USSR, Department of Technical Sciences/, 11, 1685 (1949).

6. V.I. Minenko, S.M. Petrov, N.S. Ivanova, Izv. VUZ. Khimiya i khimich. tekhnologiya /News of Higher Educational Institutions, Chemistry and Chemical Technology/, Vol. IV, Nos. 1, 3 (1961).

7. V.I. Minenko, S.M. Petrov, N.S. Ivanova, Steklo i keramika /Glass and Ceramics/, No. 6, 34 (1960).

8. F.D. Richardson, L.E. Webb, Bull. Inst. Mining and Metallurgy, July, No. 584, 529 (1955).

9. R.J. Collow, Trans. Faraday Soc., April, 47, No. 340, 370 (1951).

10. Yu.K. Delimarskiy, V.A. Andreyeva, G.D. Nazarenko, Fizicheskaya khimiya rasplavlennykh soley i shlakov /Physical Chemistry of Molten Salts and Slags/, Metallurgizdat, Moscow, p. 442, 1962.

11. O.A. Yesin, B.M. Lepinskikh, V.I. Musikhin, Izv. AN SSSR OTN, Metallurgiya i toplivo /News of the Academy of Sciences USSR, Department of Technical Sciences, Metallurgy and Fuels/, No. 4, 1959.

12. Ito, Yaganase, Suginokhar, Nikhon Koyekhay Si, J. Mining and Metallurgy Inst. Japan, 74, No. 841, 447 (1958).

13. Ito, Yaganase, Kyusyu Kodzan gakkaysi, J. Mining Inst. Kyushu, Japan, 29, No. 1, 29 (1961).

14. Yu. K. Delimarskiy, G.D. Nazarenko, Ukrainskiy khimicheskiy zhurnal [Ukrainian Chemical Journal], Vol. 27, 4, 458 (1961).

15. V.I. Minenko, S.P. Petrov, N.S. Ivanova, Izv. VUZ. Chernaya metallurgiya [News of Higher Educational Institutions, Ferrous Metallurgy], 7, 10 (1961).

Manuscript submitted 28 November 1962

REDUCIBILITY OF LEAD AGGLOMERATES

By A.Ye. Guriyev, M.B. Tsalikova, Northern Caucasian Mining and Metallurgical Institute, Chair of Heavy-Metal Metallurgy

Pages 70-76

The relative ease with which lead and its oxides and silicates can be reduced by carbon monoxide is indicated by thermodynamic data and the results of study of the kinetics of these processes. According to the data of investigators, the reduction of PbO by carbon monoxide begins at 160-185° [1]; reduction proceeds at an insignificant rate at 300°, at a marked rate at 500°, and intensively at 600° [2, 3]. The reduction of lead from lead orthosilicate by carbon monoxide goes very slowly at 550° and more markedly at 600° [4].

In connection with the fact that cases of insufficient reduction of lead from agglomerate and cases of a corresponding enrichment of the slag in the metal are observed in shaft-furnace smelting, the practically important question of the reducibility of lead from agglomerates in the upper low-temperature (400-800°) regions of shaft furnaces is of definite interest. On the basis of the compositions of typical lead agglomerates, one would expect that carbon monoxide would deoxidize primarily the oxides of iron and lead, if negligibly small quantities of copper, antimony, arsenic, and tin were present.

During the sintering of lead charges a significant percentage of the hematite in the ferrous flux is converted to magnetite. It is known that hematite ores are more easily reduced than natural magnetites, although they contain more oxygen per unit of iron. The question of the reducibility of the magnetite produced during sintering is not elucidated in the literature, although it is of similar interest. The authors know only of the opinion of V.A. Sorokin and his colleagues, who hold that "magnetite, as an intermediate reduction product, has a high chemical activity and does not need refining" [5]. The experiments on the reduction of lead agglomerates described below were therefore preceded by experiments on the reduction of artificial

Table 1

Composition of Starting Materials for Experiments (in %)

① Руда	② $Fe_{общ}$	Fe^{2+}	SiO_2	CaO	H_2O
③ Криворожский гематит 1	55,22	--	13,0	0,82	8,22
Криворожский гематит 2	54,65		24,73	--	0,50
④ Плотный гематит	68,95	нет ⑧	3,76	-	0,16
⑤ Магнетит природный	68,77	21,77	-		нет
⑥ Бурый железняк (Бакальское месторождение)	38,8	нет	-	—	11,20
⑦ Мартит (г. Магнитная)	59,78	-	10,93	нет	2,45

1) Ore; 2) total; 3) Krivorozh'ye hematite; 4) compact hematite; 5) natural magnetite; 6) limonite, (Bakalskoye deposit); 7) martite (Magnitnaya); 8) none.

magnetites and hematites from which such magnetites are obtained.

Definition of relative reducibility of artificial magnetite. In the experiments we used samples of iron ores (Table 1) from which small cubes with edge lengths of 6 mm were cut and prepared artificial magnetites by two methods: introduction of the small hematite cubes into the lead charge and subsequent sintering under laboratory conditions, and prolonged heat treatment of the cubes in a nitrogen atmosphere at 1150°. In this case we obtained samples in which the degree of reduction of hematite to magnetite was approximately 85%, as determined from the decrease in weight, from magnetic measurements, and petrographically. We used chiefly the second method for preparing the artificial magnetites, since it was rarely possible to avoid slagging of the small cubes during the sintering of the charge when employing the first method.

Preliminary experiments were conducted on the comparative reducibility of natural oxides and artificial magnetites in a hydrogen atmosphere in a horizontal furnace, the samples being weighed at intervals, and in a hydrogen and carbon monoxide atmosphere in a vertical tubular furnace with continuous weighing.

During the performance of the experiments in the horizontal furnace (Fig. 1) small cubes of the samples to be tested, having been weighed with an accuracy of up to 2 mg, were placed in a porcelain boat and reduced in a transparent quartz tube in a hydrogen atmosphere for 20 min at 800°. Heating was carried out with a small furnace which was freely movable along the reaction tube. This made it possible to observe a given reduction time precisely and to cool the samples rapidly. The velocity of the gas in the reaction zone was approximately 1.5 cm/sec. The extent of reduction was calculated from the decrease in the weight of the sample.

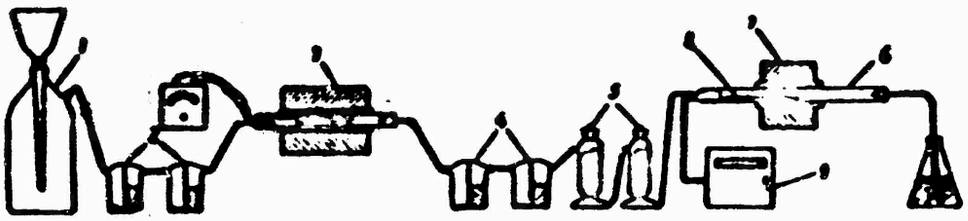

Fig. 1. Diagram of setup of horizontal furnace for reduction of iron oxides with hydrogen. 1) Gas meter; 2-5) gas purification system; 6) reaction tube; 7) heating furnace; 8) thermocouple; 9) contact galvanometer.

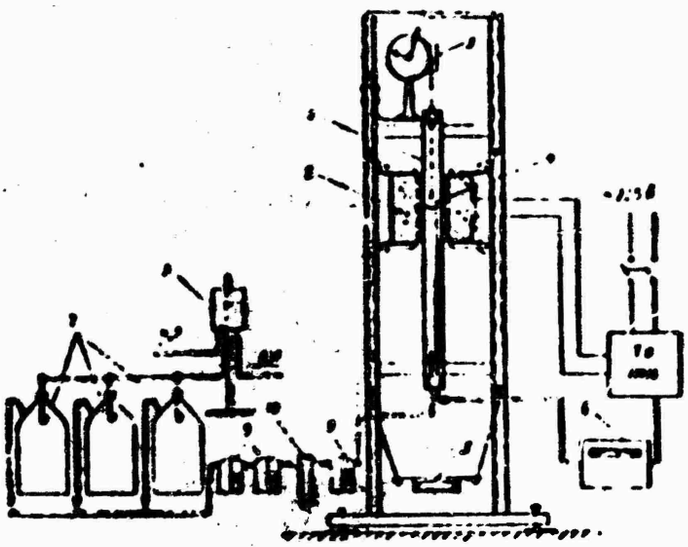

Fig. 2. Diagram of setup of vertical furnace for reduction of iron oxides and agglomerates with hydrogen and carbon monoxide. 1) Quartz tube; 2) heating furnace; 3) counterweight; 4) torsion balance; 5) nichrome basket; 6) temperature regulator; 7) gas meters; 8) pressure stabilizer; 9-10) gas purification system; 11) manometer.

Two experiments were conducted. In the first experiment two small cubes were simultaneously placed in the small boat, one of Krivorozh'ye hematite and the other of artificial magnetite obtained from it under sintering conditions. Three small cubes were used in the second experiment, one of compact hematite, one of artificial magnetite (reduction product of compact hematite), and one of natural magnetite.

The extent of reduction, qualitatively confirmed by petrographic analysis, was 32.11% for Krivorozh'ye hematite I, 26.03% for its artificial magnetite, 16.13% for compact hematite, 57.63% for its artificial magnetite, and 44.08% for natural magnetite

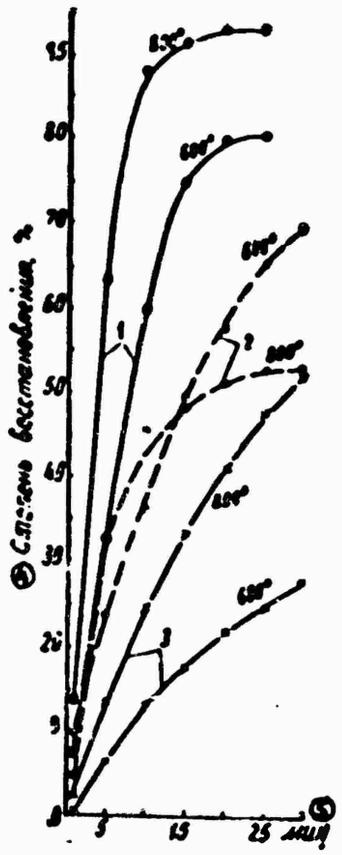

Fig. 3. Reduction of iron oxides with hydrogen. 1) Krivorozh'ye hematite; 2) artificial magnetite; 3) natural magnetite; 4) degree of reduction; 5) min.

These data show that artificial magnetite is reduced significantly more slowly than the initial Krivorozh'ye hematite and, conversely, that artificial magnetite obtained from compact hematite is reduced faster than the initial material. The latter phenomenon does not occur frequently, since such compact, difficult-to-reduce hematite, similar in these qualities to welding slag, is rarely encountered in nature.

The second cycle of experiments was conducted in a vertical furnace equipped with a torsion balance (Fig. 2). This installation made it possible to establish the weight of the sample and the loss of oxygen with time at any desired intervals.

In the first series of experiments samples of Krivorozh'ye hematite 2, artificial magnetite obtained from this hematite, and natural magnetite were tested in a hydrogen atmosphere. The results of these experiments are shown in the form of graphs in Fig. 3, which gives us some idea of the comparative reduction rate of iron oxides and shows its similarity to the data obtained in the preliminary experiments. The only decrease in activity observed is for

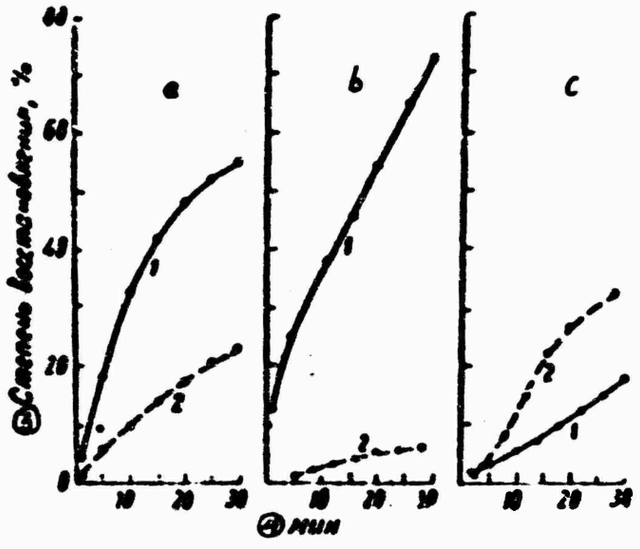

Fig. 4. Reducibility of hematite ores and magnetites obtained from them with carbon monoxide. a) Krivorozh'ye ore; b) limonite from Bakalskoye deposit; c) Magnitogorsk magnetite; 1) initial hematite; 2) corresponding magnetite; 3) extent of reduction; 4) min.

Table 2

Comparative Rate of Hydrogen Reduction

Материал	Температура опыта, °С	Исходный вес образца, мг	Потеря в весе, мг	Продолжительность опыта, мин
Криворожский гематит	600	620	130	12
	800	636	133	30
Природный магнетит	600	605	16	30
	800	583	79	30
Свинцовый шлак	600	527	3	60
	800	520	8	30

1) Material; 2) experimental temperature; 3) initial weight of sample, mg; 4) loss in weight, mg; 5) duration of experiment, min; 6) Krivorozh'ye hematite; 7) natural magnetite; 8) lead slag.

artificial magnetite (obtained from Krivorozh'ye hematite) at 800° and this is full; explained by the change which occurs in the physical structure of the sample (compaction) when the temperature rises.

The second series of experiments was conducted in a carbon monoxide atmosphere with Krivorozh'ye hematite and limonite from the Bakalskoye deposit (Fig. 4); it was established that magnetites obtained from these minerals

Table 3

Chemical Composition of Agglomerates (%)

1) Агломерат	7) $Pb_{общ}$	$Pb_{вост}$	Fe	CaO	SiO_2	$S_{общ}$
2) Лабораторный	40,76	0,09	18,52	6,25	14,88	2,13
3) Эл-ца Электроцинк	40,57	0,14	12,46	9,76	11,64	1,94
4) Лениногорский	39,53	0,44	13,64	7,52	10,70	1,61
5) Усть-Каменогорский	45,50	1,81	12,07	2,36	8,20	2,84
6) Чимкентский	36,88	0,66	12,37	6,39	10,90	1,52

1) Agglomerate; 2) laboratory; 3) Elektrotsink Plant; 4) Leninogorsk; 5) Ust'-Kamenogorsk; 6) Chimkent; 7) total.

were reduced considerably more slowly. The opposite result was obtained for Magnitnaya martite, artificial magnetite obtained from it displaying better reducibility than the initial ore sample.

Thus, of the four different hematite ores two exhibited a lower reducibility for the magnetite obtained from them, while two others displayed a higher reducibility for the corresponding magnetites. It follows from this that artifical magnetites can be reduce to a greater or lesser extent than the initial hematites, depending on the nature of the latter.

In addition to the iron oxides, the reducibility of a highly magnetic sample of lead slag containing 7% Pb with hydrogen was investigated in the vertical furnace. As one might have been led to expect, the reduction of the iron and lead of the slag by carbon monoxide was insignificant (Table 2).

Determination of reducibility of agglomerates. The same vertical tubular furnace with a torsion balance was used to determine the reducibility of lead agglomerates (see Fig. 2). Laboratory-prepared agglomerates and samples of factory agglomerates, an incomplete analysis of which is given in Table 3, were tested.

As the criterion of reducibility we used the total loss in weight due solely to loss of oxygen by the agglomerate. We selected samples weighing approximately 2 g for the experiments. The gas flow velocity was constant in all the experiments and the true gas flow velocity was calculated from the volume of gas consumed after each experiment.

In preliminary experiments we investigated the holding of samples of the laboratory agglomerates at 800° for one hour, purified nitrogen being passed over them. The weight of the samples did not change; consequently, loss of lead by evaporation was not taken into account at experimental temperatures of less than 800°.

In the first series of experiments we determined the rate of hydrogen

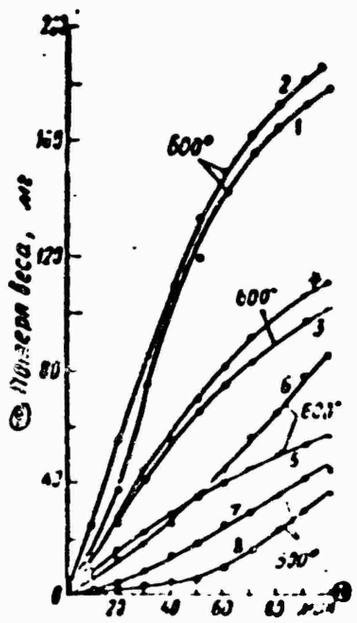

Fig. 5. Reduction of lead agglomerates by hydrogen (first series of experiments). 1, 2) porous laboratory (41-56%); 3, 4, 7, 8) porous commercial (34-40%); 5, 6) fused commercial (15-20%); 9) loss in weight, mg; 10) min.

reduction of agglomerates of varying porosity at temperatures of 500 and 600° for 100 min. The results of parallel experiments showed a definite degree of divergence (Fig. 5); this was not very great and may be fully explained by the heterogeneity of the structure of small agglomerate samples.

As the degree of reduction we used the ratio of the loss of oxygen during reduction to the oxygen bonded to the iron and lead in the initial sample. Moreover, half of the iron in the initial sample was bonded into oxide and half into magnetic oxide. Such an appraisal is grossly approximate, but is acceptable for qualitative considerations.

The curves in Fig. 5 indicate that porosity and temperature have a significant influence on the rate at which the agglomerate is reduced. Thus agglomerates of approximately the same porosity exhibited a degree of reduction of 22.0% at 500° and 53.3% at 600° (curves 7 and 4). At a temperature of 600° and an experiment time of 100 min the degree of reduction for agglomerates with porosities of 15-20, 34-40, and 41-56% were 28.1, 53.3, and 69.6% respectively (curves 2, 4, 5). Consequently, transition from fused to high-porosity agglomerate showed that reducibility increases by a factor of approximately 3, this being roughly proportional to the porosity.

The second series of experiments on the reduction of agglomerates by hydrogen was carried out as a control, at lower temperatures (400 and 450°). We tested laboratory fused agglomerate with a porosity of approximately 25% and laboratory porous agglomerate with a porosity of 45-50%.

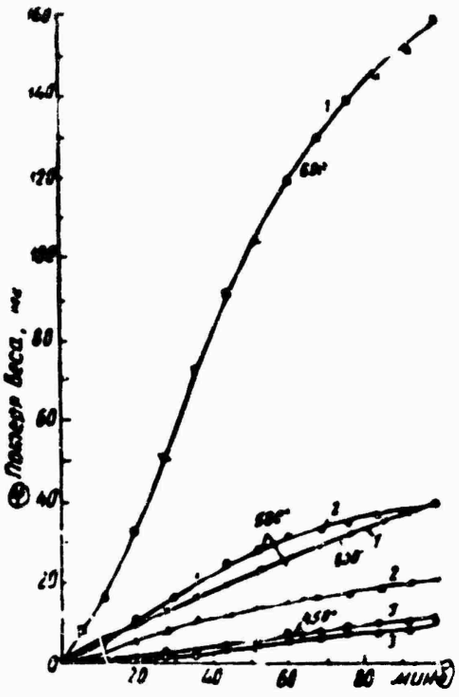

Fig. 6. Reduction of lead agglomerates by hydrogen (second series). 1, 2, 3) Porous agglomerates; 1', 2', 3') fused agglomerates; 4) loss in weight, mg; 5) min.

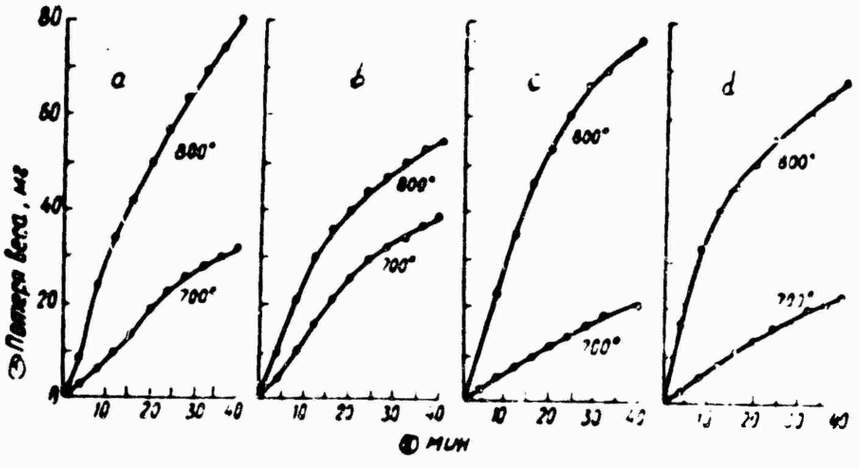

Fig. 7. Reduction of lead agglomerates from Elektrotsink (a), Leninogorsk (b), Ust'-Kamenogorsk (c), and Chimkent (d) Plants with carbon monoxide. 1) Loss in weight; 2) min.

The results of the experiments confirmed that agglomerate porosity and temperature have a considerable effect on reduction rate and showed that the influence of porosity is greatly intensified as the temperature rises. Fig. 6 contains no curve for 400°, since no agglomerate reduction was detected in

three experiments involving times of 40 min at this temperature.

The third series of experiments was devoted to elucidating the rate at which lead agglomerates are reduced by carbon monoxide.

In this series of experiments agglomerates from four lead plants were reduced at temperatures of 600, 700, and 800°, a gas flow velocity through the reaction zone of 2.0-2.3 cm/sec, and an experiment time of 40 min. Fig. 7 shows the rate of reduction of these agglomerates by carbon monoxide as a function of temperature. This figure has no curves for the reduction rates of the agglomerates at 600°, since they did not show any signs of reduction at this temperature.

The calculated degree of reduction after 40 min at 800° was 49.3% for the Elektrotsink agglomerate, 32.6% for the Leninogorsk agglomerate, 49.4% for the Ust'-Kamenogorsk agglomerate, and 45.1% for the Chimkent agglomerate. The relatively low reducibility of the Leninogorsk agglomerate is due to the high density of the sample (porosity of 15-20%).

Numerous small balls of metallic lead were visible to the naked eye on the agglomerate samples after the reduction experiments. Chemical analysis of the metallic lead content of the reduced agglomerate samples from three plants gave the following result: Elektrotsink -- 7.97% at 700° and 11.4% at 800°; Leninogorsk -- 6.41% at 700° and 9.89% at 800°; Chimkent -- 3.79% at 700° and 15.33% at 800°.

Consequently, under the experimental conditions the extent to which lead is reduced by carbon monoxide at 800° was approximately 25-40%.

Conclusions

1. We considered the behavior of ferric oxides under the conditions which obtain in the agglomeration of lead. It was established that part of the iron, which changes to magnetite during agglomeration, can be reduced to a greater or lesser extent than the initial hematite, depending on its quality.

With easily reduced hematite ores of the Krivorozh'ye or Bakalskoye types the corresponding magnetites are more difficult to reduce; magnetites obtained from compact, hard-to-reduce nonmagnetic ores are reduced relatively more easily than the initial ores.

2. We studied the influence of temperature (in the range 400-800°) on the rate at which lead agglomerates are reduced by hydrogen and carbon monoxide. Hydrogen started to reduce the agglomerates noticeably at 450° and reduced them intensively at 600°.

Carbon monoxide had no effect on the lead agglomerates at 600°, reduced them noticeably at 700°, and caused intensive reduction at 800°. At a temp-

erature of 800° and a reduction time of 40 min with carbon monoxide lead agglomerates weighing approximately 2 g lost about 50% of the oxygen bonded to their iron and lead.

3. It was established that the porosity of the agglomerates had a significant effect on their reduction rate. The reduction rate of porous agglomerates was approximately three times as great as that of compact, low-porosity agglomerates.

4. Recirculated slag rich in lead shows percept'ble signs of hydrogen reduction only at 800°.

Bibliography

1. Ya.I. Gerasimov, A.N. Krestovnikov, A.S. Shakhov, Khimicheskaya termodinamika v tsvetnoy metallurgii /Chemical Thermodynamics in Nonferrous Metallurgy/, Vol. II, 1961.

2. Yu.V. Tsvetkov, D.M. Chizhikov, Tr. in-ta metallurgii im. A.A. Baykova /Transactions of the Institute of Metallurgy imeni A.A. Baykov/, Izd-vo AN SSSR, No. 2, 1957.

3. M.M. Lakernik, L.M. Rabicheva, Sb. nauchn. trudov Gintsvetmeta /Collection of Scientific Papers of the State Scientific Research Institute for Nonferrous Metallurgy/, No. 10, 1955.

4. L.G. Berezkina, D.M. Chizhinkov, Izv. AN SSSR OTN /News of the Academy of Sciences USSR, Department of Technical Sciences/, No. 5, 1958.

5. V.A. Sorokin et al., Sb. nauchn. trudov metall. fak-ta Donetskogo industr. in-ta /Collection of Scientific Papers of the Metallurgy Faculty of the Donetsk Industrial Institute/, No. 4, 1955.

Manuscript submitted 5 January 1963

THE ROLE OF ANTIMONY DURING THE EXTRACTION OF BISMUTH FROM LEAD

By P. I. Fedorov and V. I. Shachnev,
Moscow Institute of Fine Chemical Technology.
Chair of Chemistry and Technology of Rare and
Scattered Elements

pp 77--84

For the production of highest grade lead after the removal of most bismuth by the addition of calcium and magnesium ("coarse bismuth extraction" process) a preliminary extraction of bismuth is usually carried out by introducing antimony to the lead bath. The antimony skimmings (dross) which are formed in the process concentrate bismuth, reducing its contents in the bath to a minimum ("fine bismuth extraction" process).

The fine bismuth extraction process requires a careful execution. It is sensitive to any changes of working conditions and has so far been hardly studied. The individual contradictory data on the role of antimony which are available in literature do not elucidate the practical value of the process which largely depends on the experience and skill of the service personnel.

In the first paper dealing with the possibility of preliminary bismuth extraction by antimony, D. Betterton and Yu. Lebedev [1] reported that under "appropriate conditions" antimony (and arsenic) added to lead with small quantities of bismuth, calcium and magnesium will form dross in which these admixtures are concentrated so that preliminary bismuth extraction from lead occurs. Under industrial conditions this process produced lead with 0.005% Bi and under laboratory conditions lead with 0.0005% Bi. Noting the invariable ratio

of the Bi, Ca, Mg and Sb concentration in the dross at certain temperatures, the authors emphasize the chemical role played by the introduced antimony.

Considering the process of fine bismuth extraction as described by D. Betterton and Yu. Lebedev, Holms [2] contends that the added antimony forms Ca_3Sb_2 and Mg_3Sb_2 antimonides, improving the liquation of small bismuthide crystals, i.e., the role of antimony in the process of bismuth extraction is purely physical. Because of lack of information on the quaternary compound $Bi_nCa_mMg_pSb_q$, Davy [3] concurs with the view on the role of antimony. The possibility of obtaining lead of the highest grade (up to 0.006% Bi) without antimony, provided the process of coarse bismuth extraction is carefully conducted, has also been considered [4]. Recently, a view was expressed that the effect of antimony in the extraction of bismuth stems from the formation of the quaternary compound $BiCa_5Mg_{10}Sb_5$ which has the lowest solubility in lead [5].

It follows from the above short outline that the question of the effect of antimony in the process of fine bismuth extraction from lead remains an open one. We have attempted to explain this role by studying the solubility of bismuth, calcium, and magnesium in lead in the presence of antimony. Earlier data on the common solubility of bismuth and magnesium, magnesium and antimony [6], calcium and antimony [7], bismuth and magnesium [8], bismuth and calcium [9], as well as magnesium and calcium [10] in lead at a temperature of 400°C provided the possibility of investigating the common solubility of calcium, magnesium and antimony, bismuth, magnesium and antimony, and bismuth, calcium and antimony in lead at 400°C as well as the 400°C isotherms of the systems Pb-Ca-Mg-Sb, Pb-Bi-Mg-Sb, and Pb-Bi-Ca-Sb.

The method of investigation comprised the following: the alloys were hardened after attaining equilibrium and submitted to chemical analysis, whereby the specimens for the analysis were taken from the lower "liquid" and the upper "solid residue" portion of the alloys.

A method specially developed for the determination of bismuth when substantial amounts of antimony were present was applied. Calcium and magnesium were determined by complexometric titrating: calcium with murexide, magnesium with erioferrous chromium [11]; bismuth depending upon its contents was determined by pyrocatechin titrating [11] or colorimetrically with thiourea [12]. Antimony was determined by per-

manganate titration [13] or colorimetrically with a violet crystal dye [14].

The results of the analyses were plotted on a diagram; then, the composition of the solid phase was determined by the Shkreynemaker method of residues. We have described the method of preparing alloys at greater length in earlier papers [7, 10]. Microphotographs of the alloys were prepared and the microhardness of liquated crystals was measured with the help of a "PMT-3" tester with a load of 20 and 50 g.

Table 1

Common Solubility of Calcium and Magnesium Antimonides

(a) Состав, вес. %				(d) Твердая фаза
(b) „жидкость"		(c) „твердый остаток"		
Ca_3Sb_2	Mg_3Sb_2	Ca_3Sb_2	Mg_3Sb_2	
0,119	—	—	—	Ca_3Sb_2
0,110	0,042	6,42	0,052	(e) то же
0,102	0,040	7,11	0,043	
0,093	0,063	5,14	4,42	$Ca_3Sb_2 + CaMg_2Sb_2$
0,096	0,069	5,21	3,19	
0,052	0,082	1,23	2,09	$CaMg_2Sb_2$
0,054	0,115	1,70	2,85	(e) то же
0,037	0,152	1,45	2,52	
0,039	0,22	2,06	3,57	
0,040	0,29	1,65	2,98	
0,02[illegible]	0,39	1,55	2,40	
0,027	0,46	1,91	3,48	
0,031	0,52	2,01	3,81	
0,040	0,63	1,29	2,36	
0,017	0,70	1,61	2,92	
0,033	0,81	1,64	3,20	
0,034	1,05	0,65	2,89	$CaMg_2Sb_2 + Mg_3Sb_2$
0,027	1,29	0,025	5,12	Mg_3Sb_2
0,015	1,37	0,030	4,72	(e) то же.
0,010	1,58	0,020	6,05	
—	1,80	—	—	

Key: a) Composition, weight; b) "liquid"; c) "solid residue"; d) solid phase; e) same.

The solubility of calcium and magnesium antimonides. The character of the common solubility of calcium and magnesium antimonides in lead was investigated in alloys with an invariable Pb-Ca_3Sb_2-Mg_3Sb_2 section and alloys of the quaternary system Pb-Ca-Mg-Sb. The results are given in Table 1 and Figure 1a.

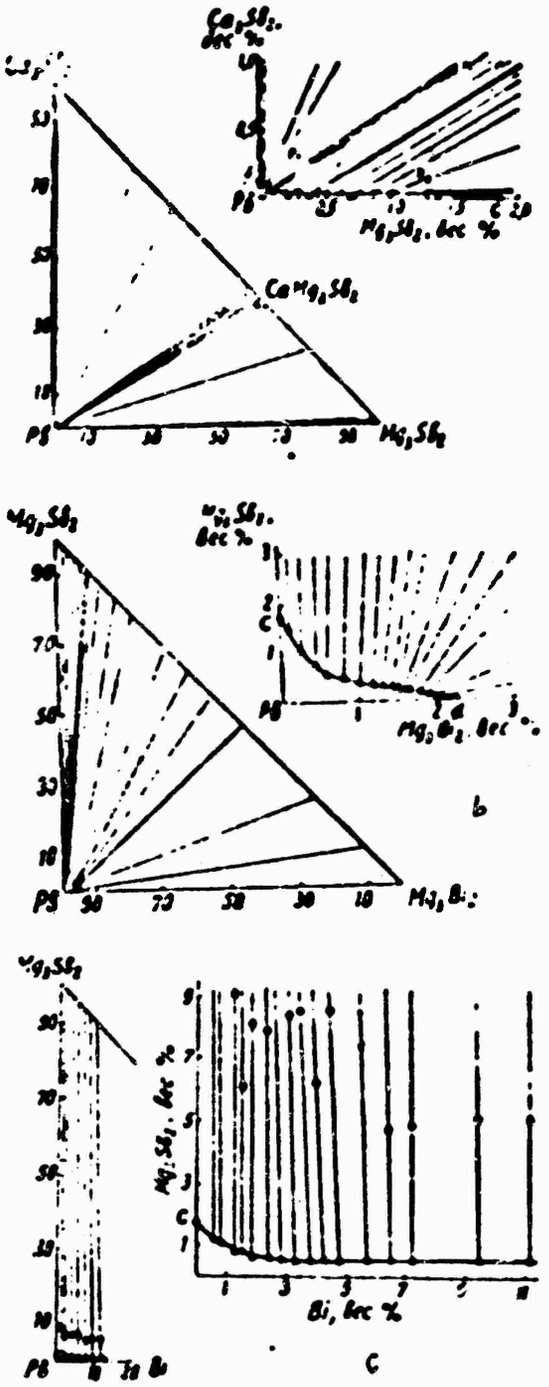

Fig. 1. Isotherms at 400°C of the lead angle of sections (a) Pb-Ca_3Sb_2-Mg_3Sb_2; (b) Pb-Ca_3Sb_2-Mg_3Bi_2 and (c) Pb-Mg_3Sb_2Bi.

The isotherm consists of three sections: section e_7 showing the solubility of the Ca_2Sb_2 compound which had crystallized in the form of small darkish round crystals [7]; section e_7e_8 defining the solubility of ternary compounds whose region of homogeneity (deflection from stoichiometry ± 0.3% calcium) includes the composition of $CaMg_2Sb_2$, i.e., the compound has a formula analogous to dibismuthide [15]. There was no way of measuring the microhardness of small $CaMg_2Sb_2$ crystals because of their small size (5 to 10 micron). The section e_8c of the isotherm showed the solubility of the Mg_3Sb_2 compound. The composition of the eutonic point e_7 was 0.093% Ca_3Sb_2 and 0.063% Mg_3Sb_2, the composition of the eutonic point e_8 0.034% Ca_3Sb_2 and 1.05% Mg_3Sb_2.

The $CaMg_2Sb_2$ compound possesses a more extensive region of homogeneity than the pertinent bismuthide [16] and crystallizes in the form of smaller crystals; the solubility of $CaMg_2Sb_2$ in lead at 400°C is 0.122% for antimony.

The solubility of magnesium bismuthide and antimonide. Results of the investigation of the Pb-Mg_3Sb_2-Mg_3Bi_2 cross-section and of the quaternary system Pb-Bi-Mg-Sb are shown

in Table 2 and Figure 1b. The solubility isotherm has one cd branch describing the composition of the specimen which is in equilibrium with solid solution Mg_3Sb_2-Mg_3Bi_2 whose disruption we have not determined. Microinvestigations revealed the presence of only one solid phase in all crystal alloys: Mg_3Sb_2-Mg_3Bi_2 solution. The detection of solid solutions between Mg_3Sb_2 and Mg_3Bi_2 was not unexpected since the latter possess all characteristics necessary for the formation of continuous metallide solutions [16].

Table 2

Common Solubility of Magnesium Antimonide and Bismuthide

(a) Состав, вес. %				(d) Твердая фаза
(b) "жидкость"		(c) "твердый остаток"		
Mg_3Sb_2	Mg_3Bi_2	Mg_3Sb_2	Mg_3Bi_2	
1,00	—	—	—	Mg_3Sb_2
1,52	0,13	6,41	0,25	(e) Твердый раствор Mg_3Sb_2–Mg_3Bi_2
1,11	0,26	5,52	0,63	(f) то же
0,92	0,43	5,01	0,90	"
0,56	0,58	3,47	1,02	"
0,49	0,88	4,52	1,52	"
0,31	0,92	5,72	1,54	"
0,26	1,27	4,37	2,26	"
0,24	1,38	6,31	2,55	"
0,20	1,42	6,05	3,72	"
0,18	1,48	6,97	4,54	"
0,12	1,56	7,90	6,30	"
0,15	1,63	7,14	7,82	"
0,13	1,77	6,25	8,81	"
0,09	1,86	5,09	9,35	"
0,06	1,98	1,90	8,44	"
0,04	2,11	0,97	8,72	"
—	2,20	—	—	Mg_3Bi_2

Key: a) composition, weight; b) "liquid"; c) "solid residue"; d) solid phase; e) solid solution; f) same.

The part of the isotherm of the lead angle of the Pb-Mg_3Sb_2-Bi section was also investigated and the findings are given in Table 3 and Fig. 1b. The section of the isotherm corresponds to the solubility of solid solution on the basis of the Mg_3Sb_2compounds.

The data obtained on alloys of the Pb-Bi-Mg-Sb system were used for a semiquantitative representation of the lead angle isotherm of the system (Fig. 2). The isotherm comprises three surfaces in accordance with the solubilities: Mg_3Sb_2 - Mg_3Pb,

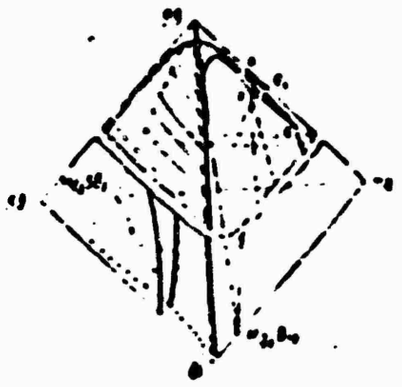

Fig. 2. Lead angle isotherm at 400°C of the Pb-Bi-Mg-Sb system.

pee$_1$ - $2Mg_2Pb$ Mg_3Bi_2 and the solubility surface of Mg_3Sb_2-Mg_3Bi_2 solid solutions. The corodes pertaining to the surface of solid solutions are basically oriented towards Mg_3Sb_2 reflecting an enrichment of the solid phase by antimony and that to a larger degree than by bismuth.

Table 3

Common Solubility of Magnesium Antimonide in Lead Bismuth

(a) Состав, вес. %				(d) Твердая фаза
(b) „жидкость"		(c) „твердый остаток"		
Mg_3Sb_2	Bi	Mg_3Sb_2	Bi	
1,80	—	—	—	Mg_3Sb_2
1,23	0,41	8,10	0, 0	(e) твердый раствор $Mg_3(Sb, Bi)_2$
1,11	0,62	9,69	0,61	(f) то же
0,83	1,19	8,92	1,22	"
0,80	1,45	5,91	1,47	"
0,71	1,85	7,90	1,80	"
0,64	2,41	7,65	2,38	"
0,60	2,81	9,19	2,75	"
0,54	3,27	8,13	3,20	"
0,47	3,76	8,21	3,70	"
0,54	4,17	6,10	4,12	"
0,50	4,72	8,16	4,65	"
0,53	5,69	7,20	5,42	"
0,50	6,51	4,90	6,29	"
0,50	7,26	4,90	7,12	"
0,52	9,41	5,11	9,31	"
0,51	11,21	5,30	11,15	"

Key: a) composition, weight; b) "liquid"; c) "solid residue"; d) solid phase; e) solid solution; f) same.

The shape of the lead angle isotherm indicates that only in the case of substantial antimony additions a negligible decrease in the bismuth contents is possible in lead which explains the usual absence of the effect of bismuth extraction from lead with magnesium whenever antimony is present.

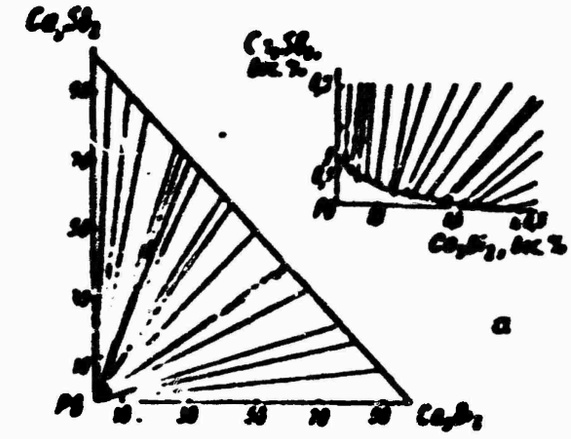

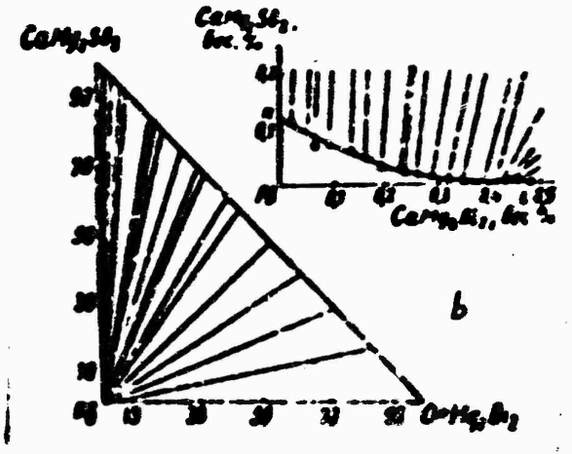

Fig. 3. Lead angle isotherm at 400°C of sections (a) Pb-Ca_3Sb_2-Ca_3Bi_2; (b) Pb-$CaMg_2Sb_2$-$CaMg_2Bi_2$.

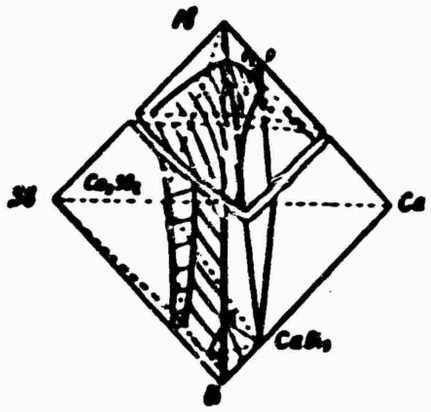

Fig. 4. Lead angle isotherm at 400°C of the Pb-Bi-Ca-Sb system.

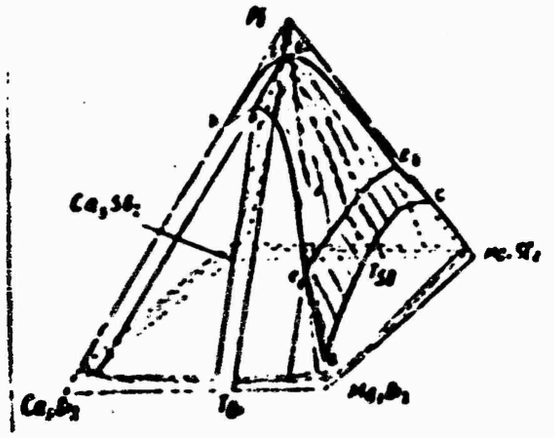

Fig. 5. Lead angle isotherm at 400°C of the quaternary reciprocal system.

The solubility of calcium bismuthide and antimonide. The results of investigating alloys of the Pb-Ca_3Bi_2-Ca_2Sb_2 cross-section of the quaternary system Pb-Bi-Ca-Sb are given in Table 4 and plotted in Fig. 3a. The character of the intersolubility is analogous to the above-described character of Mg_3Sb_2 and Mg_3Bi_2 although in this case the formed small crystals of the solid solution are of minute size (≈ 10 micron) precluding the microhardness measurement and are also much less soluble.

Although there are no data in literature about the structure, the type of bond, and so forth of Ca_3Sb_2 and Ca_3Bi_2, it

may be assumed that just like Mg_3Sb_2 and Mg_3Bi_2 these compounds correspond to all the above-described conditions which are necessary for the formation of continuous metallide solutions.

Table 4

Common Solubility of Calcium Antimonide and Bismuthide

(a) Состав, вес. %				(d) Твердая фаза
(b) „жидкость"		(c) „твердый остаток"		
Ca_3Sb_2	Ca_3Bi_2	Ca_3Sb_2	Ca_3Bi_2	
0,119	—	—	—	(e) Ca_3Sb_2
0,124	0,014	0,141	2,51	твердый раствор Ca_3Sb_2—Ca_3Bi_2
0,068	0,046	0,695	3,14	(f) то же
0,049	0,052	0,644	2,46	"
0,053	0,075	0,93	2,04	"
0,040	0,098	1,09	2,05	"
0,038	0,143	1,91	3,81	"
0,030	0,149	1,34	2,50	"
0,029	0,176	1,77	2,52	"
0,024	0,189	2,14	2,53	"
0,022	0,211	2,49	2,08	"
0,018	0,265	3,71	3,05	"
0,019	0,28	1,94	1,16	"
0,014	0,32	4,19	1,89	"
0,010	0,36	4,53	1,31	"
0,008	0,38	3,78	0,81	"
0,006	0,45	4,49	0,57	"
—	0,48	—	—	Ca_3Bi_2

Key: a) composition, weight; b) "liquid"; c) "solid residue"; d) solid phase; e) solid solution; f) same.

The lead angle isotherm of the Pb-Bi-Ca-Sb system, whose structure is analogous to the Pb-Bi-Mg-Sb isotherm in many respects, explains in a similar way the absence of bismuth extraction from lead by means of calcium whenever antimony is present (Fig. 4).

The solubility of double bismuthide and antimonide: The results of the investigation of the common solubility of $CaMg_2Sb_2$ and $CaMg_2Bi_2$ are given in Table 5 and Fig. 3b. Preceding references to sections Pb-Mg_3Sb_2-Mg_3Bi_2 (see Fig. 1b) and to Pb-Ca_3Sb-Ca_3Bi_2 make a description of section Pb-$CaMg_2Sb$ unnecessary.

Table 5

Common Solubility of Binary Bismuthide and Binary Antimonide

(a) Состав, вес. %				(d) Твердая фаза
(b) „жидкость"		(c) „твердый остаток"		
$Ca_2Mg_2Sb_2$	$Ca_2Mg_2Bi_2$	$Ca_2Mg_2Sb_2$	$Ca_2Mg_2Bi_2$	
0,122	—	—	—	$Ca_2Mg_2Sb_2$
0,114	0,023	6,17	0,141	(e) твердый раствор $Ca_2Mg_2Sb_2$ – $Ca_2Mg_2Bi_2$
0,102	0,049	7,30	0,20	(f) то же
0,053	0,058	8,02	0,26	"
0,076	0,095	8,20	0,86	"
0,074	0,102	7,51	0,95	"
0,042	0,162	8,91	1,26	"
0,024	0,189	7,19	1,39	"
0,029	0,23	5,48	1,20	"
0,029	0,24	5,42	1,84	"
0,014	0,26	4,81	2,83	"
0,012	0,28	5,25	2,43	"
0,019	0,32	5,92	3,07	"
0,009	0,34	4,43	2,45	"
0,014	0,39	4,96	3,92	"
0,034	0,41	4,16	3,41	"
0,033	0,42	2,21	3,09	"
0,035	0,43	2,63	5,29	"
0,035	0,45	1,43	5,39	"
0,004	0,46	0,82	4,81	"
—	0,47	—	—	$Ca_2Mg_2Bi_2$

Key: a) composition, weight; b) "liquid"; c) "solid residue"; d) solid phase; e) solid solution; f) same.

Figure 5 shows the solubility isotherm at 400°C of the quaternary reciprocal system consisting of Mg_3Sb_2, Mg_3Bi_2, Ca_3Sb_2 and Ca_3Bi_2 compounds and summarizes the information obtained on the common solubility of calcium and magnesium antimonides in lead. The isotherm consists of three surfaces defining the solubility in lead: solid solution Mg_3Sb_2-Mg_3Bi_2 (dce_8e_6), solid solution $CaMg_2Sb_2$-$CaMg_2Bi_2$ ($e_6e_8e_7e_5$), and solid solution Ca_3Sb_2-Ca_3Bi_2 (e_5e_7fh). The conodes of all surfaces are basically orineted towards the corresponding antimonides in view of the higher stability of the latter. The findings make it possible to visualize the role of antimony in the process of fine bismuth extraction from lead as follows. The introduction of antimony into the lead bath causes the formation of a number of Mg_3Sb_2, Ca_3Sb_2, $CaMg_2Sb_2$ antimonides which are less soluble than bismuthides owing to the fixation

of free calcium and magnesium or the destruction of finished Mg_3Bi_2, Ca_3Bi_2, $CaMg_2Bi_2$ bismuthides. The ability of the produced antimonides to form difficultly soluble solid solutions in lead leads to the formation of a phase also containing bismuth as a result of exchange ractions which is pre-extracted from lead. It may be assumed that this phase is solid solution $CaMg_2Sb_2$-$CaMg_2Bi_2$ with a considerably lower solubility than solid solution Mg_3Sb_2-Mg_3Bi_2 and a larger region of existence than solution Ca_3Sb_2-Ca_3Bi_2.

The shape of cross-sections Pb-Ca_3Sb_2-Ca_3Bi_2 and Pb--$CaMg_2Sb_2$-$CaMg_2Bi_2$ (see Fig. 3b) shows that certain optimal antimony solutions lower the bismuth contents in lead; a further increase of the antimony contents would actually not lower the contents of bismuth.

For the compositions of the lead bath as shown in the diagram of Figure 5, the composition of the solid phase would be characterized by a Bi:Sb $\approx$ 1:4 weight ratio with an optimum antimony addition while the Ca:Mg atomic ratio would be invariable (1:2) whatever the antimony addition.

With a substantial antimony content in the lead bath (over 0.1% of the weight), the resulting solid phase approximates the composition of antimonide and contains only negligible amounts of bismuth; this fact explains why bismuth cannot be eliminated from the lead bath that contains antimony by calcium and magnesium additions and why the preliminary removal of antimony is a condition <u>sine qua non</u> for a successful completion of the process of bismuth extraction from lead.

The above-mentioned minute sizes of antimonide crystals favor liquation (as observed by us in all alloy specimens containing antimony) and may impede the separation from lead due to a highly developed surface.

Summarizing the above it may be assumed that a successful implementation of the process of fine bismuth extraction from lead requires a sufficient saturation of the lead bath with calcium and a negligible (less than 0.1% of the weight) antimony content.

Conclusions

1. The common solubility of calcium and magnesium antimonides in molten lead at 400°C was established by the method of isothermal analysis. The existence of the $CaMg_2Sb_2$ ternary compound with a congruent solubility of 0.092% for antimony was determined.

2. The common solubility of Mg_3Sb_2 in lead and of Mg_3Bi_2 and Mg_3Sb_2 in bismuth lead was investigated. The existence of solid solutions Mg_3Sb_2-Mg_3Bi_2 was established.

3. The study of the common solubility of Ca_3Sb_2 and Ca_3Bi_2 and also of $CaMg_2Sb_2$ and $CaMg_2Bi_2$ showed the existence of continuous solid solutions among these pairs of compounds.

4. The lead angle isotherms at 400°C of the Pb-Bi-Mg-Sb, Pb-Bi-Ca-Sb systems and of the quaternary reciprocal of the Ca_3Sb_2, Ca_3Bi_2, Mg_3Sb_2, Mg_3Bi_2 and Pb were plotted in semi-quantitative form.

5. A theory on the role of antimony in the process of fine bismuth extraction from lead is offered.

BIBLIOGRAPHY

1. Betterton J., Lebedeff Y. Trans. AIME, 121, 205 (1936).
2. Holms L. Metal Ind., 99, No 6-8, 110 (1961).
3. Davey T. R. A. J. Metals, No 3, 341 (1956).
4. Vartanyan A. I., Krasikov A. I., Tsvetnyye metaly, No 3 18 (1946).
5. Rozhavskiy G. S., Smirnov M. P. Tsvetnyye metaly, No 6 13 (1961).
6. Fedorov P. I., Shachnev V. I., Izv. VUZ, Tsvetnaya metallurgiya, No 3, 94 (1962).
7. Fedorov P. I., Shachnev V. I. Izv. VUZ, Tsvetnaya metallurgiya, No 5, 86 (1962).
8. Fedorov P. I., Shachnev V. I., Dolgopolov A. M. Izv. VUZ, Tsvetnaya metallurgiya, No 2, 53 (1962).
9. Fedorov P. I., Shachnev V. I. Izv. VUZ, Tsvetnaya metallurgiya, No 6, 66 (1962).
10. Fedorov P. I., Shachnev V. I. Zhurnal neorg. khimii, No 6, 1962.
11. Prshibil R. Complexals in Chemical Analysis, Moscow, 1960.

12. Makaryants A. I., Zaglodina T. V., Shuvalova Ye. D., Sb. nauchnykh rabot Gosinstitua po tsvetnym metallam (Collected Works of the State Institute of Non-Ferrous Metals) No 12, 130 (1956).
13. Gillebrand V. F., Lendel G. Ye., Brayt G. A., Gofman D. I. Practical Guide for Inorganic Analysis, p 295, Moscow, 1957.
14. Lurye Yu. Yu., Filipov M. A. Zavodskaya laboratoriya, 19, 771 (1953).
15. Koster W., Soutter F., Z. Erzbergbau und Metalhuettenwesen, No 5, 303 (1952).
16. Fedorov P. I., Shachner V. I. Izv. VUZ, Tsvetnaya metallurgiya No 2, 80 (1963).
17. Kornilov N. N., Vul'f B. K. Uspekhy khimii, Vol 28, ed. 9, 1086 (1959).

Paper submitted 29 July 1962

BEHAVIOR OF ARSENIC IN THE PROCESS OF LEACHING ZINC CINDERS IN A SULFURIC ACID SOLUTION

By V. G. Ageyenkov and Z. A. Serikov,
North Caucasus Mining and Metallurgical Institute
and "Elektrozink" Plant.

pp 85--95

In zinc concentrates, arsenic occurs primarily in the form of sulfur minerals. As a rule, it is found in concentrates in quantities ranging from 0.003% to 0.02%, occasionally reaching 0.3 to 1.5%.

Above 300°C arsenic oxidizes readily in the process of sintering concentrates and volatile arsenic trioxide is formed. As_2O_3 vapor pressure at 300°C is 85 to 90 mm mercury column and at 500°C the pressure reaches 760 mm mercury column. Thus, as early as in the beginning of the sintering part of the arsenic trioxide is removed with the gases and settles together with dust in Cottrell filters. However, whenever there is a sufficient excess of air and catalysts (Fe_2O_3, CuO, PbO) are used arsenic trioxide oxidizes to nonvolatile pentoxide which forms stable arsenates $Pb_3(AsO_4)_2$, $Zn_3(AsO_4)_2$, $Cu_3(AsO_4)_2$ and others.

As a result of this process, up to 50% As remain in sintered zinc concentrates primarily in the form of pentoxide and various arsenates although the latter occur in small quantities and in the form of unoxidized arsenic sulfide in the nuclei of the sintered grains.

In the process of leaching the cinders, an attempt has been made to transfer the dissolved arsenic entirely into the sinter cake together with iron. However, in the processing of

the sinter cake by sublimation, almost all arsenic is sublimated in the oxides together with zinc, lead and cadmium. Together with the Cottrell filter dust, these oxides undergo hydrometallurgical conversion so that zinc, lead and cadmium may be extracted. At the same time, a large part of the arsenic goes into the zinc solution which is reused in the process of leaching the cinders.

Inasmuch as arsenic hardly leaves the closed cycle leaching of cinders--sublimation of the sinter cake--leaching of oxides--leaching of cinders, it gradually accumulates in the course of the process. Therefore, in practice, substantial concentrations of arsenic in circulating solutions have frequently to be considered, and occasionally they fluctuate sharply because of the variable supply of the solution from the leaching of dust and oxides.

Consequently, it is usually impossible to remove arsenic completely from the solution in the neutral leaching cycle which is one of the causes of the reconversion of cadmium into solution during the purification with zinc dust inevitably leading to the disruption of the process of zinc electrolysis and to the production of low-grade cadmium metal.

Various theories have been advanced with regard to the mechanism of arsenic removal from the solutions. As a rule, it is assumed that arsenic is eliminated from the solutions as a result of adsorption by ferrous hydroxide in the neutral leaching cycle [1]. Certain authors claim that arsenic is precipitated in the neutral cycle in the form of arsenates [2] or basic salts [3]. According to Bark and Kepls [4], precipitation of arsenic occurs during the neutralization of the solution by cinders according to the ractien

$$4Fe(OH)_3 + 3H_3AsO_3 = Fe_4O_5(OH)_3As + 5H_2O,$$

contrary to the popular view that arsenic should be in a pentavalent form in the solution to enable complete precipitation.

In spite of the diversity of views as a result of an insufficient knowledge of the mechanism of precipitation of arsenic from solutions, all authors concur that a complete precipitation of arsenic is possible only in the presence of a sufficient excess of iron in the solution and that it occurs only in the neutral leaching cycle.

According to the investigation of Bilts [5], the removal of arsenic from the solution during the precipitation of ferrous hydroxide is not as much a chemical reaction as the adsorption process which is subordinated to the equation of the adsorption isotherm:

$$x = aC^{\frac{1}{n}},$$

where x is equal to the quantity of the adsorbed substance in mg/mole per 1 g of adsorbent;
C -- the concentration of the adsorbate in the solution, mg/mole per 1 liter with an established equilibrium;
a and n -- constants. According to Bilts As and $Fe(OH)_3$ a = = 170 while 1/n = 0.195.

The calculation based on this equation shows that for a sufficiently complete precipitation of arsenic, the iron and arsenic concentrations in the solution have to correspond to a 10:1 ratio. The same conclusion was drawn on the basis of practical observations. When the iron content in the overflow of the acid thickener in the standard process amounts to 1.0 to 1.5 g/l, the arsenic content should not exceed 100 to 150 mg/l.

Together with ferrous hydroxide and an excess of cinders, the precipitated arsenic enters into an acid cycle with the lower overflow of the neutral thickener for preleaching by means of a used electrolyte. Since the precipitated arsenic easily goes into acid solutions independently of whether it is removed by adsorption or chemical reaction, a certain part of it inevitably circulates with the electrolyte that leads to the accumulation of this admixture. Finally, the concentration of arsenic may attain a value in excess of 100 to 150 mg/l that would result in its incomplete removal from a neutral solution. In practice it is usually recommended in such cases to increase the iron contents artificially in the solution until it exceeds the arsenic content ten times. This is done by adding green vitriol, iron shavings, and so forth with a corresponding quantity of manganese ore for the oxidation of iron.

Although the complete removal of arsenic becomes thus possible in the neutral cycle solution, there is no way of preventing the return of part of the arsenic into the circulating solution in the acid cycle; an accumulation of arsenic in the solution would require the addition of an ever-increasing quantity of iron in subsequent cycles.

Since 1944 a method of arsenic control [6], the so-called "low-acid leaching," developed at the Chelyabinsk electrolyte zinc plant, has been used at our plants. The essence of this process analogous to the practice at the plant in Treyl (1935) [7] consists in maintaining the acidity of the overflow of the acid thickeners not higher than 1 to 2 g/l H_2SO_4 and a pH of the neutral solution not below 5.3. However, although the solubility of the precipitated arsenic in the acid cycle decreases, the solubility of the iron compounds also diminishes considerably and its concentration in the solution declines to 0.5 to 0.8 g/l. Therefore, the danger of an incomplete precipitation of arsenic in the neutral cycle is diminished.

Thus, based on the existing idea that arsenic is removed from the solution only in the neutral leaching cycle in the presence of a large excess of iron, it is inevitably assumed that its accumulation in the circulating solution sooner or later causes an incomplete removal from the neutral solution. However, in practice if the acidity of the overflow of the acid thickeners is maintained at 5 to 7 g/l, an accumulation of arsenic in the solution is frequently not observed.

It follows that the existing theories on the behavior of arsenic in the leaching process are insufficient for an explanation of the mechanism of the process and a definite control over it. The authors of this paper have attempted the investigation of the behavior of arsenic in the process of leaching cinders and eliminating copper and cadmium from the solution as well as outlining the mechanism of its precipitation.

The materials originally used were cinder, dust and oxides and they differed not only in arsenic content but also in the form of their compounds. In cinders, it is recommended that arsenic be contained primarily as pentoxide and arsenates. In the dust of the Cottrell filters arsenic may also occur as trioxide and pentoxide. In the oxide obtained as a result of reduction processes arsenic trioxide should predominate.

It was of interest to determine the form in which arsenic goes into the solution from these materials in the process of leaching. For that purpose, its solubility in water and H_2SO_4 was determined (Table 1). From all material the predominant part of arsenic is dissolved in acid solution with a final acidity of 1 to 2 g/l. A substantial quantity of arsenic is dissolved in water from the cinders and the Cottrell filter dust. Since arsenic pentoxide is readily soluble in water while the solubility of trioxide constitutes only about 2.0 g

per 100 g water at 25°C [8], the obtained results confirm that in cinders arsenic pentoxide predominates but that trioxide occurs predominantly in oxide that forms in a deoxidized atmosphere. The increased content of insoluble arsenic in shaft furnace cinders and oxide apparently results from the presence of sulfur sulfide (in cinders 1.35%, in oxide 7.86%) with which As has gone into an insoluble compound.

Table 1

The Solubility of Arsenic Extracted from Cinders, Dust and Oxides
Agitation time: 1 hour at 25°C

(a) Наименование продуктов	(b) Содержание As, %	(c) As растворимый в воде, %	Выщелачивание в разбавленной серной кислоте (d)			(h) Нерастворимый As (по разности), %
			начальная кислотность, (e) г/л	конечная кислотность, (f) г/л	растворилось, (g) As, %	
(i) Огарок	0,04	62,0	120	1,6	87,30	12,70
(j) Пыль электрофильтров	0,17	48,4	100	2,0	96,40	3,60
(k) Окись цинка из шахтной печи	1,95	28,6	156	1,0	83,25	16,75
(l) Окись цинка из трубчатой печи	0,26	18,5	120	1,3	94,80	5,20

Key: a) designation of product; b) As content, %; c) water-soluble As, %; d) leaching in diluted sulfuric acid; e) initial acidity, g/l; f) final acidity, g/l; g) dissolved As, %; h) insoluble As (by difference), %; i) cinders; j) Cottrell filter dust; k) zinc oxide from shaft furnace; l) zinc oxide from tube furnace.

Thus, a large part of arsenic from the cinders is dissolved in the neutral leaching cycle in a pentavalent form but arsenic from dust and oxides enters the acid cycle in trivalent form.

Arsenous zinc sulfate solutions containing 80--117 g/l Zn, 0.5--2 g/l As and 20--30 g/l H_2SO_{4free} were prepared for experimental purposes.

While the solutions were being prepared it was noticed that after the addition of a portion of a neutral solution of zinc sulfate to the transparent solution of trivalent arsenic sulfate, a white mucous residue would form which would be

dissolved in acid solution after rapid agitation. Depending upon the concentration of arsenic in the solution, a lowering of acidity brings about the formation of a permanent cloudiness. Thus, with a concentration of arsenic of 2 g/l, the cloudiness appears when the acid content is less than 30 g/l. However, the concentration of arsenic is lowered by diluting it to 100--200 mg/l while the permanent residue is only formed with an acidity below 1--2 g/l H_2SO_4.

The precipitated residue remains in suspension for a long time. Only after a period of 30 to 40 hours it coagulates into shapeless transparent lumps resembling pieces of molten ice and after vigorous agitation it is once more distributed in the solution in the form of a mucous cloudiness. After filtering, a thorough washing and drying at 100°C, the residue contains 26 to 34% As and 15 to 20% Zn.

These peculiarities in the behavior of arsenic in zinc sulfate solution are attributed to the amphoteric character of arsenic acid [9]. As the neutral solution of zinc sulfate is added (pH is equal to 4--5), the acidity of the arsenic sulfate solution decreases while the relative quantity of AsO_3^{3-} ions increases and a small quantity of Zn ions added to the solution causes the formation of insoluble zinc arsenite in water. Therefore, the addition of every amount of zinc sulfate brings about the formation of the white deposit of zinc arsenite which subsequently disappears upon agitation of the solution if the acidity of the mixed solution is sufficient for the dissociation of arsenite.

According to Mellor [10], zinc arsenite can be obtained in the form of $Zn_3(AsO_3)_2$ orthoarsenite or $Zn(AsO_2)_2$ metaarsenite. The latter is produced by the addition of an As_2O_3 neutral solution in NaOH to a hot $ZnSO_4$ solution. It is usually assumed [9] that inasmuch as the dissociation of arsenic acids is in most cases accompanied by a separation of the water molecule, metaarsenic acid salts are more frequently formed. The residues obtained in our case according to the above-mentioned analyses approach the aqueous zinc metaarsenite in composition with a $Zn(AsO_2)_2 \cdot 8H_2O$ compound. The changes in the composition of deposits are attributed to the presence of various quantities of adsorbed zinc sulfate.

Furthermore, the behavior of trivalent arsenic in a zinc sulfate solution with an invariable concentration of arsenic

and a decreasing acidity was observed. For that purpose, small quantities of pure zinc oxide (triturated to 0.2 mm) were added during mixing to 1 l arsenic zinc solution containing 117 g/l Zn, 2 g/l As and 30 g/l H_2SO_4. From time to time, the solution was tested for acidity.

Under the above conditions of neutralization of the solution, the permanent zinc arsenite deposit appears in the form of a white cloudiness with an acidity of 15 g/l of H_2SO_4. The quantity of the deposit increases by further neutralization of the solution and as a result of zinc oxide additions and with a pH = 5.0--4.4, the entire mass turns into a liquid mobile jelly. Even after 48 hours no noticeable line of clarification appears in such a pulp.

The pulp loses its ability to be filtered with an acidity of 5 g/l H_2SO_4. In order to be able to filter a certain quantity of the deposit for analysis, the authors had to add up to 6--7 g/l H_2SO_4 to the pulp. The filtered and washed deposit contained 20--30% Zn and 26--32% As after drying at 100°C. The changes in the composition of the deposit are apparently a result of the presence of various quantities of adsorbed zinc sulfate and hydrate water although the weight ratio of zinc to arsenic approaches 0.9. This leads to the assumption that under these conditions basic metaarsenite $Zn_2O(AsO_2)_2$ would form which could be described by

$$2H_3AsO_3 + 2ZnO = Zn_2O(AsO_2)_2 + 3H_2O.$$

It follows from the above that trivalent arsenic can be retained in zinc sulfate solution only when the acidity and neutralization of the solution are sufficient which at a given moment inevitably evokes the precipitation of the colloidal deposit of zinc arsenic that remains in the solution in suspension for a long time in the form of a cloudiness and increases its viscosity.

Consequently, during the leaching of cinders, the presence of trivalent arsenic in the solution may be a cause of poor clarification and filtration of the acid pulp if the acidity of the acid overflow is maintained at less than 4 to 5 g/l H_2SO_4. This impairment is the more appreciable, the lower the acidity. The zinc arsenite hydrogel that precipitates in the acid cycle enters together with the overflow of the acid thickener into the neutral cycle where the precipitation of the zinc arsenite

is actually completed from the solution and the cloudiness increases hampering the settling of the neutral pulp. An increase in the trivalent arsenic content in the acid solution can lead to a substantial impairment of the settling of the neutral pulp. Moreover, a conspicuous amount of arsenic in the form of zinc arsenite will appear in the neutral overflow in the form of cloudiness and may not be detected by analysis if the solution is preliminarily filtered off.

Zinc arsenite hydrogel whose volume is increased by the precipitation of ferrous hydroxide in neutral thickeners reenters the acid cycle with the condensed product, where it goes into solution increasing the contents of trivalent arsenic. Thus, a substantial part of trivalent arsenic circulates in the process of leaching, having an adverse effect on the latter.

In comparison with the analyses of working solutions taken at different stages of the production process of leaching, we have noticed as early as in 1945 that in the process of manganese iron ore oxidation -- if produced in the acid cycle of the production process -- a substantial part of arsenic is removed from the solution. Thus, for example, in the solution of the first acid Pachuca, the arsenic content was 200 to 300 mg/l with H_2SO_4 at 30 to 40 g/l and of the second solution 400 to 500 mg/l with an acidity of 10 to 15 g/l H_2SO_4.

Repeated analyses of working solutions as well as laboratory tests confirmed this observation, each time showing that the removal of a substantial part of arsenic from the solution during the oxidation of iron in the acid cycle may occur contrary to the existing theories [1, 3]. Moreover, the removal of arsenic takes place even with an acidity of the solution in excess of 10 to 15 g/l H_2SO_4, i.e., it cannot be attributed to the adsorption of arsenic by ferrous hydroxide, inasmuch as with such an acidity the possibility of hydrolysis of ferrous sulfate is precluded.

In order to shed light on this phenomenon, experiments with arsenic-zinc solutions were carried out. The content was approximately 100 g/l Zn, 0.5 to 2.0 g/l As (in trivalent form) and 20--30 g/l H_2SO_4. Initially, iron was added to the solution in the form of concentrated dissolved or dry oxide sulfide salt and, consequently, only that part of iron was subjected to oxidation which was reduced by arsenic acid. To lower the acidity of the solution, weighed portions of pure zinc oxide were added and after a complete dissolution of the latter an

oxidizer was added through a barette in the form of 30% hydrogen peroxide and $KMnO_4$ solution (24 to 50 g/l).

In hydrogen peroxide tests fine-grained turbidity appeared only in solutions with a high concentration of iron and settled gradually after heating to 40 to 50°C in the form of a negligible yellow deposit, presumably, basic iron sulfate. In potassium permanganate tests the solution turned a deep green after adding only the initial batch of potassium permanganate, then it became a heavy ruby color and, subsequently, the solution became opaque followed by the precipitation of an abundant flesh-colored deposit. At that instant the addition of the oxidizer was stopped.

Analyses of the solution and the deposit showed that in hydrogen peroxide tests, the oxidation of iron was practically not accompanied by an appreciable decrease in the arsenic concentration in the solution and the formation of an arsenic-containing deposit. However, in the course of the oxidation of potassium permanganate, a substantial amount of arsenic was removed from the solution in the deposit. These tests confirmed the important part played by permanganic acid in the formation of insoluble arsenate.

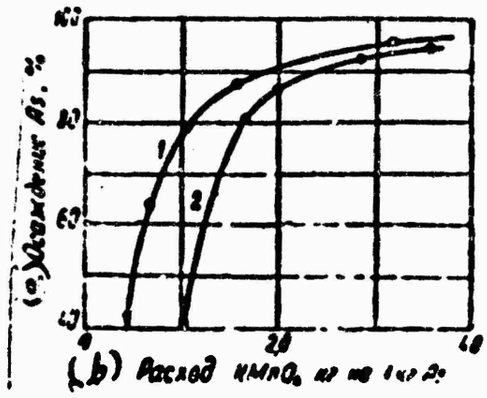

Fig. 1. The effect of the amount of $KMnO_4$ used on the degree of As precipitation from solutions: 1--11 g/l H_2SO_4 and 0.55 g/l As at 26°C; 2--11--13 g/l H_2SO_4 and 0.6 g/l As at 50°C. Key: a) As precipitation, %; b) amount of $KMnO_4$ used, kg/l kg As.

The effect of final temperature, residual acidity, iron content in the solution, and the amount of potassium permanganate

used on the completeness of arsenic precipitation from the solution was investigated in further tests. The results of these investigations are given in Figures 1, 2, and 3.

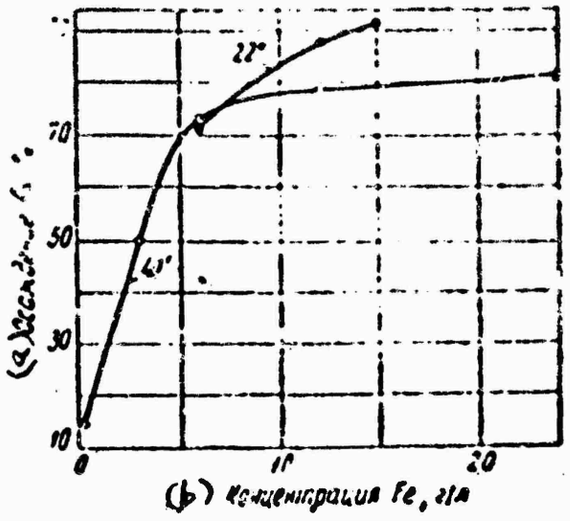

Fig. 2. The effect of Fe concentration on the degree of As precipitation with an acidity of 11 to 13 g/l H_2SO_4 and 1.6 to 1.7 g $KMnO_4$ per 1 g As. Key: a) As precipitation, %; b) Fe concentration, g/l.

The composition of the deposits in these experiments was variable. The content of the basic component changed according to the composition of the solution, precipitation conditions and dosage of precipitator. However, the total amount of iron and manganese in the deposit lies within the narrow limits of 30 to 35%, approaching in most cases 33 to 34% even in precipitating arsenic from solutions without iron. The total amount of arsenic, manganese and iron in the deposits is also invariable, approaching 50--52%. The total manganese and arsenic contents in the deposits from solutions without iron is somewhat lower, amounting to 47--48%.

In most of the tests, the manganese to arsenic weight ratio ranged from 1.43--1.59:1, with an insufficient excess of the potassium permanganate it dropped to 0.7--1.3:1, and above 45 to 50°C and, especially, when the excess of iron was appreciable, the ratio increased to 1.7--1.8 and reached 2.8:1.

Based on the findings, the mechanism of arsenic precipitation from weakly acid solutions as a result of oxidation with

potassium permanganate is assumed to proceed the following: At first, the oxidation of iron occurs and subsequently that of arsenic. Upon completion of this oxidation process, hydrated trivalent iron ions appear in the solution, lending the latter a characteristic reddish-brown color, as well as arsenic acid ions and bivalent manganese, partially bound in $Mn(H_2AsO_4)_2$ arsenate.

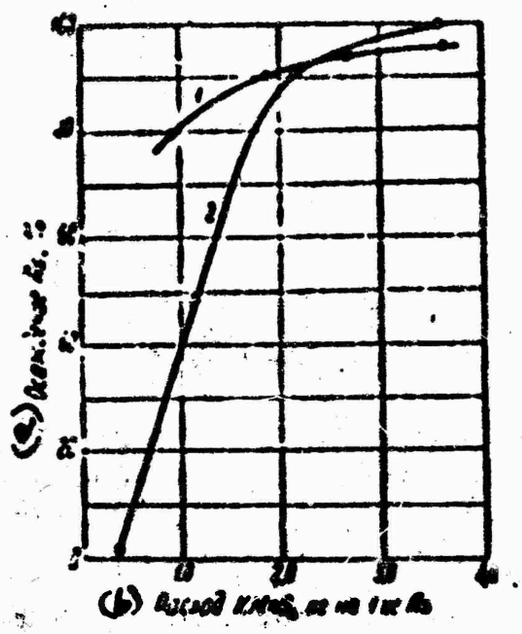

Fig. 3. Effect of the amount of $KMnO_4$ on the degree of As precipitation at 45°C and the following composition of the solution: (1) 17 g/l H_2SO_4 and 0.66 g/l As; (2) 15 g/l H_2SO_4 and 0.78 g/l As. Key: a) As precipitation, %; b) amount of $KMnO_4$ used per 1 kg As (in kg).

According to Mellor [10], bivalent manganese arsenate in the presence of arsenic acid is oxidized by potassium permanganate by the reaction

$$KMnO_4 + 4Mn(H_2AsO_4)_2 + 8H_3AsO_4 = 5H_6Mn(AsO_4)_2 + KH_2AsO_4 + 4H_2O \quad (1)$$

and is accompanied by the formation of a pinkish-red deposit of triarsenate manganic acid, readily soluble in concentrated sulfuric acid and slowly in weak sulfuric acid when the solution turns olive-green. In our case, after the oxidation of

iron and arsenic, there are all the necessary conditions for such an oxidation of bivalent manganese which occurs after further additions of potassium permanganate. However, in view of the presence of free sulfuric acid in the solution, the formed arsenate manganic acid is retained in the solution, lending it a deep green color. At the same time, inasmuch as bivalent manganese ions occur in the solution as well as an excess amount of $KMnO_4$, it is inevitable that the reaction would be

$$2KMnO_4 + 3MnSO_4 + 12H_2O = 5Mn(OH)_4 + 2KHSO_4 + H_2SO_4. \quad (2)$$

The formed manganese peroxide hydrate reacts to arsenate manganic acid producing a tetravalent manganese salt according to the formula:

$$2H_4Mn(AsO_4)_3 + 3Mn(OH)_4 = Mn_4[Mn(AsO_4)_3]_2 + 12H_2O.$$

When iron is contained in the solution, the numberof Mn^{2+} ions bound with $Mn(H_2AsO_4)_2$ arsenate is the larger after the oxidation of iron and arsenic, the higher the Fe:As ratio. An increase of the relative concentration of Mn^{2+} ions creates more favorable conditions for reaction (1). Therefore, in the presence of iron with an Fe:As ratio higher than 2--3:1 this reaction occurs fully, which is evidenced by a more intense green color of the solution in the latter case. Thus, the presence of iron seems to improve the precipitation of arsenic from the solution only indirectly. However, if iron is introduced into the solution not in a bivalent but in a trivalent form which should not affect the increase of the Mn^{2+} concentration in the solution, the arsenic also precipitates much better than without iron.

The iron content in the composition of the deposit after the precipitation of arsenic with potassium permanganate from ferrous acid solutions shows that it definitely participates in the formation of the deposit. It is known that the "red sulfate" of trivalent $HMn(SO_4)_2$ manganese produces binary salts with trivalent iron, aluminum and chrome sulfate of an aluminum iron sulfate type [11]. It follows that an analogous triarsenate manganic acid also produces binary salt with iron arsenate according to

$$2Fe^{3+} + [Mn(AsO_4)_3]^{3-} = Fe_2Mn(AsO_4)_3.$$

and with an increased acidity of the solution according to

$$Fe^{3+} + 3H^{+} + [Mn(AsO_4)_2]^{-} = FeH_3Mn(AsO_4)_2.$$

The resultant manganic arsenate or ferrous hydroarsenate precipitates at the initial stage as tetravalent manganese arsenate in colloidal form, coloring the solution a deep ruby shade. With sufficient potassium permanganate additions manganese peroxide hydrate is precipitated as described by reaction (2) with colloidal arsenate or hydroferrous arsenate and a common deposit will be precipitated without decomposition so that the arsenic precipitation in the presence of iron in the solution is more complete than without it, attaining 95--98%. The deposit precipitates within one to two minutes after the solution turns a deep ruby color. After the deposit is thoroughly settled, the solution turns greenish-yellow (from Fe^{3+} ions) provided the excess of the potassium permanganate additive does not exceed approximately 1.25 to 1.40 g per gram of As or violet (from MnO_4^- ions) when there is a substantial excess of $KMnO_4$.

With a highly acid solution and a sufficient dosage of potassium permanganate the deposit represents a mixture of ferromanganic arsenate and manganese hydroperoxide of the following composition (taking hydration into account):

$$2Fe_2O_3 \cdot Mn_2O_3 \cdot 3As_2O_5 \cdot Mn(OH)_2 \cdot nH_2O.$$

The iron to arsenic ratio in this deposit amounts to approximately 0.5:1 by weight. With approximately the same ratio of these elements, sufficiently acid deposits were precipitated in the tests (7 to 9 g/l H_2SO_4).

By increasing the acidity of the solution and also by having an excess of $KMnO_4$, hydroferrous arsenate $Fe_2O_3 \cdot Mn_2O_3 \cdot 3As_2O_5 \cdot 3H_2O$ forms in the deposit with an iron to arsenate ratio of 0.25:1. This ratio was obtained with a residual acidity of 16 g/l H_2SO_4.

By lowering the residual acidity of the solution below 4 to 5 g/l H_2SO_4, the hydrolytic decomposition of the excess of iron oxide sulfate is favored so that a certain amount of iron hydroxide goes into the residue and the Fe:As ratio in it increases to 0.6:1. An increase of this ratio in the deposit is also observed when there is a substantial excess of iron over arsenic in the initial solution (Fe:As = 6--10:1), or

when the temperature of the solution rises to 50--60°C, which is apparently caused by the adsorption of iron sulfate by a large quantity of manganese hydroperoxide which forms under these conditions.

The composition of the deposits with a different iron content in the solutions may be described by the following formula:

$$kFe_2O_3 \cdot Mn_2O_3 \cdot 3As_2O_5 \cdot mMn(OH)_2 \cdot nH_2O.$$

where coefficient k lies between 1 and 4. Under optimal precipitation conditions, namely with a residual acidity of the solution ranging from 5 to 14 g/l H_2SO_4, the Fe:As ratio in the solution is between 2 and 4, the temperature at a maximum 40 to 45°C, and the excess of $KMnO_4$ at 2 to 2.5 g/l per one part of arsenic in the solution, the value of coefficient k lies within the narrow range of 1.5 and 2, i.e., under these conditions regular arsenate with negligible amounts of hydroarsenate is produced. With acidity in excess of 14 g/l or the amount of precipitator above 3.5 g per 1 g As, the value of coefficient k changes from 1 to 1.6, and with an acidity of 4 to 5 g/l, the temperature below 50°C and an Fe:As ratio in the solution of 6--10:1, k may lie between 2--3 and higher.

The value of coefficient m is also affected by the conditions under which precipitation occurs. Under optimal conditions the Mn:As weight ratio lies between 1.43--1.59:1, which corresponds to an atomic ratio of 1.95--2.17:1. The average atomic Mn:As ratio may be assumed to be 2:1. Since there are two atoms of trivalent manganese per six atoms of arsenic in the deposit, the mean value of coefficient m will be 6 x 2 -- 2 = 10, actually ranging from 9 to 11. Whenever the excess amount of $KMnO_4$ is smaller, reaction (2) is limited and the value of coefficient m falls to 4--5 with an excess of the precipitator being 0.7 to 0.9 g per 1 g As. Its value decreases and with a small m the quantity of the iron formed during the oxidation and Mn^{2+} arsenic (i.e., with a low Fe:As ratio in the solution) also limit reaction (2). Conversely, the factors favoring the reaction, i.e., the high relative iron concentration in the solution and high temperatures with a sufficient amount of the precipitator lead to an increase of the value of m in the observed deposits to 12--13 at 60°C and 20--22 with a 6--10:1 Fe:As ratio in the solution.

The value of coefficient n changes within a wide range of 4 to 15 and stands in reverse dependence to the value of coefficient m. Under optimal conditions of precipitation, the value of coefficient n is 10--14 with a total 50--51% arsenic, manganese and iron in the deposit.

Proceeding from the above observations and assuming that the value of coefficient n = 12, m = 10, and k = 1.8, the average composition of the deposit produced under optimal conditions of precipitation may be expressed as

$$1.8Fe_2O_3 \cdot Mn_2O_3 \cdot 3As_2O_5 \cdot 10Mn(OH)_2 \cdot 12H_2O.$$

Calculations show that 7.8% Fe, 25.5% Mn, 17.4% As, amounting to a total 50.7%, remain in such a deposit.

Table 2

Calculated Composition of the Deposit (%) with Variable Coefficient Values

(a) Элемент	k = 1,8			k = 1,9		
	m = 9, n = 12	m = 10, n = 12	m = 11, n = 12	m = 9, n = 12	m = 10, n = 12	m = 11, n = 12
Fe	8,1	7,8	7,5	8,5	8,2	7,8
Mn	24,7	25,5	26,4	24,5	25,4	26,2
As	18,1	17,4	16,7	18,0	17,3	16,6
Сумма	50,9	50,7	50,5	51,0	50,9	50,6

Key: a) element.

The above-mentioned changes in the value of coefficients k, m, and n under optimal conditions of precipitation (acidity, temperature, amount of precipitator) give the changes in the calculated contents of the basic elements in the deposit (see Table 2).

Evidently, the compositions of the deposits produced in the course of experiments under optimal conditions approach each other closely and lie within possible limits of error. Consequently, deposits produced under such conditions of precipitation are manganese iron arsenate with a negligible content of hydroarsenate mixed with varying amounts of manganese hydroperoxide so that the expounded theories on the mechanism of precipitation of arsenic by potassium permanganate correspond to reality.

Conclusions

1. As a result of investigations it was established that arsenic produced during zinc leaching is obtained in the acid and not in the neutral branch and that it does not form by adsorption but occurs in the form of chemical compounds which are insoluble by diluted sulfuric acid. The process of adsorption is only a subsidiary process of deep purification of the neutral zinc solution from relatively small amounts of arsenic.

2. The mechanism of the process of formation of iron arsenate manganese and its composition is outlined.

3. The inexpediency of oxidizing and precipitating arsenic in the pulp of the acid cycle is evident considering that permanganic acid contained in the electrolyte in small quantities (300 to 1000 mg/l) is, for the most part, spent on the oxidation of readily oxidized sulfides and impurities and, consequently, it forms in insufficient quantities for the formation of the required arsenic compounds. Furthermore, a spent electrolyte, liberated from a number of detrimental impurities during the zinc electrolysis, is entirely used for the leaching of the lower overflow of the neutral thickeners under the present system, and at that stage it not only loses permanganic acid but carries many soluble and insoluble impurities (in the form of suspension) which are detrimental for the neutral cycle from the acid to the neutral cycle.

Therefore, it is most expedient to carry out the oxidation and precipitation of arsenic in a separate agitator, directing the upper overflow of the acid thickeners into it before proceeding to the sintering shop for the washout of the cinders as it is commonly practiced in certain plants. An even flow of all clarified solutions (which at present are supplied to the agitators of the acid cycle) and part of the consumed electrolyte should also be supplied to this agitator.

The amount of the used electrolyte supplied to the agitator should make the creation of the required ratio of free zinc oxide to the volume of the solution in the neutral pulp possible. For different zinc cinders and their mixtures, the quantity of the consumed electrolyte supply in this agitator varies between 25 to 45% of the total quantity obtained during the electrolysis.

BIBLIOGRAPHY

1. Chizhikov D. M. Metallurgy of Zinc, 1938.
2. Ralston O. Hydrometallurgy and Electrolytic Precipitation of Zinc, 1932.
3. Loskutov F. M. Metallurgy of Zinc, 1945.
4. Liddell, Handbook of Nonferrous Metallurgy, Vol 11, 1926.
5. Tainton, Legsen, Trans. Amer. Inst. Mining and Metallurg. Engrs., 70, 1924.
6. Gronov B. G. Tsvetnyye metally, No 4, 1945.
7. Metallurgy of Zinc, translation edited by L. M. Gazaryan and I. N. Moskvitin, 1944.
8. Remi T. Textbook of Inorganic Chemistry, Vol I, 1933.
9. Nekrasov B. V. Course of General Chemistry, Vol I, 1945.
10. Mellor, A Comp. Treatise of Inorg. Chemistry, IX, 1929.
11. Remi T. Textbook of Inorganic Chemistry, Vol II, p 119, 1935.

Manuscript submitted 15 Nov 1961

ON THE QUESTION OF SELECTING ADDITIVES FOR THE IMPROVEMENT OF THE COMPOSITION OF THE ALUMINUM BATH ELECTROLYTE

By S. V. Tararin and A. I. Beyayev,
Moscow Institute of Steel and Alloys.
Chair of the Production of Pure Metals and
Semiconductor Materials.

pp 96--99

In recent years, a large number of investigations [1] have been carried out for the improvement of the composition of electrolytes by means of various salt additions. It may be considered as an established fact that the most effective additions are salt with magnesium and chlorine ions, especially when both are contained in the electrolyte.

However, so far there has been no consensus on the form of the compounds to be used for these additions. Thus, at the Ural Aluminum Plant, MgF_2 and NaCl additions were tested. The Bogoslovskiy Aluminum Plant applied NaCl and caustic magnesite while the Dnepr Aluminum Plant is testing $MgCl_2$ additions in the electrolyte.

The results of industrial tests of these additions lead to the conclusion that all of them affect the basic physicochemical properties of the aluminum bath electrolyte almost to the same extent and the different parameters of the test baths at the above plants are accounted for by the different ratios of these elements while the elementary composition of the electrolyte was qualitatively identical, the peculiarities of the design of electrolytes and other experimental conditions.

In fact, the same elementary composition of the electrolyte with Mg^{2+} and Cl^- additions at any cryolite ratio may be obtained by applying the following mixtures of substances:

I — NaF, AlF_3, MgF_2, NaCl, Al_2O_3;
II — NaF, AlF_3, $MgCl_2$, MgF_2, Al_2O_3;
III — NaF, AlF_3, MgO, NaCl, Al_2O_3.

If an electrolyte of an aluminum bath were considered an ionic system, it would be difficult to assume that electrolytes composed of these mixtures under conditions of an equal content of corresponding elements in the mixtures had different properties. The statements to the effect that any mixture is "extraordinary," such as, for example, $MgCl_2$, result from the recognition of the particular stability of an $MgCl_2$ addition as a chemical compound in the electrolyte and of the impossibility of its synthesis in molten mixtures I and III. This, in turn, leads to the statement that MgO and NaCl are stable chemical compounds in the electrolyte and a denial of any reactions taking place among these additions and the electrolyte.

In order to estimate the relative stability of additions in the electrolyte, the changes of the isobaric-isothermal potential of certain reactions [2, 3] which may occur in the aluminum bath were calculated.

The likely reaction that takes place in the neutral electrolyte without oxides is the following:

$$2Na_3AlF_6 + 3MgCl_2 \rightarrow 3MgF_2 + 6NaCl + 2AlF_3.$$

The change of the isobaric-isothermal potential of this reaction at 1300°C $\Delta Z_1 = -58.4$ kilocalories. Equilibrium constant $K_{p1} = 6.65 \cdot 10^9$.

These quantities reflect the low stability of $MgCl_2$ in neutral melts since the reaction is noticeably shifted towards the right in the direction of the formation of MgF_2 and NaCl.

In alkaline and acid melts the following reactions may occur:

$$MgCl_2 + 2NaF \rightarrow MgF_2 + 2NaCl$$
$$3MgCl_2 + 2AlF_3 \rightarrow 3MgF_2 + 2AlCl_3.$$

the isobaric-isothermic potentials of which are equal to $\Delta Z_2 = -37.8$ kilocalories and $\Delta Z_3 = -33.4$ kilocalories, respectively.

Thus, whatever the cryolite relation, the $MgCl_2$ reaction with the melt in the absence of oxides would occur in the direction of the formation of NaCl and MgF_2. This was confirmed by the study of the chemical composition of cryolite melts containing up to 15% $MgCl_2$ [4]. The chemical analysis of a hard alloy showed that the $MgCl_2$ reaction with cryolite melts is accompanied by the formation of equivalent quantities of NaCl and MgF_2 until its completion.

When aluminum oxide is present and the electrolyte adjusted with magnesium oxide, an equilibrium corresponding to the reaction

$$2Na_3AlF_6 + 3MgCl_2 + Al_2O_3 \rightleftarrows 3MgO + 4AlF_3 + 6NaCl,$$

should be established in the melt whose isobaric-isothermal potential approaches zero. This means that in the presence of oxides the directions of the reaction are thermodynamically equivalent and the predominant formation of any one compound should not occur in the melt. It follows that all three studied mixtures (I, II, and III) must produce melts with identical physicochemical properties.

This conclusion was verified with the help of thermal analysis of the mixtures of groups I, II, and III during the preparation of which substances were taken in such quantities that the concentration of the corresponding ions in the melts would be identical.

All salts for the preparation of mixtures in addition to AlF_3 and $MgCl_2$ were graded for analysis. Graded aluminum fluoride was applied. The $MgCl_2$ compound was prepared artificially by the Erdman method [5] and contained from 96 to 98% $MgCl_2$. Thermal analysis was carried out in platinum crucibles. The crystallization point of the melts was determined from the appearance of the initial crystal and was recorded with the help of a Pt-Pt/Rh thermocouple and potentiometer.

A total of 27 specimens with three cryolite relations (3; 2.8; 2.6) were investigated. For every cryolite relation three different ratios of additives were studied as converted to MgF_2 and NaCl:

85% mixture $NaF+AlF_3$, 5% NaCl, 5% MgF_2, 5% Al_2O_3;
80% " $NaF+AlF_3$, 10% NaCl, 5% MgF_2, 5% Al_2O_3;
80% " $NaF+AlF_3$, 5% NaCl, 10% MgF_2, 5% Al_2O_3.

The results of the investigation of the fusibility of the mixtures are given in the table. The vertical lines in this table show for every cryolite relation the mixture of an identical elementary composition, while the horizontal lines show the mixtures containing different concentrations of additives converted into NaCl and MgF_2 but composed of the same group of substances.

Crystallization Point of Molten Mixtures

(a) Криолитовое отношение	(b) Группа смеси	(c) Концентрация добавок, кг/т		
		1	2	3
3	I	934	914	912
	II	932	914	912
	III	931	912	914
2,8	I	930	903	905
	II	932	901	900
	III	930	903	905
2,6	I	921	898	898
	II	921	898	898
	III	921	902	896

Key: a) crystallite relation; b) mixture group; c) concentration of additive, kg/t.

The data of the table show that the elementary composition of the mixture determines the crystallization point and from this viewpoint it does not matter from what kind of substances it is produced. Consequently, as additives containing magnesium and chlorine ions are introduced, reactions occur in the electrolyte which place the composition into equilibrium for the duration of the experiment. The practical value of this fact consists in the possibility of applying such low-cost additives for the electrolyte as table salt, caustic magnesite and industrial waste in the form of MgF_2. Inasmuch as MgF_2 is an industrial waste product, it is economically important to set a proper price for this product.

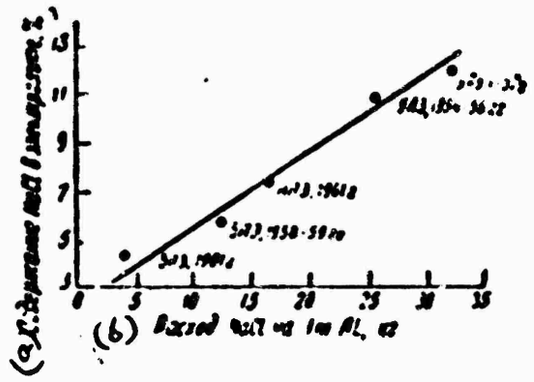

Data of industrial tests of NaCl additions in the aluminum bath electrolyte. Key: a) NaCl content in the electrolyte, %; b) amount of NaCl per ton of Al, in kg.

Proceeding from the stoichiometrical relations of reaction

$$3MgO + 2AlF_3 = Al_2O_3 + 3MgF_2,$$

one ton of dry MgF_2 should be equivalent to the total cost of 890 kg AlF_3 and 645 kg MgO with the deduction of the cost of 550 kg Al_2O_3.

Based on the findings of industrial research on NaCl and MgO (MgF_2) additives, the composition of the adjusting mixture of substances necessary for the maintenance of an invariable concentration of Mg^{2+} and Cl^- in the electrolyte of the aluminum bath can be determined. The figure shows the results of industrial tests of NaCl additives at various plants with regard to the amount of salt according to the applied NaCl concentration in the electrolyte.

According to the figure, 8 to 10 kg NaCl have to be used per 1 ton Al in order to maintain an invariable 5% concentration of NaCl in the electrolyte.

The data of industrial testing of the MgO additive into the electrolyte show that the magnesium ion concentration diminishes much slower than the concentration of chlorine ions and that it suffices to add about 3 kg MgO to the bath in order to maintain 5% MgF_2 in the electrolyte.

Thus, in working with electrolytes containing 5% NaCl and 5% MgF_2, the adjusting mixture should contain approximately 77% NaCl and 23% MgO. Whenever MgF_2 instead of MgO is used a mixture richer in magnesium salt should be prepared because of the lower contents of Mg^{2+} ions in MgF_2 as compared to MgO.

Conclusions

1. In selecting additives for aluminum bath electrolytes in order to introduce magnesium and chlorine ions, the cost of materials should be the yardstick, inasmuch as the physicochemical properties of the melts with any of the MgO + NaCl, MgF_2 + NaCl or $MgCl_2$ additives are analogous on condition that the composition of the electrolyte is the same.

2. According to the results of industrial tests of electrolytes with additives that contain magnesium and chlorine ions, an adjusting mixture with 77% NaCl and 23% MgO in quantities of 11 to 13 kg/t Al is recommended.

BIBLIOGRAPHY

1. Belyayev A. I. Elektrolit alyuminiyevykh vann (The Electrolyte of Aluminum Baths), Metallurgizdat, 1961.
2. Kubashevskiy O., Evans E. Metallurgical Thermochemistry, Pergamon Press, Ltd., London, 1958.
3. O'Brien S., Kelley K. J. Amer. Chem. Soc., Vol 70, No 21, 5116 (1957).
4. Velyayev A. I. et al., Proceedings of the All-Union Conference (22 to 25 Nov 60), Metallurgizdat, 1962.
5. Karyakin Yu. V. Chistyye khimicheskiye reagenty (Pure Chemical Reagents), Goskhimizdat, 1957.

Manuscript submitted 4 Feb 1963

ON THE QUESTION OF THE INTENSIFICATION OF CYANIDATION OF GOLD-BEARING ORES

By S. B. Leonov and M. F. Khabrov,
Irkutsk Polytechnic Institute

pp 100--105

The problem of the intensification of cyanidation of gold-bearing ores, which is one of the principal processes of gold ore extraction, has been attracting the attention of investigators for a long time. However, in spite of the availability of a great number of papers on this problem a rational method of cyanidation has still not been devised. For the purpose of intensification of the process of cyanidation, certain authors [1] propose an intensified mixing of the pulp by means of the installation of additional horizontal blades and edges on vertical mixer shafts which would act as dissectors along the periphery of the vessel and also increasing the number of revolutions of the mixing mechanism to 12--15 per minute, or using atomized air throughout the pulp volume. Other suggestions concern the mixing of the pulp during cyanidation in such highly effective devices as a flotation machine or a contact vessel or the testing of available mixer designs but with a decrease in the vessel diameter. However, all these measures did not improve the process of cyanidation.

In recent years, the interest in hydrometallurgical processes for the beneficiation of ore and concentrates under higher pressures [2, 3] has been growing, which accounts for an appreciable improvement of the hydrometallurgical method in comparison to the regular conditions under which these processes are carried out. This is accounted for by the favorable shifts in thermodynamic equilibria under increased pressures and, particularly, in the kinetics of many reactions

after putting the gaseous reagents in water solutions to the most effective use. Therefore, in the metallurgy of rare metals the increase in the partial oxygen pressure is a key factor in enhancing the process of gold dissolution in cyanogen solution since it improves the conversion of gas into solution.

As shown in the investigations of I. N. Plaksin and in our work, the most favorable conditions for maintaining the high concentration of oxygen in solutions are created with cyanidation under an air or pure oxygen pressure of up to 5--7 kg/cm^2 [4--6]. Under these conditions, the rate of gold dissolution increases 10--36 times depending upon the actual ore composition. The intensification of the process of cyanidation with increased air and oxygen pressure was verified under industrial conditions and also by S. K. Shabarin [7]. Thus, cyanidation under air or oxygen pressure is an improvement over cyanidation in open apparatus inasmuch as it allows a substantial time saving in processing the material.

However, this process has essential shortcomings, which prevent its large-scale use in industrial practice. The implementation of the process under pressure calls for special air-tight equipment which would require more complicated servicing than open apparatus. Another difficulty arises in connection with the continuity of the process and the creation of excess pressure, which requires a well-developed compressor machinery. Therefore, the quest for methods which would intensify the cyanogen process should be directed at finding simple methods and the use of equipment of simple design.

In this respect, hydrocyclones are of the greatest interest, inasmuch as they are widely used at gold beneficiation plants as classifying and enrichment equipment. We have observed an intense gold dissolution in the cyanogen pulp that was passed through a hydrocyclone. This paper deals with the results of a preliminary investigation of this phenomenon.

Experimental cyanidation of ore in hydrocyclones was carried out in two series of tests. In the first series, chalcedony quartz and chalcedony with sand and clay were used. The most important ore minerals in the test were pyrite, stibnite, and limonite. The chemical analysis of the main ore components gave the following results: SiO_2 -- 77.2%, Al_2O_3 -- 10.6%; Fe -- 3%; Sb -- 0.3%; S -- 1.08%; CaO + MgO -- 3.22%. According to the test analysis the initial gold content was 60 g/t.

In the second series of tests gangue quartz with iron hydroxide surface films was used. The ore minerals in this series were magnetite, hematite, limonite and sulfide; pyrite, galena and sphalerite were used in quantities amounting to one tenth of a percent. The gold in the ore was high-grade and occurred in quantities of 14.6 g/t. The chemical analysis of the main components gave the following results (in %): 92.5 SiO_2; 0.6 Al_2O_3; 1.67 Fe_2O_3; 3.65 FeO; 0.12 S; 0.1 Zn; 0.18 Pb; 1.3 CaO + MgO.

A 50-mm laboratory-type hydrocyclone with a 17-mm slurry and an 8-mm sand piece were used in the tests. The diameter of the feed was 20 mm and that of the spout 25 mm. The hydrocyclone was installed above a 40-liter receiving hopper. The sand and the overflow of the hydrocyclone were received by this hopper and mixed in a mechanical mixer. The mixed pulp from the hopper was fed to the hydrocyclone with the help of a sand pump, especially designed for this purpose. Thus, the continuity of the process of ore cyanidation in a hydrocyclone was made possible.

Table 1

Ore Cyanidation in the First Series of Hydrocyclone Tests

(a) Время цианирования в гидроциклоне, час	(b) Содержание золота в продуктах цианирования						(f) Извлечение золота, %	(g) Расход цианида, кг/т
	(c) песках		(d) сливе		(e) всего в руде			
	(h) г/т	%	(h) г/т	%	(h) г/т	%		
0,5	33,0	10,58	17,4	23,5	20,4	34,08	65,92	2,8
1,0	30,8	9,86	10,4	14,0	14,32	23,86	76,14	3,0
2,0	11,0	4,5	4,4	5,94	6,25	10,44	89,56	3,3
3,0	8,8	2,96	2,0	2,7	3,31	5,66	94,34	3,6
4,0	4,5	1,44	2,0	2,7	2,47	4,14	95,86	3,75

Key: a) length of hydrocyclone cyanidation, hrs; b) gold content in the cyanidation products; c) sand; d) overflow; e) total ore contents; f) gold extraction, %; g) cyanide, kg/t; h) g/t.

Sand and overflow specimens were taken separately from the hydrocyclone and analyzed for gold, whereby the sieve analysis was carried out separately.

The initial tests were conducted with the first ore specimens 74.2% of the grains being ground to 47 microns and the

liquid to solid ratio amounting to 3 : 1, the initial cyanide concentration to 0.2%. The amount of lime was 2 kg/t, and the ore batch weighed 4 kg. The test results are shown in Table 1. They reveal a highly intense dissolution of gold in the hydrocyclone. Within a more four hours of operation of the installation, 95.86% metal was dissolved while only 4.14% remained in the gangue, amounting to a gold content of 2.47 g/t.

It is noteworthy that in this test a large amount of cyanide was used, reaching 3.75 kg/t during the four-hour operation of the installation. This exceeds the amount established for ore during cyanidation in mixers by approximately four times (see Table 1).

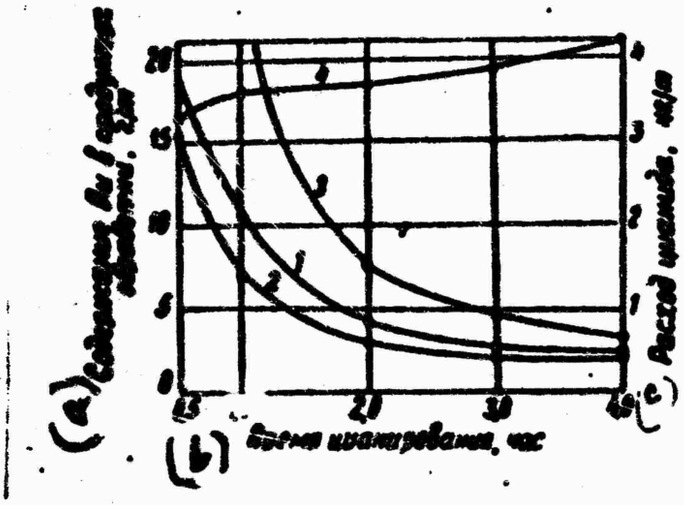

Fig. 1. Rate of gold dissolution and amount of cyanide used in the processing of ore in the first series of hydrocyclone tests (88% ground to 47 microns): 1-- Gold content in the ore; 2 -- In the discharge; 3 -- in the hydrocyclone sands; 4 -- amount of cyanide used.

Key: a) Au content in the processing products, g/t; b) cyanidation time, hr; c) amount of cyanide, kg/t.

The working parameters of the hydrocyclone were the following:

	Measuring unit	Sand	Overflow
Yield	%	19.2	80.8
Productivity	t/h	0.042	0.176
Content of 47 micron grains	%	22	86.6

After a four-hour operating period of the installation, the pulp had passed the hydrocyclone 260 times.

The results of cyanidation of finer material (88% of the grains -- 47 microns) under analogous conditions are given in Figure 1. The rate of gold dissolution in this test was even higher than in the first series of tests. This was particularly conspicuous with regard to hydrocyclone sand. It is noteworthy that ore processing in regular mixers produces analogous results only after 24 hours of cyanidation. Thus, the rate of gold dissolution in hydrocyclones for a given ore is six times higher than the rate of ordinary cyanidation in mixers.

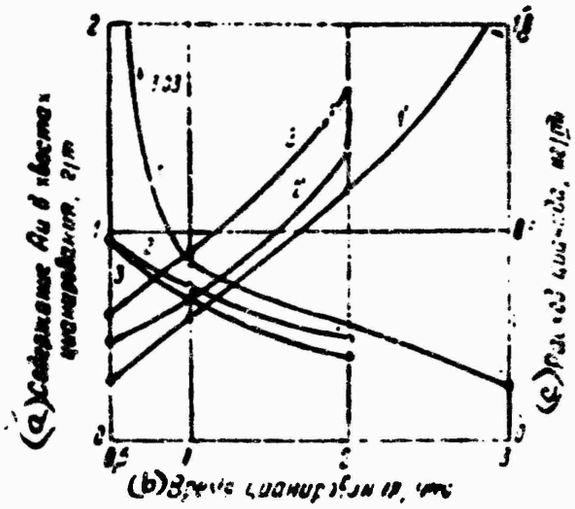

Fig. 2. The rate of gold dissolution and cyanamide used for hydrocyclone ore processing in the second test series with a grain size of 74 microns: (1) 49.6%; (2) 64.2%; (3) 79.9%; 1', 2', 3' -- respective amounts of cyanide. Key: a) Au content in the cyanidation gangue, g/t; b) cyanidation time, hrs; c) cyanide used, kg/t.

The following tests were conducted with simpler ores in a second series. In the tests an optimum degree of ore grinding and pulp consistency were determined (Fig. 2, Tables 2 and 3). It was found that after a two-hour mixing period the degree of dissolution of gold reaches 95.95 with 49.6% of the ore grains at 74 microns, and with 64.2% at 74 microns it increases to 96.6%. With 79.8% of the grain size at 74 microns, the extraction was 97.25%. The gold content in the gangue was (in g/t): 0.59; 0.48, and 0.4, respectively.

Table 2

Ore Cyanidation in the Second Test Series in a Hydrocyclone at Different Degrees of Grinding

(a) Время цианирования, час	(b) Степень измельчения руды, % класса −74 мк								
	49,6			64,23			79,46		
	(c) Содержание золота в продуктах цианирования, г/т								
	в песках	в (d) сливе	всего (f) в руде	в песках	в сливе	всего в руде	в песках	в сливе	всего в руде
0,5	12,7	1,0	3,06	1,85	0,8	0,99	1,2	0,8	0,99
1,0	1,6	0,6	0,87	1,4	0,6	0,78	1,3	0,5	0,87
2,0	1,5	0,4	0,59	0,9	0,4	0,456	0,4	0,4	0,4

Key: a) cyanidation time, hrs; b) percentage of 74-micron ore grains; c) gold content in cyanidation products, g/t; d) in sand; e) in overflow; f) total in ore.

Table 3

Ore Cyanidation in the Second Test Series in a Hydrocyclone at Different Pulp Concentration Rates

(a) Время цианирования, час	(b) Отношение ж : т								
	2:1			3:1			4:1		
	(c) Содержание золота в продуктах цианирования, г/т								
	в песках (d)	в сливе	всего в руде	в песках	в сливе	всего в руде	в песках	в сливе	всего в руде
0,5	3,4	2,2	2,44	1,85	0,8	0,99	2,0	0,6	0,835
1,0	1,2	0,8	0,99	1,4	0,6	0,75	1,2	0,5	0,619
2,0	0,8	0,4	0,44	0,9	0,4	0,48	0,4	0,4	0,4

Key: a) cyanidation time, hrs; b) liquid-solid ratio; c) gold content in the cyanidation products, g/t; d) in sand; e) in overflow; f) total in ore.

The effects of the rate of dilution of the pulp was determined in ore in which 64.2% of the grains were 74 microns. These tests differed from preceding tests in that the cyanide concentration was 0.15% NaCN. Gold extraction was 96.7% at a liquid-solid ratio of 2:1 and it increased to 97.26% at a liquid-solid ratio of 4:1. With a 3:1 liquid-solid ratio the gold extraction was 96.6%.

It follows from Table 3 that the dilution of the pulp has an essential effect only during the initial thirty minutes

of the operation of the hydrocyclone. After the initial hour of cyanidation the effect of the pulp dilution is not noticeable since good results were obtained even with a minimum liquid-solid ratio of 2:1 (see Fig. 2, Tables 2 and 3).

Since the gold occurred in the second test series in the form of large 1.5 x 0.5 mm laminae and plates, there was a certain interest in carrying out cyanidation after removing the coarse metal particles. Therefore, cyanidation was conducted with amalgamation tails containing 2.6 g/t Au. The contents of metal in the cyanidation tails was found to be 0.4 g/t after thirty minutes and it decreased to 0.3 g/t after 60 minutes. However, after a two-hour cyanidation period only traces of gold can be identified in the ore. Consequently, after the extraction of the basic mass of gold, good results are obtained by processing ore for one hour in the hydrocyclone; eight hours are required with a regular cyanidation process (see Table 4).

Table 4

Cyanidation of Amalgamation Tails in the Hydrocyclone

(a) Время цианирования, час	(b) Содержание золота в продуктах цианирования хвостов амальгамации						(f) Извлечение золота цианированием, %	(g) Расход цианида, кг/т	(h) Извлечение золота амальгамацией и цианированием %
	(c) в песках		(d) в сливе		(e) всего в руде				
	г/т	%	г/т	%	г/т	%			
0,5	0,4	13,3	0,4	12,1	0,4	15,4	84,6	0,12	97,30
1,0	0,30	2,47	0,3	9,06	0,3	11,53	88,47	0,36	97,95
2,0	0,30	1,65	сл.	—	0,012	1,65	98,35	0,68	99,8

Key: a) cyanidation time, hrs; b) gold content in the cyanidation products of the amalgamation tails; c) in sand; d) in overflow; e) total in ore; f) gold extraction by cyanidation, %; g) cyanide used, kg/t; h) gold extraction by amalgamation and cyanidation, %; i) g/t.

Thus, the process of hydrocyclone cyanidation reduces the ore processing time by 6 to 8 times as compared to the regular method and this has become possible owing to the ideal conditions under which the cyanide process is carried out in this apparatus.

First of all, the hydrocyclone cyanidation process is, apparently, not affected by the clay content in the ore, which

has an appreciably adverse effect on the performance figures of the ordinary cyanidation process. In hydrocyclones (as a result of feeding the material under excess pressure) the pulp is vigorously rubbed and mixed, the surfaces of the gold particles are cleaned of slurry residues whenever the latter occur and also flakes and other slurry accumulations in which gold grains may be enveloped are destroyed without being touched by the cyanide solution. Moreover, the circulation of the pulp through the pump installation and the hydrocyclone produces an intense oxigenation of the pulp while the vigorous friction of the particles against each other, the hydrocyclone walls, and the pump parts evidently causes a decrease of the thickness of the diffusion layer on the surface of the dissolving metal increasing thereby the rate of gold dissolution.

Table 5

Comparative Data on Ore Cyanidation in an Installation with and without a Hydrocyclone

(a) Время цианирования, час	(b) Содержание золота (в %) в хвостах обработки руды, получаемых на установке	
	с гидроциклоном (c)	без гидроциклона (d)
0,5	31,04	64,0
1,0	21,96	50,0
2,0	16,44	30,0

Key: a) cyanidation time, hrs; b) gold content in ore processing tails (%); c) with hydrocyclone; d) without hydrocyclone.

In conclusion it is noteworthy that in processing ore by means of this installation the process of gold dissolution was found to take place not only as the pulp was passing through the hydrocyclone but also during its passage through the pump. Thus, in the first series of tests during ore cyanidation with a disconnected hydrocyclone (see Table 5), i.e., as the pulp was fed to the "hopper and mixer - pump" system, approximately 50% of the metal produced during the circulation of the pulp through the pump installation by means of the hydrocyclone are gone into solution. Thus, in the system, the hydrocyclone as well as the sand pump are apparatus in which an intense dissolution of gold is achieved.

Conclusions

1. The application of a sand pump installation with a hydrocyclone shows the possibility of a substantial reduction of the cyanidation time for gold-bearing ores (six to eight times).

2. It was established that approximately half of the total amount of metal has been dissolved during the passage of the pulp through the hydrocyclone and the same amount during its passage through the pump.

BIBLIOGRAPHY

1. Galkin G. V., Chevasheva G. L. Collected Papers on Technical Information and Exchange of Experience, OBTI, Vol. 47, 1956.
2. Kurumchin Kh. A. Collected Papers on Technical Information and Exchange of Experience, OBTI, Vol. 43, 1955.
3. Forvard F. A., Halpern J. Journal of Applied Chemistry, No 1, 1957.
4. Plaksin I. N., Zefirov A. P. Sovetskaya zolotopromyshlennost' (Soviet Gold-Mining Industry), No 1, 1937.
5. Plaksin I. N., Sinelnikova A. I. Collected Scientific Proceedings of the Ministry of Nonferrous Metals and Gold, No 9, 1940.
6. Leonov S. B., Khokhlov V. R., Bessonov S. V. Izv. VUZ (VUZ Bulletin), Tsvetnaya Metallurgiya (Nonferrous Metallurgy), No 3, 94 (1958).
7. Shabarin S. K. Collected Scientific Papers of the Ministry of Nonferrous Metals and Gold, No 11, 1945.

Manuscript submitted 3 July 1962

THE EFFECT OF ULTRASOUND ON THE PROCESS OF LEACHING DIFFICULTLY-SOLUBLE RARE METAL COMPOUNDS

By M. N. Khavskiy, I. A. Yakubovich, B. A. Agranat, O. D. Kirillov and P. V. Vasil'yev,
Moscow Institute of Steel and Alloys.
Chair of Metallurgy of Radioactive Metals and Complex Polymetallic Ore Processing

pp 106--110

In connection with the industrial use of lean and difficultly-stripped ores of nonferrous and rare metals, the investigation and introduction of new effective leaching methods into practice acquires particular importance.

Along with the use of new chemical leaching reagents, the wide application of sorptional and extraction methods, the leaching of a number of ores under high pressure and at high temperatures with catalysts and oxidizers, new leaching methods are being introduced which make it possible already now to increase substantially the kinetic and technological performance figures in hydrometallurgy. Lately, a detailed investigation of the possibilities and the effectiveness of using ultrasonic effects for this purpose has been launched, in particular [1--4].

Although the mechanism of this process has been studied very little, it may be assumed that the considerable turbulent flows that appear in the liquid, the cavitation, the sound pressure and other effects change the character of diffusion of the boundary layer that is directly adjacent to the surface of the substance and the thickness of which is limited by the rate at which the process of dissolution occurs. Cavitation

leads to the formation of a great number of microcracks on the surface of the processed particles and under the effect of the accelerated molecular diffusion the solution penetrates deep into the particles through the capillaries accelerating the process of their dissolution.

In the Soviet Union as well as abroad, the possibility of using ultrasonic effects in the processes of leaching and dissolving metals, minerals, and salts in various solvents was investigated. A. P. Kapustin [5] studied the influence of ultrasound on the rate of dissolution of steel plates in acids as well as that of blue vitriol, hyposulphite, sugar and thymol crystals in water. It was found that under the action of ultrasound with a frequency of 600 kilocycles and an intensity of 4 wt/cm^2, the rate of dissolution increases sharply and that the quantity of the dissolved substance is proportional to the length of sound application on condition of invariable intensity and temperature.

In all the described cases a sharp intensification of the process of dissolution was observed. Obviously, intensity plays an important role since weak ultrasounds did not appear to influence the acceleration of the process of dissolution very much.

With the help of ultrasound Pfefferkorn [6] produced fine etching patterns of crystals for their subsequent study under an electron microscope. The same method was used by Kh. S. Bagdasarov [7], who produced etching patterns along the edges of alum alumopotash crystals. He also investigated the action of ultrasound of different frequencies on the rate of dissolution of rock salt crystals in water. It was established that at identical intensity of the ultrasound the rate of dissolution of this salt with a frequency of 22 kilocycles is seven times higher than with a frequency of 410 kilocycles.

N. N. Dolgopolov, V. M. Fridman, and N. M. Karavayev have increased the rate of dissolution of ferrous potassium cyanide in water and that of copper plates in nitric acid (as compared to the ordinary mixing) one and a half times subjecting these substances to the effects of a 1.2 milligram frequency ultrasound and an intensity of 8 wt/cm^2 [8].

Paper [9] investigates halogenating and germanium extraction from coal by the application of ultrasonic fields, while paper [10] deals with the leaching of uranium hydroxide and oxide from tuff sandstone by means of ultrasound at room temperature and with a 5% soda solution. After 13 minutes it was

sible to extract up to 16% metal contained in the rock, reas 90 minutes of processing under ordinary conditions ures a maximum extraction of 8%.

In this paper, which is of an exploratory character, the ect of ultrasound on the process of carbonate leaching of tain difficultly-soluble substances was investigated. The er deals with the effects of temperature, mixing rate and alyst quantity on the rate of metal extraction from its pounds under the action of an ultrasonic field. By way of parison, experiments were conducted with ultrasound appli- ion. A copper ammonium complex $[Cu(NH_3)_4]SO_4$ was employed a catalyst.

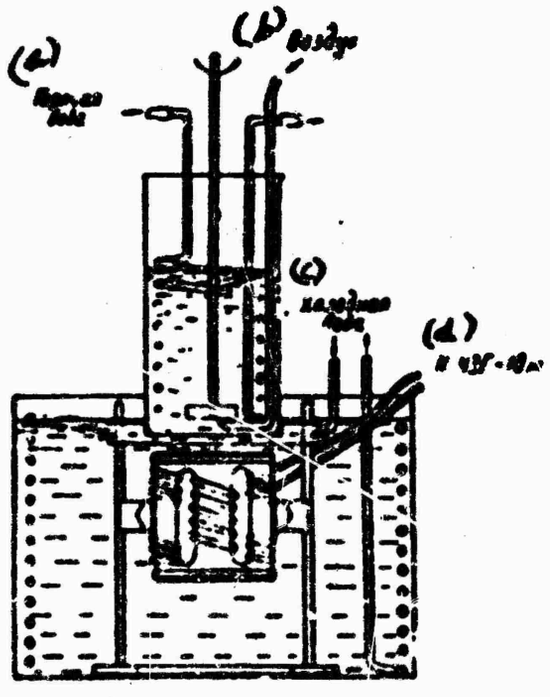

Fig. 1. Diagram of leaching installation with the help of ultrasound. Key: a) hot water; b) air; c) cold water; d) ultrasonic generator - 10 m.

The laboratory installations consisted of a chemical glass h a 2-liter capacity in which the pulp was processed and o which a glass coil and a mechanical mixer were lowered as l as of a system for the supply of diffused air (see Fig. The pulp was mixed in a four-blade glass mixer with aight blades and with controllable rpm; furthermore, air bles were diffused through the pulp. Air diffusion oc- red at a speed of 65 l/h under a pressure of 0.8 atm. In

addition to the mixing of the suspension the air served as a source of oxidizer-oxygen enhancing the solubility of the specimens. In the tests the glass was placed on the water-cooled surface of a magnetostrictive radiator that was supplied with power by ultrasonic generator "UZG-10M." The intensity of the oscillations in the glass measured by calorimetric method was 0.55 wt/cm^2.

Initially, the tests concerned the treatment of an Na_2CO_3 with a view of establishing the possibility of changing the carbonate ratio and the necessary amount of the cuprammonium compound (Fig. 2).

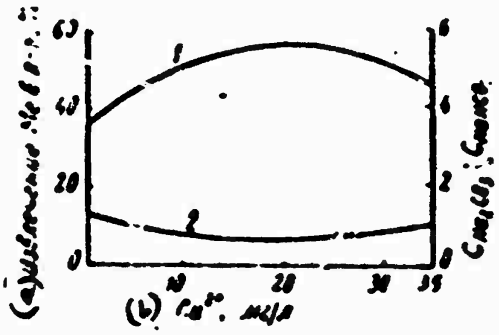

Fig. 2. The effect of the amount of the catalyzer used in an ultrasonic field on the leaching and the change in the carbonate ratio with n = 400 rpm; t = 80°C within 60 minutes: (1) extraction; (2) ratio of concentrations. Key: a) Me extraction, in solutions, %; b) Cu^2 milligram/liter.

Similar to high-basicity salt and weak acids, sodium carbonate goes through hydrolysis in water according to the equation

$$CO_3^{2-} + H_2O \rightleftarrows HCO_3^- + OH^-.$$

The degree of hydrolysis depends on temperature, time, concentration and the content of an analogous ion in the solution. By way of acid titration of the soda solution specimen we determined the Na_2CO_3 and $NaHCO_3$ concentrations in the solution and calculated the carbonate ratio:

$$z = C_{Na_2CO_3} : C_{NaHCO_3}.$$

According to the obtained data, this ratio in the initial solution was 9--10, and decreased in a solution submitted to

the action of an ultrasonic field owing to the increase of the $NaHCO_3$ content which enhances the leaching process. The change of the carbonate ratio made the determination of the intensification of the dissolution process possible. The mechanism of this phenomenon is attributed to the fact that in solutions chemical reactions are completed only when an insoluble deposit is precipitated from the solution as a result of the process, gas evolves or a little-dissociated compound forms in the solution.

It is known that under the influence of ultrasound in water nitric acid forms from dissolved nitrogen [1]; however, usually its concentration in a solution is negligible since equilibrium is established at an early stage. But sodium carbonate reacts with nitric acid according to the equation

$$HNO_3 + Na_2CO_3 \rightarrow NaNO_3 + NaHCO_3$$

and due to the decrease in the acid concentration new portions are formed as a result of which the content of sodium bicarbonate in the solution is increased and the carbonate ratio decreased.

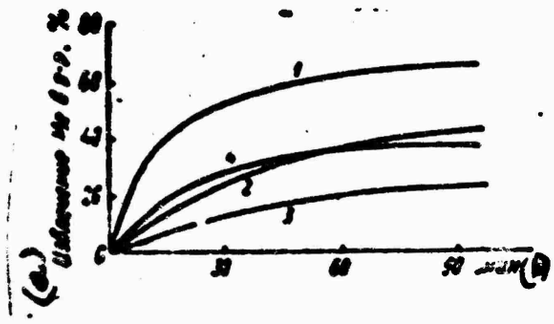

Fig. 3. Effects of the duration and temperature on the degree of leaching: 1, 2 and 3 -- with ultrasound at a temperature of 80, 60, and 45°C, respectively; 4--without ultrasound at 80°C.
Key: a) Mo extraction in solutions, %; b) min.

In the course of the tests one liter of the tested solutions was poured into a two-liter chemical glass and heated by means of a glass coil. The application of ultrasound was combined with the bubbling of the solution and mixing with a 400 to 1200 rpm mixer. Soda solution was treated for 30 minutes at 45°C, 60°C, and 80°C. Figure 3 gives the effects of temperature on the degree of leaching at a rotation speed of the mixer of 400 rpm. The diagrams show that at 80°C the

ultrasound intensifies the leaching process as compared with ordinary mixing. However, a decrease in the temperature sharply lowers the degree of leaching and the effect of the ultrasound becomes negligible.

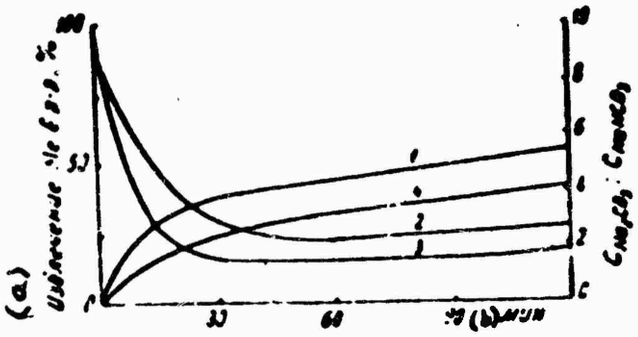

Fig. 4. The effect of the leaching time on the degree of leaching and the carbonate ratio with n = 400 rpm, t = 80°C: 1, 3 -- with ultrasound; 2, 4 -- without ultrasound; 1, 4 -- extraction; 2, 3 -- ratio of concentrations. Key: a) Me extraction in solutions, %; b) minutes.

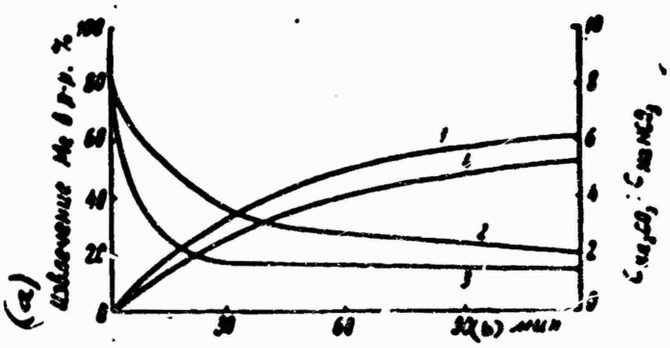

Fig. 5. The effect of the leaching time on the degree of leaching and the carbonate ratio with n = 800 rpm, t = 80°C. Designations of the curves same as in Figure 4. Key: a) Me extraction in solutions, %; b) minutes.

Figures 4, 5, and 6 show the results of analogous experiments with increased pulp mixing speeds of 400, 800, and 1200 rpm at 80°C. By increasing the mixing speed of the pulp the effectiveness of the ultrasonic field is lowered. The asymptotic approach of the curves characterizing the kinetics of the process with and without the application of the ultrasonic field at high mixer speeds leads to the assumption about the similarity of the mechanism of dissolution in both cases,

namely about the cavitational disruption of the diffusion layer on the phase boundary [11].

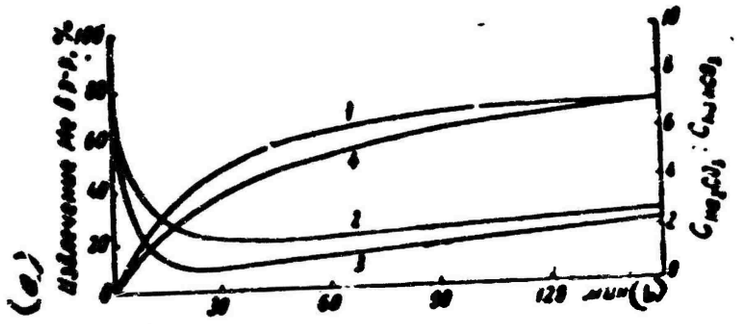

Fig. 6. The effect of the leaching time on the degree of leaching and the carbonate ratio with n = 1200 rpm, t = 80°C. Designations of the curves same as in Figure 4. Key: a) Me extraction in solutions, %; b) minutes.

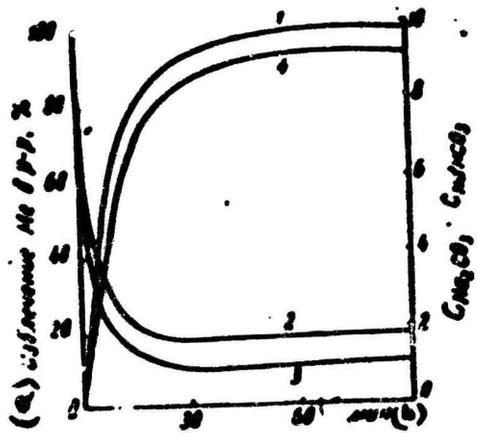

Fig. 7. The effect of the leaching time and of the ultrasonic field on the degree of leaching and the carbon ratio with n = = 400 rpm, t = 80°C. Designations of the curves same as in Fig. 4. Key: a) Me extraction in solutions, %; b) minutes.

Figure 7 illustrates the relation of the degree of leaching of more soluble compounds. Although the rate of the leaching process in this case is higher, the general character of the relation remains unchanged.

The obtained results show that with the help of ultrasound a 5 to 15% increase in the rate of extraction of certain rare metal compounds can be achieved. The effect of ultrasonic sound is most conspicuous when mixing of the pulp is rather slow (400 rpm).

Conclusions

1. Investigations showed that the effect of ultrasound on Na_2CO_3 + $NaHCO_3$ aqueous solution decreases the $C_{NaCO_3} \cdot C_{NaHCO_3}$ ratio of concentrations in the solution. The authors attempt to explain this phenomenon.

2. The effect of ultrasound on the completeness of the dissolution of difficultly-soluble rare metal compounds in carbonate solutions was investigated. It was found that an ultrasonic field created by magnetostrictive transformer with a frequency of 18 to 20 kilocycles and an ultrasound intensity of 0.55 wt/cm^2 appreciably accelerates the dissolution of these compounds in soda solutions.

3. The ultrasonic effect proved most conspicuous with a slower mechanical mixing.

4. The combined use of slow mechanical mixing and ultrasonic action is recommended for practical application.

5. It is suggested in the paper that the effect of ultrasound application prevents diffusion and capillary limitations enhancing the intensification of dissolution processes of substances.

BIBLIOGRAPHY

1. Fridman V. M. Zvukovyye i ul'trazvukovyye kolebaniya i ikh primeneniye v legkoy promyshlennosti (Sound and Ultrasound Oscillations and Their Application in Light Industry), Gizlegprom, 1956.
2. Bergman L. Ul'trazvuk i yego primeneniye v nauke i tekhnike (The Ultrasound and Its Application in Science and Technology), IL, Moscow, 1957.
3. Krouford A. E. Ul'trazvukovaya tekhnika (Ultrasonic technology), IL, 1958.

4. Fridman V. M. Primeneniye ul'trazvuka v legkoy i tekstil'noy promyshlennosti (The Use of Ultrasound in Light and Textile Industry), Series 1 and 2, TsINTI Light Industry, Moscow, 1959.
5. Kapustin A. P. Vliyaniye ul'trazvuka na protsessy kristallizatsii i rastvoreniya (The Effect of Ultrasound on Crystallization and Dissolution Processes), Proceedings of the All-Union Conference on Ultrasound, MDNTP, 1957.
6. Pfefferkorn G. Optik, No 7, 208 (1950).
7. Bardasarov Kh. S. Vliyaniye ul'trazvukovykh kolebaniy na skorost' rastvoreniya monokristallov (The Effect of Ultrasonic Oscillations on the Dissolution Rate of Single Crystals), Proceedings of the All-Union Conference on Ultrasound, MDNTP, 1957.
8. Dolgopolov N. N., Fridman V. M., El'piner I. E. Izv. AN SSSR (News of the Acad. Sci. USSR), Vol 93, No 9, 305 (1953).
9. Losev V. N., Mel'nikova A. N., El'piner I. E. Izv. AN SSSR, Division of Technical Sciences, No 9, 90 (1957).
10. Andreyev P. F., Rogozina E. M., Rogozin Yu. M. Zh. fiz. khimii Vol, 34, No 112429 (1960).
11. El'piner I. E. Zh. priroda, No 11, 23, 1958.

THE BEHAVIOR OF THE BASIC CONSTITUENT BLAST-FURNACE SLAG COMPONENTS DURING HYDROCHEMICAL PROCESSING

By A. R. Rakhimov, V. D. Ponomarev and L. P. Ni,
Kazakh Polytechnic Institute.
Chair of Metallurgy of Light and Rare Metals.

pp 111--115

As a result of the substantial growth of aluminum consumption anticipated in the near future in our country, the problem of expanding the raw-material base of the aluminum industry acquires particular significance.

One of the promising types of aluminum raw material is blast-furnace slag produced during the melting of aluminum iron ores [1--3]. This problem is particularly topical in Kazakhstan with its extraordinary rich reserves of such ores in Tselinnyy Kray (Lisakovo and Ayat deposits).

In extracting alumina from blast-furnace slag in which the molecular $CaO:SiO_2$ ratio is 1.0 to 1.5, the method of soda sintering is comparatively expensive. In our opinion, the processing of this type of slag by hydrochemical alkaline method is more promising and gives good results for various forms of natural and artificial aluminum silicates [4--8]. However, the organization of the alumina production from blast-furnace slag by means of hydrochemical leaching calls, in the first place, for a clarification of the behavior of the basic constituent aluminum slag components, namely the behavior of anorthite, gelena calcium dialuminate and their mixtures inasmuch as the practically possible compositions of this type of slag lie in the field of gelena (in the phase diagram of the $CaO-Al_2O_3-SiO_2$ system) and these components will be contained in them during crystallization.

The weight ratios of these compounds in the solidified slag vary depending on the composition of the slag. Therefore, knowing the behavior of every compound the assessment of the behavior of any slag during hydrochemical processing will be made possible. The investigations conducted by the authors were devoted to this task.

Al_2O_3 was experimentally leached from the basic constituents of blast-furnace slag such as anorthite, gelena, and its eutectic mixture with calcium dialuminate in a steel autoclave with external electric heating. The autoclave was set up under an angle of 15° on a horizontal plane and revolved at 55--60 rpm. Together with the batch of the specimens the necessary amount of the initial aluminate working solutions was poured into the autoclave so as to obtain a rated caustic pulp modulus after the test. Then, the autoclave was rotated and the electric heating turned on simultaneously. The starting time of the test was recorded as soon as the predetermined temperature was attained in the autoclave.

Chemical Composition of the Compounds Used in the Experiments

(a) Материалы	Содержание, %(b)			$CaO : SiO_2$, (c) мол.
	CaO	Al_2O_3	SiO_2	
Геленит (d)	40,26	37,84	21,50	2,0
Анортит (e)	20,70	37,04	43,30	0,5
Эвтектическая смесь (f)	35,47	51,20	14,02	2,5

Key: a) compounds; b) content, %; c) mole; d) gelena; e) anorthite; f) eutectic mixture.

Upon the completion of the test, the autoclave was cooled and the pulp discharged on a filter. After separating it from the liquid phase, the residue was washed off with hot water. The experiments were controlled by means of the liquid phase which was analyzed for Al_2O_3 and Na_2O contents by a method developed by VAMI (All-Union Alumina Metals Institute). The chemical composition of the tested alumina components is given in the table.

The reactions that take place during autoclave leaching with concentrated alkaline solutions may be expressed as follows:

for anorthite:

$$2(CaO\cdot Al_2O_3\cdot 2SiO_2) + 6NaOH + nH_2O \rightarrow Na_2O\cdot Al_2O_3 + Na_2O\cdot 2CaO\cdot 2SiO_2\cdot nH_2O + Na_2O\cdot Al_2O_3\cdot 2SiO_2\cdot nH_2O; \quad (1)$$

for galena:

$$2(2CaO\cdot Al_2O_3\cdot SiO_2) + 6NaOH + nH_2O \rightarrow 2(Na_2O\cdot Al_2O_3) + Na_2O\cdot 2CaO\cdot 2SiO_2\cdot nH_2O + 2Ca(OH)_2; \quad (2)$$

for the eutectic mixture:

$$2(2CaO\cdot Al_2O_3\cdot SiO_2) + CaO\cdot 2Al_2O_3 + 10NaOH + nH_2O \rightarrow 4(Na_2O\cdot Al_2O_3) + Na_2O\cdot 2CaO\cdot 2SiO_2\cdot nH_2O + 3Ca(OH)_2. \quad (3)$$

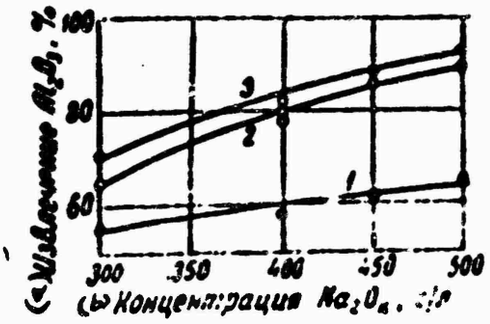

Fig. 1. The effect of Na_2O concentration in the initial solution on alumina extraction from: (1) anorthite; (2) galena; (3) eutectic mixture at 290°C, time: 30 minutes, calculated caustic pulp modulus: 13. Key: a) Al_2O_3 extraction, %; b) Na_2O_k, g/l.

The effect of the concentration of the initial working solution. Test results of the effect of Na_2O concentration in initial aluminate working solutions are shown in Figure 1. For galena and eutectic mixture a high Al_2O_3 extraction (90 to 93%) is attained by using solutions containing 450 g/l Na_2O and more. For anorthite Al_2O_3 extraction is much lower at this concentration of the solution amounting to 62--65%. This is attributed to the fact that the molecular $CaO:SiO_2$ ratio in anorthite

is equal to 0.5:1.0. It follows from reaction (1) that the insufficient quantity of calcium oxide accounts for losses of aluminum oxide due to the formation of $Na_2O \cdot Al_2O_3 \cdot 2SiO_2 \cdot nH_2O$ permutite.

A weakening of the sodium oxide concentrations causes a sharp decrease in the Al_2O_3 content in the solution for all three tested minerals. Therefore, a high concentration of the alkaline solution is an important factor for a rapid and effective extraction of Al_2O_3.

The effect of temperature. The temperature has a considerable effect on the extraction of Al_2O_3 during the leaching of artificial alumina raw material. This is confirmed by experimental data (Fig. 2), which show that the extraction of Al_2O_3 is particularly sharply increased after raising temperatures from 270 to 300°C. For galena and eutectic mixture the extraction increases from 85--88% to 90--93% and from 61% to 65% for anorthite.

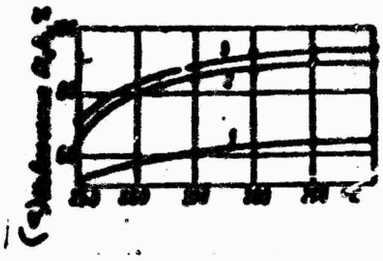

Fig. 2. The effect of leaching temperature on alumina extraction from: (1) anorthite; (2) galena; (3) eutectic mixture; time: 30 minutes; calculated caustic pulp modulus: 13. Composition of initial solution: 500 g/l Na_2O; α_k = 30. Key: a) Al_2O_3 extraction, %.

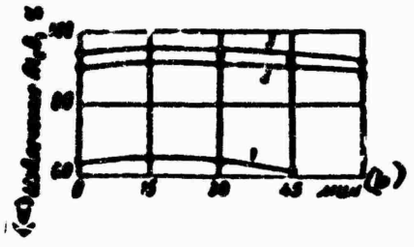

Fig. 3. The effect of leaching time on the alumina extraction from: (1) anorthite; (2) galena; (3) eutectic mixture at 290°C, calculated caustic pulp modulus: 13. Composition of the initial solution: 500 g/l Na_2O; α_k = 30. Key: a) Al_2O_3 extraction, %; b) minutes.

Consequently, the high yield of Al_2O_3 during the dissociation of the basic blast-furnace slag constituents by hydrochemical method may be attained at 280 to 290°C as a result of the increased activity in the interaction of the tested substance with alkali.

The effect of leaching time. The leaching time and temperature are closely connected. An increase in temperature

usually reduces the leaching time. A 0 to 30-minute increase in the leaching time (see Fig. 3) somewhat lowers the extraction of Al_2O_3 which is attributed to secondary processes which occur between the solid phase and the aluminate solution.

The effect of the calculated caustic pulp modulus. According to earlier hydrometallurgical findings, the calculated caustic modulus has a considerable effect on the extraction of Al_2O_3 during leaching [3, 6].

Fig. 4. The effect of the calculated caustic modulus on alumina extraction from: (1) anorthite; (2) galena; (3) eutectic mixture at 290°C, time: 30 minutes; composition of the initial solution: 500 g/l Na_2O; α_k = 30. Key: a) Al_2O_3 extraction, %; b) calculated caustic pulp modulus.

A study of the effect of the calculated caustic pulp modulus showed (Fig. 4) that the optimum value of a modulus is 13. (The calculation of the amount of raw material was based on the formula recommended by L. P. Ni [9]). With all other conditions at an optimum and a pulp modulus of 13 and higher, a high Al_2O_3 extraction is ensured in the solution prepared of galena and its eutectic mixture with calcium dialuminate reaching 90--93% and 64--65% for anorthite. It is noteworthy that an increase in the calculated caustic pulp modulus above 13 is inexpedient since aluminum solutions with lower oxide concentrations are obtained.

Optimal conditions were established as a result of systematic testing of hydrochemical processing of the basic constituent alumina blast-furnace slag components which would ensure a high extraction of Al_2O_3: Na_2O concentration in the initial aluminate working solution was 450--500 g/l; the

caustic modulus of the initial working solution was 30--35; the calculated caustic pulp modulus was 13; leaching time: 15 to 30 minutes; temperature: 280--290°C.

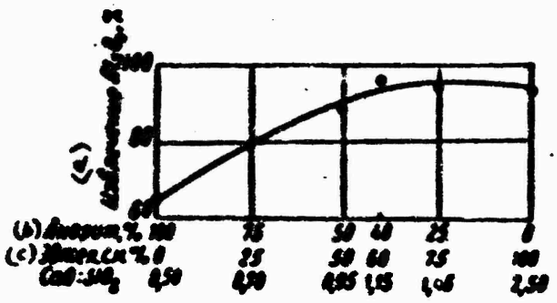

Fig. 5. The effect of the percentile relationship in the anorthite and galena specimens on alumina extraction at 290°C; time: 30 minutes; calculated caustic pulp modulus: 13; composition of the initial solution: 500 g/l Na_2O; α_k = 30. Key: a) Al_2O_3 extraction, %; b) anorthite; c) eutectic mixture.

A study of the effects of the main technological factors on the process of decomposition (Al_2O_3 extraction) of the main constituents of blast-furnace slag during the hydrochemical process showed that there is a similarity of behavior with nepheline and red slurry although the latter is, primarily, represented by aluminum oxide in the form of $Na_2O(K_2O)\cdot Al_2O_3\cdot 2SiO_2\cdot nH_2O$ aluminumsilicate alkaline metals and in the slag in the form of calcium aluminosilicates.

Tests were carried out under optimal conditions with a combined hydrochemical treatment of galena - anorthite and a eutectic mixture - anorthite with various weight ratios (see Figures 5 and 6). The test results show that the degree of Al_2O_3 extraction in the solution depends on the ratio of the above-mentioned compounds in the mixtures. A sufficiently high extraction (93--94%) is attained with 40% anorthite plus 60% galena and 40% anorthite plus 60% eutectic mixture. At the same time, an optimum molecular $CaO:SiO_2$ ratio of 1.10--1.15 is provided for the batch.

Consequently, a combined hydrochemical processing of the mixture of these compounds ensures a higher extraction of Al_2O_3

as compared to the processing of separate compounds. This fact is highly significant for the hydrochemical alkaline method of processing alumina blast-furnace slags inasmuch as the method is suitable for the processing of galena and galena dialuminate blast-furnace slags by soda solutions that are not readily decomposed.

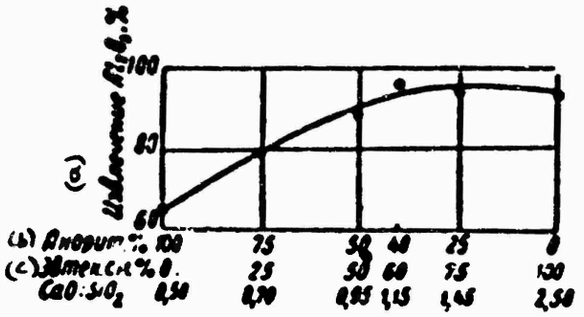

Fig. 6. The effect of the percentile relationship in the anorthite and eutectic mixture specimens on alumina extraction at 290°C; time: 30 minutes; composition of the initial solution: 500 g/l Na_2O; α_k = 30. Key: a) Al_2O_3 extraction; b) anorthite; c) eutectic mixture.

Conclusions

1. The behavior of the main alumina blast-furnace slag constituents such as anorthite, galena and its eutectic mixture calcium dialuminate was studied during leaching by hydrochemical method.

2. The possibility of decomposing the main constituent components of blast-furnace alumina slag by hydrochemical methods was shown for the first time.

3. The most suitable components for hydrochemical alkaline processing were found to be galena and galena-dialuminate high-alumina blast-furnace slags.

BIBLIOGRAPHY

1. Sushkov A. I., Troitskiy I. A., Eydenzon M. A. Metallurgiya legkikh metalloy (The Metallurgy of Light Metals), Sverdlovsk, 1957.

2. Khodak L. P., Kuznetsov S. I. et al. Byull. glinozemnoy promyshlennosti (Bulletin of the Main Institute for Industrial Alumina), Legkiye metally, No 1, 5 (1958).
3. Mikhaylov V. V., Korotich V. I., Khodak L. P., Ivanov A. I. Vestnik AN KazSSR (Herald of Acad. Sci. Kazakh SSR), No 7, 198 (1961).
4. Ponomarev V. D., Sazhin V. V. S. Tsvetnyye metally (Nonferrous metals), No 12, 1957.
5. Ni L. P., Izv. Akademii Nauk KazSSR (News of the Acad. Sci. Kazakh SSR), Series of Metallurgy, Beneficiation and Refractories, Vol. 1, 1958.
6. Ponomarev V. D., Nurmagambetov Kh. N., Putilin Yu. M. Trudy in-ta metallurgii i obogashcheniya AN KazSSR (Proceedings of the Institute of Metallurgy and Beneficiation of Acad. Sci. Kazakh SSR), Vol. IV, 1962.
7. Ponomarev V. D., Sazhin V. S. NDVSh. Metallurgiya (Metallurgy), No 2, 1959.
8. Ni P. P., Ponomarev V. D. Izv. AN KazSSR, Series of Metallurgy, Benefication and Refractories, Vol 1, 4 (1959).
9. Ni L. P., Izv. AN KazSSR, Series of Metallurgy, Beneficiation and Refractories, Vol 1, 7 (1960).

Manuscript submitted 23 Oct 1962

SEPARATION OF VANADIUM AND URANIUM IN FLUORIDE SOLUTIONS WITH THE HELP OF ANIONITES

By V. S. Pakholkov and A. Ya. Korbut
Ural Polytechnical Institute

pp 116--121

The method of ion exchange chromatography was used by many investigators for the separation of uranium from vanadium and from other elements. To separate uranium from vanadium and molybdenum, N. T. Voskresenskaya [1] carried out a sorption of these elements by "PFSK" paraphenol sulfocationite, and then washed out vanadium and molybdenum in the form of per acid with a 5% solution of hydrogen peroxide. Uranium was washed with 5% solution of sulfuric acid.

D. I. Ryabchikov, P. N. Paley, and Z. K. Mikhaylova [1] separated uranium from vanadium, iron, molybdenum, tungsten, copper and lead by passing the solutions of these elements with the addition of ethylene tetradiamine acetic acid through a column with a "KU-2" cationite. Only uranium was retained by this while all remaining elements which formed resistant complex anions passed into the filtrate.

D. I. Ryabchikov, M. M. Senyavin, Z. K. Mikhaylova [1] and Klement [2] also used cation exchange for the separation of uranium from vanadium, aluminum and phosphorus. After sorption from solutions with pH = 1.5--2.0, the cationite was at first washed out from the vanadium and aluminum with a 10% solution of ammonia, then the uranium with a 5% solution of ammonium carbonate. The use of anionites for the precipitation of elements from solutions and for separation has become popular only in the last ten to fifteen years. Therefore, the problems dealing with the separation of the above elements are insufficiently described in literature.

Yu. V. Korachevskiy and M. M. Gordeeva [3] took advantage of the difference in the sorptive ability of complex uranium (VI) and vanadium (V) chloride anions and separated these elements in hydrochloric acid solutions (8 N NCl) by means of "PE-9" and "EDE-10P" anionites.

A. L. Arnfelt [4] carried out the separation of uranium and vanadium from sulfate solutions with the help of strong-base anionite "daueks-2" in the form of SO_4^{2-}. In a number of other papers [5--7] the use of anionic exchange in the technology of nuclear fuel is reported as a method for the separation of vanadium from uranium. In this case the process is conducted in two stages: common sorption V (V) and U (VI) and selective washing out of vanadium by solutions which contain a reducing agent to convert the vanadium into a tetravalent state.

In all the above papers, with the exception of paper [3], the separation of uranium and vanadium with the help of ion exchange resins was conducted in weak acid solutions. All proposed methods were used for the separation of small quantities of uranium and vanadium during the quantitative determination of these elements in ores and minerals.

This paper is devoted to the separation of uranium and vanadium from hydrochloric acid solutions, containing hydrofluoric acid, with the help of anionites "AB-17," "AB-16," "EDE-10P," and "AH-2F." The use of fluoride solutions makes it possible to prevent the hydrolysis of pentavalent vanadium and to carry out the process of separation in solutions with a high content of hydrochloric acid.

For the determination of conditions of separation the sorption of uranium (VI) from 0.05 N UO_2Cl_2 by anionites was studied as it depends upon the concentration of salt and hydrofluoric acids. Furthermore, the washing out of tetra- and pentavalent vanadium, sorbed from HCl--HF solutions, from anionites by various washing solutions and water was studied.

The study of the sorption of uranium (VI) from HCl--HF solutions was conducted under dynamic conditions in organic glass columns with a 1.4 cm^2 section and a height of 30 cm. The air-dry grains size of the used anionites was 0.1--0.25 mm. The quantity of ionite in the column was 2 g (converted into a dry state).

The filtration of the solution was carried out until the complete saturation of ionite by uranium. The ionite was assumed to be saturated if two days after the stopping of the column the concentration of uranium in the filtrate was equal to its concentration in the initial solution. Uranium was washed from the saturated ionite with a weakly acid solution of ammonium chloride. The content of uranium in the washing solution was determined by weight analysis. The results of the analyses were used to calculate the absorbability of uranium.

Experiments concerned with the washing out of vanadium from anionite and with the separation were conducted in the same organic glass columns. The quantity of ionites for the study of washing and separation was 6 g of each (converted into the dry state). In using "AB-16G" anionite its quantity was decreased in all experiments to 4 g (converted into dry material). The sorption of vanadium (IV) in the washing experiments was carried out from 0.1 M $VOCl_2$ solutions, containing 0.1 mole/l HCl and 0.5 mole/l HF. The filtration of the solution through the ionite layer was carried out until vanadium (VI) appeared in the filtrate, i.e., before it passed through the filter. The correct time was determined by the qualitative reaction with dimethylglyoxine [8]. The filtration rate of the solutions during sorption and washing was equal to 1 $ml/cm^2 \cdot min$ in all experiments.

The washing action of water, 0.1 and 0.3 HCl solutions containing 5 g/l HF was investigated. The filtrate that was discharged from the columns was removed by 30 ml fractions in calibrated organic glass tubes. The content of V in the batches was determined by volumetric analysis, titrating 0.1 potassium permanganate solution with a Reyngard mixture [9]. In order to eliminate the effect of the fluorine ion on the results of permanganate titrating, boric acid or aluminum sulfate were added to the specimen of the solution.

According to the results of analyses of individual fractions, integral diagrams of vanadium washing from anionites were plotted. The experiments of separating uranium (VI) and vanadium (IV) were conducted with the use of "AB-17," "AB-16G," "EDE-10P" and "AN-2F" anionites. Uranium (VI) and V (IV) were separated from a solution with the following composition (in mole/l): 0.05 UO_2CL_2, 0.1 $VOCl_2$, 0.1 HCl and 0.5 HF.

During the filtration of the solution through the column uranium (VI) was completely sorbed by anionite, while the tetravalent vanadium would partially pass into the filtrate. After

the sorption of uranium (VI) and vanadium (IV) the ionite was washed with a 0.3 N HCl + 5.0 g/l HF solution. Vanadium then passed entirely into the filtrate. In using a high-basicity "AB-17" anionite for the separation of uranium and vanadium, vanadium was displaced from the ionite by water after the sorption of uranium.

Uranium in all experiments was washed from anionites with 1 N HCl. In washing out vanadium as well as in washing out uranium the filtrate from the column was removed in 30 ml fractions. Results of analysis of every fraction for the vanadium and uranium contents were plotted in a separation diagram. For the separation of uranium (V) and vanadium (V), sorbed from HCl--HF solutions by anionites, solutions were used containing a reducing agent. We have used sodium sulfite and hydrochloric hydroxylamide acid as reducing agents. In filtrating the hydrochloric acid solution containing fluorine ions and a reducing agent through anionite, vanadium was restored to the tetravalent state and transferred entirely into the filtrate. In this case the method of separation was analogous to the above described method.

Fig. 1. Uranium (VI) and vanadium (V) sorption from HCl--HF solution with a high basicity AB-17 anionite. Concentration of HCl (in mole/l): 0.1 (1), 0.3 (2), 0.5 (3), 1.0 (4) and 2.0 (5). Key: sorbability $M_{mole}UO_2^{2+}$; b) HF concentration, mole/l.

Figure 1 represents the results of uranium (VI) sorption from 0.05 M UO_2Cl_2 solutions, containing hydrofluoric acid with a high-basicity AB-17 anionite. By way of comparison the same figure shows data on the sorption of pentavalent vanadium

from HCl--HF solutions by the same ionite. We have taken the data on vanadium sorption from the preceding paper [10].

Character of the dependence of uranium sorption (VI) and the HCl and HF concentration for all four studied ionites is identical. Therefore, the experimental data on the sorption of uranium from HCl--Hf solutions by anionites "AH-2F," "EDE-10P" and "AB-16G" are not given in this paper.

Fig. 2. Sorption of vanadium (VI) from HCl--HF solutions by EDE-10P anionite. HCl concentration (in mole/l): 0.1 (1), 0.3 (2), 0.5 (3). Key: a) Sorbability Mmole VO_2^{2+}; b) HF concentration, mole/l.

From the data of Fig. 1 it follows that pentavalent vanadium from HCl--HF solutions as well as uranium (VI) is very well sorbed by anionites. In this connection it is not expedient to use pentavalent vanadium for the process of separation. It is obvious that only a method based on the use of anion exchange properties of tetravalent vanadium is suitable as a simple, convenient and fast method of separation of uranium and vanadium. This is confirmed by the data in Figure 2, which show that tetravalent vanadium is absorbed in insignificant quantities by anionite EDE-10P (and also AB-16, AH-2F). The sorption from solutions with a low content of hydrofluoric acid is particularly low. The high-basicity AB-17 anionite does not sorb tetravalent vanadium at all. The substantial difference in the absorbability of uranium (VI) and vanadium (IV) from solutions by anionites was used for their separation. For the purpose of determining the conditions of complete separation we have studied the washing of sorbed tetravalent vanadium from AV-2F, EDE-10P and AV-16G anionites using 0.1 N and 0.3 N HCl solutions containing 5 g/l HF, and water.

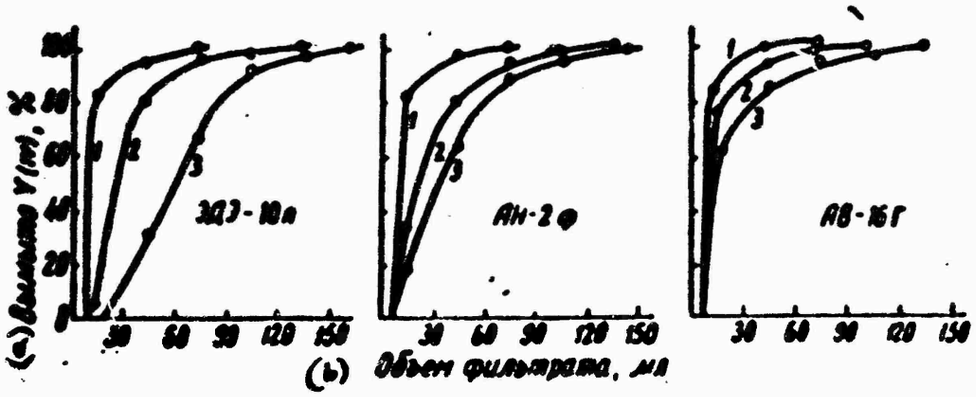

Fig. 3. Washing out of vanadium (IV) from AV-2F, EDE-10P and AB-16G anionites. Quantity of sorbed vanadium 2 mg·equiv VO^{2+}. Elution solutions: 0.3 N HCl + 0.25 N HF (1), H_2O (2) and 0.1 N HCl + 0.25 N HF (3). Key: a) washed out V (IV), %; b) volume of filtrate, ml.

The integral washing diagrams of sorbed vanadium (IV) from anionites are represented in Figure 3; they show that tetravalent vanadium is comparatively easily washed out from all anionites by water and hydrochloric acid solutions with an addition of 5 g/l HF. Vanadium is washed out particularly thoroughly with 0.3 N HCl, containing 0.25 mole/l HF. Water, despite its good washing ability, cannot be applied for separation with AB-16G, EDE-10P and AH-2F anionites, since it also washes out uranium in small quantities. In this case, a complete separation of uranium and vanadium is not attained. High-basicity anionite AB-17 does not hydrolize in the form of salt, and uranium sorbed from HCl--HF solutions by this ionite is not washed away by water. Therefore, water is suitable as a washing solution for vanadium during the separation with anionite AB-17. Hydrochloric acid solutions, containing fluorine ions, did not wash out uranium from all investigated anionites and it was not detected in the filtrate.

Results of experiments of uranium (VI) and vanadium (IV) separation with the help of AB-16G, EDE-10P, AH-2F and AB-17 anionites are represented in Figure 4. In using hydrochloric acid with hydrofluoric acid additions as a washing solution a complete separation of uranium and vanadium is attained. In vanadium fractions uranium is not qualitatively revealed. From all investigated anionites the most suitable is high-basicity anionite AB-17, which does not absorb tetravalent vanadium at all.

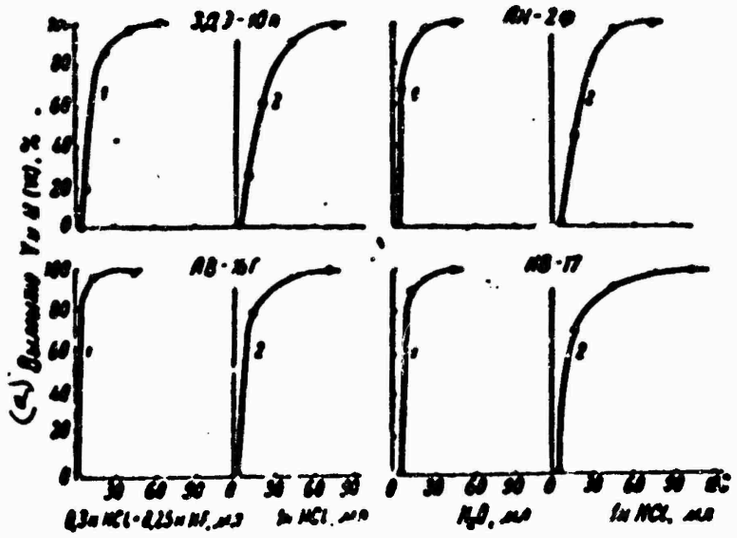

Fig. 4. Separation of vanadium (IV) (1) and uranium (VI) (2) with anionites. Quantity of separated vanadium and uranium: 2 mg·equiv VO^{2+} and 3 mg·equiv UO_2^{2+}. Key: a) washed out V and U (VI), %.

The results of the above experiments show the possibility of indicating the conditions of separation of uranium (VI) and of pentavalent vanadium with the use of fluoride solutions. These conditions will evidently be the following: joint sorption of uranium (VI) and vanadium (V) from HCl--HF solutions, washing of vanadium with 0.1 N or 0.3 N HCl solution, containing HF and a reducing agent. In filtrating this solution through ionite with sorbed elements, vanadium would be reduced to tetravalent state and pass into the filtrate. Sulfuric acid or sodium sulfite are suitable as reducing agents.

In order to investigate the possibility of using solutions with a reducing agent in the separation of uranium (VI) and vanadium (V) experiments were conducted with anionite AB-17. For the washing of vanadium sorbed from HCl--HF solutions 0.1 N HCl, containing 5 g/l HF and 10 g/l Na_2SO_3 was used. In addition to Na_2SO_3 we used also hydrochloric hydroxylamine. Results of experiments of separation are represented in Fig. 5 and 6.

It is clear that in both cases a complete separation of uranium and vanadium takes place. Hydroxylamine is a more

effective reducing agent, although its use creates substantial inconveniences as a result of the discharge of gaseous nitrogen in process of reduction.

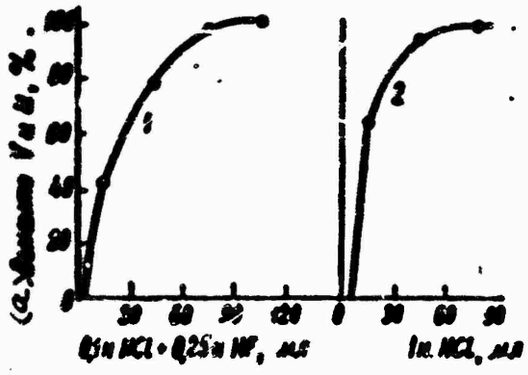

Fig. 5. Separation of vanadium (V) (1) and uranium (VI) (2) anionite AB-17. Quantity of separated vanadium and uranium: 4 mg·equiv VO_2^+ and 4.3 mg·equiv UO_2^{2+}. Reducing agent: 1.0% Na_2SO_3. Key: a) washed out V and U (%).

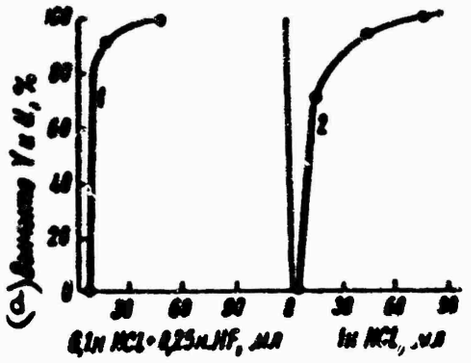

Fig. 6. Separation of vanadium (V) (1) and uranium (VI) (2) anionite AB-17. Quantity of separated vanadium and uranium: 4 mg·equiv VO_2^+ and 4.03 mg·equiv UO_2^{2+}. Reducing agent: 1.0% hydrochloric hydroxylamine solution. Key: a) washed out V and U, %.

Conclusions

1. The sorption of uranium (VI) from HCl--HF solutions was investigated and the results of the study compared with results of vanadium sorption to determine the conditions of separation of the above two elements with the help of AH-2F, AB-17, EDE-10P and AB-16G anionites.

2. The washing out of vanadium (IV), sorbed from HCl--HF solutions from AB-17, EDE-10P, AB-16 and AH-2F anionites with water and hydrochloric acid solutions with addition of hydrofluoric acid was investigated.

3. A complete separation of uranium (VI) and vanadium (IV) with the help of all studied anionites was carried out.

4. A method of uranium (VI) and vanadium (V) separation in solutions, containing hydrofluoric acid, with the help of anionites has been proposed and experimentally verified.

BIBLIOGRAPHY

1. Ryabchikov D. I., Senyavin M. M. Materials of the International Conference on the Peaceful Use of Atomic Energy (Geneva, 1955), Vol. 8, 328, Metallurgizdat, M., 1958.
2. Klement R. Chemiker-Ztg, V. 74, 334 (1953).
3. Morachevskiy Yu. V., Gordeyev M. N. Vestnik Len. Univ. (Herald of Leningrad University), Series of Physics and Chemistry, No 10, 2, 148 (1957).
4. Arnfelt A. Z. Acta Chem. Scand. V. 9, 1484 (1955).
5. Foos R. A. Mining Engng, V. 8, No 9, 893 (1956).
6. Galkin N. P., Mayorov A. A., Voryatin U. D. Technology of Processing Uranium Concentrates, M., Atomizdat, 1960.
7. Chem. and Engng. News, No 15, 49 (1959).
8. Blok N. I. Qualitative Chemical Analysis. Goskhimizdat, 1952.
9. Gillebrand V. F., Lendel G. Ye. Practical Guide of Inorganic Analysis, M., Goskhimizdat, 1957.
10. Pakholkov V. S., Korbut A. Ya. Izv. VUZ Nonferrous Metallurgy, No 5, 100 (1962).

Manuscript submitted 16 Apr 1962

Influence of Preliminary Deformation on Self-Diffusion in Silver and Its Alloys

By M. E. Yanitskaya,
Moscow Institute of Steel and Alloys. Chair of physical chemistry

pp 122-124

This work is dedicated to the study of parameters of self-diffusion in metals, subjected to preliminary deformation, and the influence of small additions of a second component on these parameters.

The literature contains data on the influence of deformation on diffusion in metals and alloys, however systematic research in the influence of concentration on self-diffusion in deformed alloys was not conducted until now. Self-diffusion in pure iron, diffusion of tin in nickel and its alloy during imposition of stretching efforts, but also later on preliminary deformation was studied in work [1]. In all cases there is a considerable increase of diffusion mobility and decrease of activation energy, especially in aging nickel alloy. At significant degrees of deformation, volume deformation is accelerated more than threshold. Authors explain this by a larger orderliness of volume, as compared with boundaries, and insignificant changes in the latter during deformation. Coefficient of diffusion during diffusion annealing of preliminarily deformed alloys remained constant, which proves the formation during deformation of such structural changes, which do not disappear during annealing, and are nonreversible, or require for removal a longer time.

Work [2] considered diffusion in chrome-nickel alloy in connection with the study of the problem of recrystallization. Increase of coefficients of diffusion, obtained at the beginning of diffusion annealing, in distinction from results of work [1], decreased in time. Authors, discussing this

non-correspondence, consider that, judging by temperature rates, recrystallization in work [1] occurred earlier than the study of diffusion.

For manifestation of the influence of additions on the effect of influence of preliminary deformation on self-diffusion, we measured parameters of self-diffusion in silver and its alloys, containing 1.3 and 5% Sn, in both deformed and annealed specimens.

In these alloys, we had earlier [3] determined parameters of self-diffusion in samples subjected to a long diffusion annealing near the temperature of melting. Meanings of these magnitudes were used now for checking reproducibility of results. In the present work, experiments with equilibrium samples were performed during all investigated temperatures.

Diffusion constants were determined by the film method [4], making it possible to observe the kinetics of the process. Specimens before annealing were deformed to 75% cold rolling. With such deformation, following conclusions of work [1], it is possible to consider that the influence of it on volume diffusion is significantly greater than on threshold. Diffusion was determined at temperatures of 560, 600, and 660°.

Annealed and deformed specimens experienced diffusion annealing simultaneously; this eliminated error due to fluctuations of temperature in checking the effect of deformation on diffusion mobility.

Kinetic curves, slope of which determines the coefficient of self-diffusion, in all cases represented straight lines, and besides slope of them in experiments with deformed specimens is larger than with annealed (table). This proves an increase of mobility of atoms due to definite structural changes, which are not destroyed under the conditions of the experiment. Similar long increased mobility of atoms is noted by Pines [5] during cold working of powder materials, which considerably accelerates sintering in spite of the fact that recrystallization succeeds to pass during a time tens of times smaller than the duration of sintering.

During comparison of the influence of additions of tin on mobility of atoms of main metal in equilibrium and deformed alloys, there is revealed an essential distinction. If in annealed samples there occurs an increase of speed of self-diffusion with concentration, then for deformed samples all three temperatures are minimum at 1% Sn. Consequently during introduction of small additions of tin, there occurs a decrease

of mobility of atoms of silver, apparently due to the location of tin in regions with an increased mobility that closes these regions for diffusion of main atoms.

Coefficients of Self-Diffusion of Silver in Annealed and Deformed Specimens

(a) Sn, вес. %	560°			600°			660°		
	$D_{отж} \cdot 10^{12}$ (b)	$D_д \cdot 10^{12}$ (c)	$D_д : D_{отж}$	$D_{отж} \cdot 10^{12}$	$D_д \cdot 10^{12}$	$D_д : D_{отж}$	$D_{отж} \cdot 10^{12}$	$D_д \cdot 10^{12}$	$D_д : D_{отж}$
0	2,0	9,3	4,63	4,5	17,5	3,8	16,0	37,0	2,3
1	2,8	6,1	2,18	6,0	10,0	1,67	20,0	21,0	1,0
3	3,5	8,4	2,4	6,67	12,2	1,80	20,0	24,0	1,2
5	—	—	—	7,3	16,4	2,24	24,0	27,0	1,1

a -- Sn, weight %; b -- Annealed; c -- Deformed.

Such atomic arrangement of tin is like in the Cottrel cloud [6]. Impurities, according to Cottrel, lower elastic energy of dislocations and their mobility is stronger, the bigger the difference in radii of atoms and their valence. In the Ag-Sn system, this difference is essential. Further increase of concentration decreases the effect connected with saturation by atoms of defective places and dissolution of them in volume.

The ambiguity found in the work in influence of additions on self-diffusion in annealed and deformed specimens can be compared with the ambiguity discussed in works [6-7] in influence of alloying on self-diffusion in equilibrium materials and recrystallization.

From work [8] it is known that a small addition in all cases retards recrystallization in deformed specimens and at the same time very frequently accelerate self-diffusion in the annealed one.

It is possible that in work the delay obtained of self-diffusion reflects an increase of the temperature threshold of beginning of recrystallization, proceeding basically by means of diffusion, corresponding, as a rule, to 1% impurity.

The meaning of activation energy considered in the work in equilibrium alloys coincides within limits of experiment errors with those which we obtained in work [3] (44 kilocalories). In deformed specimens, activation energy hardly depends

upon concentration and in interval of temperatures investigated constitutes 24-26 kilocalories.

Manuscript submitted 8 December 1962

Bibliography

1. S. Z. Bokshteyn, T. I. Gudkov, A. A. Zhukhovitskiy, Kishkin. DAN USSR, 121, 6, 1015 (1958).
2. S. S. Gorelik, Romashov, Shchedrin. Collection MIS, No 39, 1955.
3. M. E. Yanitskaya, A. Zhukhovitskiy, S. Z. Bokshteyn. DAN USSR, 112, 4 (1957).
4. S. N. Kryukov, A. A. Zhukovitskiy. DAN USSR, 90, 380 (1953).
5. Pines. UFAN, 52, 4 (1954).
6. Zomer, Cottrel. Phil. Mag., 46, 7, 11 (1955).
7. S. S. Gorelik. Author's abstract of dissertation, 1962.
8. Smit. Principles of Physics of Metals, 1959.

Investigation of Influence of Compositions and Temperature Conditions on Hot-Brittleness of Alloys of Aluminum With Magnesium During Casting in Chill Mold

By Ma Chia-chi, A. G. Spasskiy,
Krasnoyarsk Institute of Nonferrous Metals. Chair of foundry production

pp 125-127

Alloys of aluminum with magnesium for shaped casting, due to their small specific gravity, excellent stability in corrosional relation and high mechanical properties as compared with other alloys on aluminum basis found at present practical application in various branches of industry. In technological relation these alloys present known difficulties, since, possessing a large temperature interval of crystallization they are inclined to formation of friability, porosity, hot cracks, oxidation in melted state and so on.

Representing this group of alloys are alloys AL-8 and AL-13. For improvement of quality of these alloys were conducted a number of works [1, 2], which in definite measure increased their property and expanded region of their application. However many technological peculiarities of these alloys remain still unexplained.

This work is dedicated to an investigation of influence of contents of magnesium in aluminum alloys, temperatures of filling and temperatures of chill mold on inclination of alloys to appearance of hot cracks during casting in chill mold.

Hot-brittleness was determined by method of S. I. Spektorovoy and T. V. Lebedevoy [3], supplemented by A. M. Osokin [4] in reference to chill casting. By this method in metallic form are poured rings of thickness 5 mm, width from 5.0 to 42.5 mm through every 2.5 mm to appearance of cracks. The less the width of ring poured without cracks, the less the

the tendency of the alloy in question to exhibit cracks in period of crystallization under the conditions of hampered shrinkage. Casting of annular test it is possible to see on Fig. 1.

Every experiment for determination of hot-brittleness was repeated not less than two times. Microsections were etched 0.5% water solution of hydrofluoric acid. For color of chill mold was applied always the same paint, having followed composition (in parts by weight): 50 prepared chalk, 50 oxide of zinc, 5 soluble glass in 100 parts water.

Fig. 1.

Fig. 1
Ring test for hot-brittleness

For determination of influence of composition of alloy on hot-brittleness of investigation were conducted on aluminum alloys, containing 3, 6, 9 and 12% Mg respectively. All alloys were prepared from aluminum of brand A0 (99.6%) and aluminum-magnesium alloy, containing 20% Mg alloyed from aluminum of brand A0 and magnesium of brand MG-1 (99.92%).

Alloys for investigation were prepared preliminarily. Smelting was conducted in the following order: in gas hearth in warmed up to 300-350 graphite-fire clay crucible was loaded pig aluminum. After melting it and bringing of temperature melting to 700 from surface of liquid bath was removed slag and metal was covered protective layer of flux VI-3; then during turned off hearth in crucible under layer of flux is careful was

introduced warmed up to 150-200° magnesium for alloy or aluminum-magnesium alloy for alloys; mixing of metal was produced by graphite mixer slowly, without disturbance of flux cover. After mixing prepared for experiment alloy was flooded at a temperature 660-670° in preliminarily warmed up cast-iron casting moulds. Received small pigs of alloy served as further main working alloy for carrying out of all investigations.

Every alloy from above-mentioned compositions during determination of inclination of it to hot-brittleness was remelted in graphite-fire clay crucibles in electric furnace with silit heaters. Melting of aluminum alloys, containing 9 and 12% Mg was produced under layer of flux VI-3, and alloys with 3 and 6% Mg -- without application of flux.

For investigation of influence of temperature on hot-brittleness of alloys filling of them was carried out at temperatures 700, 760 and 800°. Temperature of alloys was checked with a chromel-Alumel thermocouple. For study of influence of temperature of chill mold, it was heated in muffle to temperatures 50, 200 and 300°. Filling of chill mold was produced in all cases through central funnel of short continuous stream, and besides, if extreme cylinders (see Fig. 1) were not filled completely, no metal was added. After filling and holding 2-3 minutes, chill mold was opened and ring casting extracted from it.

Received as result of experiments data shown in Fig. 2. From these data it is clear that to the extent of increase of contents of magnesium inclination to formation of hot cracks due to shrinkage stresses is lowered continuously. At definite temperature rate for alloys, containing 9 and 12% Mg, hot cracks at all are not revealed and with this width of ring, not giving cracks, is equal to 5 mm.

Continuous lowering of hot-brittleness of alloys with increase of contents of magnesium it is possible to explain by decrease of effective interval of crystallization and appearance of eutectic, which at definite quantity of it, closes up the previously formed cracks [5, 6] (Fig. 3).

It is necessary to underline that in given investigations, reproducing real conditions of casting, alloys were in unequal state and therefore point, corresponding in these conditions to highest solubility of magnesium at eutectic temperature, lies at significantly smaller concentration, than point on state of equilibrium diagram.

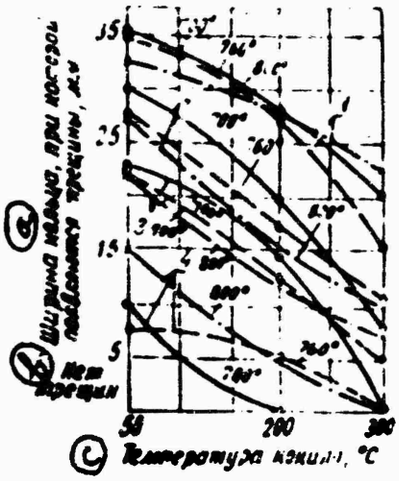

Fig. 2. Depencence of Inclination of Alloys to Hot-Brittleness from Temperatures of Filling and Temperatures of Chill Mold. Content in aluminum alloys of magnesium: 1 -- 3%, 2 -- 6%, 3 -- 9%, 4 -- 12%. Temperature of filling: 700, 760, 800.

a -- Width of ring, with which cracks appear, mm; b -- No cracks; c -- Temperature of chill mold.

Cited data clearly show also that increase of temperature of chill mold always beneficially affects crackstability of alloys. At a temperature of chill mold 300 for alloy with 9% Mg and at a temperature of chill mold 200 for alloy with 12% Mg hot cracks at definite temperature of filling do not appear. Decrease of hot-brittleness with increase of temperature of chill mold it is possible to explain by decrease of stresses in connection with decrease of difference of temperatures of metal and chill mold in period of crystallization.

Regarding influence of temperature of filling, results of experiments show that change of temperature little affects inclination to crack formation of aluminum-magnesium alloys. In our experiment from the viewpoint crackstability optimum temperature of filling lies within limits 700-760°.

Conducted investigations allow to make correct approach to selection of alloys for chill casting and to establish corresponding conditions by temperature of metal and chill mold: alloy of aluminum with 12% Mg in filling at a temperature of metal 700-760° and temperature of chill mold 200-300° cracks on samples do not appear. For alloy with 9% Mg it is necessary to heat chill mold to 300°.

To article of Ma Chia-chi, A. G. Spasskiy "Investigation of Influence of Composition and Temperature Rate on Hot-Brittleness of Alloys of Aluminum with Magnesium During Casting in Chill Mold."

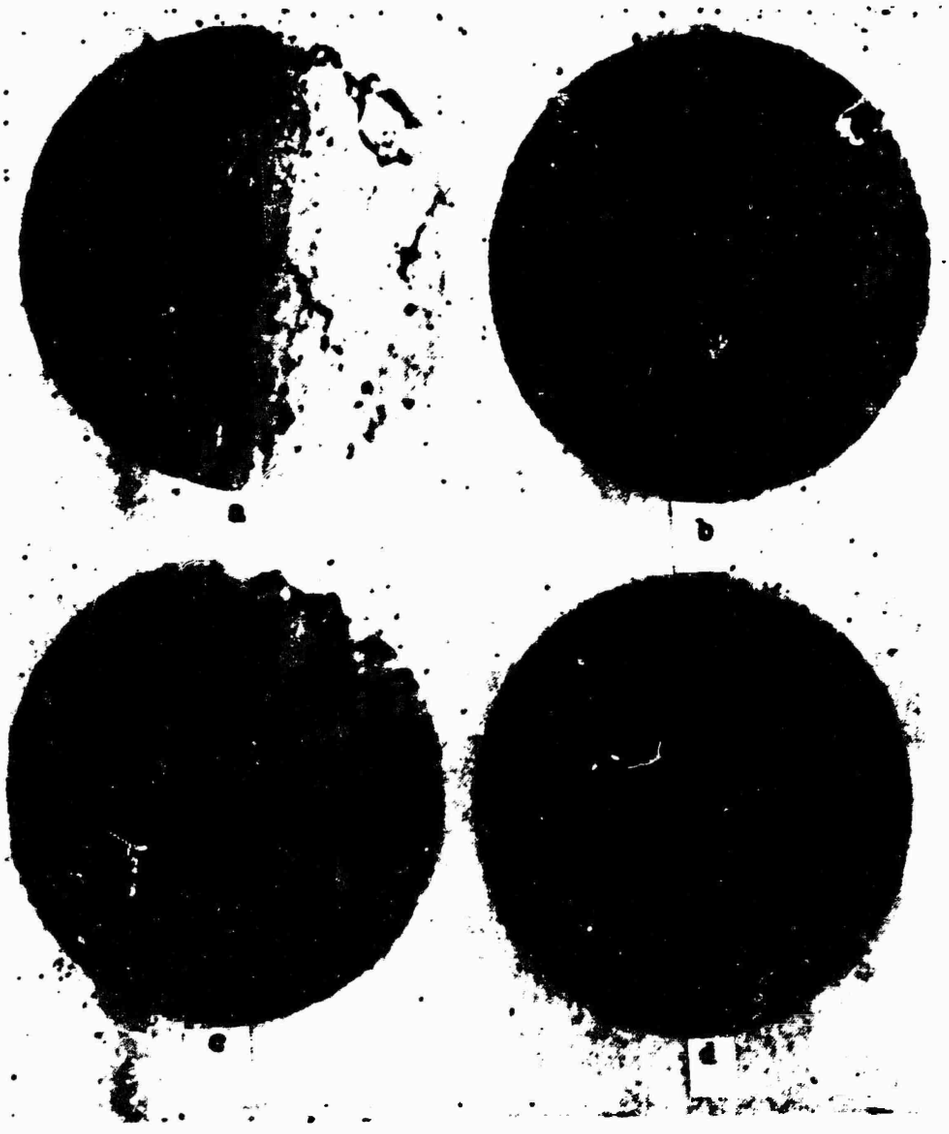

Fig. 3. Microstructure of Aluminum-Magnesium Alloys. Content of magnesium in them: a -- 3%, b -- 6% c -- 9%, d -- 12%.

Manuscript submitted 10 May 1961

Bibliography

1. M. V. Sharov, M. F. Odin. Tr. MATI, in. 11, Oborongi z, 1951.

2. L. Kubichek, M. V. Maltsev. Collection. "Investigation of Alloys of Nonferrous Metals," Izv. Acad. Sci. USSR, in. 2, 1960.
3. S. G. Glazunov, S. I. Spektorov. Technological Properties of Foundry Aluminum and Magnesium Alloys. Oborongiz, 1950.
4. A. M. Osokin. Foundry Production, No 1, 1956.
5. A. A. Bochvar, I. I. Novikov. Izv. Acad. Sci. USSR, OTN, No 2, 1952.
6. A. A. Bochvar, N. N. Rykalin, N. N. Prokhorov, I. I. Novikov, B. A. Movchan. Foundry Production, No 10, 1960.

Force Conditions During Pressing of Pipes With Arbitrary Internal Relief

By M. F. Zakharov, Yu. P. Glebov, M. Z. Yermanok

pp 128-136

Process of pressing of pipes with relief on internal surface consists in the following (Fig. 1): on split segment mounted with relief hollow ingot is put. Mounting with ingot is introduced in container, with one end of mounting placed in hole of mouthpiece, but on other end from side of press-stamp is put mobile die centered on container.

During dislocation of sloping press-stamp with die at first occurs deposit of ingot, after which starts direct pressing, with which relief of mounting is filled. The prepressed ingot will be cut by internal edge of die and remains in the form of thin-walled ribbed pipe on mounting, but surplus of metal is pressed out in the form of strips by reflux through windows in peripheral part of the die.

Proceeding from law of least resistance for shaping of ribs of pipe it is necessary, so that stresses, necessary for flow of metal to windows of die σ_d were larger than stresses necessary for filling of ribs σ_{rib}, i.e., $\sigma_d > \sigma_{rib}$.

In this work we consider questions of analytic determination of magnitudes σ_d and σ_{rib} and establishment on this basis of magnitude of minimum deformation during pressing out of strips, necessary to produce in the metal stresses necessary for filling of relief of mounting.

Initial relationships of geometric parameters of ingot and ribbed pipe.

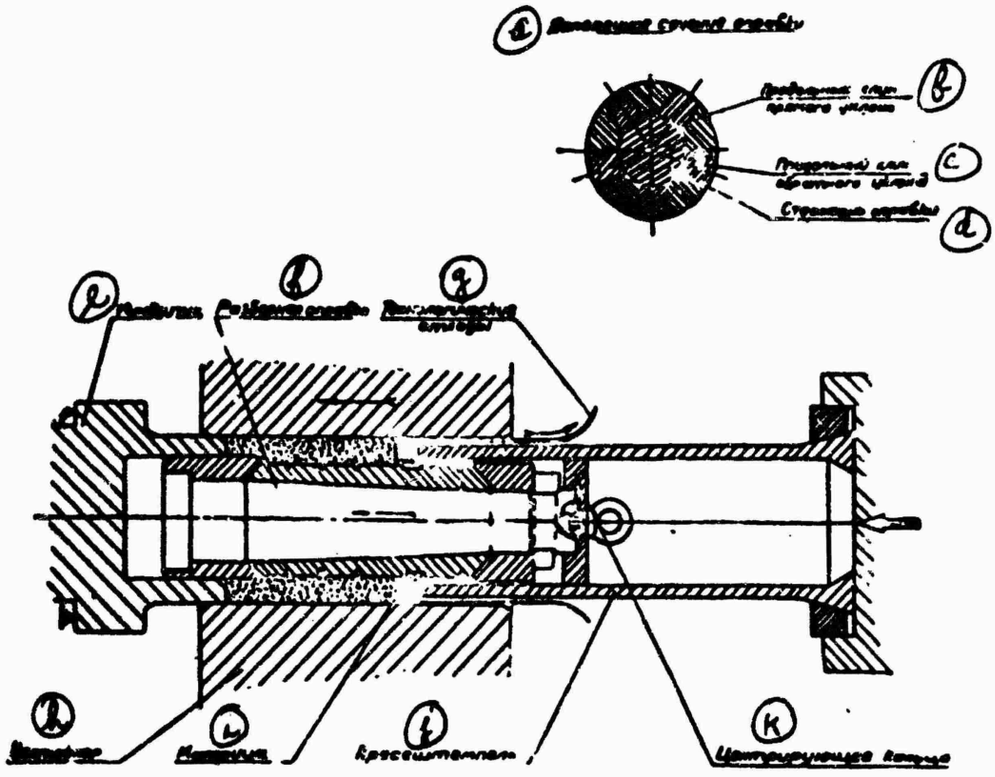

Fig. 1. Diagram of Process of Pressing of Pipes With Internal Relief.

a -- Cross section of mounting; b -- Longitudinal wedge of straight inclination; c -- Longitudinal wedge of reverse inclination; d -- Rod of mounting; e -- Mouthpiece; f -- Demountable mounting; g -- Technological waste; h -- Container; i -- Die; j -- Press-stand; k -- Centering ring.

Area of section of prestressed ingot

$$F = F_p + \Sigma F_s \lambda$$

where F_p -- area of section of ribbed pipe,

ΣF_s -- total area of section of strips,

λ -- coefficient of drawing during pressing of strips.

Area of section of ribbed pipe (Fig. 2)

$$F_p = F_{cloth} + \Sigma F_{rib},$$

where ΣF_{rib} -- total area of section of ribs in given section of pipe.

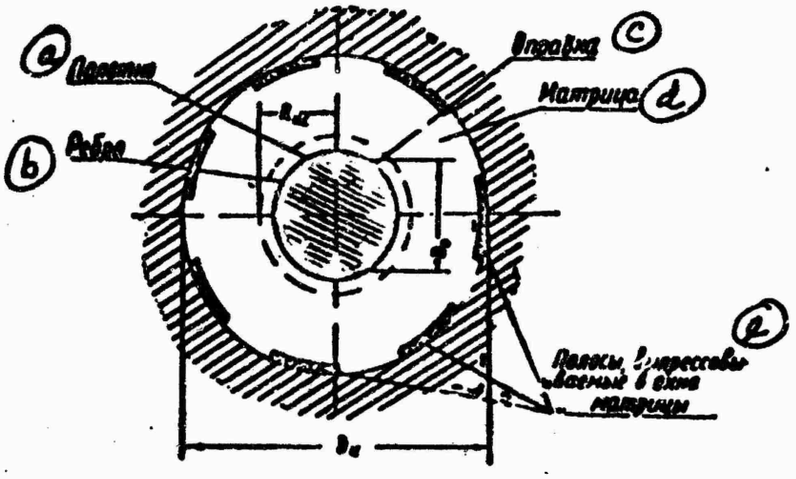

Fig. 2. Diagram for Determination of Conventional Boundary Flow of Metal.

a -- Cloth; b -- Rib; c -- Mounting; d -- Die; e -- Strip, pressed out to windows of die.

Coefficient of drawing at pressing of strips

$$\lambda = \frac{F_c - F_p}{\Sigma F_s}. \qquad (1)$$

On the basis of the above one can determine in cross section of ingot conditional boundary of flow of metal, proceeding to formation of ribbed pipe and on pressing of strips (neutral layer). This boundary represents circumference with radius $R_{n\ell}$ (see Fig. 2)

$$R_{n\ell} = \frac{1}{2}\sqrt{D_p^2 - 4\frac{\Sigma F_{rib}}{\pi}}$$

where D_p -- external diameter of ribbed pipe.

Thickness of layer of ingot, from which is formed ribbed pipe (see Fig. 2)

$$H = R_{n\ell} - \frac{D_m}{2},$$

where D_m -- diameter of cylindrical part of mounting.

Definition of stress, necessary for flowing of metal through outlet window of die σ_d. The process of flow of metal through outlet window of die is analogous to process of pressing of glass with counter flow on punch. On this basis in

pressing on flat die the full stress, necessary for dislocation of die equals

$$\sigma_d = \sigma_{R_d} + \sigma_{f_d} + \sigma_{f_{sh}}, \qquad (2)$$

where σ_{R_d} -- stress for realization of main deformation without calculation of losses on friction;
σ_{f_d} -- stress for surmounting of friction in die and hearth of deformation;
$\sigma_{f_{sh}}$ -- stress for surmounting of friction in calibrating shoulder of die.

According to conclusions cited in work [1], magnitude σ_{R_d} can be represented by expression

$$\sigma_{R_d} = \frac{1}{\cos^2 \frac{\alpha}{2}} \ln \lambda \beta s_{def} \qquad (3)$$

where λ -- coefficient of drawing, determined by formula (1);
S_{def} -- resistance to deformation;
α -- average-suspended angle of inclination of forming inert zone.

On the basis of data of works [2, 3] we assume $\alpha = 80°$. In view of absence of noticeable deformations in circumferential direction, the deformed state during pressing out of strips approaches the flat. On this basis coefficient $\beta = 1.1$ at $\alpha = 80°$ and $\beta = 1.15$

$$\sigma_{R_d} = 2S_{def} \ln \lambda. \qquad (4)$$

Stress for surmounting friction in die and focus deformation can be determined at equality of active and reactive forces and condition that in die passes metal, limited by container and "neutral" layer of diameter $2R_{n\ell}$.

Surfaces of friction are surfaces of container in focus of deformation and surface of retarded zone, for simplicity assumed to be conical with angle of inclination of generstrix α (Fig. 3). The force expended on friction during dislocation of elementary layer by height dx, is determined by expression

$$dN \quad V_1 \tau = D_\ell dx + V_x \tau = D_x \frac{dx}{\cos \alpha}.$$

From condition of constancy of volume, and also from the fact that in section AA $V_x = 0$

$$V_x = V_0\left(\frac{D_0^2 - D_{n\ell}^2}{D_0^2 - D_x^2} - 1\right).$$

and since $dx = \frac{dD_x}{tg\,\alpha}$, expression (3) can be represented in the form

$$dN = \frac{V_0 \pi}{tg\,\alpha}\left(\frac{D_0^2 - D_{n\ell}^2}{D_0^2 - D_x^2} - 1\right)\left(D_d + \frac{D_x}{\cos\alpha}\right) dD_x.$$

Integrating this equation from D_d to $D_{n\ell}$ and considering that the determined total force equals

$$N_{flow} = T_d V_0,$$

where T_d -- force on splint for surmounting friction in die and forcus of deformation, we will obtain

$$T_d = m(D_0^2 - D_{n\ell}^2)\left[\ln\frac{(D_0 + D_{n\ell})(D_0 - D_d)}{(D_0 - D_{n\ell})(D_0 + D_d)} + \frac{1}{\cos\alpha}\ln\frac{D_0^2 - D_{n\ell}^2}{D_0^2 - D_d^2}\right]D_d^2 -$$
$$- m(D_{n\ell} - D_d)\left[2D + \frac{1}{\cos\alpha}(D_{n\ell} + D_d)\right]. \qquad (5)$$

where $m = \frac{\pi}{2tg\alpha}$.

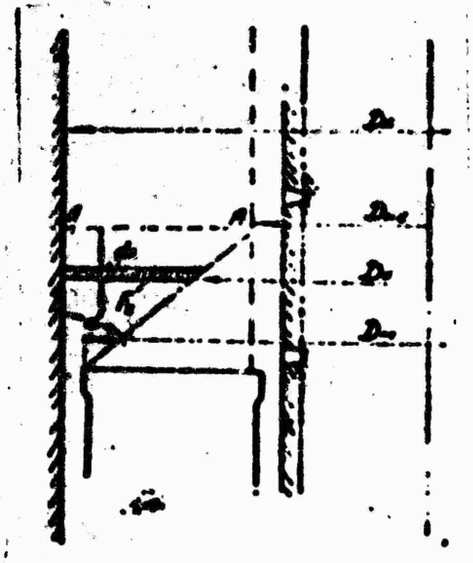

Fig. 3. Diagram to Determine Losses for Friction During Flow of Metal in Windows of Die.

On the basis of formula (5)

$$\sigma_{f_d} = \frac{T_d}{F_d}, \qquad (6)$$

where F_d -- area of force of die.

Losses on friction in calibrating shoulder of die are determined by known dependence

$$\sigma_{f_{sh}} = \lambda\frac{1}{F_d} f S_{def} F_p, \qquad (7)$$

where $F = F_{pw} + F_p$;

F_{pw} -- surface of shoulder in outlet windows;

F_{fp} -- surface of friction touching upon pipe.

Determination of stress necessary for filling of relief of mounting σ_{rib} is produced by analogy with stamping of ribbed panels [4]. Deformed state is assumed to be flat which does not lower accuracy of calculation, since cloth of pipe in considered process is shaped to cut and flow of metal in direction of forming mounting is practically absent. Distribution of stresses during flow of metal along longitudinal ribs is represented in Fig. 4.

The solution of the problem is conducted by elements. Let us define normal stress σ_y' in regions of cloth of pipe along length $t/2$ by analogy with deposit of strip in plane-parallel plates, but with that distinction that the upper block will be the boundary of metal. Here the shifting stress τ_{xy} will change from 0 on the line of division to τ_c on the contact surface.

Let us assume that stress σ_x does not depend on coordinates y, and, consequently, $\frac{\partial \sigma_x}{\partial x} \quad \frac{d \sigma_x}{d x}$.

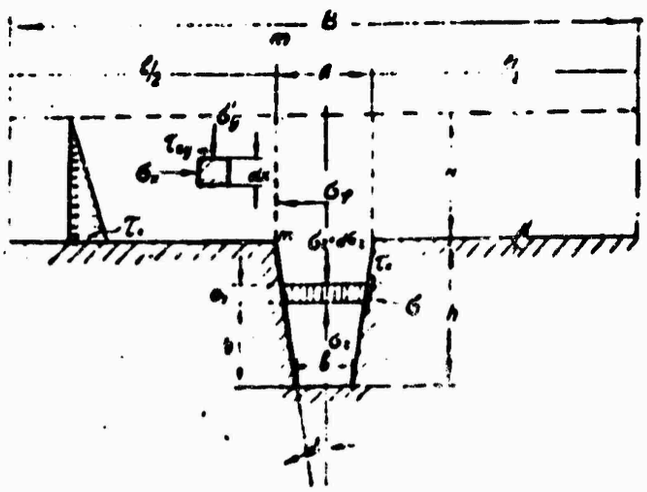

Fig. 4. Diagram to Determine Magnitude of Stress, Necessary for Flow of Metal in Slot of Mounting and for Deformation of it During Passage in Slots of Mounting.

Then it is sufficient from system of equations for plane problem

$$\left.\begin{aligned} \frac{\partial \sigma_x'}{\partial x} + \frac{\partial \tau_{xy}}{\partial y} = 0 \\ \frac{\partial \tau_{xy}}{\partial x} + \frac{\partial \sigma_y'}{\partial y} = 0 \end{aligned}\right| \qquad (8)$$

to assume only the first and, integrating it from 0 to H, we will obtain

$$\int \frac{\partial s_x'}{\partial x} dy + \int_0^H \frac{\partial \tau_{xy}}{\partial y} dy = 0.$$

Considering that $\frac{\partial s_x'}{\partial x}$ does not depend on y after integration and substitution of limits, we will receive an approximate equation of equilibrium

$$\frac{ds_x'}{dx} + \frac{\tau_0}{H} = 0. \qquad (9)$$

Using the approximate condition of plasticity

$$(s_y' - s_x')^2 + 4\tau_{xy}^2 = 4k^2$$

and assuming that tangential stress on contact attains its own maximum ($\tau_{xy} = \tau_0 = K$), we find the expression, attained earlier by E. P. Unksov [4]

$$ds_x' = ds_y'. \qquad (10)$$

On the basis of this after integration of equation (9) we obtain

$$s_y' = -\frac{\tau_0}{H} x + c.$$

The constant of integration we find from the condition that in the cross-section

mm at $x = \frac{l}{2}$ on the basis of (10)

$$s_y' = s_x' = \sigma_0,$$

then

$$c = \sigma_0 + \frac{\tau_0}{H} \cdot \frac{l}{2},$$

whence

$$s_y' = \sigma_0 + \frac{\tau_0}{H}\left(\frac{l}{2} - x\right).$$

The average surface tension on frontal surfaces can be represented by the expression

$$\sigma_R = \frac{2}{l}\int_0^{\frac{l}{2}} \sigma_y' \, dx.$$

After integrating and the necessary transformations we obtain

$$\sigma_R = \sigma_\varphi + \frac{\tau_c l}{2H}. \qquad (11)$$

In this equation σ_φ and l are unknown. Value l characterizing the extent of the plastic zone, feeding the rib of the relief, can be approximately determined on the basis of analysis of grids of slip lines.

L. A. Shofman [5], analyzing rigidly-plastic boundaries and fields of slip lines during stamping with a flow into two slots, located in mutually-perpendicular planes (in our case slot in mounting and slot in die), found that the magnitude of the extent of the plastic zone depends on the ratios $\frac{L}{A}$ and $\frac{h_1}{2a}$ (Fig. 5). And besides, for values $\frac{L}{A} > 10$ the value h_1 does not show an essential influence on magnitude $\frac{l}{2}$. Relationship $\frac{L}{A} > 10$ practically corresponds to the entire assortment of pressed ribbed pipes. Thus, for the most wide applied dimension of ribbed pipes the distance between the nearest neighboring ribs L = 100 mm, and thickness of rib at the base ≈ 10 mm, i.e., A = 5 mm and ratio $\frac{L}{A} = 20$. For this relationship magnitude $\frac{l}{2A}$, according to the data of L. A. Shofman, equals 8, i.e., $l = 16$ A. (12)

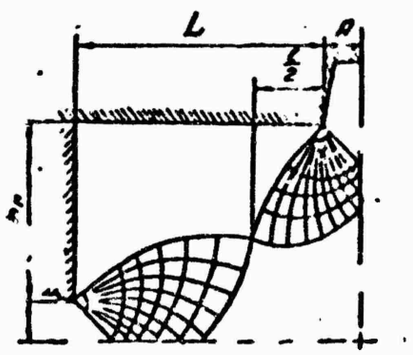

Fig. 5. Diagram to Determine Boundaries of Plastic Zones and Fields of Slip Lines During Stamping With Flow in Two Slots (according to L. A. Shofman).

The value $\sigma_\varphi = \sigma_{r\,max}$ (see Fig. 4) is determined by conditions of pressing metal along cone of slot and full shaping of angles of ribs. We will present σ_r in the form of two components

$$\sigma_{r\ max} = \sigma_{r\ def} + \sigma_{r\ p}.$$

where $\sigma_{r\ def}$ stress, necessary for deformation, i.e., for passing of metal in cone of slot without calculation of losses for friction,

but σ_{rf} stress, conditioned by friction of metal along wall of slot.

Value $\sigma_{r\ def}$ will approximately be defined from the condition of equilibrium of elementary volume. Inasmuch as angle α equals 3-5°, and by obtaining condition $r = 0$, then σ_r and σ_{sh} without great error can be assumed for principal normal stress and condition of plasticity, it is possible to register in the form

$$\sigma_{sh} - \sigma_{r\ def} = \beta S_{def}.$$

The condition of equilibrium of elementary by height dy is recorded in the form

$$(\sigma_{r\ def} + d\sigma_{r\ def})(F_y + dF_y) - \sigma_{r\ def}F_y - 2\sigma_s\frac{dy}{\cos\alpha}\sin\alpha = 0, \quad (13)$$

where $F_y = v + 2y\ tg\ \alpha$.

Substituting the values of F_y and σ_{sh} in (13) and neglecting infinitely small magnitudes of the second order, we will obtain

$$d\sigma_{r\ def} = \beta S_{def}\frac{2\ tg\ \alpha\ d\ y}{b + 2\ y\ tg\ \alpha}.$$

After integrating

$$\sigma_{r\ def} = \beta S_{def} ln(v + 2\ tg\ \alpha\ y) + c,$$

$$\text{at } y = 0,\ \sigma_{r\ def} = 0 \quad c = -\beta S_{def} ln\ v,$$

then

$$\sigma_{r\ def} = \beta \cdot S_{def} ln(1 + 2\ tg\ \alpha\ \frac{y}{v}).$$

The maximum value of $\sigma_{r\ def}$ will be taken $y = t$

$$\sigma_{r\ def} = \beta S_{def} ln(1 + 2\ tg\ \alpha\ \frac{t}{v}). \quad (14)$$

Losses for friction during filling by metal of rib of mountings are determined by method of I. L. Perlin [1] from the equality of input power and power, expended on surmounting of friction (Fig. 6).

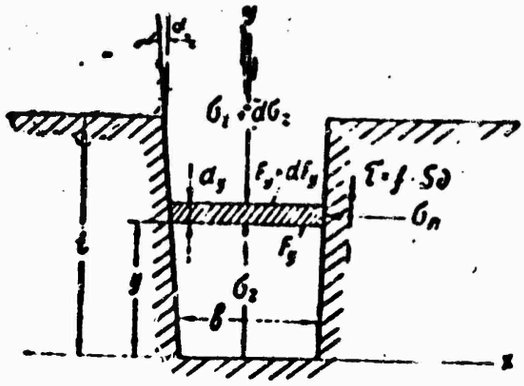

Fig. 6. Diagram to Determine Losses for Friction During Transfer of Metal into Slots of Mounting.

Power, expended on passage of the elementary layer dy at speed v_y, equals

$$dN_y = 2fS_{def}\frac{dy}{\cos\alpha}tv_y,$$

where f -- coefficient of friction at yield point;
dN_y -- in turn, is equal to input power, which one can determine by the formula

$$dN_{inp} = dpv_{flow},$$

where dp -- elementary force, conditioned by friction of elementary volume;
v_{flow} -- rate of flow of metal in slot in section y = t.

Then we can write

$$dpv_{flow} = 2fS_{def}\frac{dy}{\cos\alpha}tv_y. \qquad (15)$$

v_y from condition of constancy of second volumes will be determined from expression

$$v_y = v_{flow}\frac{v + 2\,\mathrm{tg}\,\alpha\, t}{v + 2\,\mathrm{tg}\,\alpha\, y},$$

then expression (15) will assume the form

$$dp = 2fS_{def}\frac{t}{\cos\alpha}(v + 2\,\mathrm{tg}\,\alpha\, t)\cdot\frac{dy}{v + 2\,\mathrm{tg}\,\alpha\, y}.$$

Integrating along the entire surface of friction, we will obtain

$$p = 2fS_{def}\frac{l}{\cos\alpha}(v+2\operatorname{tg}\alpha\, l)\int_0^l \frac{dy}{v+2y\operatorname{tg}\alpha},$$

$$p = 2fS_{def}\frac{l}{\cos\alpha}(v+2\operatorname{tg}\alpha\, l)\frac{1}{2\operatorname{tg}\alpha}\ln\left(1+2\operatorname{tg}\alpha\frac{l}{v}\right).$$

The surface, on which force p acts equals

$$\ell(v + 2\ \operatorname{tg}\alpha\ t);$$

than the necessary stress for surmounting of forces of friction at the cone of the slot

$$\sigma_r\ p = fs\ \frac{1}{\sin\alpha}\ln\left(1+2\operatorname{tg}\alpha\frac{l}{v}\right). \qquad (16)$$

On the basis of function (14) and (16), magnitude

$$\sigma_r = \beta S_{def}\left(1+\frac{f}{\beta\sin\alpha}\right)\ln\left(1+2\operatorname{tg}\alpha\frac{l}{v}\right). \qquad (17)$$

Substituting into equation (11) values $\sigma_\varphi = \sigma_r$ from (17) and ℓ from (2), we obtain the average magnitude of stress on boundary of flow of metal, necessary for filling of relief of mounting

$$\sigma_R = \beta S_{def}\left(1+\frac{f}{\beta\sin\alpha}\right)\ln\left(1+2\operatorname{tg}\alpha\frac{l}{s}\right)+4\frac{S_{def}A}{H}. \qquad (18)$$

The obtained value of stress σ_R, as follows from the condition of plasticity, differs from the fractional maximum by magnitude βs_{def} on the condition that $\tau = 0$.

Considering the approximate character of the conducted solution, it is possible to assume R_d and σ_d the main radial and functional stresses respectively and to consider that for realization of filling of ribs we should observe the ratio

$$\sigma_d > \sigma_R + \beta S_{def}. \qquad (19)$$

The determination of the magnitude of the minimum degree of deformation during pressing out of strips is conducted:

σ_R by the formula (18),
σ_d by the formula (19),
σ_{f_d} by the formulas (5) and (6).

Considering that at a definite thickness of strip (determined by the preliminarily assumed value D_d, see Fig. 3) the

magnitude of the degree of deformation can be modified owing to a change of quantity of strips, as well as their width, obtain possibility of conducting process at a constant value σ_{f_d}.

The value of sum $\sigma_{R_d} + \sigma_{f_d} = \sigma_d - \sigma_{f_d}$.

The magnitude of minimum drawing λ_{min} is determined from formulas (4) and (7).

It is obvious that during calculations one should consider section of pipe with minimum thickness of cloth and at maximum height of the thinnest ribs, since filling of relief in such sections is the most energy holding.

Manuscript submitted 29 August 1962

Bibliography

1. I. L. Perlin. Tsvetnyye metaly (Nonferrous Metals), No 9, 1957.
2. V. V. Zholobov, G. I. Zverev. Pressing of Metals, Metallurgizdat, 1960.
3. P. A. Sarychev. Flow of Aluminum Alloys During Pressing, Oborongiz, 1946.
4. Ye. P. Unksov. Engineering Theory of Plasticity, Mashgiz, 1959.
5. L. A. Shofman. Fundamentals of Calculation of Processes of Stamping and Pressing, Mashgiz, 1961.

Appearance of Lines of Fluidity During Deformation of Highly Durable Aluminum Alloys

By A. T. Zakharov,
Moscow Engineering-Economic Institute. Chair of technology of metals

pp 137-143

Production of parts of aircraft and motor vehicles from sheet aluminum alloys of high durability occurs with the help of processes, stamping, drawing and covering on stamping and stretching presses.

Flat preparation, formchanging in process of transformation of it into an article, undergoes a complicated state of strain. Separate stages of preparation undergo evenly stretched stresses in uniaxial and biaxial directions, at the same time other sections undergo compressed tensile stress. Process of formchange of preparations occurs with growing degree of deformation from minimum in initial period to significantly large elastic-plastic flows during final obtaining of articles.

In the process of formchange of preparation and transformation of it into an article of a given configuration, lines of fluidity appear on surfaces of the preparation, which rapidly move on the surface of the preparation in this or that direction but usually under a certain angle to the applied load, causing dullness of the surface of the preparation. During further deformation, there is observed repeated appearance of lines of fluidity and movement of them along the surface of the preparation, evoking considerable dullness, changing into ripples.

Disappearing strips of fluidity, observed during deformation of sheets from aluminum alloys of high durability, sharply differ from lines of fluidity, described [1, 2] during deformation of preparations from low-carbon steels, revealing site of

fluidity. In these cases, on preparation appears a characteristic figure, recording the state of stress of formchange of preparation [3], which does not disappear even at the end of deformation.

For a study of the physical essence of the mechanism of plastic flow of aluminum alloys, experiments were conducted for the purpose of determination of the moment of appearance of lines of fluidity depending upon the degree of deformation, nature and state of the aluminum alloy. It was necessary also to fix the speed of lines of fluidity and to make observations of the change of the polished surface of the alloy depending upon the speed of deformation.

For observation of lines of fluidity, we used highly durable deformed aluminum alloys of brands AMtsM, D-16 and V-95. Specimens were prepared from one-millimeter sheet metal, differently heat treated(annealed, fresh-hardened and aged); one side of specimens was polished to mirror surface, of which observations were made.

Specimens were subjected to uniaxial elongation on breaking machine with force of 1200 kg at speeds of leading clamp 40, 10 and 3 mm/minute. Change of polished surface of specimen was observed visually, and speed of appearing and moving lines of fluidity was fixed with the help of a movie camera with subsequent treatment of films in the form of stills. From this, the speed of lines of fluidity was fixed.

Observation showed that during the test of alloy of brand AMtsM, possessing high plasticity, site and line of fluidity on samples during their test and on articles during formation are not observed. Curve diagram of elongation has a smooth character independent of the speed of the leading clamp of machine--speed of deformation.

Test of specimens from aluminum alloy of brand D-16, with various thermal treatment and various speeds of deformation, showed that on polished surface of specimen there are observable visually fast moving lines of fluidity which, depending upon the thermal treatment and the speed of deformation, appear differently, but a definite regularity in manifestation of them and character of motion is maintained.

At speed of deformation 40 mm/min, independently of thermal treatment on polished surface of specimen after achievement of 3% ratio, appear fast transferred lines of fluidity at first in one, and then in the other direction on the polished surface of the specimen. The motion of the lines

of fluidity is continued with diminishing speed with certain interruptions. During every appearance of lines of fluidity, the arrow of forcemeter oscillates by jerks, leaving a trace on the curve diagram of elongation (Fig. 1) in the form of eroded stretched deflections from the normal curve of elongation. The process of elongation of the specimen to break occurs after 30 sec., therefore, to trace appearance of dullness and transition of it into a ripple on the polished surface of the specimen is difficult, but with the help of a movie camera we fixed the moment of appearance of lines of fluidity and speed of their motion. In fresh-hardened state, appearance of lines of fluidity occurs more intensely. We hear crackling at the moment of appearance of next lines of fluidity.

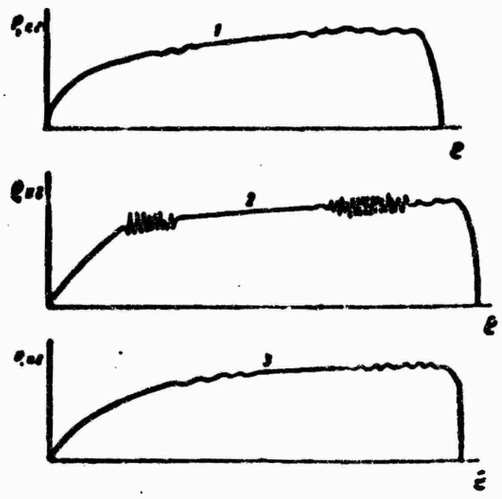

Fig. 1. Curve Diagram of Elongation of Specimens of Alloy D-16 at Speeds of Deformation: 1 -- 40 mm/min, specimen 8; 2 -- 10 mm/min, specimen 1; 3 -- 3 mm/min, specimen 12.

After the end of the process of deformation on the surfaces of the specimen no traces of the movement of lines of fluidity remain, just as during formchange of flat preparation in article during stamping-drawing, figures of fluidity are not fixed from diagram of stress deformed state, undergone by the preparation.

In the process of deformation of the same specimens with speed 10 mm/min, there is the possibility to conduct visual observation for changes, occurring on the polished surface of deformed specimen and the moment of appearance of lines of fluidity and speed of their movement to fix with the help of a motion picture camera; vacillations of loads are fixed by a recording apparatus of a machine on a curve of the diagram of elongation.

Analysis of the curve diagram of elongation and the charge on the polished surface of the specimen is performed jointly with visual observations and deciphering the film. Results of analysis showed that there are seven stages of deformation of specimen, which correspond to seven sections on the curve diagram of elongation, shown in Fig. 2. Corresponding with the analysis of the curve diagram of elongation, we will list a description of the results of the observations.

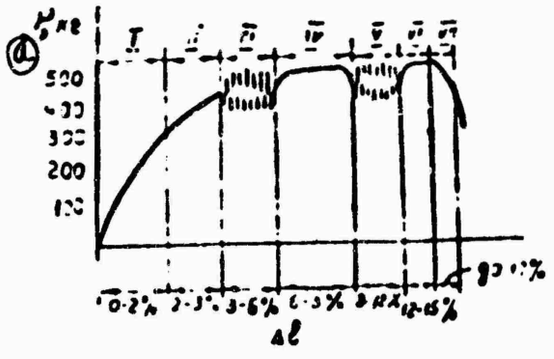

Fig. 2. Curve of Diagram of Elongation of Specimen of Alloy D-16 with Sections Revealing Strips of Fluidity.

a -- R, kilogram.

Section I -- stage of elastic deformation 2% relative elongation. Curve diagram of elongation does not have deflection from normal curve. Polished surface of specimen does not change.

Section II -- stage of plastic flow to 3% relative elongation. Polished surface of specimen grows foggy, becomes slightly dull.

Section III -- stage of plastic flow 3-6% relative elongation. Is characterized by the appearance of the first line of fluidity on polished surface of specimen, which in the beginning is not brightly expressed and moves with a speed 17 mm/sec and then is clearly expressed and moves with a speed 15 mm/sec; we hear crackling.

Polished surface of specimen becomes duller with appearance of ripples. On curve diagram of elongation appear teeth in result of load variations, which reach to 8-12 kilograms. Every variation corresponded to the appearance of lines of fluidity, attenuation of speed of motion which gave more eroded figure of curve diagram of elongation.

Section IV -- stage of plastic flow, which corresponds 6-8% relative to the elongation of the specimen. With this,

on the polished surface of the specimen there is not observed appearances of lines of fluidity. On this section of load, variations were not noticed, curve of diagram of elongation has a smooth section without teeth. Surface of the specimen changes from dull to rippled.

Section V -- stage of plastic flow, corresponding 8-12% relative to the elongation of the specimen. With this deformation on surfaces of specimen, there again appeared lines of fluidity of second period. Speed of their movement is delayed as compared with speed in first period. First wave of lines of fluidity moved with speed 1.7 mm/sec, the second -- with a speed of 1.5 mm/sec; the counter movement of lines of fluidity passed with speed of 1.0 mm/sec. On surfaces of specimen, appear more clearly expressed ripples.

On three samples out of twelve tested, lines of fluidity stopped at the end or at the middle part of the specimen; they were the focus of destruction of the specimen, but, as a rule, no traces on surfaces of it remain. On curve diagram of elongation, as a result of load change, there appeared teeth. Every tooth characterizes deflection of load 10-15 kilograms.

Section VI -- stage of plastic flow, corresponding 12-15.5% relative to the elongation of the specimen. With this deformation, there occurs uniform elongation to the moment of formation of neck on sections VII and break. Surface of deformed specimen is covered with shallow dull ripples, most clearly expressed on section of neck. The curve of the diagram of elongation does not have teeth, but has normally increasing inclination and characteristic slump of load during break.

In the process of deformation of the same specimens with speed 3 mm/min, it was found that the character of appearance of lines of fluidity has the same regularity as at a speed 10 mm/min, with the only difference that the speed of them in the first and second period is delayed in accordance with deformation 3-6% relative to the elongation of the specimen with speed 1.7 mm/sec, in second period during deformation 8-12% relative to the elongation of the specimen with speed 0.15 mm/sec; counter movement of lines of fluidity with the same deformation occurred with speed 0.1 mm/sec. The polished surface became in the beginning dull, and then appeared rippled. With this speed of load of oscillation of loads occur less than at speed of deformation 10 mm/minute. They correspond to 6-8 kg, in consequence of which the saw of teeth obtained is less noticeable, and given a more sloping-eroded drop of the curve, and speeds of lines of fluidity are delayed.

It is necessary to note that curves of elongation on diagrams at speed of deformation 3 and 10 mm/min have a more sloping character than at speed of deformation 40 mm/min: at high speed of deformation the metal hardens more intensely and for further deformation requires a large load.

Watching the polished surface of the specimen in the period of its deformation, it is difficult to note the moment of appearance of the first lines of fluidity, since in the beginning of their appearance they are insufficiently clear, but with increase of deformation they become more distinct and therefore there appears the possibility to conduct observations.

The character of movement of lines of fluidity on the polished surface of the specimen is the most varied. They do not appear in most cases on the surfaces of the specimen in place of transition from working part to clamp and under angle near 53° to applied load start fast to be transferred on working surface of specimen. As a rule, they appear in groups one after another, one line seems to chase the other and, passing the whole working surface of the specimen, return back with slope to the other side at angle of 37-53°. Separate lines of fluidity do not reach to the end of the specimen, disappear anywhere on working part, subsequent lines cover this place, moving further. Sometimes, lines appear simultaneously at two ends of the specimen, also at angle of 37-53°, only with slope in different directions and, moving toward each other, meet, crossing and parting in various directions. At the moment of crossing, speeds of movement are retarded.

Watching for changes on both sides of specimen showed identity of movement of strips of fluidity and allowed to establish that lines of fluidity are not a surface phenomenon, but plastic flow spreading on all area of cross section of the specimen. As a result of deformation of the polished surface of the specimen and passage on it of lines of fluidity, after the first period on working surface there appears dullness, but after second period, ripples appear. The lines of fluidity disappear and do not leave traces (Fig. 3).

At deformation of highly durable aluminum alloy V-95 with various thermal treatments, it was found that in all cases on the polished surface of the specimen during its deformation there are revealed fast moving lines of fluidity. Their movement is analogous to regularities observed during testing of alloy D-16.

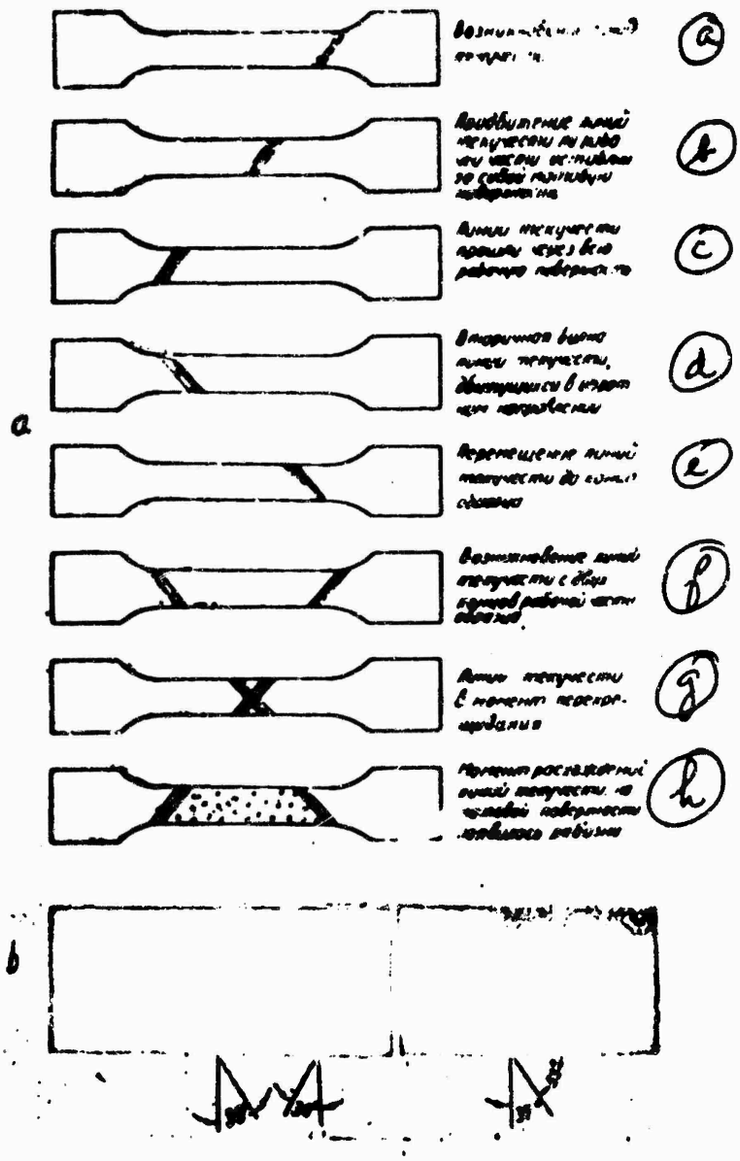

Fig. 3. Diagram of Variants of Strips of Fluidity during Deformation of Specimens from Aluminum Alloy D-16 (a); Photograph from Film during Appearance of Strips of Fluidity and Their Angles of Inclination in Reference to the Applied Load (b).

a -- Appearance of line of fluidity; b -- Advance of line of fluidity on working part, leaving a dull surface; c -- Line of fluidity passed through the whole working surface; d -- Secondary wave of lines of fluidity, moving in the opposite direction; e -- Dislocation of lines of fluidity to the end of the specimen; f -- Appearance of lines of fluidity from two ends of working part of specimen; g -- Line of fluidity at moment of crossing; h -- Moment of divergence of lines of fluidity, on dull surface appeared ripples.

Fresh-hardened state of alloy V-95 gives more intense quantity of lines of fluidity as compared with the aged state. In the fresh-hardened state there is heard intense crackling during deformation of specimen, coinciding in time with the appearance of lines of fluidity that evoked load variation, which was fixed on diagram of elongation in the form of teeth.

In the aged state, the curve diagram of elongation has a steeper rise that is explained by strengthened separate crystallites as compared with the fresh-hardened state, but the annealed state gives a smoother character of rise of curve as compared with the preceding. Measurements of speed of separate lines of fluidity gave the same results as those during investigation of alloy D-16 with the same conditions of deformation.

Explaining the appearance and movement of lines of fluidity from the viewpoint of the theory of dislocations, separate authors affirm that movement of dislocation leaves a visible trace [4]. This phenomenon is ascribed to local deformation, appearing on the frontal surfaces between metal and surface film (oxide or carbonic) [5]. When dislocations move, on the surfaces should be formed a step. In the presence of surface layer a step cannot appear. Therefore, on frontal surfaces remain two long dislocatory lines, allowing to see trace of slipping. In aluminum, trace of slipping disappears approximately after 10 sec as a result of the process of relaxation; in stainless steels it remains visible for a longer time. This distinction, probably, is explained by various durability of the connection between metal and surface film [4].

Deformation of aluminum alloys is accompanied by an increase of density of slip lines. Increase of deformation approximately double causes decrease of average distance between neighboring lines from 640 to 380 Å. Magnitude of shift in every step remains equal to 30 Å [4]. Plastic flow in this region mainly occurs by means of appearance of new slip lines, which are rippled. Boundaries of grains, as it is known, during plastic flow are an obstacle to propagation of shift. Usually plastic shifts start inside grains and are braked near own boundaries, evoking appearance of nonuniform field of stresses and bends near boundaries of grains [6]. Thanks to such action of boundaries, yield point of polycrystal is always higher than single crystal and is increased with decrease of dimension of grains. Effectiveness of influence of boundaries, as investigation shows [7], grows with increased disorientation of grains. During plastic flow, boundaries of grains obtain toothed structure, and position of teeth coincides with slip bands inside grains [6]. Simultaneously with this,

on the boundaries of grains of aluminum alloys occurs a falling of hardening component $CuAl_2$, and further deformation brings to slipping by means of local deformation by jumps. Speed of dislocation during jump is very great. Sound of specimen during deformation is explained by jump-like plastic flow.

Distortion of curve diagram of elongation (in the form of teeth) is explained by braking of plastic flow during falling of the hardening component on boundaries of grains and its stabilization, since it is easy to prove that for stabilized plastic flow a larger effort is required than for free flow.

Conclusions

1. It has been found that lines of fluidity appear only in highly durable deformed aluminum alloys, able to take heat treatment.

2. It was shown that highly durable aluminum alloys, revealing lines of fluidity, have on the curve diagram of elongation seven independent sections and two zones, revealing lines of fluidity: the first zone is on section 3-6%, and second -- 8-12% relative to the elongation. Both zones on curve diagram of elongation are marked by change of curve in the form of a saw indicating a change of load, and every load variation corresponds to appearance of new line of fluidity and evokes intermittent plastic flow, giving sound.

Manuscript submitted 14 February 1963

Bibliography

1. Luders. Dinglars Polytechn. Iomn., 1854.
2. D. K. Chernov. Generalization Because of Certain New Observations during Treatment of Steel, 1884.
3. S. I. Gubkin, A. D. Tomlenov et al. Principles of Theory of Pressure Treatment of Metals, Mashgiz, p 244, 1959.
4. V. A. Pavlov. Physical Bases of Plastic Flow of Metals. Publishing House of Academy of Sciences USSR, 1962.
5. M. I. Whelan, P. B. Hirsch, W. Bollmann. Proc. Roy. Soc., A, 240, 524 (1957).
6. E. S. Yakovleva, M. V. Yakutovich. DAN USSR, 90, 1027 (1953).
7. B. Chalmers. Proc. Roy. Soc., A, 162, 120 (1937).
8. V. I. Syutkina, E. S. Yakovleva. Physics of Metals and Metal Science, 7, 829 (1959).

Copper Plating from Pyrophosphate Electrolytes

By V. I. Lainer and V. A. Bardina,
Moscow Institute of Steel and Alloys. Chair of corrosion of metal

pp 144-150

Of all uncyanogen electrolytes for the copper plating of steel, zinc alloy, and aluminum the long since known pyrophosphate electrolytes deserve the greatest attention. However, they have not had wide industrial application until now, and sufficiently stable results concerning durability of cohesion of covering with a base began to be obtained only in the last five years.

In Soviet and foreign literature is published large quantity of original and review articles, and many patents were granted for copper plating in pyrophosphate electrolytes. A. I. Gershevich and L. V. Gamburg [1], proceeding from solution of sodium pyrophosphate, indicated necessity of introduction in electrolyte along with pyrophosphates also doubly decomposed sodium orthophosphate.

V. I. Layner and G. F. Gromotkov [2], studying polarization curves, arrived at conclusion that sodium orthophosphate somewhat improves durability of cohesion of copper covering with a steel base. However, later investigations [3-5] showed that for guarantee of durable cohesion of thick copper coverings with a base it is necessary to deposit on steel articles first a fine film of copper (0.05-0.2 microns) from pyrophosphate electrolyte with large content of free pyrophosphate (P_2O_7:Cu = 25), and on articles from zinc alloy -- film of copper from cyanogen electrolyte. Besides that it was found that stability of electrolyte and obtaining of reproducible results are assured by introduction of certain quantities of salts of nitric acid and ammonia, but for application of first layer of copper we need a supplementary additive, for example $C_2O_4^{2-}$.

For pyrophosphate copper electrolytes to be full-value substitutes of cyanogen, cathode polarization in them should be of the same order, i.e., approximately one volt at D = 0.3-0.5 and/dm^2. This it is necessary also for guarantee of durable cohesion between steel and electroprecipitated copper in salts of sufficient thickness and for equal distribution of metal on surfaces of covered profiled articles.

From pyrophosphate electrolytes we obtain comparatively well polished copper deposits with thin structure. They can be used for protection from cementation and nitration [6]. For successful protection from nitration at 520° for the duration 72 hours it is sufficient to have a thickness of layer of copper of 10 microns.

In films up to 15-20 microns deposits are obtained by brilliant or semibrilliant that is very valuable during subsequent brilliant nickel-plating without polishing of copper layer. In more thick layers, the order 50-100 microns, they do not have growths. It is possible also to apply copper layers of thickness in 0.5-1.0 mm on articles of complicated form. Advantages of pyrophosphphosphate electrolytes over acids consist of a better dispersing ability and of the fact that due to insignificant alkalinity of electrolyte there is no corrosion of deep, uncovered places.

Due to these properties of copper coverings from pyrophosphate electrolytes it is expedient during protective-decorative coverings by the formula copper-nickel-chromium to apply relatively thick layers of copper on comparatively coarsely prepared surface of steel and after mechanical polishing of copper to apply brilliant layers of nickel and chrome. Although full replacement of nickel by copper during protective-decorative chromium-plating does not give proper effect, it is fully expedient to decrease thickness of nickel layer, considerably increasing thickness of copper. Due to causes, above-indicated, pyrosphosphate electrolytes are better for this purpose than others. The above applies in significant measure also to articles from zinc alloy, which are subjected to protective-decorative chromium plating.

Pyrophosphate electrolytes for copper plating and conditions of their work. Electrolyte for copper plating is prepared in the following manner. To water solution of sulfate of copper at 30-40° gradually is added warm solution of pyrophosphate of potassium from calculation[1]):

1) Application of potassium salt is stipulated by the fact that salt [$K_6Cu(P_2O_7)_2$] is more soluble and its solutions are better electric conductors than corresponding sodium salts. In-

$$2CuSO_4 + K_4P_2O_7 \rightarrow Cu_2P_2O_7 \downarrow + 2K_2SO_4. \quad (1)$$

Falling deposit of pyrophosphate of copper is filtered out and is washed to full removal of ions SO_4^{2-}. To the washed deposit is added heated to 30-40° solution of pyrophosphate of potassium from such calculation, so as to form a soluble complex copper salt and so that in solution remained needed surplus of pyrophosphate in free form.

As a result of conducted investigations for preliminary copper plating of steel we recommend electrolyte of composition (in g/l): 10 Cu, 250 $P_2O_{7tot}^{4-}$ (P_2O^{4-}:Cu = 25) 5-10 $C_2O_4^{2-}$ at following conditions of precipitation: temperature room; current density 0.5-1.0 a/dm^2; time 0.5-1 minute that corresponds to thickness of layer 0.05-0.2 mk; pH = 8.5-9.

In working bath is recommended to maintain following composition of electrolyte (in g/l): 22.5-30 Cu, 170-210 $P_2O_7^{4}$, 7.5-15 NO_3, 0.5-2.0 NH_3 at conditions: temperature 38-60°; current density to 7 a/dm^2, mixing-air or mechanical; pH = 8-8.5.

The most harmful impurity in pyrophosphate electrolytes are lead and cyanides, which are introduced by articles from zinc alloy after applying to them film of copper in cyanogen electrolyte, and fats. Traces of cyanide evoke formation of spotty nonuniform coverings. Inasmuch as alkalinity of pyrophosphate electrolytes is very insignificant, article it is necessary thoroughly to defat before covering.

In bath of preliminary copper plating are introduced $C_2O_4^{2-}$, improving dissolution of anodes and buffering of electrolyte.

It is believed that introduction in working bath of ions of ammonia, improves appearance of deposits and dissolution of anodes; NO_3^- increases upper limit of permissible current densities, possibly, as a result of the fact that ions of hydrogen combine

$$NO_3^- + 10H^+ + 8e \rightarrow NH_4^+ + 3H_2O.$$

At usual temperature pyrophosphate is somewhat subject to hydrolysis according to the reaction

---

soluble pyro[illegible]hate of copper can also be prepared by means of interact[illegible] sulfate of copper with sodium pyrophosphate according [illegible]tion (1).

$P_2O_7^{4-} + H_2O \rightarrow 2HPO_4^{2-}$.

Although anions HPO_4^{2-} are not complexforming, they promote dissolution of anodes and to certain degree buffer the electrolyte.

For preventing of contamination of electrolyte by cyanide is recommended preliminary brief cathode treatment of articles in solution of pyrophosphate of potassium. Remainders of traces CuSN, formed as a result of hydrolysis of coppercyanogen complex, are removed by precipitating hydrogen, or are restored to metal.

Organic impurities or cyanide, polluting the working bath are removed by: treatment with activated carbon from calculation 2-5 g/l for the duration 4-8 hours at 50-55°; introduction of $KMnO_4$ from calculation 0.1-0.2 g/l with subsequent treatment with activated carbon; addition of 30% H_2O_2 (0.5-2.0 ml/l) with subsequent treatment with activated carbon or addition of certain quantity of hypophosphite for destruction of remainders of hydrogen peroxide.

Control of electrolyte for contents of copper, pyrophosphate and ammonium should be conducted during two-shift work once a week; measurement of pH is made every 24 hours of work of bath. Content of NO_3^- and $C_2O_4^{2-}$ are usually not checked, they are added periodically proportionally to the pyrophosphate. Ammonia is added daily, the quantity of which is established depending upon operating temperature, intensity of mixing and surface of electrolyte. During constant working conditions this quantity is established after 4-5 analyses.

The following methods of analysis are recommended.

For determination of copper specimen of electrolyte (5 ml) is carefully heated with sulfuric acid to precipitation of vapors of SO_3. Then add 10 ml 40% KJ and titrate by hyposulphite in presence of starch to nonvanishing blue coloring.

For determination of pyrophosphate, specimen is processed with sulfuric acid and then solution of sulfate of hydrazine, after which copper is filtered through activated carbon. Part of filtered specimen (50 ml) is transferred to retort for 400 ml, add 50 ml of water, 3-4 drops of 1% phenolphtalein and by drops add concentrated HCl as long as red coloring will not turn into weak pink or will be discolored. After that the specimen is electrometrically titrated with intense mixing from 0.5 n H_2SO_4

to pH ≈ 3.8, add 50 ml of solution $ZnSO_4$ (125 g/l) and let stand for 4-5 minutes, periodically agitating. Then titrate with continuous mixing 0.3 n NaOH to pH ≈ 3.8 and mark volume of consumed alkali. Contents of pyrophosphate (in g/l $P_2O_7^{4-}$) are determined by multiplying volume of alkali (in ml) by 7.5.

Operating conditions of baths. Usually in baths it is recommended to maintain cathod current density near 3.0 a/dm^2. However, in mixed electrolyte or with moving cathode rods and temperature 50-55° it is possible to receive good deposits in the structural sluse with yield along current near 90% with current density 6-8 a/dm^2. Anode yield along current is somewhat larger than the cathode, in consequence of which there is no need for periodic addition of relatively expensive copper salts. Anode current density is recommended to be maintained near 2.0 a/dm^2 and in any case lower than 4 a/dm^2, at which on surfaces of anodes will be formed difficult soluble film. At current density lower than 2.0 a/dm^2 anode yield along current is higher than 100% and a film is formed from products of anode dissolution which is sufficiently soluble. Dependence of anode and cathode yield along current from current density is show in Fig. 1.

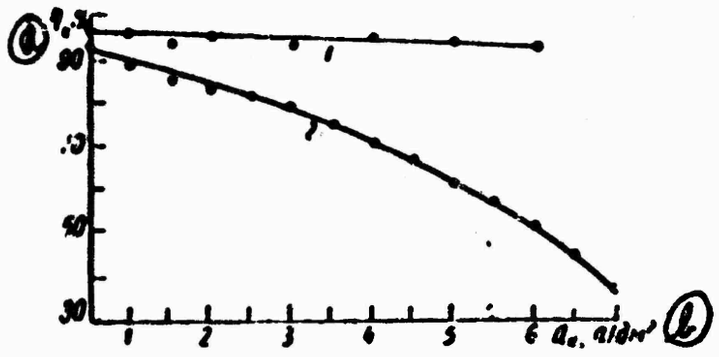

Fig. 1. Dependence of Anode and Cathode Yield Along Current from Current Density in Pyrophosphate Copper Electrolyte: 1 -- Anode Yield, 2 -- Cathode Yield.

a -- 1_k, %; b -- D_k a/dm^2.

Cathode polarization in pyrophosphate copper electrolytes. It was shown above that for guarantee of durable cohesion of electroprecipitated copper with main metal and uniform distribution of metal on covered articles it is necessary that cathode be of the same order as that in cyanogen electrolytes. Fig. 2 shows polarization curve in electrolyte of preliminary copper plating (ratio $P_2O_7^{4-}$:Cu = 25) at 20°. At density current 0.1 a/dm^2 in this electrolyte cathode potential is equal --

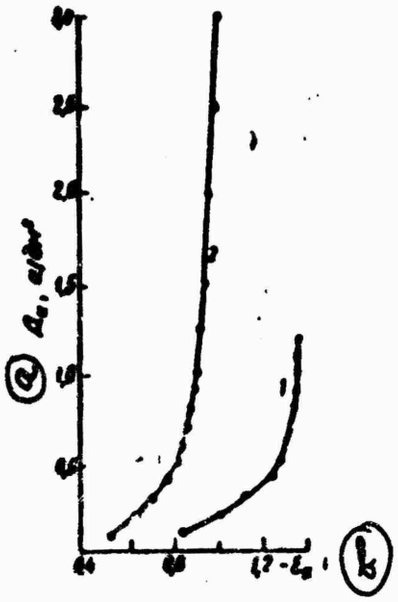

Fig. 2. Cathode Polarization in Copper Pyrophosphate Electrolytes: 1 -- in Bath of Preliminary Copper Plating, 2 -- in Working Bath.

a -- D_k, a/dm^2; b -- ε_k.

0.842 volt, and in working electrolyte it is 320 millivolt more positive. This can be explained lower ratio $P_2O_7^{4-}$:Cu(5 instead of 25) and increased temperature (see Fig. 2).

Curves of cathode polarization at constant contents of free pyrophosphate (1.2 n) and various concentration of copper salt (0.5; 0.8 and 1.0 n) are displaced to the left (in the direction of less electronegative meanings) approximately by 100 millivolt (Fig. 3 a). Increase of concentration of free pyrophosphate from 0.1 to 3.5 n at constant contents of copper in electrolyte (0.8 n) shifts polarization curve to the right (in the direction of electronegative meanings) by 150-200 millivolt (see Fig. 3 b). Noticeably decreases cathode polarization (on 100-200 millivolt) at increase of temperature from 40 to 70° (see Fig. 3 b). All these facts indicate the mixed character of polarization -- concentration and chemical.

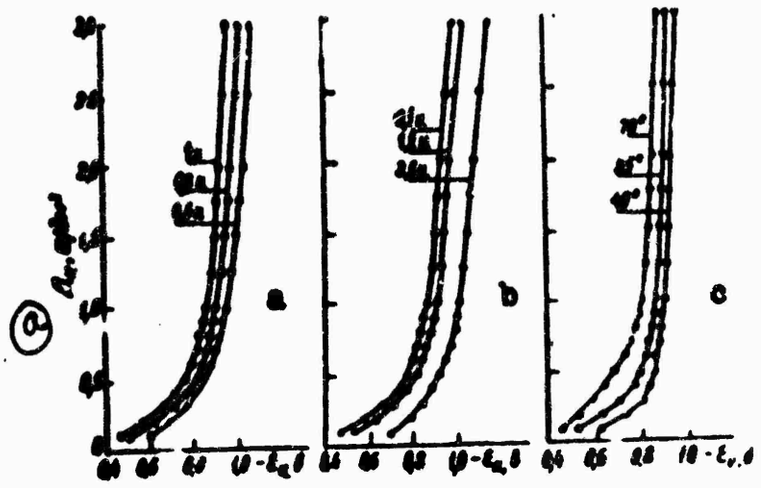

Fig. 3. Influence on Cathode Polarization of Concentration of Copper Salt (a), Concentration of Pyrophosphate (b) and Temperature (c).

a -- D_k, a/dm^2.

Distribution of copper on cathode and influence of main parameters on appearance of copper deposits. Experiments were conducted in Hull cell [7], diagram of which is shown on Fig. 4. As cathode served iron tape of thickness 0.5 mm and area 0.55 cm^2, anode-copper plate. All experiments were conducted in thermostat at 55° and average current density 1 a/dm^2; duration of experiment 30 minutes. For establishment of distribution of copper cathode was cut into stripes by width 10 mm. Every even strip, counting from the nearest to anode of edge, was weighed together with copper with accuracy up to 0.2 milligrams and then was weighed after dissolution of copper from it. Copper was removed in solution containing 450 g/l CrO_3 and 50 g/l H_2SO_4 at room temperature.

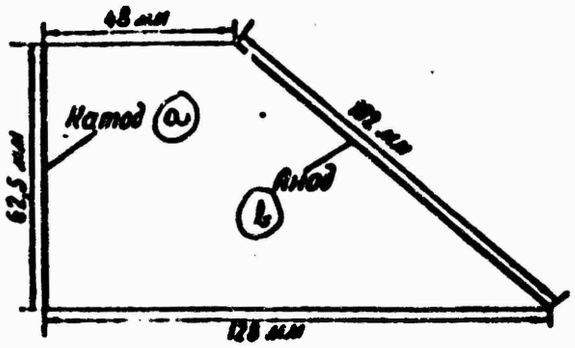

Fig. 4. Diagram of Hull Cell.

a -- Cathode; b -- Anode.

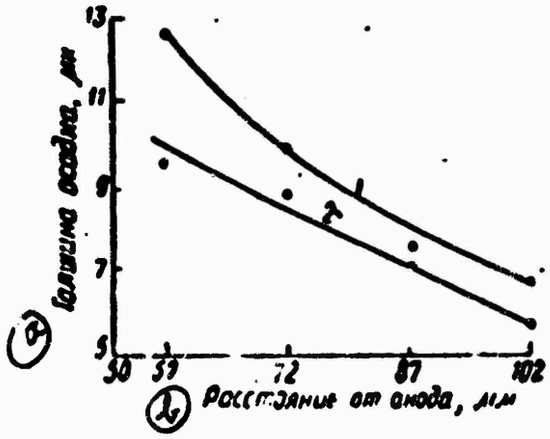

Fig. 5. Uniformity of Distribution of Metal in Copper Electrolytes in Hull Cell: Cyanogen (1) and Pyrophosphate (Working Bath) (2).

a -- Thickness of deposit, microns; b -- Distance from anode, mm.

For comparison, analogous experiments were conducted in that cell with cyanogen electrolyte, containing 60 g/l

$KNaC_4H_4O_6 \cdot 4H_2O$, at a temperature of 40°. Obtained data are graphically presented on Fig. 5. As can be seen, in pyrophosphate electrolyte metal is distributed somewhat more uniformly than in cyanogen. In the latter the ratio of weight of copper (or thickness) to the nearest and the most remote stripe equals 86, whereas in the pyrophosphate electrolyte it equals 1.71.

In that same cell was investigated influence of concentration of copper salt at constant contents of free pyrophosphate (1.2 n) and influence of contents of free pyrophosphate at constant contents of copper (0.8 n) on appearance of various cathode sections at average current density 1 and 1.5 a/dm^2. Obtained data are presented in Fig. 6.

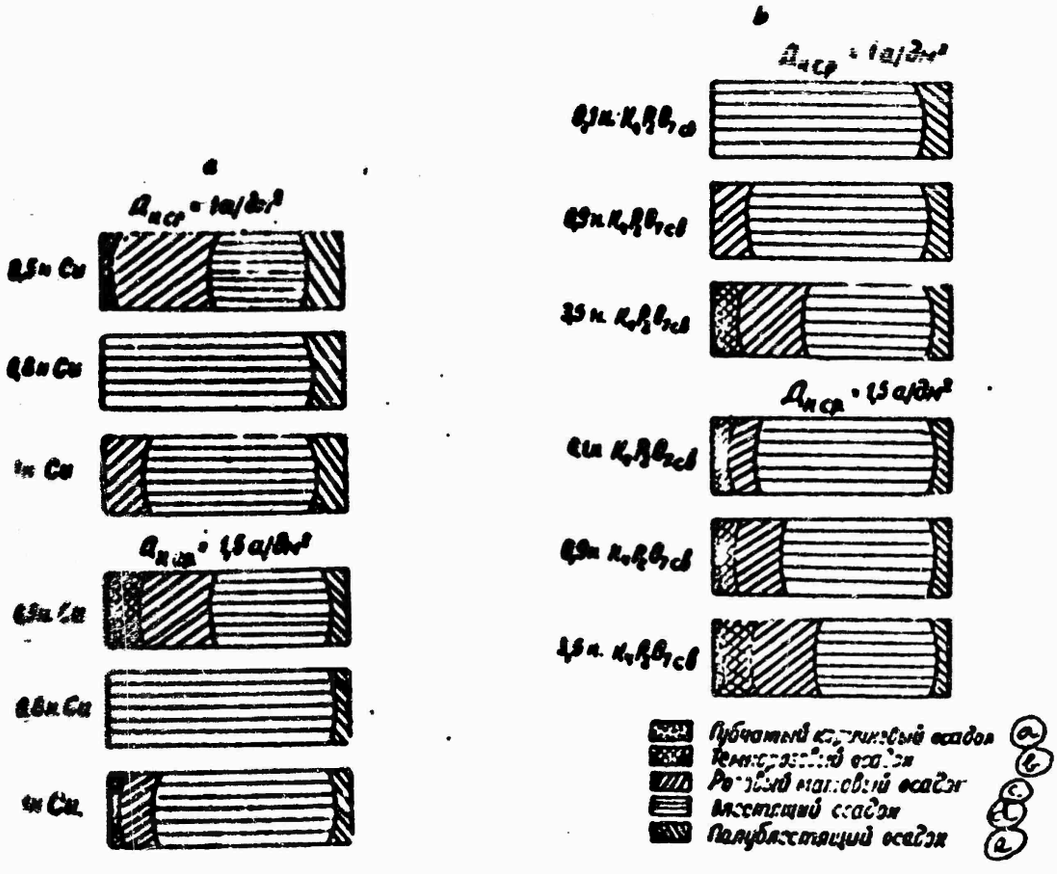

Fig. 6. Influence of Concentrations of Copper Salt (a) Free Pyrophosphate (b) on Appearance of Deposits in Hull Cell.

a -- Spongy brown deposit; b -- Dark-rose deposit; c -- Rose dull deposit; d -- Brilliant deposit; e -- Semibrilliant deposit.

As can be seen, at average current density 1 a/dm^2 we get good externally appearing deposits almost on all surface of cathode in Hull cell. With increase of concentration of copper

salt region of obtaining of brilliant deposits is expanded. At average current density 1.5 a/dm^2 and concentration 0.5 n Cu on the nearest anode of cathode sections is observed inclination to formation of spongy deposits. These data indicate large inclination to formation of spongy deposits to the extent of increase of average current density and content of free pyrophosphate.

Conclusions

1. According to basic indications pyrophosphate copper electrolytes are not inferior to those of copper cyanogen.

2. Cathode polarization in pyrophosphate copper electrolyte is somewhat lower than in cyanogen. Yield of metal along current on anode and cathode is close to theoretical. Uniformity of distribution of metal in pyrophosphate copper electrolyte approximately such, as and in cyanogen.

3. Guarantee of durable cohesion with steel in layers of significant thickness 100 microns and larger) is possible with application of first film of copper (0.05-0.2 microns) in pyrophosphate electrolyte with large surplus of pyrophosphate ($P_2O_7^{4-}$:Cu = 25) and in presence of second additive, for example, $C_2O_4^{2-}$ (5-10 g/l). Before copper plating of zinc alloy is recommended preliminarily to apply film of copper in cyanogen electrolyte.

4. For baths of preliminary copper plating is recommended composition of electrolyte (in g/l): 10 Cu, 250 $P_2O_{7gen}^{4-}$, 372 $K_4P_2O_{7free}$(4.5 n), 5-10 $C_2O_4^{2-}$ at following conditions of precipitation: temperature room, current density 0.4-0.8 a/cm^2, time 0.5-1.0 minute, pH = 8.5-9. Composition of electrolyte for working baths is recommended (in g/l): 25 Cu, 190 P_2O_{7gen}, 102 $K_4P_2O_{7free}$(1, 2 n), 5-10 KNO_3, 1-3 NH_3 and conditions of precipitation: temperature 50-60°, current density 2-3 a/cm^2 (with mixing to 6-8 a/dm^2), pH = 8.2-8.8.

Manuscript submitted 17 December 1962

Bibliography

1. A. I. Gershevich, L. V. Gamburg. Corrosion and Struggle with it, No 2, 1940.
2. V. I. Layner. Atmospheric Corrosion of Metals, Metallurgizdat, 1951.

3. J. E. Starek. Modern Electroplating. N.Y., 1953.
4. D. E. Weimer. Trans. Inst. Metal Finish., Vol XXXV, 1957-1958.
5. F. Passal. Plating, June 1959.
6. C. E. Heussner, A. R. Balden, L. M. Morse. Plating, June, Jul, 1948.
7. R. O. Hull. Proc. Amer. Electroplaters Soc., 27, 52 (1939).

On the Problem of Mathematical Model of Zone of Active Heat Exchange of Shaft Furnace for Purpose of Automation of Smelting of Oxidized Nickel Ores

By A. Ashimov, D. I. Lisovskiy,
Moscow Institute Steel and Alloys. Chair of automation of production of rare and radioactive metals

pp 151-156

One of the important sections of shaft furnace is zone of active heat exchange [1] between charge and gases, which is carried out intensely to temperature of melting of the entire mass of material.

The dynamic of heating materials in this zone plays an important role in the course of processes in shaft furnace. Therefore a study of this question is important.

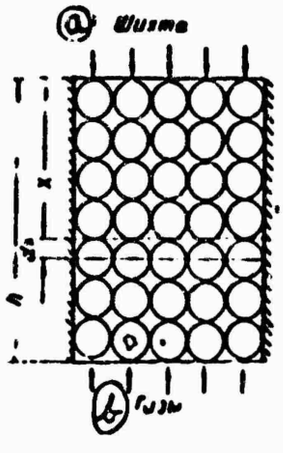

Fig. 1. Diagram of Heating Material in Countercurrent.

a -- Charge; b -- Gases.

An approximate solution of problem of heat exchange between loose material and penetrating gas under conditions of their countercurrent taking into account heating of piece along thickness was obtained by B. I. Kitayev [2].

G. P. Ivantsov and B. Ya. Lobov [3] resolved this problem more accurately in the following arrangement (Fig. 1). Through shaft in height h and cross section f charge moves down from above, consisting of spheres of radius r_o with initial temperature t_{1s}, where $r_o \ll h$ and $r_o^2 \ll f$. The coordinate of center of sphere, read off down from above, equals x.

From below upwards through shaft gas is ventilated with initial temperature t_{1g}. The coefficient of heat emission α from gases to surface of spheres is constant, as are all parameters, characterizing the physical properties of the system. Water equivalent of flow of gas W_g, spheres W_s. Full surface of all n spheres, filling shaft, equals F, time of stay of each of them in shaft τ_0.

We are considering the case of an established process, i. e., such a process, when temperature on any horizon does not change in time. Temperature field inside every sphere, as a function of time, can be depicted by the derivative

$$\frac{\partial t_s}{\partial \tau} = a\left(\frac{\partial^2 t_s}{\partial r^2} + \frac{2}{r}\cdot\frac{\partial t_s}{\partial r}\right). \qquad (1)$$

Change of temperature of gases along height of shaft can be connected with temperature of surface of spheres by differential equation

$$\alpha\left(t_g - t_{s\,g=g_0}\right) F \frac{dx}{h} = W_g\, dt_g.$$

Substituting in this equation $\frac{dx}{h}$ for $\frac{d\tau}{\tau_0}$ and considering that $\tau_0 = \frac{4}{3}\pi r_0^3 n \gamma_s c_s W_s$ and $F = 4\pi r_0^2 n$, we will get

$$\frac{dt_g}{d\tau} = -\frac{3\alpha W_s}{r_0\,\gamma_s c_s W_g}\left(t_g - t_{s\,g=g_0}\right). \qquad (2)$$

On surface of sphere

$$\lambda\left(\frac{\partial t_s}{\partial r}\right)_{g=g_0} = \alpha\left(t_g - t_{s\,g=g_0}\right) \text{ and } \left(\frac{\partial t_s}{\partial r}\right)_{g=0} = 0. \qquad (3)$$

Furthermore, at $\tau = 0$ $t_s = t_{1s}$ and at $\tau = \tau_0$ $t_g = t_{1g}$.

Resolution of problem is given in complicated form by method of operational calculus that complicates its application in engineering practice. Expression [1] refers to equation of parabolic type. On boundary is given linear relationship between derivative and function. This boundary condition corresponds to heat exchange according to law of Newton on surfaces of body with environment, temperature of which isknown. For determination of temperature on getting out of zone of active heat exchange we use method of final differences.

Main idea consists of the fact that differential equations, initial and boundary conditions are replaced by system of finite-difference equations, approximately representing the given boundary value problem. If, however, in initial and boundary conditions do not enter derivative resolutions, then boundary condition directly determine meaning of searched function. If, however, boundary conditions contain derivative searched function, then these derivatives can be replaced by differential approximations. With this we obtain differential boundary conditions, approximating with certain error of boundary conditions for differential equation. Thus, have

$$\frac{\partial t_s}{\partial \tau} = a\left(\frac{\partial^2 t_s}{\partial r^2} + \frac{2}{r}\cdot\frac{\partial t_s}{\partial r}\right);$$

$$\frac{dt_g}{d\tau} = \frac{3\alpha G_s}{r_0 \gamma_s c_g G_g}\left(t_g - t_{s\,g=g_0}\right);$$

$$\lambda\left(\frac{\partial t_s}{\partial r}\right)_{g=g_0} = \alpha\left(t_g - t_{s\,g=g_0}\right);\quad \left(\frac{\partial t_s}{\partial r}\right)_{g=0} = 0;$$

at $\tau = 0$ $t_s = t_{1s}$ and at $\tau = \tau_0$ $t_g = t_{1g}$.

Here G_s and G_g -- quantity of charge and gas in zone.

Time interval τ_0 for transition to equation in boundary conditions will be broken into $\tau_0 = \sum_{j=1}^{3} \Delta\tau_j$ (Fig. 2).

Combining equation (2) and (3), we will receive

$$\lambda\left(\frac{\partial t_s}{\partial r}\right)_{g=g_0} = \frac{r_0 \gamma_s G_g c_g}{3G_s}\cdot\frac{dt_g}{d\tau} \qquad (4)$$

or

$$\left(\frac{\partial t_s}{\partial r}\right)_{g=g_0} = \frac{r_0 \gamma_s G_g c_g}{3G_s}\cdot\frac{dt_g}{d\tau}.$$

Designating $\frac{r_0 \gamma_s G_g}{3G_s}$ with A, we will receive

$$\left(\frac{\partial t_s}{\partial r}\right)_{g=g_0} = A\frac{G_g}{G_s}\cdot\frac{dt_g}{d\tau}.$$

Let us consider third section $\Delta\tau_3$, for which potential of temperature along gas will be $(t_{g_2} - t_{g_3})$. For transition to differential equation we will assume radius of particle r_0 =

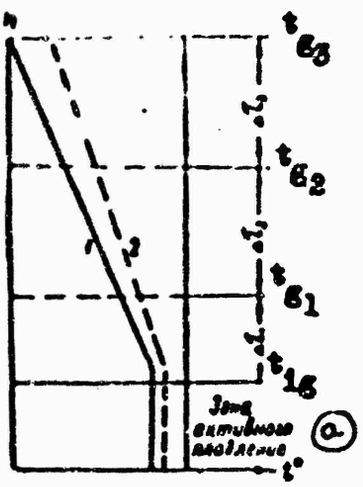

Fig. 2. Process of Heating Materials:
1 -- Materials, 2 -- Gases.
a -- Zone of active melting.

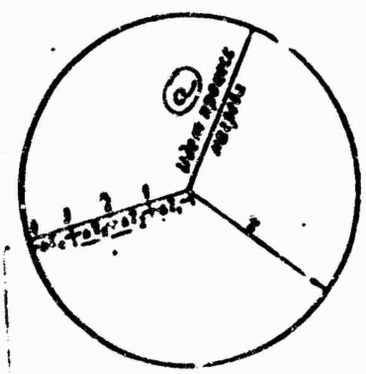

Fig. 3. Diagram of Heating of Particle.
a -- Course of Heating process.

$= i\Delta r (i = 1, 2, 3, 4, \ldots, n)$; for example radius of particle r_0 will be presented as $4\Delta r$.

Replacing boundary conditions by differential approximation we will get (Fig. 3)

$$\frac{t_{s_4} - t_{s_3}}{\Delta r_4} = A \frac{G_g}{G_s} \cdot \frac{t_{g2} - t_{g3}}{\Delta r_3} \qquad (5)$$

Differential approximation Fourier equation will be

$$\frac{dt_{s_i}}{d\tau} = a\left(\frac{t_{s_{i+1}} - 2t_{s_i} + t_{s_{i-1}}}{\Delta r_{i+1}^2} + \frac{2}{r} \cdot \frac{t_{s_{i+1}} - t_{s_i}}{\Delta r_{i+1}}\right).$$

For $i = 3$ (beginning of heating of materials)

$$\frac{dt_{s_3}}{d\tau} = a\left(\frac{t_{s_4} - 2t_{s_3} + t_{s_2}}{\Delta r_4^2} + \frac{2}{r} \cdot \frac{t_{s_4} - t_{s_3}}{\Delta r_4}\right),$$

and taking into account equation (5)

$$\frac{dt_{s_3}}{d\tau} = a\left(\frac{t_{s_4} - t_{s_3}}{\Delta r_4^2} + \frac{t_{s_2} - t_{s_3}}{\Delta r_4^2} + \frac{2}{r} \cdot \frac{t_{s_4} - t_{s_3}}{\Delta r_4}\right),$$

$$\frac{dt_{s_3}}{d\tau} = a\left(A \frac{G_g}{G_s} \cdot \frac{t_{g2} - t_{g3}}{\Delta\tau_3 \Delta r_4} + \frac{t_{s_2} - t_{s_3}}{\Delta r_4^2} + \frac{2}{r} \cdot \frac{t_{g2} - t_{g3}}{\Delta\tau_3} A \frac{G_g}{G_s}\right),$$

$$\frac{dt_{s_3}}{d\tau} = Aa \frac{G_g}{G_s} \cdot \frac{t_{g2} - t_{g3}}{\Delta\tau_3 \Delta r_4} + a \frac{t_{s_2} - t_{s_3}}{\Delta r_4^2} + \frac{2}{r} Aa \frac{G_g}{G_s} \cdot \frac{t_{g2} - t_{g3}}{\Delta\tau_3} \qquad (6)$$

For $i = 2$

$$\frac{dt_{s_2}}{d\tau} = a \frac{t_{s_3} - 2t_{s_2} + t_{s_1}}{\Delta r_3^2} + \frac{2a}{r} \cdot \frac{t_{s_1} - t_{s_2}}{\Delta r_3} \qquad (7)$$

For i = 1 (approximate temperature in center of sphere)

$$\frac{dt_{s_1}}{d\tau} = a \frac{t_{s_2} - 2t_{s_1} + t_{s_0}}{\Delta r_1^2} + \frac{2a}{r} \cdot \frac{t_{s_2} - t_{s_1}}{\Delta r_1}. \qquad (8)$$

Let us consider second section $\Delta\tau_2$, for which potential of temperature for gas will be $(t_{g_1} - t_{g_2})$.

Replacing boundary condition by differential approximation we will receive

$$\frac{t_{s_1} - t_{s_3}}{\Delta r_1} = A \frac{G_g}{G_s} \cdot \frac{t_{g_1} - t_{g_2}}{\Delta \tau_2}. \qquad (9)$$

For i = 3 taking into account equation (9)

$$\frac{dt_{s_3}}{d\tau} = Aa \frac{G_g}{G_s} \cdot \frac{t_{g_1} - t_{g_2}}{\Delta r_1 \Delta \tau_2} + a \frac{t_{s_2} - t_{s_3}}{\Delta r_1^2} + \frac{2a}{r} \cdot A \frac{G_g}{G_s} \cdot \frac{t_{g_1} - t_{g_2}}{\Delta \tau_2}. \qquad (10)$$

For i = 2 equation (7) is valid and for i = 1 -- equation (8).

Let us consider first section $\Delta\tau_1$, for which potential of temperature for gas will be $(t_{ig} - t_{g_1})$.

Replacing boundary condition by differential a, we will obtain

$$\frac{t_{s_4} - t_{s_3}}{\Delta r_4} = A \frac{G_g}{G_s} \cdot \frac{t_{ig} - t_{g_1}}{\Delta \tau_1}. \qquad (11)$$

For i = 3 taking into account equation (11)

$$\frac{dt_{s_3}}{d\tau} = aA \frac{G_g}{G_s} \cdot \frac{t_{ig} - t_{g_1}}{\Delta \tau_1 \Delta r_4} + a \frac{t_{s_2} - t_{s_3}}{\Delta r_4^2} + \frac{2a}{r} \cdot A \frac{G_g}{G_s} \cdot \frac{t_{ig} - t_{g_1}}{\Delta \tau_1}.$$

For i = 2 we have equation (7), and for i = 1 (end of zone of active heat exchange) -- equation (8).

Thus, processes of zone of active heat exchange are described by nine equations, which first corresponds to equation (6), in which $t_{s_2} = t_{is}$; second equation -- (7), where $t_{s_1} = t_{is}$; third -- (8), where $t_{s_0} = t_{is}$; remaining equations:

$$\frac{dt_{s_3}}{d\tau} = aA \frac{G_g}{G_s} \cdot \frac{t_{g_1} - t_{g_2}}{\Delta r_4 \Delta \tau_2} + a \frac{t_{s_2} - t_{s_3}}{\Delta r_4^2} + \frac{2a}{r} \cdot A \frac{G_g}{G_s} \cdot \frac{t_{g_1} - t_{g_2}}{\Delta \tau_2}.$$

where $t_{s_2} = t_{s_2}$;

$$\frac{dt_{s_2}}{d\tau} = a\frac{t_{s_3} - 2t_{s_2} + t_{s_1}}{\Delta r_2^2} + \frac{2a}{r}\cdot\frac{t_{s_3} - t_{s_2}}{\Delta r_2} \text{ where } t_{s_1} = t_{s_1};$$

$$\frac{dt_{s_1}}{d\tau} = a\frac{t_{s_2} - 2t_{s_1} + t_{s_0}}{\Delta r_2^2} + \frac{2a}{r}\cdot\frac{t_{s_2} - t_{s_1}}{\Delta r_2} \text{ where } t_{s_0} = t_{s_1};$$

$$\frac{dt_{s_3}}{d\tau} = aA\frac{G_g}{G_s}\cdot\frac{t_{1g} - t_{g_1}}{\Delta r_1 \Delta r_1} + a\frac{t_{s_2} - t_{s_3}}{\Delta r_1^2} + \frac{2a}{r}\cdot A\frac{G_g}{G_s}\cdot\frac{t_{1g} - t_{g_1}}{\Delta r_1},$$

where $t_{s_2} = t_{s_2}$;

$$\frac{dt_{s_2}}{d\tau} = a\frac{t_{s_3} - 2t_{s_2} + t_{s_1}}{\Delta r_2^2} + \frac{2a}{r}\cdot\frac{t_{s_3} - t_{s_2}}{\Delta r_2} \text{ where } t_{s_1} = t_{s_1};$$

$$\frac{dt_{s_1}}{d\tau} = a\frac{t_{s_2} - 2t_{s_1} + t_{s_0}}{\Delta r_2^2} + \frac{2a}{r}\cdot\frac{t_{s_2} - t_{s_1}}{\Delta r_2} \text{ where } t_{s_0} = t_{s_1}.$$

After substituting the indicated meanings of temperatures we will receive system of equations:

$$\frac{dt_{s_3}}{d\tau} = aA\frac{G_g}{G_s}\cdot\frac{t_{g_2} - t_{g_3}}{\Delta r_3 \Delta r_4} + a\frac{t_{1g} - t_{s_3}}{dr_4^2} + \frac{2a}{r}\cdot A\frac{G_g}{G_s}\cdot\frac{t_{g_2} - t_{g_3}}{\Delta r_3},$$

$$\frac{dt_{s_2}}{d\tau} = a\frac{t_{s_3} - 2t_{s_2} + t_{1g}}{\Delta r_3^2} + \frac{2a}{r}\cdot\frac{t_{s_3} - t_{s_2}}{\Delta r_3};$$

$$\frac{dt_{s_1}}{d\tau} = a\frac{t_{s_2} - 2t_{s_1} + t_{1g}}{\Delta r_3^2} + \frac{2a}{r}\cdot\frac{t_{s_2} - t_{s_1}}{\Delta r_3};$$

$$\frac{dt_{s_3}}{d\tau} = aA\frac{G_g}{G_s}\cdot\frac{t_{g_1} - t_{g_2}}{\Delta r_4 \Delta r_2} + a\frac{t_{s_2} - t_{s_3}}{\Delta r_4^2} + \frac{2a}{r}\cdot A\frac{G_g}{G_s}\cdot\frac{t_{g_1} - t_{g_2}}{\Delta r_2},$$

$$\frac{dt_{s_2}}{d\tau} = a\frac{t_{s_3} - 2t_{s_2} + t_{s_1}}{\Delta r_3^2} + \frac{2a}{r}\cdot\frac{t_{s_3} - t_{s_2}}{\Delta r_3};$$

$$\frac{dt_{s_1}}{d\tau} = a\frac{t_{s_2} - 2t_{s_1} + t_{s_1}}{\Delta r_3^2} + \frac{2a}{r}\cdot\frac{t_{s_2} - t_{s_1}}{\Delta r_3};$$

$$\frac{dt_{s_3}}{d\tau} = aA\frac{G_g}{G_s}\cdot\frac{t_{1g} - t_{g_1}}{\Delta r_1 \Delta r_1} + a\frac{t_{s_2} - t_{s_3}}{\Delta r_4^2} + \frac{2a}{r}\cdot A\frac{G_g}{G_s}\cdot\frac{t_{1g} - t_{g_1}}{\Delta r_1},$$

$$\frac{dt_{s_2}}{d\tau} = a\frac{t_{s_3} - 2t_{s_2} + t_{s_1}}{\Delta r_3^2} + \frac{2a}{r}\cdot\frac{t_{s_3} - t_{s_2}}{\Delta r_3};$$

$$\frac{dt_{s_1}}{d\tau} = a\frac{t_{s_2} - 2t_{s_1} + t_{s_1}}{\Delta r_3^2} + \frac{2a}{r}\cdot\frac{t_{s_2} - t_{s_1}}{\Delta r_3}.$$

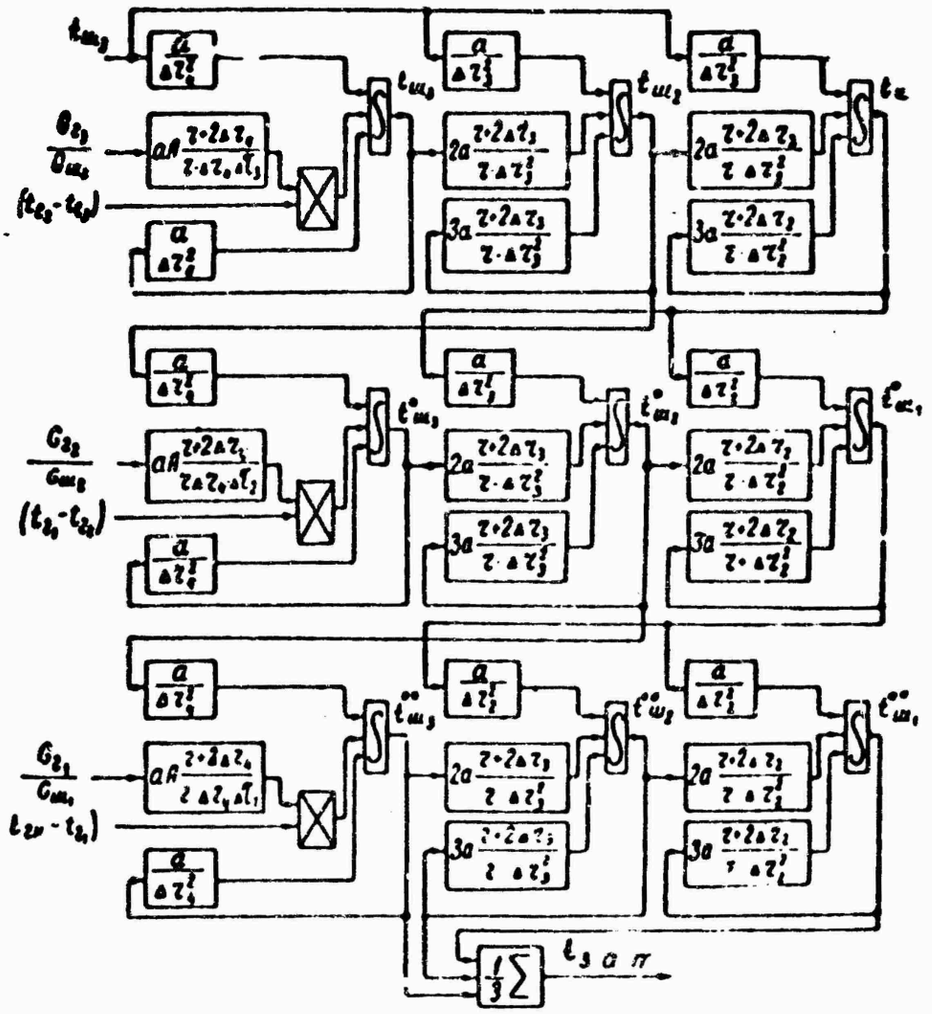

Fig. 4. Equivalent Structural Diagram of Process of Active Heat Exchange.

Average temperature for mass of materials is determined

$$\frac{t''_{s_3} + t''_{s_2} + t''_{s_1}}{3}.$$

For construction of mathematical model of zone we will register also condition of material balance for gas and material:

$$\frac{dG_s}{dt} = Q'_s - Q_s; \quad \frac{dG_g}{dt} = Q'_g - Q_g$$

where Q'_s, Q'_g -- flows, proceeding in the zone;

Q_s, Q_g -- flows, departing from zone.

Fig. 4 gives equivalent structural diagram of process of active heat exchange.

Conclusions

1. Shown is approach to construction of mathematical model of zone of active heat exchange of shaft furnace for purposes of automation of smelting of oxidized nickel ores.

2. Presents possibility of modeling of zone with the help of computers.

3. Obtained mathematical description can be used for analogous processes of heating of loose material in countercurrent.

Manuscript submitted 4 July 1962

Bibliography

1. A. Ashimov, D. I. Lisovskiy. Izv. VUZ (Nonferrous Metallurgy), No 1, 1963.
3. B. I. Kitaevi and others. Heat Exchange in Mine Ovens, Sverdlovsk, 1957.
4. G. P. Ivantsev, B. Ya. Lobov. DAN USSR, Vol 85, No 5, 1952.

Calculation of Time of Building with Comparison of Variants of Capital Investments

By U. B. Baymuratov, S. Ya. Rachkovskiy,
Moscow Institute of Steel and Alloys. Chair of economics and organization of production

pp 157-164

(In Order of Discussion)

In projection and building of objects, it is important to ensure not only maximum economy of public labor, but also the shortest periods of its realization. It is obvious that variants, having an identical coefficient of effectiveness, but various duration of building, are economically unequal.

In connection with this, the method of calculation of comparative effectiveness of variants of new building and technical reconstruction of effective enterprises should consider the influence of the time of building. Meanwhile, existing methods of calculation and estimate of the factor of time, in our opinion, need in the future improvement. This article makes an attempt to consider various points of view with respect to calculation of duration of building with determination of effectiveness of capital investments and to indicate certain ways of improvement of the method of this calculation.

When we consider the question of the influence of periods of building on the effectiveness of capital investments in nonferrous metal industry, it is necessary to consider that its development determines the rate of growth of such most important branches of the national economy as power engineering, machine building and others. Growth of these branches increases technical capacity and productivity of public labor in the entire national economy. Therefore, if large periods of building delay delivery of necessary production, one should

determine what kind of losses to the national economy are caused by such delays. For example, by one variant an enterprise of annual productivity of 15,000 tons of metal can be built in three years, but by another variant -- in six years. For the duration of three years of difference of periods of building it will be necessary to import the necessary metal. The cost of imported metal is 100 rubles higher than the cost of one ton of metal of domestic production. Additional expenditures as a result of the importation of metal for the duration of three years of difference of periods of building will constitute 4.5 million rubles. These additional expenditures should be added to the sum of capital investments by the variant of building in six years.

It is especially important to accelerate building in those cases where metal cannot be received, for some reason, by means of import or other method, but it is certainly necessary to guarantee the proportionality of development of the national economy. Even in those cases when various periods of building do not touch the interests of the national economy on the whole, it is necessary to consider the damage evoked by these circumstances.

Karl Marx emphasized that building projects "for long periods of time, a year or more, do not deliver either production tools, nor means of living and in general fail to give any beneficial effect, but, naturally, subtract from the entire annual economy both labor, production tools, and means of living" [1].

For this reason it has been found expedient to put charges on capital investments and thus account for economic losses during the process of building. For this purpose it was suggested [2-6] that in determining the economic effectiveness of capital investments, to use "reduced" capital investments K_r, differing from the estimated cost of project K_0 by the magnitude of losses from the freezing of means P

$$K_{\text{р}} = K_{\text{о}} + \text{P}.$$

In calculations it is more convenient to use not the reduced investments, but their ratio to the estimated cost of the project, which we will call the coefficient of losses from the freezing of means in an unfinished building

$$\text{е} = \frac{K_{\text{р}}}{K_{\text{о}}}.$$

For hydroelectric power plants [2], in comparison of variants, it is recommended for calculation of factor of time

to compare with each other variants of cited capital investments, determined by the formula of simple percentages

$$K_T = K_0(1 + E_n T), \qquad (1)$$

where T -- duration of building, years;
E_n -- coefficient of normative effectiveness.

Model method of Academy of Sciences USSR [3] offers to produce calculation and estimate of factor of time, proceeding from average effect, which can be obtained in given branch during productive use of capital investments. It is necessary to figure capital investments by the formula of compound interest

$$K_T = K_0(1 + E_n)^T. \qquad (2)$$

Both methods recommend to us formulas (1) and (2) in those cases, when compared variants are distinguished by duration of building or capital investments are carried out in various periods.

However with these methods of calculation there is a complete omission of the distribution of capital investments by years of building that does not reflect real picture of process of building production.

In the work of Prof. A. E. Gibshman [4] is offered formula of reduced capital investments, considering annual capital investments

$$K_T = K_1(1 + E_n)^T + K_2(1 + E_n)^{T-1} + K_3(1 + E_n)^{T-2} + \cdots + K_t(1 + E_n),$$

where $K_1, K_2, K_3 \cdots, K_t$ -- capital investment of first, second, third and Tth year of building, rubles.

Assuming that capital investments are produced evenly, i.e.,

$$K_1 = K_2 = K_3 = K_t = \frac{K_0}{T},$$

then

$$K_T = \frac{K_0}{T}[(1 + E_n)^T + (1 + E_n)^{T-1} + (1 + E_n)^{T-2} + \cdots + (1 + E_n)] =$$

$$= \frac{K_0}{T}(1 + E_n)\frac{[(1 + E_n)^T - 1]}{E_n}. \qquad (3)$$

Formula (3) is obtained on the assumption that the total annual capital investments is advanced in the beginning of every year of building.

Almost analogous method of calculation of reduced capital investments is offered also for enterprises of power engineering [5]. The distinction consists in the fact that annual capital investments are considered investment as embedding, made at the end of every year. The sum of capital investments, brought to moment of completion of building, should constitute

$$K_{пр} = K_1(1 + E_н)^{T-1} + K_2(1 + E_н)^{T-2} + K_3(1 + E_н)^{T-3} \dots + \\ + \dots K_{T-1}(1 + E_н) + K_T;$$

at $K_1 = K_2 = K_3 = \dots K_{T-1} = K_T = \frac{K_0}{T}$, we will get

$$K_{пр} = \frac{K_0}{T} \cdot \frac{[(1 + E_н)^T - 1]}{E_н(1 + E_н)^{T-1}}. \qquad (4)$$

Deficiency of formulas (3) and (4) consists of groundlessness of assumption that capital investments are made once a year. In reality process of capital investments represents a more or less continuous process, accomplished during the entire period of building.

Proceeding from actual conditions of building, Prof. B. S. Vaynstein [6] correctly considers that expenditures K(t) made in time interval Δt toward the end of building will be equivalent to $K(t)(1 + E_н)^{T-t} \cdot \Delta t$.

Then the sum of reduced capital investment will constitute

$$K_{пр} = \int_0^T K(t)(1 + E_н)^{T-t} dt.$$

With uniform capital investments, i.e., when $K(t) = \frac{K_0}{T}$,

$$K_{пр} = \frac{K_0}{T}\int_0^T (1 + E_н)^{T-t} dt = \frac{K_0}{T} \cdot \frac{(1 + E_н)^T - 1}{\ln(1 + E_н)} = K_0 z. \qquad (5)$$

Comparing formulas (3), (4) and (5) we see that the latter allows more correctly to consider influence of duration of building on value of calculating reduced capital investments.

However application of formula (5) gives insufficiently accurate results, in sequence of which selection of best variant is hampered. In this method it is assumed that yearly volume of capital investments is constant and therefore building should be conducted evenly. We will show on example that given solution is not best from the viewpoint of optimum distribution of capital investments by years of building and of maximum increase of their effectiveness.

Table 1.

Distribution of Capital Investments by Years of Building

a Варианты	b Капитальные вложения, млн. руб			
	1 год c	2 год c	3 год c	4 год c
I	5	8,33	11,67	15
II	10	10	10	10
III	15	11,67	8,33	5

a -- Variants; b -- Capital investments, million rub; c -- Year.

Let us assume that a metallurgic plant with estimated value $40 \cdot 10^6$ rubles can be built in 4 years. Normative coefficient of effectiveness in nonferrous metallurgy is assumed to be 15%. Let us consider three variants of distribution of capital investments by years of building (Table 1) and we will calculate reduced capital investments for the end of building proceeding from continuity of investments (Table 2).

Table 2.

Reduced Capital Investments by Years of Building

a Варианты	b Приведенные капитальные вложения, млн. руб				c Суммарные приведенные капитальные вложения, млн. руб.
	1 год d	2 год d	3 год d	4 год d	
I	8,1	13,5	13,1	16,1	50,8
II	16,2	14,2	12,4	10,8	53,6
III	24,6	16,7	10,4	5,5	57,2

a -- Variants; b -- Reduced capital investments, million rubles; c -- Total reduced capital investments, million, rubles; d -- Year.

With the same estimated value and duration of building of object we obtain various reduced capital investments and, consequently, various level of losses depending upon distribution of capital investments by years. For guarantee of least losses from freezing of mean it is more profitable to conduct building at an accelerated rate. In this case total expenditures taking into account losses from diverted means will be lowered as

compared with building with diminishing rate and uniform building at 8 and 12%, respectively.

Therefore, comprising graphs of construction and installation works, it is most necessary to see to it that the biggest fraction of capital investments is carried out in completing stage of building. Thus, delivery and assembling of technological and auxiliary equipment, means of mechanization and automation of production of as far as possible have to be produced in preoperational period.

We will define dimensions of annual major investments, proceeding from condition that magnitude of yearly absolute increase of capital investments a should remain constant (figure). As initial base we assume variant II (uniform building).

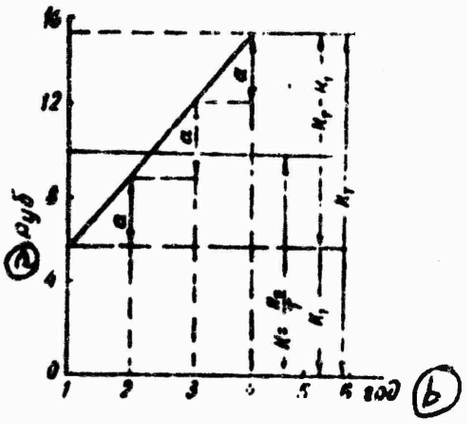

Growth of Annual Volume of Major Investments at Constant of Yearly Absolute Increase of Capital Investments (a)

a -- Rub; b -- Year.

From figure it follows that magnitude of estimated value of object in II variant equals

$$K_0 = KT,$$

in I variant

$$K_0 = K_1 T + \frac{1}{2} T(K_T - K_1) = \frac{K_1 + K_T}{2} T.$$

Equating these expressions, we find

$$K = \frac{K_1 + K_T}{2},$$

whence

$$K_1 + K_T = 2K.$$

We will now define limiting value K_1 and K_T

$$\text{at } K_{1\min} = 0 \quad K_{T\max} = \frac{2K_0}{T};$$

$$\text{at } K_{1\max} = K = \frac{K_0}{T} \quad K_{T\min} = K = \frac{K_0}{T}.$$

Their average magnitudes will equal:

$$K_1 = \frac{K_{1\min} + K_{1\max}}{2} = \frac{K_0}{2T};$$

$$K_T = \frac{K_{T\min} + K_{T\max}}{2} = \frac{3K_0}{2T}.$$

Since

$$K_T - K_1 = a(T-1), \text{ then } a = \frac{K_0}{T(T-1)}.$$

It is obvious that capital investments for second, third and remaining years of building will constitute:

$$K_2 = K_1 + a \frac{K_0}{2T} \cdot \frac{T+1}{T-1}; K_3 = K_1 + 2a \frac{K_0}{2T} \cdot \frac{T+3}{T-1};$$

$$\ldots \text{and } K_{T-1} = K_1 + (T-2)a \frac{K_0}{2T} \cdot \frac{3T-5}{T-1}.$$

Reduced capital investments accordingly will be equal

$$K_{E_n}^1 = \int_0^{T_1} \frac{K_0}{2T}(1+E_n)^{T-t}\,dt = \frac{K_0}{2T} \cdot \frac{E_n(1+E_n)^T - 1}{\ln(1+E_n)};$$

$$K_{E_n}^2 = \int_{T_1}^{T_2} \frac{K_0(T+1)}{2T(T-1)}(1+E_n)^{T-t}\,dt = \frac{K_0}{2T} \cdot \frac{T+1}{T-1} \cdot \frac{E_n(1+E_n)^{T-2}}{\ln(1+E_n)}; \ldots$$

$$\ldots \text{and } K_{E_n}^T = \int_{T_1}^{T} \frac{3K_0}{2T}(1+E_n)^{T-t}\,dt = \frac{3K_0}{2T} \cdot \frac{E_n}{\ln(1+E_n)},$$

and total reduced capital investments will constitute:

$$K_T = \frac{K_0}{2T} \cdot \frac{E_n(1+E_n)^{T-1}}{\ln(1+E_n)} + \frac{K_0(T+1)}{2T(T-1)} \cdot \frac{E_n(1+E_n)^{T-2}}{\ln(1+E_n)} + \ldots$$

$$\ldots + \frac{3K_0}{2T} \cdot \frac{E_n}{\ln(1+E_n)} + \frac{K_0}{2T} \cdot \frac{E_n}{\ln(1+E_n)}\left|(1+E_n)^{T-2} + \right.$$

$$\left. + \frac{T}{T-1}(1+E_n)^{T-3} + \ldots + 3\right|. \qquad (6)$$

The multiplier at K_0 corresponds to the earlier mentioned loss factor

$$z = \frac{E_n}{2T\ln(1+E_n)}\left|(1+E_n)^{T-1} + \frac{T}{T-1}(1+E_n)^{T-2} + \ldots + 3\right|.$$

In Table 3 are brought meanings of loss factor depending upon duration of building, calculated, proceeding from formulas (5) and (6). If we were to be distracted from distribution of major investments with growing yearly volume of them, then the magnitude of reduced capital investments will be significantly overrated: from 2.6% during biennial period of building to 6% during five-year period. Much larger errors result from application of formulas (1), (2), (3), (4), not considering

continuity of putting in of capital investments in building of objects. Thus, in calculation of reduced capital investments by the formula (2), during period of building, equal to five years, we have

$$K_r = K_0(1 + E_n)^T = K_0(1 + 0{,}15)^5 = 1{,}9\,K_0.$$

i.e., the loss factor is equal to 1.9 which is 40% larger than calculated by us.

Table 3.

Loss Factors from Freezing of Means in Incomplete Building at Various Methods of Calculation and Various Periods of Building and at E_n 0.15%

	a Продолжительность строительства, год				
	1	2	3	4	5
b При строительстве с нарастающими темпами	1,00	1,13	1,19	1,27	1,26
c При строительстве с равномерными темпами	1,00	1,16	1,23	1,31	1,14

a -- Duration of building, year; b -- During building at accelerated rate; c -- During building at uniform rate.

Comparison of norms [7] of distribution of capital investments by years of building of pits of nonferrous and ferrous metallurgy prove (Table 4) that in ferrous metallurgy is foreseen relatively the best distribution of capital investments, ensuring with respect to periods of building their higher effectiveness.

Norms provide for introduction of production facilities already toward the end of the fourth year of building, for which to the share of fifth year falls only 11 and 15% of all major investments.

Data of Table 4 show that to moment of introduction of production facilities distribution of capital investments by

years in ferrous metallurgy is foreseen at growing rate, but in nonferrous metallurgy -- almost evenly. As a result at identical value of building of pit 20 million rubles, four year period of building and normative coefficient of effectiveness, equal 0.1 reduced capital for pit of ferrous metallurgy will constitute 24.0 million rubles, and for pit of nonferrous metallurgy -- 24.9 million rubles. With distribution by offered method reduced capital investments will be lowered to 22.6 million rubles.

Table 4.

Norm of Distribution of Major Investments by Years of Building of Pits of Ferrous and Nonferrous Metallurgy in % of Their Value During Period of Building Five Years

a Годы строительства	b Рудники черной металлургии, %	Рудники цветной металлургии (при c штольневом вскрытии), %
1	10	15
2	16	20
3	24	25
4	39	25
5	11	15
d Итого	100,0	100,0

a -- Years of building; b -- Pits of ferrous metallurgy, %; c -- Pits of nonferrous metallurgy (during gallery opening), %; d -- Total.

A comprehensive appraisal of effectiveness of variants of capital investments, as is known, assumes to consider both direct, as well as joint capital investments. Therefore a consistent national-economic approach cannot be limited only to calculation of time of realization of given variant without calculation of time of building analogous objects in adjacent branches. Therefore, in appraising concrete variants of new building or reconstruction of operating enterprises it is necessary to add charges also to joint investments by the formula (6), proceeding from normative periods of building of corresponding objects in adjacent branches of the national economy.

Calculated by us loss factors from freezing of joint investments in process of building for some affiliated with metallurgy branches of the national economy are brought in Table 5. Calculated loss factors a can be used in comparative calculations of effectiveness of technical variants of major investments by the formula

$$E \quad \frac{C_1 - C_2}{(K' + \alpha' \Sigma K'_i \alpha'_i) \quad (K'' + \alpha'' \Sigma K''_i \alpha''_i)}$$

where C_1 and C_2 -- annual operating expenditures by first and second variants, rub;
K' and K'' -- corresponding direct major investments, rub;
K'_i and K''_i -- corresponding joint major investments by i -- that branch, rub;
α' and α'' -- corresponding loss factor by direct capital investments;
α'_i and α''_i -- corresponding loss factors by joint capital investments by i -- that branch.

Table 5.

Loss Factors From Freezing of Means in Process of Building in Certain Branches of Industry

(a) Смежные отрасли цветной металлургии	(b) Отраслевой нормативный коэффициент эффективности	(c) Нормативные сроки строительства[1]				
		1	2	3	4	5
(d) Сырьевая база	0,10	1,08	1,10	1,15	1,22	1,29
(e) Топливная база	0,15	1,09	1,13	1,19	1,27	1,36
(f) Энергетическая база	0,125	1,09	1,12	1,18	1,25	1,33
(g) Транспорт	0,10	1,08	1,10	1,15	1,22	1,29

[1] Periods of building of objects are standardized depending upon productivity of enterprises.

a -- Adjacent branches of nonferrous metallurgy; b -- Branch normative coefficient of effectiveness; c -- Normative periods of building[1]; d -- Raw-material base; e -- Fuel base; f -- Power base; g -- Transport.

This formula allows more correctly to consider loss not only as result of various periods of building, but also depending upon dimension of major investments by years.

Manuscript submitted 5 July 1962

Bibliography

1. K. Marks and F. Engels. Works, V. XVII, p 334, 1939.
2. Method of Determination of Economic Effectiveness of Hydro-Electric Power Plants. State Power Engineering Publishing House, 1961.

3. Model Method of Determination of Economic Effectiveness of Major Investments and New Technology in National Economy USSR. Gosplanizdat, 1960.
4. A. E. Gibshman. Symp. Economic Effectiveness of Major Investments and New Technology. Soekekgiz, 1959.
5. Basic Methodical Positions of Technical Economic Calculations in Power Engineering. Metallurgizdat, 1959.
6. B. S. Vaynstein. Sb. Problems of Economic Effectiveness of Major Investments and New Technology in Building, 1959.
7. Norms of Duration of Building of Enterprises, Starting Complexes, Workshops, Buildings and Construction. SN 164-61, M. 1961.

Scientific Chronicle

Short Information on Session of Scientific Seminar on Mining Thermotechnics of the Ac Sc UkSSR

pp 165-166

From 5 to 8 June in Kiev took place the fifth session of scientific seminar on mining thermotechnics, organized by commission for mining thermotechnics of State Committee of Council of Ministers of Ukrainian Soviet Socialist Republic. At sessions were heard 14 reports in plenary sessions and 46 papers in five sections. Reports were dedicated to the most important problems of contemporary state of mining thermotechnics and were of very great scientific interest.

Working sections (five) of the seminar were represented by reports of following scientific directions:

geothermy of various regions of USSR and technical possibilities of use of terrestrial heat;
sources of best emission in mines and their influence on forming of climatic conditions in working mines;
methods of thermal calculations of mines and other underground construction, based on results of investigations of thermal regimes in mines under the conditions heated up and perennial-frozen deposits;
on the selection of rational diagrams of conditioning air in mines taking into account heat and humidity conditions in mines;
nature of endogenic mine fires and preventive measures.

This information gives a short account of contents of certain reports, heard at sessions of separate sections.

Report of senior scientific collaborator of Institute of Geology of Academy of Sciences of USSR B. A. Pokrovskiy: "Geothermic Conditions of European Part of USSR" was devoted to the

study of magnitude of geothermic degree in various geographic regions of the country. In report was marked that in connection with search for oil and gas was drilled near 1000 holes, the data of which were processed and from them composed thermograms, map isotherms and isothermal profiles. It turned out that at depth of 500 m from day surface temperature of rocks in European zone of USSR is equal approximately to 15°, and in subcaucasus and South 40-45°. At depths 1000 m temperature of rocks in the north of the European part of USSR constitutes 6-13°, in central part 20-25°, and in south is within limits of 40-50°. At depth 1500 m occurs sharp temperature increase of rocks; thus, for example, in the north of country it constitutes 20°, in central part of Union is equal to 40° and in south reaches 130-140°.

As can be seen from above-cited data, the magnitude of geothermic degree representing such vertical distance, at deepening on which in bowels of earth temperature of rocks increases by 1°, in south of European part of USSR constitutes less than 30 m, whereas in central and north regions it is significantly higher. Therefore in designing mines and pits in these regions one should consider this circumstance for the purpose of creation of normal temperature rate.

The report by Doctor of Technical Sciences G. V. Duganov "Investigation and Forecast of Heat Emmission in Deep Mines, and Investigation of Heat Physical Constants of Rocks in Mine Conditions" contained a short technical characteristic and description of new instrument-heat meter for determination of heat emission from a mass of 1 cubic meter.

Measurements, performed by heat meter in certain mines of Donets Basin, give following magnitudes of heat emission from oxidation: in workings, passed through hard rocks without bracing 1.5-3.0 kilocalorie/m^2·hour; in foundation laying of working space 10-15 kilocalorie/m^2·hour.

As can be seen from cited examples, main source of heat emission in clean cuts are oxidation of rocks and filling of worked out space with lumber.

Great interest was caused by repott "Method of Forecast of Thermal Conditions in Preparatory Workings with Deadend Cuts," by cand. techn. sciences E. I. Baratov and Engineer E. N. Malashenko (Institute of Heat-Power Engineering Ac Sc UkSSR). Data of this report show that dead-end workings as compared with through workings have the worst parameter of ventilation and temperature rate. Main sources of emission of heat in dead-end workings are fresh-bared rocks massifs and cutting machines.

As a result of number of analytic investigations by authors of above method formulas were drawn, reflecting character of heat exchange in air conduit in pre-cut space in mines with heated up mine massif, also in hydro-mines. Resolution of these equations with sufficient accuracy depicts real temperature rate of dead-end working mines. Besides formulas are developed also nomographs, accelerating calculating operations as compared with calculations by the formulas.

In report by cand. of technical sciences N. N. Khokhotva (MAK. NII) "About Rational Diagram of Cooling of Air in Deep Mines of Donets Basin" was given analysis of developed classification of division of all deep mines of Donets Basin into six groups with recommendations for mines of every group. This work represents great scientific and practical interest, inasmuch as it is one of the first works in this field.

Besides other reports, done on plenary sessions, was heard also information of E. I. Baratov on mine air-cooling installations in Belgium, in which was reported much interesting material on solution of problem of lowering of temperature in deep mines. Thus, for example, in one of the mines in Belgium acts refrigerating installation of Freon type, refrigerating machines of which are placed on surfaces of earth with supplying of refrigerating heat-transfer agent to operating cuts. All pipe lines for the refrigerant are heat-isolated with cork material or fiberglass.

Besides above-stated reports and appearances at session was done many valuable from scientific and practical points of view of communications about forecast and adjustment of thermal regime of mines and pits. Therefore collection of scientific reports of this seminar, which will be published by the Academy of Sciences Ukrainian SSR, will present great interest for mining engineers and thermotechnicians.

Value of past session of seminar consists in the fact that it generalized performed investigations in field of mining thermotechnics that will serve as a stimulus to further still more extensive investigations in this direction and make a valuable contribution to science on mining thermotechnics.

The session showed that the question of temperature rate of mines is thus far resolved basically only for coal deposits, whereas in practice we have a number of high-temperature ore deposits, in which are inherent conditions of disturbances due to strong hydrothermal treatment and mineralization of rocks. These processes are still studied insufficiently although they appear to have a large influence on climatic conditions in pits.

E N D

T. S. Guriev

1163, 1169 and 2478
CSO: 1500-S/3